17 June 2005

Science

Vol. 308 No. 5729
Pages 1697-1824 $10

125 YEARS OF GLOBAL Science

AAAS

The perfect assortment.

With GeneMorph® mutagenesis kits, a balanced spectrum of mutations is right at your fingertips.

GeneMorph® random mutagenesis kits* feature our patented Mutazyme® II DNA polymerase, which delivers a balanced mutational spectrum with more robust yields than *Taq* polymerase under error-prone PCR conditions. This allows you to discover more key residues responsible for protein function easier and faster than before, thus enhancing the evolution of your protein.

- **Simple protocol to control mutation frequency**
- **Efficient mutagenesis rates of 1 to 16 bases per kb**
- **Overcome poor PCR yield and mutational bias of *Taq* polymerase**

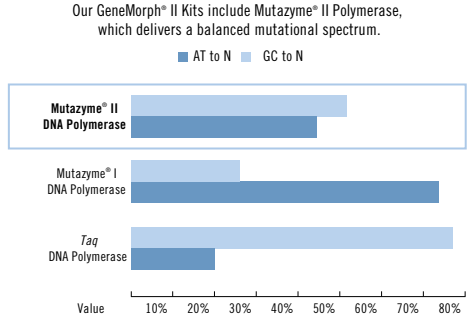

Need More Information? Give Us A Call:

Stratagene USA and Canada
Order: (800) 424-5444 x3
Technical Services: (800) 894-1304

Stratagene Europe
Order: 00800-7000-7000
Technical Services: 00800-7400-7400

Stratagene Japan K.K.
Order: 03-5159-2060
Technical Services: 03-5159-2070

* U.S. Patent No. 6,803,216 and patent pending

www.stratagene.com

Ask us about these great products:

GeneMorph® II Random Mutagenesis kit	30 rxns	200550
GeneMorph® II EZClone Domain Mutagenesis kit	10 rxns	200552

Purchase of these products is accompanied by a license to use them in the Polymerase Chain Reaction (PCR) process in conjunction with a thermal cycler whose use in the automated performance of the PCR process is covered by the up-front license fee, either by payment to Applied Biosystems or as purchased, i.e., an authorized thermal cycler.

STRATAGENE

The great thinkers of our time are out there—a handful of idealistic souls driven to discover something that will improve the human condition. Maybe you're one of them.

accelerate > rock stars

But breakthroughs don't happen independently of one another. Inevitably, the act of answering one question in science automatically leads to another. Even if you're just one link in a string of related discoveries, that string could lead to a breakthrough of epic proportions.

Science has changed the world dramatically in the last 100 years by answering many of the questions facing humankind. But there are still many things we don't know. Invitrogen's innovative products and services make the job of answering the next great question easier and more efficient, covering all areas of biological discovery, including disease research, drug development, and commercial bioproduction.

Chances are your work will never result in a crowd of groupies asking for your autograph. But maybe one day, our collaboration will result in a discovery that truly changes people's lives for the better.

The spotlight might be fleeting, but the effect is bound to make a lasting reverberation.

www.invitrogen.com

invitrogen™

GE Healthcare

Ni Sepharose™

4x greater binding capacity in histidine-tagged protein purification

Ni Sepharose™ products from GE Healthcare give you the highest binding capacity available for histidine-tagged protein purification. With up to four times the binding capacity, it's no longer pure imagination to dramatically increase your yield, while saving time and costs. Maximum target protein activity is assured, thanks to tolerance of a wide range of additives and negligible nickel ion leakage. The flexibility to use a variety of protocols ensures the highest possible purity. Ni Sepharose 6 FF is excellent for manual procedures such as gravity/batch and easy scale-up, while the HP version is designed for high-performance in automated purification systems – both are available in different formats, including prepacked columns. Outstanding performance has never been easier to achieve.

www.amershambiosciences.com/his

imagination at work

GE10-05

Science

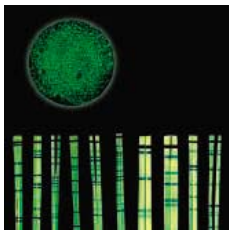

COVER Human embryonic stem cells derived by nuclear transfer (green moon) match the donor cells genetically and immunologically (human leukocyte antigen data sets represent bamboo), regardless of the age, sex, or disease status of the donor of the nucleus. The patient-specific cell lines described on page 1777 may aid in the discovery of complex disease mechanisms and human developmental processes. [Image: H. Qidwai]

Volume 308
17 June 2005
Number 5729

DEPARTMENTS

NEWS OF THE WEEK

NEWS FOCUS

1730

1744

NASA/GSFC, MODIS Rapid Response Team.

1753

LETTERS

BOOKS *ET AL.*

POLICY FORUM

PERSPECTIVES

Contents continued

Systems Biology — RNAi and Gene Expression Analysis

GeneGlobe — the world's largest database of matching siRNAs and RT-PCR assays

New

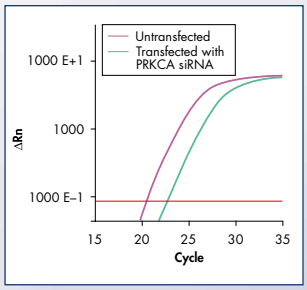

Reliable quantification after knockdown.

Visit www.qiagen.com/GeneGlobe .

New genomewide solutions from QIAGEN provide potent, specific siRNAs and matching, ready-to-use, validated primer sets for SYBR® Green based real-time RT-PCR assays.

- **One database** — easy online access to RNAi and gene expression solutions at the GeneGlobe™ Web portal
- **Two matching solutions** — siRNAs and matching real-time RT-PCR assays you can rely on
- **Three complete genomes** — siRNAs and RT-PCR assays are available for the entire human, mouse, and rat genomes

For matched siRNAs and real-time RT-PCR assays, go to www.qiagen.com/GeneGlobe !

QIAGEN

SCIENCE EXPRESS www.sciencexpress.org

ATMOSPHERIC SCIENCE: Marked Decline in Atmospheric Carbon Dioxide Concentrations During the Paleogene

M. Pagani, J. C. Zachos, K. H. Freeman, B. Tipple, S. Bohaty

Atmospheric CO_2 levels fell from 1500 parts per million to modern levels of 300 parts per million from 35 to 25 million years ago, coincident with the buildup of ice in Antarctica.

GEOCHEMISTRY: ^{142}Nd Evidence for Early (>4.53 Ga) Global Differentiation of the Silicate Earth

M. Boyet and R. W. Carlson

A difference in the relative abundance of neodymium-142 in chondrite meteorites and sampled rocks on Earth imply that Earth's mantle rapidly separated into two reservoirs. *related News story page 1723*

STRUCTURAL BIOLOGY: Crystal Structure of Human Toll-Like Receptor 3 (TLR3) Ectodomain

J. Choe, M. S. Kelker, I. A. Wilson

A Toll-like receptor, which helps the immune system sense microbes, is a large horseshoe-shaped glycoprotein that may be activated when double-stranded RNA binds to its side.

MOLECULAR BIOLOGY: Genome-Scale Identification of Nucleosome Positions in *S. Cerevisiae*

G.-C. Yuan, Y.-J. Liu, M. F. Dion, M. D. Slack, L. F. Wu, S. J. Altschuler, O. J. Rando

The proteins that pack DNA into the yeast nucleus are usually found next to genes, whereas large regulatory regions, which have evolved little, are left exposed. *related News story page 1724*

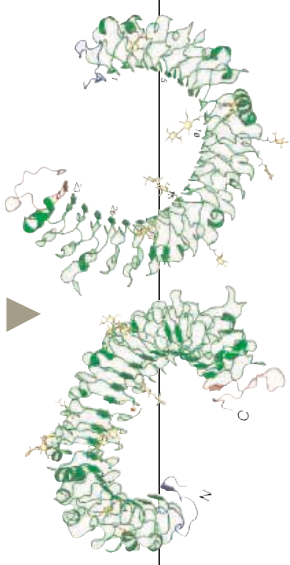

TECHNICAL COMMENT ABSTRACTS

1750 & 1756

BREVIA

RESEARCH ARTICLES

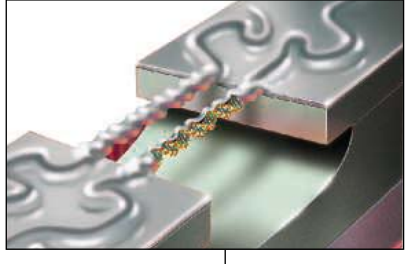

1762

REPORTS

Contents continued

PIERCE

Grasp the Proteome™

Protein Purification/Detection

Still using Streptavidin?

NeutrAvidin™ Protein offers ultra-low nonspecific binding at an *unbelievably* low price

NeutrAvidin™ Protein offers the highest possible specificity for biotin, yielding the lowest nonspecific binding. NeutrAvidin™ Protein provides exceptional performance for both purification and detection of biotin-labeled proteins. If you're still using Streptavidin, it's time to discover the advantages of NeutrAvidin™ Tools.

Advantages over streptavidin:

- Highest specificity for biotin binding
- No nonspecific binding to cell-surface proteins
- High signal-to-noise ratio in detection systems
- Saves money without sacrificing quality

Properties of biotin-binding proteins

	Avidin	Streptavidin	NeutrAvidin™ Protein
Molecular Weight	67K	53K	60K
Biotin-binding Sites	4	4	4
Isoelectric Point (pI)	10	6.8-7.5	6.3
Specificity	Low	High	Highest
Affinity for Biotin (K_d)	10^{-15} M	10^{-15} M	10^{-15} M
Nonspecific Binding	High	Low	Lowest

Available in bulk quantities and in the following convenient formats:

- Immobilized NeutrAvidin™ Protein on Agarose
- UltraLink® Immobilized NeutrAvidin™ Protein
- Soluble NeutrAvidin™ Protein
- HRP- and Alkaline Phosphatase-labeled NeutrAvidin™ Protein
- Fluorescein-labeled NeutrAvidin™ Protein
- Maleimide-activated NeutrAvidin™ Protein
- 96- and 384-well NeutrAvidin™ Plates

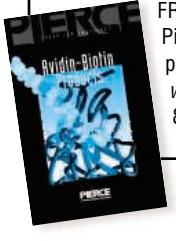

FREE Avidin-Biotin Handbook from Pierce, the leader in avidin-biotin products! Visit the Pierce web site at *www.piercenet.com/ab95d* or call 800-874-3723 to request your copy today.

www.piercenet.com/neu22d

PIERCE

Tel: 815-968-0747 or 800-874-3723 • Fax: 815-968-7316
Technical Assistance E-mail: TA@piercenet.com • Customer Assistance E-mail: CS@piercenet.com

Outside the United States, visit our web site or call 815-968-0747 to locate your local Perbio Science branch office (below) or distributor

Belgium & Dist.:	China:	France:	Germany:	Hong Kong:	The Netherlands:	United Kingdom:	Switzerland:
Tel +32 53 85 71 84	Tel +86 10 8049 9033	Tel 0800 50 82 15	Tel 0228 9125650	Tel 852 2753 0686	Tel 076 50 31 880	Tel 0800 252185	Tel 0800 56 31 40
euromarketing@perbio.com	support@perbio.com.cn	euromarketing@perbio.com	de.info@perbio.com	SalesHK@perbio.com	euromarketing@perbio.com	uk.info@perbio.com	euromarketing@perbio.com

PERBIO

REPORTS CONTINUED

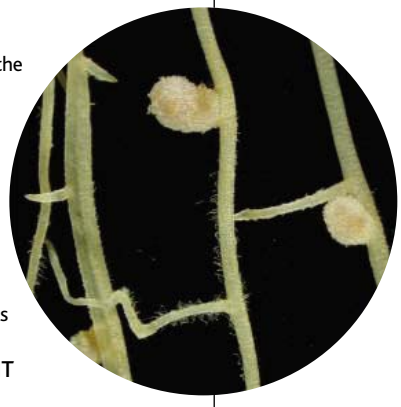

1749, 1786, & 1789

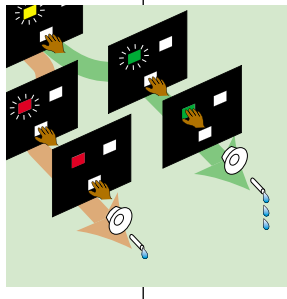

1798

AAAS
ADVANCING SCIENCE, SERVING SOCIETY

SCIENCE (ISSN 0036-8075) is published weekly on Friday, except the last week in December, by the American Association for the Advancement of Science, 1200 New York Avenue, NW, Washington, DC 20005. Periodicals Mail postage (publication No. 484460) paid at Washington, DC, and additional mailing offices. Domestic individual membership and subscription (51 issues): $135 ($74 allocated to subscription). Domestic institutional subscription (51 issues): $550; Foreign postage extra: Mexico, Caribbean (surface mail) $55; other countries (air assist delivery) $85. First class, airmail, student, and emeritus rates on request. Canadian rates with GST available upon request, GST #1254 88122. Publications Mail Agreement Number 1069624. **Printed in the U.S.A.**

Change of address: allow 4 weeks, giving old and new addresses and 8-digit account number. **Postmaster:** Send change of address to *Science*, P.O. Box 1811, Danbury, CT 06813–1811. **Single copy sales:** $10.00 per issue prepaid includes surface postage; bulk rates on request. **Authorization to photocopy** material for internal or personal use under circumstances not falling within the fair use provisions of the Copyright Act is granted by AAAS to libraries and other users registered with the Copyright Clearance Center (CCC) Transactional Reporting Service, provided that $15.00 per article is paid directly to CCC, 222 Rosewood Drive, Danvers, MA 01923. The identification code for *Science* is 0036-8075/83 $15.00. *Science* is indexed in the *Reader's Guide to Periodical Literature* and in several specialized indexes.

Contents continued ▶

One just right for you.

Find your perfect match among the full line of Bio-Rad amplification products.

Bio-Rad is committed to providing you with the best tools for your PCR needs. This dedication is proven by our history of innovation, quality, and regard for researchers' needs.

- The most complete line of thermal cyclers available anywhere
- The only modular real-time cycler upgrade with a thermal gradient; choose from 1 to 5 colors
- Innovative enzymes that work where others fail
- PCR tubes, plates, and sealers for any application
- Dedicated technical support by experienced scientists

For more information, visit us on the Web at: **www.bio-rad.com/amplification/**

Photo: Pete with his MiniOpticon™ real-time system and Patty with her DNA Engine Dyad® cycler with a Dual Alpha™ unit and a single Alpha™ unit.

Visit us on the Web at **discover.bio-rad.com**
Call toll free at 1-800-4BIORAD (1-800-424-6723);
outside the US, contact your local sales office.

BIO-RAD

Science
www.scienceonline.org

sciencenow www.sciencenow.org Daily News Coverage

Supreme Court Rules on Patent Suits
Decision seen as boost for drug researchers.

There's Life in That Oil!
Ancient crude indicates young Earth teemed with organisms.

Fungi's Little Helper
Compound made by plants encourages growth of symbiotic fungi.

Spark your job search with a positive attitude.

science's next wave www.nextwave.org Career Resources for Young Scientists

US: Tooling Up—Time for an Attitude Adjustment? *D. Jensen*
A positive mindset gives you a better chance of ending up in the ranks of the employed.

Canada: Rising Canadian Stars Win Cottrell Scholar Awards *A. Fazekas*
A U.S.-based foundation offers $100,000 awards for young university faculty members.

UK: On the Road to Health and Safety *CareerDoctor*
The CareerDoctor spells out health and safety acronyms and offers advice on entering the industry.

UK: The Write Initiative *L. Blackburn*
A bunch of budding science communicators, teamwork, and a failed marathon training plan helped get a science magazine off the ground.

MiSciNet: NAMSS—Recruiting Minorities for STEM Careers *E. Francisco*
A marine and space science program recruits Native Americans into science, engineering, and math careers.

GrantsNet: International Grants and Fellowships Index *Next Wave Staff*
Get the latest listing of research funding, scholarships, fellowships, and internships offered outside the U.S.

science's sage ke www.sageke.org Science of Aging Knowledge Environment

Genetically Altered Mice: CB1 Knockout Mice *M. Russell*
Cannabinoid receptors are involved in the control of bone mass and osteoclast activity.

News Focus: Before Their Time *R. J. Davenport*
Eggs falter prematurely in mice without signaling molecule.

News Focus: Premature Emission *M. Leslie*
Early surge in fat-fighting hormone might trigger obesity later in life.

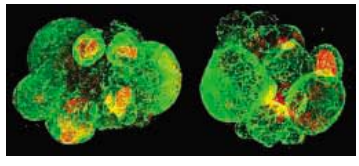

Speeding up ovarian aging.

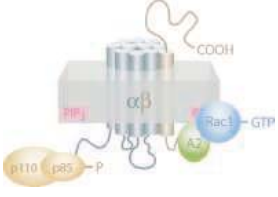

Sodium pump as adaptor protein.

science's stke www.stke.org Signal Transduction Knowledge Environment

Perspective: Oxygen Sensing—Getting Pumped by Sterols *B. M. Emerling and N. S. Chandel*
Sterol depletion activates anaerobic gene expression in fission yeast.

Perspective: A Moving New Role for the Sodium Pump in Epithelial Cells and Carcinomas *J. H. Kaplan*
Sodium pump abundance controls MDCK cell motility.

Teaching Resource: Nuclear Transactivators and Repressors *Z.-Q. Pan*
Prepare a graduate-level lecture on the regulation of eukaryotic gene transcription machinery.

Separate individual or institutional subscriptions to these products may be required for full-text access.

“Novartis drove my cancer into remission in 35 days. Now I’m going for my PhD.”

Suzan was fighting a losing battle against a deadly form of cancer. She dropped out of school. She lost weight, her hair, and at times, her will to live. Then, a Novartis medicine put her cancer into remission in just 35 days. No one can promise what the future holds for any cancer patient, but today Suzan is back—into life and into a PhD in biology.

Think what’s possible

NOVARTIS

www.us.novartis.com

edited by Stella Hurtley and Phil Szuromi

Freshening Up Slowly

The strength of large-scale ocean thermohaline circulation depends in part on the saltiness of the waters of the North Atlantic Ocean. The salinity of the upper waters there has been decreasing during the past 30 or more years, but how much fresh water must have been added to produce those changes has been unclear. **Curry and Mauritzen** (p. 1772) reconstruct the history of the ocean temperature, salinity, and density of the Nordic Seas and Subpolar Basins for last 50 years in order to determine what must have been the fresh water inputs there. Although the fluxes that they calculate are high, they do not appear to be great enough to slow or shut down thermohaline circulation within the next century or two.

Nanowires and SQUIDs

Using molecules as templates onto which metal wires can be deposited is opening up opportunities for self-assembled circuitry and the formation of devices. **Hopkins *et al.*** (p. 1762) used two strands of DNA stretched across a trench as a template to deposit two finely coupled superconducting nanowires. Although the structure superficially resembles a superconducting quantum interference device (SQUID), and the resistance oscillates as a function of magnetic field, close inspection of the magnetotransport behavior suggests somewhat different behavior from that of standard mesoscopic superconducting devices.

Beyond H_3O^+

Despite the ease with which we can now measure pH, a molecular picture of aqueous protons remains elusive, and recent studies have shown that the standard H_3O^+ structure is more of a shorthand than an accurate description of bonding. **Headrick *et al.*** (p. 1765) used infrared spectroscopy to probe the structure from the bottom up, starting with a proton shared between just two water molecules. They then watched the bonding structure change as one to nine additional water molecules were added. Enlarging the solvation shell varied the dominance of structures in which the proton is bound to one water molecule (H_3O^+) or shared equally between two ($H_2O–H–OH_2^+$). These results suggest that coordination in the bulk may fluctuate between these extremes.

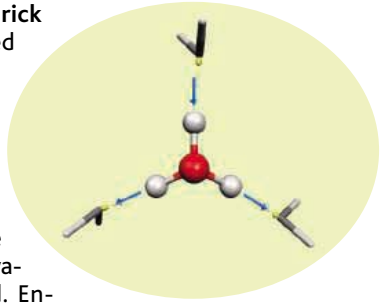

CREDITS (TOP TO BOTTOM): JANKE *ET AL.*; HEADRICK *ET AL.*

Tubulin-Modifying Enzymes Identified

Polyglutamylation of tubulin has been implicated in several functions of microtubules. **Janke *et al.*** (p. 1758, published online 12 May 2005) present evidence that the neuronal tubulin polyglutamylase is a protein complex containing a conserved tubulin tyrosine ligase–like (TTLL) protein, TTLL1. The unicellular, ciliated freshwater protozoan *Tetrahymena thermophila* has at least two conserved types of TTLLs that act as polyglutamylases. The polyglutamylases differ in substrate preference and subcellular localization and contribute in *Tetrahymena* to ciliary motility and cell division.

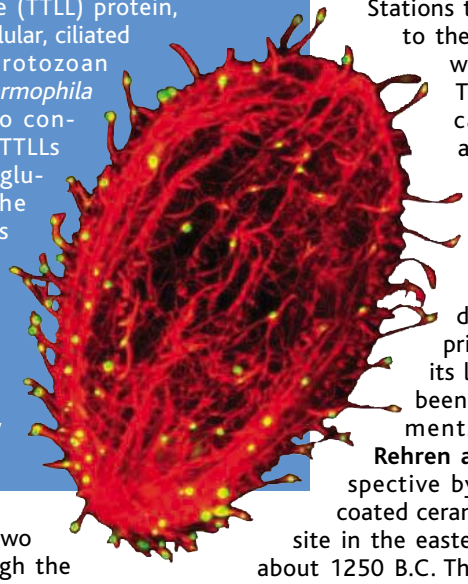

A Long-Lived Earthquake

The 26 December 2004 Sumatra-Andaman earthquake produced noticeable deformation over most of Earth. **Banerjee *et al.*** (p. 1769 published online 19 May 2005) used global positioning satellite measurements from both far from and near to the earthquake to provide an estimate of how the rupture progressed and the amount of energy it released. Stations to the east of the rupture moved to the west, and vice versa, consistent with the quake's thrust motion. The inversion implies that significant energy was released even after 1 hour after the quake.

Clearing Up Glass

Glass artifacts can be found in Mesopotamia and Egypt that date from 1000 to 1500 B.C. The primary source of the glass, before its later reworking by craftsmen, has been uncertain, although most arguments have favored Mesopotamia. **Rehren and Pusch** (p. 1756; see the Perspective by **Jackson**) now describe glass-coated ceramic vessels and slag discovered in site in the eastern Nile Delta in Egypt dating to about 1250 B.C. The nature of the material implies that it was fired to nearly 1000°C and is consistent with this site being a major center of primary glass production.

Patient-Specific Embryonic Stem Cells Become a Reality

The generation of pluripotent patient-specific cell lines is a first step toward specifically tailored cellular therapies. **Hwang *et al.*** (p. 1777; published online 19 May 2005; see the 20 May news story by **Vogel**) have isolated embryonic stem cell lines via an improved somatic cell nuclear transfer method. These cell lines match the nuclear DNA and show in vitro immunological compatibility with cells from the original somatic nucleus donor patients. However, these patient-specific cells could only be used for preclinical analyses until the remaining animal components introduced during culture are removed and until reliable methods provide efficient, directed differentiation of stable cells of whichever cell type may be needed for therapeutic transplantation. In a related Policy Forum, **Magnus and Cho** (p. 1747; published online 19 May 2005) discuss the ethical issues raised by nonclinical oocyte donation.

CONTINUED ON PAGE 1711

Traditional Mini Preps are Over.

Start automating with the latest in plasmid DNA purification. The Mini Prep 96 can perform up to 96 preps in 1 hour of processing time. Up to 8 µg of plasmid DNA per lane at less than $1 a prep.

Start with easy operation. Disposable cassettes allow for direct loading of culture with no centrifugation.

Start the Mini Prep 96 with the push of a button. Remove high purity DNA and use in most microbiology protocols — including sequencing and cell transfection.

Start saving time and money with the Mini Prep 96.

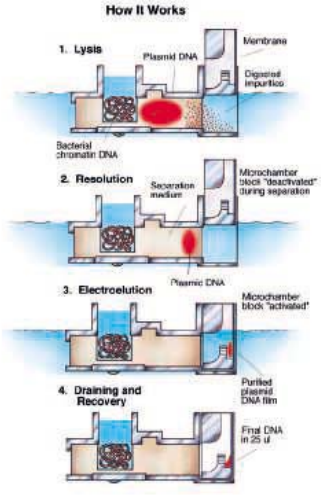

Four Easy Steps to
Plasmid DNA Purification

Stop Manual Mini Preps 

Start the Mini Prep 96™

1-800-466-7949
www.macconnell.com

Mini-Preps at the Push of a Button.
6195 Cornerstone Court, San Diego, California 92121, Fax: 858-452-6753

MacConnell Research

Home Sweet Home

Leguminous plants fix atmospheric nitrogen with the aid of symbiotic rhizobial bacteria. When rhizobia infect the root, a complex developmental program is initiated to form the nodules that house the symbiotic bacteria (see the Perspective by **Udvardi and Scheible**). **Smit *et al.*** (p. 1789) and **Kaló *et al.*** (p. 1786) identify key elements in the signaling cascade by which the bacteria signal their presence to the host plants. The constitutively expressed plant proteins NSP1 and NSP2 are likely transcription factors poised to respond early to the bacterial nodulation factor signal. It appears that NSP1 and NSP2 respond to the initial nodulation factor–induced calcium signal to generate changes in gene transcription.

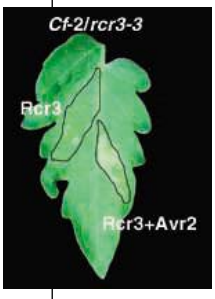

Indirect Defenses

Some plants defend against fungal infection by using the hypersensitive response, in which plant cells at the site of invasion are killed off to retard spread of the infection. The process relies upon an elicitor from the pathogen and a corresponding resistance gene in the plant. When *Cladosporium fulvum* infects tomato leaves, these two factors do not, however, seem to interact directly. **Rooney *et al.*** (p. 1783, published online 21 April 2005) analyze the function of the plant protease Rcr3 in mediating the defense response. The pathogen avirulence factor, Avr, is secreted extracellularly, where it interacts with the tomato plant Rcr3 protease. Together, this interaction signals to the membrane-bound host resistance factor, Cf-2, to initiate plant defense responses.

Of Mice and Men

Differences between the left and right hemispheres of the brain mean that each side is somewhat specialized, the right being more "artistic" and the left being more "mathematical." These differences are laid down early in development, and the skills associated with each side honed as we mature. **Sun *et al.*** (p. 1794, published online 12 May 2005) have now analyzed gene expression in the early developing human brain and identified a number of genes that are asymmetrically expressed. In-depth analysis of one of the genes, *LMO4*, and comparison of how the related gene is expressed in developing mouse brains, indicates that human brains consistently attain a similar left-right asymmetry, whereas in the mouse the asymmetry is established randomly.

The Neural Signature of Disappointment

Neurons in several brain structures respond to dopamine in a way that is positively correlated with the difference between reward magnitude and reward expectation. However, what happens when our expectations are frustrated, as often happens in real life? **Minamimoto *et al.*** (p. 1798) observed a reward-related signal in the centromedian nucleus of the thalamus that is correlated with the expectation or delivery of a small reward. This signal seems to be specifically related to disappointment or unhappiness. Electrical stimulation of this nucleus specifically disrupted behavior in a task with differential reward structure. Thus, the feeling of disappointment interferes with the execution of a straightforward behavioral process.

TRP'ing Up the Kidney

In focal and segmental glomerulosclerosis (FSGS), scarring or hardening of the tiny blood vessels within the kidney leads to leakage of protein into the urine. FSGS is a significant cause of end-stage renal disease, and its prevalence is increasing. Disruption of cytoskeletal and structural proteins are known to play a role in pathogenesis. Now, **Winn *et al.*** (p. 1801, published online 5 May 2005) describe an alternative route to the disease. Studying a large family with a hereditary form of FSGS, they find that the causative mutation occurs in the gene encoding transient receptor potential cation channel 6 (TRPC6), a protein believed to mediate calcium entry into cells. Because channels are often amenable to pharmacological manipulation, this study raises the possibility that TRPC6 may be a useful therapeutic target in chronic kidney disease.

CREDIT: ROONEY *ET AL.*,

Science

AAAS

AFFYMETRIX®

AAAS Newcomb Cleveland Prize

Supported by

AFFYMETRIX

CALL FOR NOMINATIONS

This $25,000 prize is awarded to the author or authors of an outstanding paper published in the Research Articles or Reports sections of *Science*.

Readers are invited to nominate papers published during the period 1 June 2004 – 31 May 2005. An eligible paper is one from the relevant sections that includes original research data, theory, or synthesis or one that presents a fundamental contribution to basic knowledge or a technical achievement of far-reaching consequence. Reference to pertinent earlier work by the author may be included to give perspective.

DEADLINE: 30 JUNE 2005

Phone ..... (202) 326-6507

E-mail ..... skihara@aaas.org

Additional information about the prize and the nomination procedure can be found at:
www.aaas.org/about/awards/

The Fight of the Decade

At the inauguration of the United Nations (UN) World Environment Day 2005 Conference in San Francisco on 2 June, California Governor Arnold Schwarzenegger did an astonishing thing in his opening speech. Such occasions normally invite specimens of banal hospitality: "We welcome this distinguished gathering of international leaders to our great state…" Well, the Gubernator wasn't having any of that. Instead, he talked about global warming, laying out a real challenge to climate policy as it is practiced in Washington, DC, today. His talk has set up a heavyweight bout between two powerful Republican leaders over the proper role of science in politics. Best of all, we won't even have to pay to watch it!

So imagine that it's Fight Night. Before the action begins in the ring, I'll set the scene and report some of the background. In the lower right corner is President George Bush, the champion by virtue of his office as leader of the world's largest economy. He's wearing the red trunks. In various pre-fight interviews he has said that he thinks the climate may be changing, but his seconds are instructed to talk about "climate variability" and avoid the phrase "climate change" at international meetings. He didn't want to sign the Kyoto Protocol, which would have set targets for timed reductions in greenhouse gas emissions to below 1990 levels. As a White House official now explains, signing it would have cost jobs and raised energy prices. Bush's Climate Change Science Program, at first criticized by a National Academies report, now gets better reviews from the Academies. It focuses heavily on long-range research, but it contains no targets for reductions in greenhouse gas emissions, the primary cause of global warming. In a pre-fight meeting with reporters, the champ praised the virtues of fuel cells and the hydrogen economy envisioned in his climate plan, and added that his critics are "disassembling."

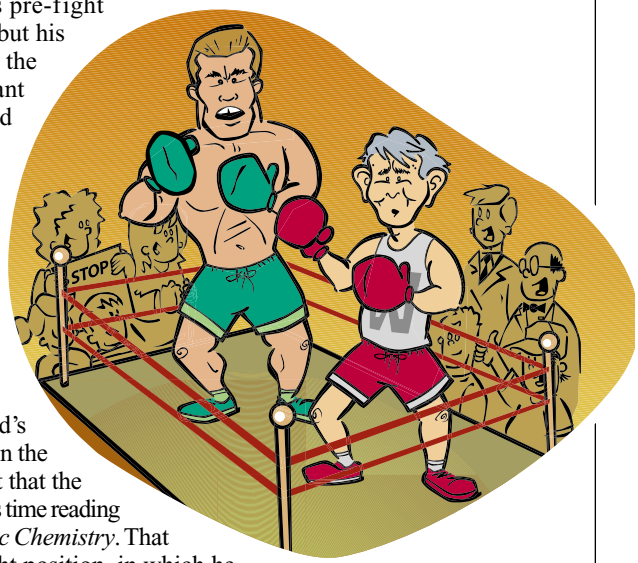

In the upper left corner is the challenger, representing the world's fifth-largest economy: California Governor Arnold Schwarzenegger, in the green trunks. Sportswriters who have visited his training camp report that the weight machines sit unused in a corner, and that the governor spends all his time reading journals like *Science*, *Climatic Change*, and the *Journal of Atmospheric Chemistry*. That may be why he selected the UN conference to stake out his pre-fight position, in which he asserted: "We know the science, we see the threat, and we know that the time for action is now." The plan he announced sets tough targets for reducing California's emissions of greenhouse gases: to 2000 levels by 2010, to 1990 levels by 2020, and to 80% below 1990 levels by 2050. These will require stringent regulatory measures, building on California's existing commitments to reduce automobile emissions. But the governor said: "We have no choice but to meet this challenge. We must leave a better world for our children and their children."

Early pre-fight commentary has produced newsworthy partisans on both sides. Representative John Dingell of Michigan, who represents the "Big Three" automakers in Congress, is said to be forming a Democratic Transportation Caucus to offer its crossover support to the president. The mayors of over 100 U.S. cities, who earlier had declared their own intentions to reduce emissions, voiced their enthusiasm for the challenger's plan. The mayor of Seattle, a prime mover in that effort, has offered to wager a 40-pound Washington salmon against an equivalent stake put up by a backer of the champ. Famed Bush strategist Karl Rove promptly designated a small striped bass, claiming that it's worth more than its 8-pound weight because it's a celebrity fish, having been boated by the president in an event pictured on the front page of the *New York Times*.

Folks, this promises to be the Fight of the Decade in this division, so keep your dial where it is. The charismatic California challenger has a lively rooting section, including soccer moms and children, some carrying signs saying "Stop Polluting Our Greenhouse." On the other side, NASCAR dads and numbers of elegantly dressed older gentlemen are voicing enthusiastic support for the president. We asked for quick pre-fight statements from each contestant. The champ said that everything was just fine with the climate. His challenger, in a comment directed at his constituency or perhaps his opponent, merely said, "Hasta la vista, baby."

Donald Kennedy
Editor-in-Chief

10.1126/science.1115709

ILLUSTRATION: TIM SMITH

GetInfo

science.labvelocity.com

Get the lab product info you need — FAST

Science announces a new online life science product information system, **GetInfo**, powered by **LabVelocity**

- Quickly find and request free information on products and/or services found in the pages of *Science* magazine
- Ask vendors to contact you with more information
- View detailed product information
- Link directly to vendors' websites

Visit GetInfo today at
science.labvelocity.com

Science
AAAS

EDITORS' CHOICE

edited by Gilbert Chin

PHYSIOLOGY

Regulating Salt Intake

Euryhaline fish, such as Mozambique tilapia (*Oreochromis mossambicus*), are able to live in waters with a wide range of salinity. Mitochondrion-rich cells (MRCs, also known as ionocytes) are located in the gills of adult fish and are thought to regulate internal ionic composition, either by secreting excess salt in a seawater environment or by taking up needed ions during a freshwater stage of life.

Hiroi *et al.* have examined the adaptive deployment of ion transporters in MRCs, which are found in the yolk sac membrane in developing embryos, by transferring the embryos from fresh water to salt water or vice versa. The three primary molecular components are a Na/K-ATPase, a Na/K/2Cl cotransporter, and a chloride channel, and the authors used immunoflurorescence microscopy to group the MRCs into four types: (i) an immature type-I MRC that can give rise to any of the other three types; (ii) a salt-accumulating type-II cell for freshwater living; (iii) a dormant type-III cell held in reserve; and (iv) a seawater, salt-extrusion type-IV cell derived from and apparently convertible back into type-III cells. The remarkable changeover from absorption to secretion (fresh water to sea water) is achieved by moving the Na/K/2Cl cotransporter from the apical to the basolateral surface and by replacing it with the chloride channel. — GJC

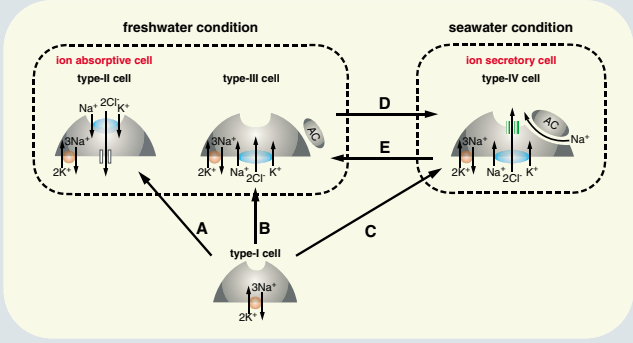

Locations in the four types of MRCs of Na/K-ATPase (red), Na/K/2Cl cotransporter (blue), and chloride channel (green).

J. Exp. Biol. **208**, 2023 (2005).

CHEMISTRY

Scattershot Patterning

Although many methods exist for the patterning of semiconductor surfaces, for large-scale fabrication, a system that can self-assemble would be ideal. Recent work has shown that block copolymers are compatible with industrial silicon-based processing, thus these materials are attracting renewed interest.

Aizawa and Buriak have devised two methods to use block copolymers to direct reactions at semiconductor surfaces in a spatially defined manner. In the first approach, block copolymer micelles are loaded with reagents that react with the semiconductor surface on deposition. In the second, they can deposit a monolayer of self-assembling block copolymers onto a substrate, which is then immersed in the reactive reagent. This variation has the advantage of not limiting the reagent concentration to that available in the loaded micelles. The reactions studied were based on the galvanic reduction of oxidizing metal ions, which can bond to the substrates as particles, films, or other morphologies. The diblock copolymer consisted of polystyrene joined to poly-4-vinylpyridine (P4VP); the latter material is known to associate with metal ions or complexes. Thus, by controlling the location of the P4VP blocks, one can control the size and spacing of the metal particles. — MSL

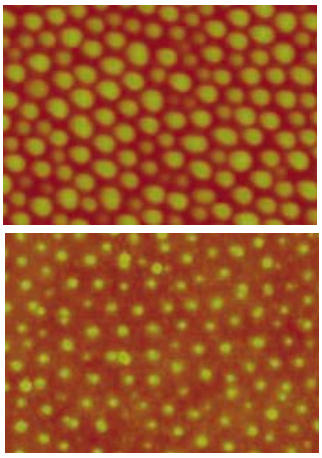

Deposited copolymer micelles (top) and the resultant pattern of Ag nanoparticles (bottom).

J. Am. Chem. Soc. 10.1021/ja052281m (2005).

BIOMEDICINE

Cultured Cancer Killers

Adoptive cell transfer represents a highly promising therapy for treating some forms of cancer. Isolated antitumor T cells are stimulated and expanded in culture before they are transferred back into the patient. Although this approach has yielded encouraging success in treating malignant melanoma, there is room for improvement.

Using a mouse tumor model, Gattinoni *et al.* observed that the duration of stimulation of antitumor T cells in culture had a negative impact on their subsequent ability to kill tumors in vivo. As expected, T cells that had undergone successive rounds of stimulation in vitro did acquire the capacity to kill tumor cell lines when tested in vitro, indicative of a persistently robust cytotoxic activity. However, the acquisition of an activated phenotype—including changes in the pattern of lymph node–homing receptors and responsiveness to the T cell growth factor interleukin-2—was accompanied by a reduced ability to replicate and to eradicate tumors upon subsequent transfer into mice. These results highlight important parameters to consider, as efforts to select and generate effective antitumor T cells for adoptive cellular immunotherapy are refined. — SJS

J. Clin. Invest. **115**, 1616 (2005).

GEOLOGY

Coastal Ups and Downs

A subduction zone extending along the northwest margin of North America, from northern California up to the Aleutians, is capable of generating giant earthquakes and tsunamis. One means for assessing the current hazard is to reconstruct records of past major tremblors. From a coastal lake in Oregon, Kelsey *et al.* have obtained a detailed and well-dated history of tsunamis stretching back 7000 years. The lake sediments reveal the periodic input of beach sand and saline water, which likely was associated with tsunami incursions. Tsunami-generating earthquakes clustered, with

CONTINUED ON PAGE 1717

Institutional Site License Available

Q What can *Science* SAGE KE give me?

A Essential online resources for the study of aging

SAGE KE – Science of Aging Knowledge Environment offers:

- Perspectives and Reviews on hot topics
- Breaking news stories
- A database of genes and interventions
- PDFs of classic papers

SAGE KE brings the latest information on aging related research direct to your desktop. It is also a vibrant virtual community, where researchers from around the world come together to exchange information and ideas. For more information go to www.sageke.org

To sign up today, visit promo.aaas.org/sageas

Sitewide access is available for institutions.
To find out more e-mail sagelicense@aaas.org

Science
SAGE KE
AAAS

three to four occurring every 1000 years, and clusters were separated by earthquake-free periods lasting about 1000 years; the most recent large event, in 1700, followed a 700-year quiescent span.

Separately, Hawkes *et al.* show that noticeable changes in the foraminifera and diatom populations in tidal marshes near two recent large earthquakes along the Alaskan and Oregon coasts may reveal subtle subsidence that began several months before the earthquakes. Additional verification of this provocative signal is needed, including whether such changes are connected to recently recognized aseismic slip along these subduction zones. — BH

Geol. Soc. Am. Bull. **117**, 1009; 996 (2005).

CHEMISTRY

Gaseous Dihydrides

The reduction of solutions of zinc, cadmium, and mercury ions generates gas-phase compounds that likely are the dihydrides of these metals, but the identity of these gas-phase products has been uncertain, and the solid forms of these compounds decompose back to the elements rather than vaporize. Shayesteh *et al.* synthesized the dihydrides of Hg, Cd, and Zn by the direct reaction of excited-state atoms with H_2 and were able to characterize the products through analysis of their infrared emission. The short bond lengths obtained by fitting the rotational-vibrational spectra indicate that the dihydrides are more stable than the monohydride radicals. The authors note that, given the production of other hydrides, such as SnH_4 and AsH_3, by anaerobic bacteria, these species might be produced naturally as well. — PDS

Chem. Eur. J. 10.1002/chem.200500332 (2005).

CELL BIOLOGY

Perfect Peroxisome Partitioning

During successful cell division, mother and daughter cells arrive at an equitable allocation of each type of membrane-bounded organelle. Molecular mechanisms that guarantee faithful organelle partitioning in budding yeast involve the polarized actin cytoskeleton and myosin-related motors and are well established for mitochondria, the vacuole, secretory vesicles, and the endoplasmic reticulum. However, peroxisomes are low-copy-number organelles involved in lipid metabolism whose inheritance has been less well characterized.

Fagarasanu *et al.* examined the role of a peripheral peroxisomal membrane protein, Inp1p (for inheritance of peroxisomes protein 1). In budding yeast, overexpression of Inp1 led to the failure of efficient peroxisome delivery to the bud, whereas deletion of the *INP1* gene often left the mother cell without any peroxisomes. It appears that Inp1p helps to anchor peroxisomes within cells, and having the right amount of it is critical to a fair and harmonious division of accumulated assets. — SMH

Peroxisomes (green) partition between mother and bud in wild-type cells

CREDITS: FAGARASANU *ET AL.*, *J. CELL BIOL.* **169**, 765 (2005)

J. Cell Biol. **169**, 765 (2005).

HIGHLIGHTED IN *SCIENCE*'S SIGNAL TRANSDUCTION KNOWLEDGE ENVIRONMENT

Science's stke www.stke.org

Screening for Sensitivity to Drugs

Inappropriate cell death or survival can lead to various diseases, such as neurodegenerative disorders and cancer. MacKeigan *et al.* performed large-scale screens using short interfering RNAs (siRNAs) transfected into cultured human cell lines to identify kinases and phosphatases involved in cell survival. Seventy-three kinases and 72 phosphatases were identified as contributing positively to cell survival, based on an increase in markers for programmed cell death (apoptosis) when the levels of these proteins were reduced. The phosphatase siRNA library was used to screen for phosphatases involved in cell death induced by cisplatin, Taxol, or etopside; 12 such death-promoting phosphatases were identified. The RNA interference screen was also used to identify kinases that, when downregulated, conferred an increased sensitivity to apoptosis-inducing drugs. For instance, Taxol combined with the siRNA for serum and glucocorticoid-regulated kinase increased cell death as compared with the siRNA or the drug alone. Taken all together, these results may suggestion new combination therapies. — NG

Nat. Cell Biol. **7**, 591 (2005).

GE Healthcare

What do you call making protein purification easy right from the start?

Pure imagination brought to life.

GE Healthcare is the one name behind all the leading tools in biomolecular research. Our focus is on providing protein purification systems, columns and media that make drug discovery simpler and faster from the outset to help you compete more effectively. Innovations like HiTrap™ and HisTrap™ columns, which offer outstanding convenience and reproducibility. Or the ÄKTAdesign™ platform, combined with the seamless control of UNICORN™ software, which gives you speed, ease and confidence whatever your application or scale.

At GE Healthcare we never stand still. We're constantly working to improve our offering – finding new ways of bringing pure imagination to life, to give you even better performance in tomorrow's race.

Visit www.amershambiosciences.com/pureimagination

imagination at work

GE08-05

www.sciencemag.org

Science

1200 New York Avenue, NW
Washington, DC 20005
Editorial: 202-326-6550, FAX 202-289-7562
News: 202-326-6500, FAX 202-371-9227

Bateman House, 82-88 Hills Road
Cambridge, UK CB2 1LQ
+44 (0) 1223 326500, FAX +44 (0) 1223 326501

SUBSCRIPTION SERVICES For change of address, missing issues, new orders and renewals, and payment questions: 800-731-4939 or 202-326-6417, FAX 202-842-1065. Mailing addresses: AAAS, P.O. Box 1811, Danbury, CT 06813 or AAAS Member Services, 1200 New York Avenue, NW, Washington, DC 20005

INSTITUTIONAL SITE LICENCES please call 202-326-6755 for any questions or information

REPRINTS Ordering/Billing/Status 800-635-7171; Corrections 202-326-6501

PERMISSIONS 202-326-7074, FAX 202-682-0816

MEMBER BENEFITS Bookstore: AAAS/BarnesandNoble.com bookstore www.aaas.org/bn; Car purchase discount: Subaru VIP Program 202-326-6417; Credit Card: MBNA 800-847-7378; Car Rentals: Hertz 800-654-2200 CDP#343457, Dollar 800-800-4000 #AA1115; AAAS Travels: Betchart Expeditions 800-252-4910; Life Insurance: Seabury & Smith 800-424-9883; Other Benefits: AAAS Member Services 202-326-6417 or www.aaasmember.org.

science_editors@aaas.org (for general editorial queries)
science_letters@aaas.org (for queries about letters)
science_reviews@aaas.org (for returning manuscript reviews)
science_bookrevs@aaas.org (for book review queries)

Published by the American Association for the Advancement of Science (AAAS), *Science* serves its readers as a forum for the presentation and discussion of important issues related to the advancement of science, including the presentation of minority or conflicting points of view, rather than by publishing only material on which a consensus has been reached. Accordingly, all articles published in *Science*—including editorials, news and comment, and book reviews—are signed and reflect the individual views of the authors and not official points of view adopted by the AAAS or the institutions with which the authors are affiliated.

AAAS was founded in 1848 and incorporated in 1874. Its mission is to advance science and innovation throughout the world for the benefit of all people. The goals of the association are to: foster communication among scientists, engineers and the public; enhance international cooperation in science and its applications; promote the responsible conduct and use of science and technology; foster education in science and technology for everyone; enhance the science and technology workforce and infrastructure; increase public understanding and appreciation of science and technology; and strengthen support for the science and technology enterprise.

INFORMATION FOR CONTRIBUTORS

See pages 135 and 136 of the 7 January 2005 issue or access www.sciencemag.org/feature/contribinfo/home.shtml

EDITOR-IN-CHIEF **Donald Kennedy**
EXECUTIVE EDITOR **Monica M. Bradford**
DEPUTY EDITORS **R. Brooks Hanson, Katrina L. Kelner**
NEWS EDITOR **Colin Norman**

EDITORIAL SUPERVISORY SENIOR EDITORS Barbara Jasny, Phillip D. Szuromi; SENIOR EDITORS Gilbert J. Chin, Lisa D. Chong, Pamela J. Hines, Paula A. Kiberstis (Boston), Beverly A. Purnell, L. Bryan Ray, Guy Riddihough (Manila), H. Jesse Smith, Valda Vinson, David Voss; ASSOCIATE EDITORS Marc S. Lavine, Jake S. Yeston; ONLINE EDITOR Stewart Wills; CONTRIBUTING EDITOR Ivan Amato; ASSOCIATE ONLINE EDITOR Tara S. Marathe; BOOK REVIEW EDITOR Sherman J. Suter; ASSOCIATE LETTERS EDITOR Etta Kavanagh; INFORMATION SPECIALIST Janet Kegg; EDITORIAL MANAGER Cara Tate; SENIOR COPY EDITORS Jeffrey E. Cook, Harry Jach, Barbara P. Ordway; COPY EDITORS Cynthia Howe, Alexis Wynne Mogul, Sabrah M. n'haRaven, Jennifer Sills, Trista Wagoner; EDITORIAL COORDINATORS Carolyn Kyle, Beverly Shields; PUBLICATION ASSISTANTS Chris Filiatreau, Joi S. Granger, Jeffrey Hearn, Lisa Johnson, Scott Miller, Jerry Richardson, Brian White, Anita Wynn; EDITORIAL ASSISTANTS Ramatoulaye Diop, E. Annie Hall, Patricia M. Moore, Brendan Nardozzi, Michael Rodewald; EXECUTIVE ASSISTANT Sylvia S. Kihara; ADMINISTRATIVE SUPPORT Patricia F. Fisher

NEWS SENIOR CORRESPONDENT Jean Marx; DEPUTY NEWS EDITORS Robert Coontz, Jeffrey Mervis, Leslie Roberts, John Travis; CONTRIBUTING EDITORS Elizabeth Culotta, Polly Shulman; NEWS WRITERS Yudhijit Bhattacharjee, Jennifer Couzin, David Grimm, Constance Holden, Jocelyn Kaiser, Richard A. Kerr, Eli Kintisch, Andrew Lawler (New England), Greg Miller, Elizabeth Pennisi, Charles Seife, Robert F. Service (Pacific NW), Erik Stokstad; Amitabh Avasthi (intern); CONTRIBUTING CORRESPONDENTS Marcia Barinaga (Berkeley, CA), Barry A. Cipra, Adrian Cho, Jon Cohen (San Diego, CA), Daniel Ferber, Ann Gibbons, Robert Irion, Mitch Leslie (NetWatch), Charles C. Mann, Evelyn Strauss, Gary Taubes, Ingrid Wickelgren; COPY EDITORS Linda B. Felaco, Rachel Curran, Sean Richardson; ADMINISTRATIVE SUPPORT Scherraine Mack, Fannie Groom BUREAUS: Berkeley, CA: 510-652-0302, FAX 510-652-1867, New England: 207-549-7755, San Diego, CA: 760-942-3252, FAX 760-942-4979, Pacific Northwest: 503-963-1940

PRODUCTION DIRECTOR James Landry; SENIOR MANAGER Wendy K. Shank; ASSISTANT MANAGER Rebecca Doshi; SENIOR SPECIALISTS Vicki J. Jorgensen, Jessica K. Moshell; SPECIALISTS Jay R. Covert, Stacey Ferebee; **PREFLIGHT** DIRECTOR David M. Tompkins; MANAGER Marcus Spiegler; SPECIALIST Jessie Mudjitaba;

ART DIRECTOR Joshua Moglia; ASSOCIATE ART DIRECTOR Kelly Buckheit; ILLUSTRATOR Katharine Sutliff; SENIOR ART ASSOCIATES Holly Bishop, Laura Creveling, Preston Huey, Julie White; ASSOCIATE Nayomi Kevitiyagala; PHOTO RESEARCHER Leslie Blizard

***SCIENCE* INTERNATIONAL**

EUROPE (science@science-int.co.uk) EDITORIAL: INTERNATIONAL MANAGING EDITOR Andrew M. Sugden; SENIOR EDITOR/PERSPECTIVES Julia Fahrenkamp-Uppenbrink; SENIOR EDITORS Caroline Ash (Geneva: +41 (0) 222 346 3106), Stella M. Hurtley, Ian S. Osborne, Peter Stern; ASSOCIATE EDITOR Stephen J. Simpson; EDITORIAL SUPPORT Emma Westgate; Deborah Dennison ADMINISTRATIVE SUPPORT Janet Clements, Phil Marlow, Jill White; NEWS: INTERNATIONAL NEWS EDITOR Eliot Marshall DEPUTY NEWS EDITOR Daniel Clery; CORRESPONDENT Gretchen Vogel (Berlin: +49 (0) 30 2809 3902, FAX +49 (0) 30 2809 8365); CONTRIBUTING CORRESPONDENTS Michael Balter (Paris), Martin Enserink (Amsterdam and Paris); INTERN Mason Inman

ASIA Japan Office: Asca Corporation, Eiko Ishioka, Fusako Tamura, 1-8-13, Hirano-cho, Chuo-ku, Osaka-shi, Osaka, 541-0046 Japan; +81 (0) 6 6202 6272, FAX +81 (0) 6 6202 6271; asca@os.gulf.or.jp JAPAN NEWS BUREAU: Dennis Normile (contributing correspondent, +81 (0) 3 3391 0630, FAX 81 (0) 3 5936 3531; dnormile@gol.com); CHINA REPRESENTATIVE Hao Xin, + 86 (0) 10 6307 4439 or 6307 3676, FAX +86 (0) 10 6307 4358; haoxin@earthlink.net; SOUTH ASIA Pallava Bagla (contributing correspondent +91 (0) 11 2271 2896; pbagla@vsnl.com); CENTRAL ASIA Richard Stone (+7 3272 6413 35, rstone@aaas.org)

EXECUTIVE PUBLISHER **Alan I. Leshner**
PUBLISHER **Beth Rosner**

FULFILLMENT & MEMBERSHIP SERVICES (membership@aaas.org) DIRECTOR Marlene Zendell; MANAGER Waylon Butler; SYSTEMS SPECIALIST Andrew Vargo SENIOR SPECIALIST Pat Butler; SPECIALISTS Laurie Baker, Tamara Alfson, Karena Smith

BUSINESS OPERATIONS AND ADMINISTRATION DIRECTOR Deborah Rivera-Wienhold; BUSINESS MANAGER Randy Yi; SENIOR BUSINESS ANALYST Lisa Donovan; BUSINESS ANALYST Jessica Tierney; FINANCIAL ANALYST Farida Yeasmin; RIGHTS AND PERMISSIONS: ADMINISTRATOR Emilie David; ASSOCIATE Elizabeth Sandler; MARKETING: DIRECTOR John Meyers; MEMBERSHIP MARKETING MANAGER Darryl Walter; MARKETING ASSOCIATE Julianne Wielga; RECRUITMENT MARKETING MANAGER Allison Pritchard; ASSOCIATES Mary Ellen Crowley, Amanda Donathen, Catherine Featherston; DIRECTOR OF INTERNATIONAL MARKETING AND RECRUITMENT ADVERTISING Deborah Harris; INTERNATIONAL MARKETING MANAGER Wendy Sturley; MARKETING/MEMBER SERVICES EXECUTIVE: Linda Rusk; JAPAN SALES AND MARKETING MANAGER Jason Hannaford; SITE LICENSE SALES: DIRECTOR Tom Ryan; SALES AND CUSTOMER SERVICE Mehan Dossani, Catherine Holland, Adam Banner, Yaniv Snir; ELECTRONIC MEDIA: INTERNET PRODUCTION MANAGER Lizabeth Harman; ASSISTANT PRODUCTION MANAGER Wendy Stengel; SENIOR PRODUCTION ASSOCIATES Sheila Mackall, Amanda K. Skelton, Lisa Stanford; PRODUCTION ASSOCIATE Nichele Johnston; LEAD APPLICATIONS DEVELOPER Carl Saffell

PRODUCT ADVERTISING (science_advertising@aaas.org); MIDWEST Rick Bongiovanni: 330-405-7080, FAX 330-405-7081 • WEST COAST/W. CANADA B. Neil Boylan (Associate Director): 650-964-2266, FAX 650-964-2267 • EAST COAST/E. CANADA Christopher Breslin: 443-512-0330, FAX 443-512-0331 • UK/SCANDINAVIA/FRANCE/ITALY/BELGIUM/NETHERLANDS Andrew Davies (Associate Director): +44 (0)1782 750111, FAX +44 (0) 1782 751999 • GERMANY/SWITZERLAND/AUSTRIA Tracey Peers (Associate Director): +44 (0) 1782 752530, FAX +44 (0) 1782 752531 JAPAN Mashy Yoshikawa: +81 (0) 33235 5961, FAX +81 (0) 33235 5852 ISRAEL Jessica Nachlas +9723 5449123 • TRAFFIC MANAGER Carol Maddox; SALES COORDINATOR Deiandra Simms

CLASSIFIED ADVERTISING (advertise@sciencecareers.org); U.S.: SALES DIRECTOR Gabrielle Boguslawski: 718-491-1607, FAX 202-289-6742; INTERNET SALES MANAGER Beth Dwyer: 202-326-6534; INSIDE SALES MANAGER Daryl Anderson: 202-326-6543; WEST COAST/MIDWEST Kristine von Zedlitz: 415-956-2531; EAST COAST Jill Downing: 631-580-2445; LINE AD SALES Emnet Tesfaye: 202-326-6740; SENIOR SALES COORDINATOR Erika Bryant; SALES COORDINATORS Rohan Edmonson, Christopher Normile, Joyce Scott, Shirley Young; INTERNATIONAL: SALES MANAGER Tracy Holmes: +44 (0) 1223 326525, FAX +44 (0) 1223 326532; SALES Christina Harrison, Suitlana Barnes; SALES ASSISTANT Helen Moroney; JAPAN: Jason Hannaford: +81 (0) 52 789 1860, FAX +81 (0) 52 789 1861; PRODUCTION: MANAGER Jennifer Rankin; ASSISTANT MANAGER Deborah Tompkins; ASSOCIATE Amy Hardcastle; SENIOR TRAFFICKING ASSOCIATE Christine Hall; SENIOR PUBLICATIONS ASSISTANT Robert Buck; PUBLICATIONS ASSISTANT Natasha Pinol

AAAS BOARD OF DIRECTORS RETIRING PRESIDENT, CHAIR Shirley Ann Jackson; PRESIDENT Gilbert S. Omenn; PRESIDENT-ELECT John P. Holdren; TREASURER David E. Shaw; CHIEF EXECUTIVE OFFICER Alan I. Leshner; BOARD Rosina M. Bierbaum; John E. Burris; John E. Dowling; Lynn W. Enquist; Susan M. Fitzpatrick; Richard A. Meserve; Norine E. Noonan; Peter J. Stang; Kathryn D. Sullivan

AAAS
ADVANCING SCIENCE, SERVING SOCIETY

NetWatch

edited by Mitch Leslie

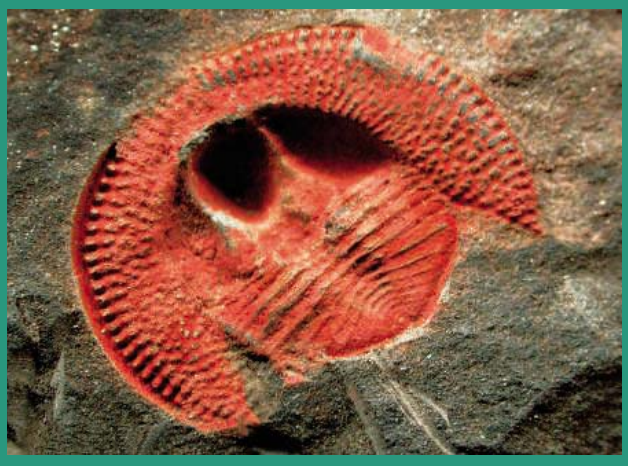

IMAGES

Life's Family Album

Step into The Virtual Fossil Museum for a peek into life's past. The growing site, created by physicist-turned-bio-informaticist Roger Perkins of Jefferson, Arkansas, offers a gallery of eye-catching fossil photos—from a cave bear's toothy skull to this more than 440-million-year-old impression of the trilobite *Nankinolithis* extricated from Moroccan rock. Users can browse the images by taxonomic group and by fossil location. Another section profiles famous sites such as the Chengjiang formation in China, which teems with remains of some of the earliest known animals, and the fossil-rich slate of Bundenbach in Germany. Visitors can use the museum's images, which come from fossil collectors, researchers, and other contributors, for research and education purposes.

www.fossilmuseum.net

TOOLS

West Nile Watch

Because of wet weather this year, some western states are expecting a surge in infections from the West Nile virus. The mosquito-borne disease, which first struck the United States in 1999, sickened more than 2400 people across the nation last year, killing 88. You can track this year's outbreak using a mapper from the U.S. Geological Survey. Updated twice weekly during prime mosquito months, the site charts human cases, along with reports of infected birds, horses, and sentinels—chickens or other animals that scientists test regularly to reveal the disease's presence. You can also chart where mosquitoes carrying the virus have turned up. An archive lets you compare this season's results to those from past years. Above, counties with confirmed human infections in 2004.

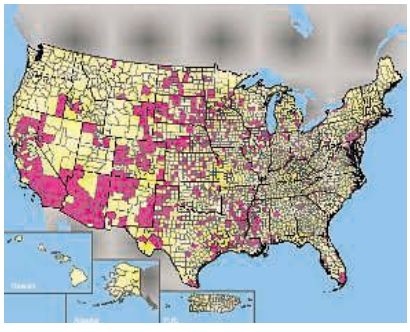

westnilemaps.usgs.gov

EDUCATION

Sense and Sensitivity

This tutorial from Tutis Vilis of the University of Western Ontario in Canada offers 12 animated chapters on the basics of vision, hearing, and the other senses, along with topics such as memory. Students can probe the workings of the vestibular system in the inner ear, which maintains our balance, or learn how receptors in the skin transform pressure into the sensation of being touched. The chapters also include exercises demonstrating concepts such as working memory, the mental scratch pad for temporarily storing information.

www.med.uwo.ca/physiology/courses/sensesweb

EDUCATION

Illuminating Special Relativity

One hundred years ago this month, Albert Einstein submitted his paper describing special relativity to the journal *Annalen der Physik*. Ever since, students have struggled to grasp the theory's mind-bending implications. The new tutorial Einstein Light, hosted by physicist Joseph Wolfe of the University of New South Wales in Australia, offers help. In a 10-minute multimedia program, Wolfe and a pair of animated assistants explore the intellectual background for special relativity and its counterintuitive consequences, such as that a spaceship traveling near the speed of light would seem to shorten to an observer on Earth (above). Visitors hungry for more can tuck into more than 30 pages of additional explanation.

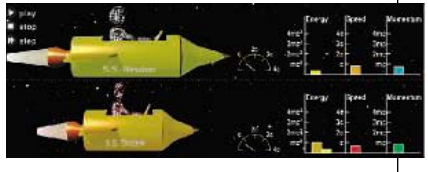

www.phys.unsw.edu.au/einsteinlight

WEB PROJECTS

Grassroots Math Guide

If your favorite Web site suddenly shut down, you could grumble about life's unfairness, or you could decide to build a replacement. Nathan Egge and Aaron Krowne, math and computer science students at Virginia Polytechnic Institute and State University in Blacksburg, chose the second course when a math reference they often consulted went offline. Five years later their handiwork, PlanetMath, holds nearly 4400 entries on topics from the ABC conjecture to Zsigmondy's theorem.

PlanetMath's encyclopedia section resembles Wikipedia, with site users writing and reviewing the content. Krowne, now a computer scientist at Emory University in Atlanta, Georgia, estimates that math grad students contribute the largest share of the articles, with college professors, undergrads, and other visitors supplying the rest. Anyone can critique an article, but the author decides whether to revise it. PlanetMath also links to 70 free math texts, more than 30 tutorials and lectures, and a collection of published and unpublished papers.

planetmath.org

Send site suggestions to netwatch@aaas.org. Archive: www.sciencemag.org/netwatch

CREDITS (TOP TO BOTTOM): THE VIRTUAL FOSSIL MUSEUM; JOSEPH WOLFE/UNIVERSITY OF NEW SOUTH WALES; USGS

This Week

PAGE 1724
Nucleosomes and gene regulation

1726
Foot-and-mouth tussle in Spain

ITALIAN SCIENCE

Abstentions Scuttle Drive to Liberalize Italy's Embryo Laws

An attempt to loosen tight restrictions on in vitro fertilization (IVF) in Italy failed when only 26% of the electorate turned out to vote in a referendum on 12 and 13 June, missing a required 50% quorum. The result was precisely what Catholic Church leaders sought; it means Italy will continue to forbid research using embryos from IVF procedures. Italian scientists are still allowed to work with any imported human embryonic stem (hES) cells—although funding is scarce—but they cannot derive new ones.

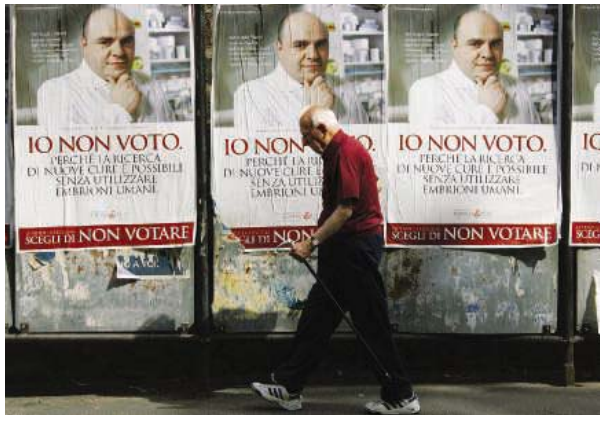

Opposed. On campaign posters, stem cell researcher Angelo Vescovi urged people to abstain from Italy's referendum on IVF techniques, saying "new cures are possible without the use of human embryos."

The Catholic Church campaigned strongly to persuade voters to stay away from the polls. Under Italian law, a referendum is invalid if fewer than half the eligible voters participate. The abrupt fade-out marked the end of a bitterly fought campaign. Referendum opponents accused proponents of overstating the promise of embryo research, comparing it to Nazi experiments. Many scientists and referendum supporters accused the government of dirty tricks and distortions.

Until January, Italy had no laws on IVF treatments or embryo research, enabling the infamous claims of gynecologist Severino Antinori, who said he was trying to create the first cloned human. But a law passed in February 2004 put tight restrictions into effect 6 months ago. It forbids the creation of more than three embryos per IVF attempt, all of which must be implanted in the potential mother, and it outlaws the donation of sperm or eggs. It also imposes a fine of more than $1 million for any attempt at human cloning. The law was controversial from the start: Members of Parliament offered more than 350 amendments. But none were allowed, and the law passed 277 to 222.

Before the law took effect, Italy's far-left Radical Party collected nearly twice as many signatures as the 500,000 required for a petition to put four parts of the law up for review in a referendum—the ban on embryo research; giving legal rights to the human embryo; the ban on gamete donation; and the requirement that only three IVF embryos can be created, all of which must be implanted.

In the weeks leading up to the vote, the campaign intensified, with researchers and patient groups staging several days of hunger strikes to protest what they called an unfair attack on the referendum. Opponents, including Pope Benedict XVI and Catholic bishops, calculated that a combination of voter apathy, summer vacations, and deliberate abstentions would nullify the vote.

Scientists were active on both sides, with several researchers, including Angelo Vescovi of the Stem Cell Research Institute at the University of Milan–Bicocca, saying new hES lines were not necessary to advance stem cell research. Vescovi appeared on campaign posters saying he planned not to vote. On the other side, more than 130 scientists from around the world signed a letter urging Italians to change the law.

Elena Cattaneo of the University of Milan, one of a handful of researchers working with hES cells in Italy, says she is bitterly disappointed by the vote. "It is a pity for science," she says. "The scientific community wasn't able to express itself the way we should have done."

Marco Cappato, a member of the Radical Party and a leading campaigner for the referendum, says he and his colleagues will try to make the law an issue in the next elections, expected next spring, and win enough votes to change it in Parliament. **–GRETCHEN VOGEL**

SCIENTIFIC PUBLISHING

Society Bars Papers From Iranian Authors

Six months after scientific societies and publishers won a hard-fought battle with the U.S. government to edit and publish manuscripts from countries under a U.S. trade embargo, the American Institute of Aeronautics and Astronautics (AIAA) has decided to bar such submissions from its journals and conferences. The institute says the ban, which falls hardest on scientists from Iran, is necessary to protect national security. But other scientific associations say the decision is wrong-headed and could actually limit U.S. access to scientific developments in the four embargoed countries: Iran, Cuba, North Korea, and Sudan.

The policy, adopted last month, states that the institute, "consistent with U.S. laws and policies, shall not knowingly provide products or services to, or engage in formal, technical information exchange with individuals or entities residing in embargoed nations." As a result, AIAA pulled 24 Iranian-authored submissions from its seven journals and cancelled presentations by Iranian researchers scheduled to attend an AIAA-sponsored fluid dynamics conference in Toronto. The conference, held 6 to 9 June, was subsequently exempted from the ban after protests by Iranian attendees who had already finalized their travel plans. ▶

Barred. AIAA pulled Masoud Darbandi's paper from one of its journals.

CREDITS (TOP TO BOTTOM): MAX ROSSI/REUTERS; M. DARBANDI

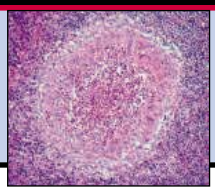

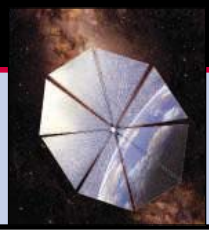

AIAA's position that the ban is "consistent with U.S. laws" is incorrect, says Marc Brodsky, executive director of the American Institute of Physics (AIP), which has pushed hard to assure open communication with scientists in the embargoed countries. "There is no law or regulation I know of that requires AIAA to take the actions it has announced," he says. "Certainly it hurts our security to bury our head in the sand and not learn about what scientists and engineers are doing in the countries the institute has targeted."

In December, the Treasury Department's Office of Foreign Assets Control (OFAC) clarified that publications did not need the government's permission to edit and print papers from anywhere in the world (*Science*, 24 December 2004, p. 2170). That decision, which reversed an earlier ruling requiring journals to obtain a license in order to edit papers from embargoed countries, came after AIP and other publishers filed a lawsuit against OFAC in October 2004 alleging that the agency was violating freedom of speech. The suit cited a 1988 legal amendment that exempts information from trade embargoes.

AIAA did not institute the ban "in response to a specific legal constraint," institute Executive Director Robert Dickman told *Science* in an e-mail. Dickman said the board "is balancing our responsibilities as a professional society to foster open exchange in scholarly, scientific, and engineering information with our social responsibility to avoid assisting a nation such as North Korea in its efforts to develop nuclear weapons and the capability to deliver them."

One of the first victims of that policy was Masoud Darbandi, an aerospace engineer at Sharif University of Technology in Tehran, who received a note from Dickman on 26 May that AIAA had withdrawn his paper on high-temperature irradiance from a forthcoming issue of the *Journal of Thermophysics and Heat Transfer*. "It was a basic science paper, and I am not involved with any military projects," he says. "If the paper *had* been about a military application, the U.S. would actually benefit from its publication; what better way to get inside information about Iran's military?"

The policy has triggered internal dissent, according to some AIAA staff members who requested anonymity. "We're hopeful that it will be reversed," says one.

–YUDHIJIT BHATTACHARJEE

CREDIT: WILLIAM K. HARTMANN/PLANETARY SCIENCE INSTITUTE

GEOCHEMISTRY

New Geochemical Benchmark Changes Everything on Earth

Whether you're navigating the expanse of the Pacific or Earth's 6370-kilometer-deep interior, it's best to have a star to guide you. Geochemists exploring the dark realms of the planet's rocky mantle and iron core depend on the elemental and isotopic composition of magmas, which have risen from the deep interior, and meteorites, which were the building blocks of the rocky planets. Their pole star has been an assumption about the composition of Earth's rock—until now.

Far from done. New isotopic data suggest that the rock of the accreting Earth soon separated into two layers.

According to a paper published online this week by *Science* (www.sciencemag.org/cgi/content/abstract/1113634), for decades researchers have been following the wrong star. New, more-precise measurements of the neodymium isotope composition of meteorites show that geoscientists have been using an incorrect composition of the rocky Earth as a benchmark to infer everything from mantle compositions to the amount of interior heat being generated by radioactive decay.

"It's a fantastic paper," says geochemist Stanley Hart of Woods Hole Oceanographic Institution in Massachusetts. "This is going to change the way we think about the interior of the Earth. There are so many things this is going to impact." For starters, either Earth was made from only one part of an inexplicably lumpy primordial pudding, or very different rock unlike anything sampled so far settled to the bottom of the mantle early on and has been altering the behavior of the rest of the planet ever since.

A key to the geochemical benchmarking of Earth has been the ratio of the isotope neodymium-142 to neodymium-144 ($^{142}Nd/^{144}Nd$), which can be used to trace geologic processes. In the early 1980s, researchers measured this ratio in both chondritic meteorites—which are made of the same primordial rock that formed Earth—and a variety of terrestrial rocks. The ratio was the same on Earth and in meteorites, within the error of the analyses. So everyone assumed that the average $^{142}Nd/^{144}Nd$ ratio of terrestrial rock had not been changed since Earth formed. Any chemical processing in the first several hundred million years—such as partial melting of rock or crystallization of magma—would have tended to separate samarium-146—whose radioactive decay produces neodymium-142—from neodymium-144, altering the $^{142}Nd/^{144}Nd$ ratio seen today.

No one seriously tested the result until geochemists Maud Boyet and Richard Carlson of the Carnegie Institution of Washington's Department of Terrestrial Magnetism in Washington, D.C., used a markedly improved mass spectrometer to measure the $^{142}Nd/^{144}Nd$ ratio of a variety of chondrites. Their value fell in the range published 25 years ago, but their much more precise analytical technique revealed that $^{142}Nd/^{144}Nd$ is 20 parts per million lower in chondrites than in terrestrial rocks.

Boyet and Carlson think that the meteorite-Earth difference most likely arose just 30 million years after Earth formed. Some process—perhaps the progressive crystallization of Earth's early "magma ocean"—may have concentrated certain elements in the remaining melted rock, the way frozen seawater loses most of its salt to the sea. Such an "enriched" part of the interior has never shown up in volcanic rocks. If it's there, geochemists have calculated the composition of the rocky Earth ▶

from samples of "depleted" rock, with misleading results.

Boyet and Carlson suggest that the enriched rock ended up at the bottom of the mantle. To judge by other isotopic and chemical data, this enriched region could make up as much as 30% or as little as 5% of the whole mantle. At the low end, it would be small enough to fit into the 200-kilometer-thick D″(pronounced "D double prime") layer, a mysterious region seismologists have spotted at the bottom of the mantle, hard against the molten-iron core.

A geochemically enriched bottom layer "explains a lot of things," says Carlson. One might be Earth's missing heat. The average Earth rock—as previously calculated—didn't contain enough radioactive, heat-generating uranium, thorium, and potassium to account for half of the heat seeping out of the planet. But an enriched layer would contain 43% of all heat-producing elements. From the bottom of the mantle, a hot, enriched layer could help drive the core's geodynamo, which generates Earth's magnetic field. And the hot layer could also produce rising plumes of hot mantle rock that feed volcanic hot spots such as Hawaii and Iceland.

"It's a very exciting result," says geochemist Stein Jacobsen of Harvard University, who co-authored the 1980s papers on the first $^{142}Nd/^{144}Nd$ measurements. "I don't doubt their measurements at all, and the interpretation is reasonable. But at this early stage, I don't think it's the only one." Boyet and Carlson acknowledge that the Earth-meteorite difference might have arisen when the planets formed. Perhaps the primeval disk of gas and dust differed in composition from place to place. True enough, says planetary physicist David Stevenson of the California Institute of Technology, but such heterogeneity "is not an attractive idea. There is no obvious physical reason why it would be so." Wherever the truth lies, "this is going to create an incredible hum and a lot of work," says Hart.

–RICHARD A. KERR

MOLECULAR BIOLOGY

Nucleosomes Help Guide Yeast Gene Activity

If traffic lights aren't precisely coordinated, accidents and traffic jams result. Likewise, for an organism to develop and remain healthy, cells need to turn their genes on and off at exactly the right times. Numerous proteins known as transcription factors assist in this task, settling in on regulatory sequences in DNA and activating or inactivating associated genes as needed. But genetic material is more than just strands of DNA. It also includes complexes of proteins arranged with the DNA in beadlike structures called nucleosomes. Recently, studies have suggested that these chromosomal beads also contribute to gene regulation.

The latest example comes from Oliver Rando and his colleagues at Harvard University. In a paper published online this week by *Science* (www.sciencemag.org/cgi/content/abstract/1112178), they describe a technique that has allowed them to determine the exact positions of all the nucleosomes over large stretches—roughly 500 kilobases—of the yeast genome. The work, which cell biologist Bradley Cairns of the University of Utah in Salt Lake City calls a "technical tour de force," suggests that nucleosomes help direct transcription factors to the regulatory sites of their target genes.

For many years, researchers thought that nucleosomes were distributed more or less evenly along a chromosome's DNA. However, examination of a few genes revealed that their promoters, regulatory regions that contain binding sites for transcription factors, lacked nucleosomes. Then, last year, two groups, one led by Jason Lieb of the University of North Carolina, Chapel Hill, and the other by Bradley Bernstein and Stuart Schreiber of Harvard University, reported that this seemed to be the case for promoters throughout the yeast genome.

The Rando team has now provided the most detailed look yet at nucleosome positioning in the yeast genome. The researchers first treated yeast DNA with a DNA-digesting enzyme that removes the regions that connect one nucleosome bead with the next. The nucleosomal DNA itself survives because it is protected by associated proteins called histones.

After isolating the nucleosomal DNA and labeling it with a green fluorescent dye, they mixed it with digested fragments of total genomic yeast DNA labeled with a red fluorescent dye. The researchers then applied the mixture to a microarray chip covered with thousands of overlapping 50-base DNA sequences that covered the length of chromosome 3, a span of nearly 500 kilobases. These probes latched onto the corresponding fluorescently labeled fragments of yeast DNA. By plotting the green-to-red ratio for each spot on the chip, Rando's team could determine the exact position of nucleosomes along chromosome 3.

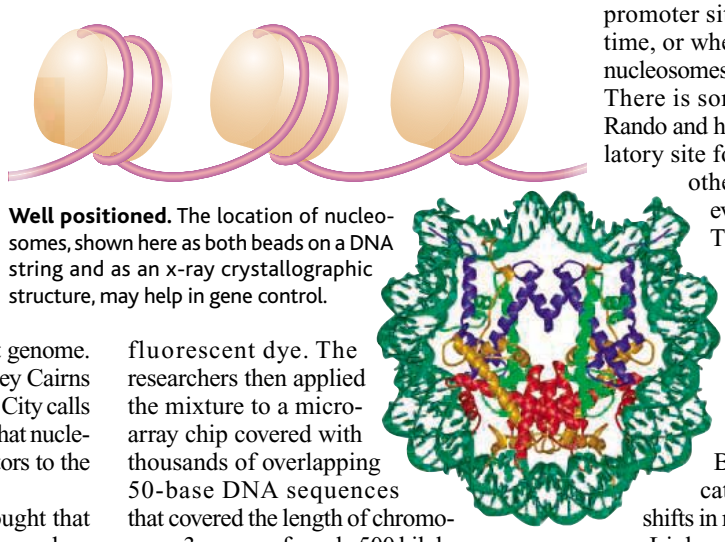

Well positioned. The location of nucleosomes, shown here as both beads on a DNA string and as an x-ray crystallographic structure, may help in gene control.

This analysis showed that most—nearly 70%—of nucleosomes occupy the same chromosomal locations in every yeast cell. This was indicated by the fact that the green-to-red ratio peaks indicating their positions were sharp and not smeared out across the DNA. That finding was surprising. "If nucleosomes were left to their own devices, they would be pretty happy [thermodynamically] sitting almost anywhere," Rando says.

In keeping with the previous results, those positions are outside the promoter-containing regulatory sites for most genes. Indeed, nucleosomes usually flanked those sites, creating what Lieb calls "helicopter landing pads" for transcription factors.

A question that remains is whether those promoter sites are nucleosome-free all the time, or whether transcription factors push nucleosomes out of the way so they can land. There is some evidence for the first idea. Rando and his colleagues found that the regulatory site for a gene turned on by heat and other stresses lacked nucleosomes even before the stress was applied. The promoter sites may be held open, Rando says, because they contain stretches of adenine-thymine nucleotide pairs, which tend to incorporate poorly into nucleosomes because of their rigidity. However, other work, including that of the Lieb and Bernstein-Schreiber teams, indicates that gene activation leads to shifts in nucleosome positioning.

Lieb suggests that the Rando team's finding may help explain other phenomena in addition to gene regulation. He points out that chromosome exchanges during meiosis and the insertion of moveable elements called transposons both tend to occur just before the beginning of genes—regions now known to often lack nucleosomes. Nucleosome positioning could "provide a structural basis for a broad range of observations," Lieb predicts.

–JEAN MARX

CREDITS (TOP TO BOTTOM): P. HUEY/*SCIENCE*; C. L. WHITE *ET AL.*, *THE EMBO JOURNAL* **20**, 5207 (2001)

INTELLECTUAL PROPERTY

U.S. Patent Reform Begins Long Journey Through Congress

Enshrined in the original text of the Constitution, the U.S. patent regime is showing its age. Last week, Representative Lamar Smith (R–TX), an influential House member, introduced a bill intended to bring the system into the 21st century. But his proposed reforms have sharpened a debate between biopharma and other high-tech sectors over whether to strengthen or weaken the power to enforce an issued patent. The road to patent reform is not going to be an easy one.

There is general agreement that reform is needed, however. A 2004 National Research Council (NRC) panel identified many "new strains" on the system, including increasingly complex technologies, more applications, and new forms of intellectual property, that are threatening to overwhelm the U.S. Patent and Trademark Office (PTO) as well as the courts. The panel argued that the office needs more examiners to handle a rising workload and that U.S. examiners are more likely to say yes than are their counterparts around the world. "Inventors are induced to make marginal applications by their likelihood of success, and the resulting flood of applications overwhelms the patent office," Harvard Business School professor Joshua Lerner wrote in testimony last week before the House Judiciary Committee panel on intellectual property that Smith chairs. Drugmakers and bench researchers alike complain of litigation costs, and lawyers now advise scientists not to read patents—undercutting the system's basic aim of dissemination—so that they can claim ignorance if they are later sued for infringement.

Smith's bill, the Patent Reform Act of 2005 (H.R. 2795), draws heavily on 5 years of discussion among patent attorneys, inventors, and academics on needed changes. One point of agreement was that individuals or companies should be able to challenge a patent through an administrative process up to 9 months after the patent is granted. Reformers hope that step—in which the PTO would review the scope and validity of a patent—will speed up the resolution of disputes, reduce the number of suits, and prevent bad patents. Smith's bill would also adopt the international norm of according priority to the first inventor to file an application rather than the first to come up with the invention.

Other aspects of the bill are more contentious. The disagreements generally reflect a fundamentally different view of intellectual property in the computer and pharmaceutical industries. Computer hardware and software technologies change so fast that the industry generally considers patent protection less important. But big high-tech companies say patents are being awarded for small changes in software code, and they regularly receive threats of infringement suits that they have sometimes settled for millions of dollars. The computer industry therefore generally wants to make enforcing patents more difficult. Biotech companies, whose products can have a market life of many years and bring in billions of dollars in revenues, on the other hand, generally want to strengthen patent protection.

Building bridges. Representative Smith (R–TX) is trying to reconcile opposing views in the computer and drug industries.

An April draft of the bill had biotech lobbyists apoplectic over language regarding injunctions: the way judges stop infringers from selling another's intellectual property. Reflecting the wishes of the computing industry, it would have barred injunctions unless the patent holder could show potential ▶

CREDITS: JUDY GOSS/THE NATIONAL ACADEMIES (INSETS) PHOTOS.COM

ScienceScope

House Targets Conflicts at FDA

The U.S. House of Representatives last week tackled conflicts of interest at the Food and Drug Administration (FDA) head on, approving a bill that would set new restrictions on who can advise the agency. Voting 218 to 210, with most Democrats in favor, the House passed a measure that aims to end a common FDA practice: waiving conflicts of interest for potential panel members, such as accepting consulting fees from a company whose drug is under FDA consideration.

FDA has been under pressure to crack down on possible conflicts in its advisory committees, which guide drug approvals. Earlier this year, for instance, *The New York Times* reported that 10 of 32 panel members examining COX-2 inhibitors had recent ties with companies producing the drugs.

But politicians worry that the change could erode the quality of the panels. "The effect would be that the top experts ... would not be able to advise the federal government about vaccines, biological products, medical devices, and drugs," says Tom Latham (R–IA), who opposed the amendment.

Longtime FDA critic Sheldon Krimsky of Tufts University in Medford, Massachusetts, called the measure "an important signal to the FDA to get its act together." Now the Senate will consider the bill.

–JENNIFER COUZIN AND GENEVRA ORNELAS

Supreme Court on Drug Research

Drug researchers cheered a Supreme Court ruling this week that a scientist may use a competitor's patented invention during early investigations related to government approval of drugs. But it remained silent on the larger question of whether all basic research with patented materials is exempt from infringement suits. Now the onus is on Congress to consider that blurred area.

In reviewing a 9-year-old patent-infringement case between Merck KGaA of Germany and New Jersey–based Integra, the court reversed a lower court ruling that had narrowed a legal exemption from infringement for "preclinical" studies. Now the lower court will re-review the case in light of the high court's decision. "This is a big win for discovery drug companies," says attorney Kevin Noonan of McDonnell Boehnen Hulbert & Berghoff LLP in Chicago.

–ELI KINTISCH

"irreparable harm" to its business. Biotech attorneys argued that would render many patents unenforceable. After marathon negotiations with both sides, Smith softened that language, calling instead for the judge to consider "relevant interests."

But a clause Smith added—one that would essentially require the judge to stay the injunction during an appeal—opened a new line of disagreement. The new language would mean a "fundamental sea change," said federal judge T. S. Ellis, speaking before a patent-reform conference last week at the National Academy of Sciences. "Nearly every case will be appealed," predicts Carl Gulbrandsen, head of the Wisconsin Alumni Research Foundation, which manages intellectual property for the University of Wisconsin. "The [university] start-up program will be sorely interfered with." Attorney Robert Armitage of Eli Lilly commented wryly that the 63-page bill was "one page too long."

Another concession to the computing industry involves a clause that would allow an accused infringer to challenge the validity of the patent administratively years after the patent was issued and thus avoid court costs. Biotech officials believe this so-called second window would significantly weaken their ability to enforce patents. And Yale president Richard Levin, who co-chaired the NRC panel, called it a "terrible idea."

Even if those issues are resolved, a thicket of others has interest groups jostling for position. Universities like the idea of first-to-file because it could eventually save on filings overseas if the United States harmonizes with foreign systems. But they worry that large companies will beat them to the patent office. "The current system has given the university time to file," said Theodore Poehler, vice provost of Johns Hopkins University in Baltimore, Maryland, speaking at the academy conference on behalf of several university consortia.

Poehler says Congress should adopt rules that ensure academic scientists could publish results and not "get scooped by their own work or someone they work with." But Poehler threw his own monkey wrench into the works by suggesting that universities should receive an exemption from infringement suits for academic research using patented material. That idea—a preliminary one, he stresses—bothers companies that sell patented tools such as reagents and could harm universities that license them.

Smith knows he has his work cut out for him. After all, the previous attempt, a relatively minor measure introduced in 1991, took 8 years to pass. "We have a ways to go," he says gamely.

–ELI KINTISCH

INFECTIOUS DISEASES

Turf War Halts Spain's Foot-and-Mouth Disease Studies

A bureaucratic turf battle has forced Spain's premier animal disease center to halt all research on an important veterinary infection, foot-and-mouth disease (FMD), scientists say. Studies on the viral disease by four groups at the Research Center for Animal Health (CISA), in Valdeolmos, 40 kilometers from Madrid, stopped last month because the European Union last year issued a directive that shifted FMD studies to a smaller Spanish lab—one that experts say is ill equipped for this work.

Virologists have decried the move as a blow to Spanish FMD research and claimed the move was plotted by the Ministry of Agriculture, Fisheries, and Food to wrest control over the FMD portfolio from Education and Science. But the government has so far given no official rationale for the shift. "Nobody really understands what has been going on," says virologist Rafael Fernández Muñoz of the Hospital Ramón y Cajal in Madrid.

CISA has been doing research on FMD in its extensive biosafety level 3 facilities since the lab was built in 1993; it also became the country's national reference center for FMD. Nobody disputes that it is home to the bulk of the research in this area, says Luís Enjuanes, a virologist at the Universidad Autónoma in Madrid who is not involved in FMD. The lab is part of the National Institute for Agricultural and Food Research and Technology (INIA), administered by the Ministry of Education and Science.

But CISA was snubbed by a September 2003 E.U. directive setting guidelines for FMD control. An annex that listed European centers authorized to handle the highly infectious FMD virus mentioned the Central Veterinary Laboratory (LCV) in Algete—a part of the Ministry of Agriculture—as the only authorized lab in Spain. The Spanish government confirmed the move in a November 2004 law. LCV was an odd choice, says Enjuanes, because it specializes in diagnostics and surveillance, and it has inferior facilities and no basic research program.

Despite the decree, CISA continued working on FMD until last month, with the tacit approval of the Education and Science Ministry, says former CISA director Esteban Domingo. But it stopped in May, and on 8 June, an official at INIA headquarters sent CISA staff an e-mail declaring that all FMD work was prohibited.

E.U. officials compiled the 2003 list based on the recommendations of member countries, including Spain, but the Spanish government has not explained why it agreed to CISA's exclusion. Researchers suspect a bureaucratic motive: They say Spain's Ministry of Agriculture wants to wrest back control of FMD research, which it lost in a reorganization 5 years ago. The Brussels directive apparently took the science ministry by surprise, says Francisco Sobrino, a CISA researcher studying FMD. A spokesperson says that the two ministries "are working to find a solution."

Researchers are outraged, however. In an open letter sent to the ministries in March, 135 virologists asked that CISA be allowed to study FMD again, giving Spain two research centers. France and Germany also have two designated FMD labs, notes Enjuanes. Sobrino says the scuffle over FMD shows that science policy lacks coherence. The Spanish Society for Virology has asked both ministries to resolve the issue. "I hope they work it out," says Muñoz, who chairs that group, "because there really is no justification at all for this."

–MARTIN ENSERINK

Shutting the door. In Spain's reference center for foot-and-mouth disease, all work on the virus was halted.

CREDIT: CISA

ASTRONOMY

Extrasolar Planets Get Smaller and (Possibly) Harder

Planet hunters are edging toward an alien version of home. Astronomers have identified the littlest planet known to orbit a normal star, with a likely mass just 7.5 times that of Earth—half the size of the previous record-holder. But the finding's uniqueness isn't quite on firm ground: Although its discoverers say the world is "plausibly rocky," it may be similar to a batch of exoplanets unveiled last year by competing teams from the United States and Europe (*Science*, 3 September 2004, p. 1382).

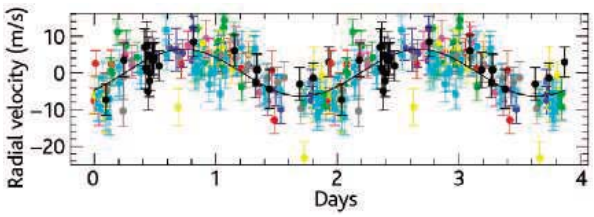

Solid find? Eight years of data (*top*) exposed the smallest exoplanet yet (artist's conception).

The planet circles a red dwarf star called Gliese 876, a dim neighbor just 15 light-years from Earth. It gained notice only because of a striking gravitational resonance between two big gaseous bodies that revolve around the star. The inner planet takes 30 days to orbit, whereas the outer one takes twice as long. As astronomers monitored the planets' back-and-forth tugs on Gliese 876—revealed as regular wobbles in the star's light—a slight distortion in the resonant pattern suggested that a third world was in the mix.

Theorists Eugenio Rivera of the University of California (UC), Santa Cruz, and Jack Lissauer of NASA's Ames Research Center in Mountain View, California, created a detailed model of the system. It pointed to a low-mass inner planet speeding around the star in a mere 1.94 days, the shortest exoplanet "year" yet seen. But to be sure, the team's observers monitored the star as often as possible using the 10-meter Keck I Telescope at Mauna Kea, Hawaii, including an intense program last fall with an improved spectrograph to tease out fine details of the wobbles. It took more than 150 observations spread over 8 years to pinpoint the inner planet, says team leader Geoffrey Marcy of UC Berkeley.

Without the pas de deux between the more distant gas giants, their little sibling would have eluded detection thus far, says team member Paul Butler of the Carnegie Institution of Washington, D.C. Moreover, the precise gravitational waltz allowed the team to calculate the planetary system's tilt relative to our view. That geometrical measure—known only for a few other "edge-on" systems—yielded a range of six to nine times Earth's mass for the new planet, rather than simply a minimum mass that astronomers calculate for other exoplanets. The group announced its results on 13 June at a National Science Foundation press briefing in Arlington, Virginia.

At its distance of just 3 million kilometers from Gliese 876, the new world probably roasts with a surface temperature of 200 to 400 degrees Celsius. The team leans toward a solid nickel-iron rocky body for the hot planet, perhaps with a steamy atmosphere. "But it could be something more akin to a small Neptune," notes Lissauer, with a thick, vaporous mantle of water, hydrogen, and other gases. "It could go in either of those directions."

Indeed, too much equivocation remains to claim the first terrestrial analog, says Carnegie theorist Alan Boss, who did not participate in the study. At half the size of the three exoplanets announced last year—with masses 15 to 20 times that of Earth—the new planet probably isn't a distinct beast. "I view these as likely to be members of a single class," says Boss. "They are possibly rocky worlds." The question won't remain open too long, he adds. By finding more such planets, astronomers should spot one that crosses directly in front of its star. That would yield a convincing measure of the object's size and density, and thus its composition.

Red dwarf stars are appealing targets for another reason, says team member Steven Vogt of UC Santa Cruz: Their energy output is so feeble that rocky planets in 10-day to 20-day orbits might be cool enough for liquid water to exist. "If nature makes those planets, that's where we want to be looking," Vogt says.

–ROBERT IRION

CREDITS (TOP TO BOTTOM): ADAPTED FROM E. RIVERA *ET AL.*/UC SANTA CRUZ; TRENT SCHINDLER/NSF

ScienceScope

Cancer Trials Revamp

A panel convened by the National Cancer Institute last week recommended a sweeping restructuring of NCI-funded clinical trials.

Among the most far-reaching of the group's 22 recommendations is to create scientific steering committees to coordinate all phase III trials for major cancers. "That's a huge change," says panel member Richard Schilsky of the University of Chicago, noting that the varied ways trials are currently reviewed can lead to redundant studies.

The 77-page report also calls for a central database of trials with summary results, and it sets aside new funds for molecular medicine. Total costs of the restructuring plans are estimated at $113 million over 5 years. NCI Director Andrew von Eschenbach, who called for the review 18 months ago, said on 7 June that the reorganization "will change the future of clinical research."–JOCELYN KAISER

Want Ads Go Up at NASA

The new NASA chief is wasting no time sweeping out the old to make way for the new. Last week, a number of senior managers said they would leave the agency in the coming months; other departures were confirmed by agency and industry sources. Those leaving include NASA science chief Al Diaz and his deputy Ghassem Asrar, space-flight chief William Readdy and his deputy, and exploration directorate head Craig Steidle, a retired Navy admiral brought on board last year. To the surprise of many space insiders, Steidle's deputy Steve Isakowitz, a long-time influential insider, will also resign. Expect replacements to be named after NASA returns the space shuttle to flight, now scheduled for mid-July.

–ANDREW LAWLER

U.K. Space Program Criticized

A committee of the British House of Commons slammed the U.K. space program in a report last week, charging that it doesn't properly assess the risks of projects or analyze whether they achieve their goals. Particular criticism was leveled at the failed Beagle 2 Mars lander. Mass constraints, a tight timetable, and poor management gave the mission "no real prospect of success," the report charged, adding that uncertain funding was a factor. Beagle 2 chief Colin Pillinger of the Open University says the government has learned its lesson and has "already put aside money for the next flight opportunity."

–DANIEL CLERY

eppendorf PhysioCare Concept criteria 1 and 2

- Highest level of precision and ergonomics
- Pipettes for any application and budget
- Ceramic pistons
- Ergonomics approved by TÜV

A complete picture.

Integrated systems – Exceptional durability

PhysioCare Concept pipettes.
In this highly developed world shouldn't you be afforded the best possible work environment, one that is highly efficient and also satisfies your physiological needs? Absolutely.

Eppendorf helps you give it your best every day with optimum pipetting systems. Shorter work processes, reduced stress and low error rates will contribute to your total satisfaction with the new eppendorf **PhysioCare Concept**.

TÜV Rheinland approved our manual pipettes as: ergonomic, user-friendly and user tested.

PhysioCare concept

Check out how good your pipette really is!
PhysioCare Concept™ website
www.physiocare-concept.info

eppendorf

In touch with life

Your local distributor: www.eppendorf.com/worldwide · Application Hotline: +49 180-3 66 67 89

Eppendorf AG · Germany · +49 40 538 01-0 • Eppendorf North America, Inc. 800-645-3050

GENETICS

Jumping DNA Mixes It Up in the Developing Brain

We usually attribute the unique temperaments and talents of each person to a mysterious mix of heredity and environment. A provocative new study, however, suggests that a third factor also plays a role in generating individual differences: bits of genetic material that spontaneously hop around the genome of neurons in the developing brain, altering patterns of gene expression. In the 16 June issue of *Nature*, the discoverers of this phenomenon, led by Fred Gage at the Salk Institute for Biological Studies in La Jolla, California, propose that the process adds a random twist to neural development that ensures that no two brains—not even those of identical twins—are put together in exactly the same way.

Other researchers are intrigued by the idea but say much more work is needed to extend the team's findings, which come from experiments on cultured rat cells and genetically engineered mice, to normal animals—let alone people. "It has the potential to open a new paradigm, but it's not there yet," says Haig Kazazian, a geneticist at the University of Pennsylvania in Philadelphia.

Gage and colleagues, including postdocs Alysson Muotri and Vi Chu, were investigating a major puzzle in developmental neuroscience: how neural stem cells decide whether to turn into neurons or support cells called astrocytes and oligodendrocytes. Searching for genes that guide this decision, the team noticed that rat cells in the process of becoming neurons contained increased levels of RNAs corresponding to L1 retrotransposons, bits of DNA that can jump from one place in the genome to another by first copying themselves into RNA and then reversing the process. In so doing, they can alter the activity of genes they hop into.

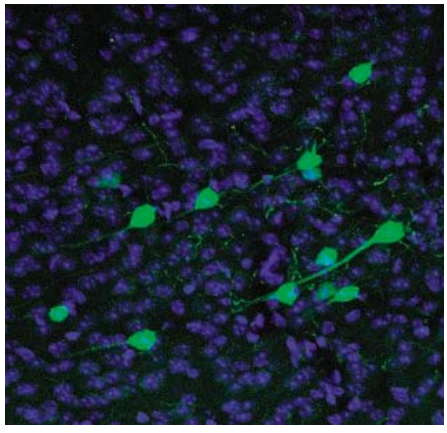

Shuffling the deck. Random genetic changes inside some neurons (green) may help ensure that every brain is unique.

Intrigued, the team inserted a human version of L1 into rat neural stem cells, along with a marker that would make the cells glow green whenever L1 made a jump. Many cells lit up, and when the researchers took a closer look, they found that L1 jumped into several genes typically expressed by neurons. In some cases, the jump altered gene expression in a way that influenced the stem cells' fate—making them more likely to turn into neurons, for example.

In an additional set of experiments, the team created transgenic mice by endowing the rodents with the same human retrotransposon. L1 did its jumping act in a subset of brain cells but not in cells of other tissues, with the exception of the testes and ovaries, where such retrotransposition was already know to occur. In principle, Gage says, this process could generate distinct neural circuitry in each individual by altering the proportion of different neuron types or levels of gene expression in the brain. The next step, he says, will be to prevent L1 from jumping around and see what effect—if any—that has on brain development in mice.

If L1 does prove to have an important role in brain development, that would come as a surprise to many researchers, says Kazazian: "These are genetic parasites as far as we know, and we never thought they might have a function like this."

Indeed, not everyone is willing to bet that they do. Anthony Furano, who studies retrotransposons at the National Institute of Diabetes and Digestive and Kidney Diseases in Bethesda, Maryland, applauds the Salk team's efforts but harbors doubts about the implications. "It seems unlikely that the relatively random changes caused by L1 could be a serious player in producing individual variation," he says. "But if they prove otherwise, well, then, wouldn't that be something?" **–GREG MILLER**

BIOMEDICAL POLICY

House Approves 0.5% Raise for NIH, Comments on Database

A House panel this week approved a 0.5% increase in the 2006 budget for the National Institutes of Health (NIH). The $142.3 million increase, to $28.5 billion, matches the Bush Administration's request. House lawmakers also declined to fully support a scientific society in its dispute with NIH over the agency's new chemicals database.

The modest budgetary rise falls far short of the projected 2006 biomedical inflation rate of 3.2%, say NIH's supporters. Representative David Obey (D–WI), who voted against the bill, predicted that it would lead to fewer new grants. "We are concerned about the momentum of biomedical research being affected by this," says Jon Retzlaff, legislative relations director for the Federation of American Societies for Experimental Biology in Bethesda, Maryland. Backers of NIH hope that the corresponding Senate panel, chaired by Senator Arlen Specter (R–PA), will continue its track record of bestowing more generous increases on the agency. The Senate panel could mark up its bill as soon as July.

The House Appropriations Labor/Health and Human Services/Education subcommittee also appears to have listened to NIH in its fight with the American Chemical Society (ACS) over PubChem, a free NIH database on biologically active compounds. ACS contends that PubChem will duplicate its own vast subscription-based chemical database and should therefore include only data generated by NIH's new molecular libraries screening effort. This spring, ACS took its case to the subcommittee's chair, Ralph Regula (R–OH), whose state is home to the headquarters of the ACS database (*Science*, 6 May, p. 774). Librarian groups and advocates of open-access publishing, meanwhile, blasted ACS's position.

According to several sources, subcommittee staffers discussed whether the House bill should order NIH to scale back PubChem. But after last-minute negotiations between ACS and NIH officials, including NIH Director Elias Zerhouni, the subcommittee settled on less restrictive wording. A report accompanying the House bill notes that PubChem's mission is to "house both compound information from the scientific literature as well as" data from the molecular libraries initiative, but it says the committee is "concerned that NIH is replicating" private information services. The report "urges NIH to work with private sector providers to avoid unnecessary duplication and competition."

ACS issued a statement saying it "is very pleased" and expects "to work diligently with NIH toward a collaborative model." Supporters of PubChem, for their part, see the House language as a victory for NIH. ACS official Brian Dougherty declined to say whether the society will ask the Senate for help. "We're focused on working with NIH," he says.

–JOCELYN KAISER

CREDIT: A. R. MUOTRI *ET AL.*, *NATURE* **435**, 903 (2005)

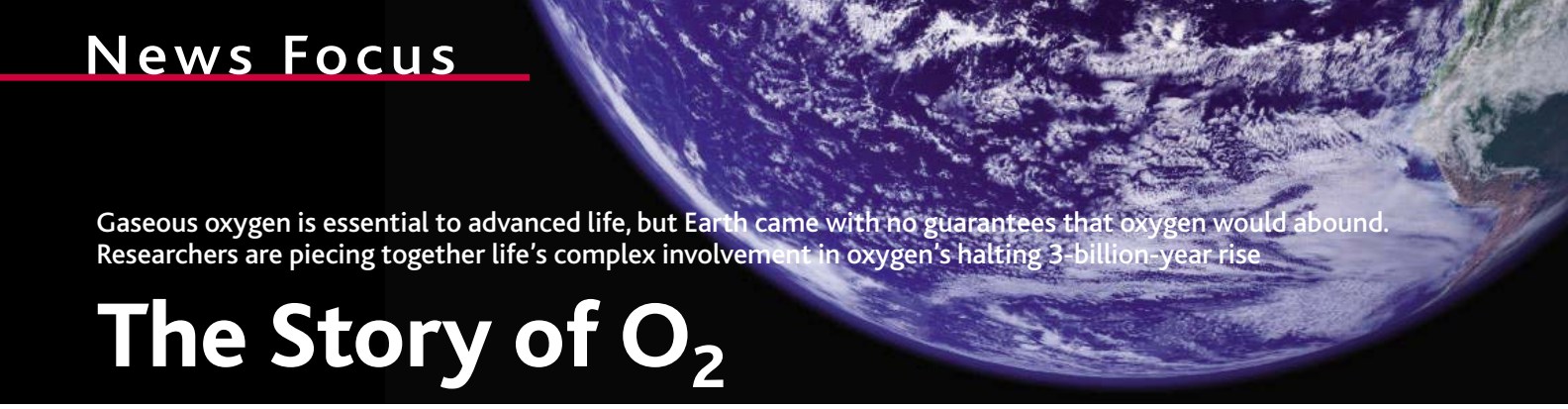

Gaseous oxygen is essential to advanced life, but Earth came with no guarantees that oxygen would abound. Researchers are piecing together life's complex involvement in oxygen's halting 3-billion-year rise

The Story of O_2

In the beginning, Earth was devoid of oxygen, and then life arose from nonlife. As that first life evolved over a billion years, it began to produce oxygen, but not enough for the life-energizing gas to appear in the atmosphere. Was green scum all there was to life, all there ever would be? Apparently, yes, unless life and nonlife could somehow work together to oxygenate the planet from the atmosphere to the deep sea.

Earth scientists are flocking to the emerging field of astrobiology to tease out the history of oxygen on Earth from a maddeningly subtle and fragmented rock record. The rise of atmospheric oxygen from nothing to abundance, they are finding, came in two big steps about 2 billion years apart. Relatively simple life probably facilitated the first step up and possibly the second, much to its own detriment but to the benefit of more complex life.

"The rise of oxygen changed the course of evolution," says astrobiologist David Catling of the University of Bristol, U.K. "Atmospheric oxygen was a precursor to advanced life on Earth, and, I would argue, to life elsewhere." With the new interest in 3 billion years of oxygen history, "there's been a great deal of progress," says geochemist Donald Canfield of the University of Southern Denmark in Odense. "The field has matured; it used to be a hobby area for most people. I credit NASA's [astrobiology funding] for much of that." An invigorated field is attacking a host of big questions: When did free oxygen first appear in Earth's atmosphere? What made it appear in the first place? What held it back for so long? And what caused the second, delayed surge of oxygen that allowed advanced animals to appear?

A certain beginning

Historians of oxygen have always agreed on one thing: Earth started out with no free oxygen—that is, diatomic oxygen, or O_2. It was all tied up in rock and water. For half a century, researchers have vacillated over whether the gases that were there favored the formation of life's starting materials (see sidebar, p. 1732). Without free oxygen, in any case, the first life that did appear by perhaps 3.5 billion years ago had to "breathe" elements such as iron, processing them to gain a mere pittance of energy.

For decades, scientists have argued about just how long the planet remained anoxic, and thus home to nothing but tiny, simple, slow-living microorganisms. Until recently, the idea that early Earth was anoxic for more than 2 billion years—as advanced primarily by geochemist Heinrich Holland of Harvard University—dominated the field but had not won the day. Its proponents pointed to diverse evidence. Minerals older than about 2.2 billion to 2.4 billion years found in ancient soils, streambeds, and other sediments seemed to show no sign of ever having been exposed to oxygen. There were no "red beds" of sediment stained with rusted iron minerals, for example. But a small but vocal opposition, headed by Holland's former student Hiroshi Ohmoto of Pennsylvania State University (PSU), University Park, had long believed that Earth's atmosphere was oxygenated back as far as geologists can peer. He and other opponents pointed to mineral bits here and there that they believed had been oxidized 3 billion years ago or longer.

"The rise of oxygen changed the course of evolution."
—David Catling

A step up

That teacher-student debate now appears to be resolved in the teacher's favor. Researchers have in hand an unequivocal method for determining the presence or absence of oxygen early in Earth's history. Introduced by geochemist James Farquhar of the University of Maryland, College Park, and his colleagues in 2000, the sulfur isotope method depends on the way sunlight breaks down sulfur dioxide in the atmosphere. These photochemical reactions can shuffle sulfur isotopes in weird ways, without respect to the mass of the isotopes. But free atmospheric oxygen wipes out such mass-independent fractionation (MIF) before the sulfur reaches Earth's surface, where the odd mix of isotopes could be preserved in sediments. Farquhar and colleagues found MIF of sulfur in rocks older than 2.4 billion years but not in younger rocks, apparently pinning down atmospheric oxygen's first appearance at levels of at least 1 part per million.

Slow leak. Escaping hydrogen (imaged as blue) would have slowly oxidized early Earth, but only if methane sped things up.

That discovery—now buttressed by theoretical work and studies of other rocks—pretty much clinches the case for a late "Great Oxidation Event," as Holland has dubbed it. "Skeptics would have to reinvent physics to counteract Farquhar's results," says atmospheric physicist James Kasting of PSU. Although Ohmoto and some associates have yet to give in, "there's a strong consensus in the rest of the community," says Catling. "In the MIF of sulfur, you have a clear signal that something changed at about 2.4 billion years."

And that permanent rise in oxygen to detectable atmospheric levels seems to have spurred evolution. The earliest known fossil of a eukaryote—the term for organisms, from yeast to humans, that have a cell nucleus and usually require oxygen—is about 2 billion years old. The first fossil big enough to be seen without a microscope—the spiral-chained algae *Grypania*—appeared 1.9 billion years ago.

Rumors of oxidation

So what about those signs of earlier oxygen that helped fuel years of debate? Some could be markers of ancient "oxygen oases" in which cyanobacteria—oxygen-producing blue-green algae—seem to have been capturing the sun's energy through photosynthesis for hundreds of millions of years before atmospheric levels exceeded the sulfur MIF limit.

In rocks from the Hamersley Basin of western Australia, researchers have found signs that such oxygen did manage to permeate at least small parts of the environment—perhaps just a sea-floor skim of microbial scum—while the rest of the world remained anoxic. When

CREDITS (TOP TO BOTTOM): NASA GODDARD SPACE FLIGHT CENTER; ISTP/GSFC/NASA

oxygen-producing microorganisms die, they leave behind a telltale mix of carbon isotopes biased toward the lighter isotope, as well as distinctive organic molecules such as steranes.

At the astrobiology meeting, geochemist Jennifer Eigenbrode of the Carnegie Institution of Washington's Geophysical Laboratory and colleagues reported finding those geochemical fingerprints in Hamersley rocks. The mix of isotopes and biomarkers changed as the researchers traced them into geologically more recent rocks. Eigenbrode said the shifts point to an increasing role for oxygen-dependent ecosystems, perhaps confined to thick films on the sea floor. In such oxygenated islands, eukaryotes may have appeared hundreds of millions of years earlier than their first recognized fossils, giving them that much more time to evolve their more sophisticated lifestyle.

What was the holdup?

Better records of the history of oxygen don't always make the historian's job easier. They can also make gaps in the timing harder to explain. For example, evidence from sterane and other biomarkers indicates that oxygen-generating cyanobacteria were in business by 2.7 billion years ago or earlier. Yet the Great Oxidation Event didn't come along for another 300 million years. Why the delay?

Researchers have suggested several possible reasons. Geobiologist Joseph Kirschvink of the California Institute of Technology in Pasadena and his doctoral student Robert Kopp note that early cyanobacteria didn't produce oxygen. They argue that the type of photosynthesis that liberated the gas did not appear until 2.4 billion years ago. The explanation discounts a number of geochemical indicators, such as steranes, which are commonly thought to require oxygen for their synthesis.

Other geoscientists suspect that the supply of oxygen-devouring volcanic gases such as hydrogen might have started petering out by 2.4 billion years ago, finally allowing oxygen levels to rise. But recent studies of trace metals in ancient rock derived from the deep Earth seem to show that the supply of reducing gases held steady right up to and through the oxidation event.

Catling and colleagues have proposed that high levels of methane (CH_4) in the early atmosphere greatly increased the rate at which hydrogen "leaked" into space, allowing photosynthetically produced oxygen to oxidize Earth. In 2001, they pointed out that 3 billion years ago methane produced by anoxia-loving bacteria was probably 100 to 1500 times more abundant than it is today. And hydrogen-bearing methane can freely diffuse to the atmosphere's outer fringes where its hydrogen can make the final jump to space; water's hydrogen gets condensed out at lower altitudes.

To test the idea, Catling, astrobiologist Mark Claire of the University of Washington, Seattle, and planetary physicist Kevin Zahnle of NASA's Ames Research Center in Mountain View, California, recently programmed methane into a computer model that keeps tabs on oxygen's comings and goings on early Earth. In the model, volcanic gases and reactions with crustal minerals sop up oxygen as fast as cyanobacteria can churn it out. Without abundant methane to carry hydrogen away to space, Earth remains anoxic indefinitely. But with high atmospheric methane, hydrogen losses to space eventually overwhelm the anti-oxygen forces, and oxygen levels begin to rise. So the lowly methane-generating bacterium may have unwittingly given oxygen—its deadly enemy—a leg up on the road to an oxidizing world.

The boring billion

Even more puzzling than the 300-million-year run-up to the Great Oxidation Event is what came next. The advent of oxygen ushered in geology's red beds and life's eukaryotes. Then, for a good billion years, the newcomer eukaryotic algae went nowhere evolutionarily, frozen in time as an advanced sort of green scum. And there is growing geochemical evidence that the Great Oxidation Event wasn't actually all that great. To understand why not, scientists look to the ocean.

Doubts about the oxidation event's greatness arose in 1998 when geochemist Canfield first proposed—on the basis of sulfur isotopes—that all of the ocean's waters except the uppermost layer had remained anoxic for more than a billion years after atmospheric oxygen made its first appearance. In 2002, geochemist Ariel Anbar of Arizona State University, Tempe, and paleontologist Andrew Knoll of Harvard University linked Canfield's idea to the history of life. They suggested that what oxygen the atmosphere held during the time of the "Canfield Ocean"—perhaps 1% to 10% of present levels—had actually starved eukaryotic algae and held them back evolutionarily (*Science*, 16 August 2002,

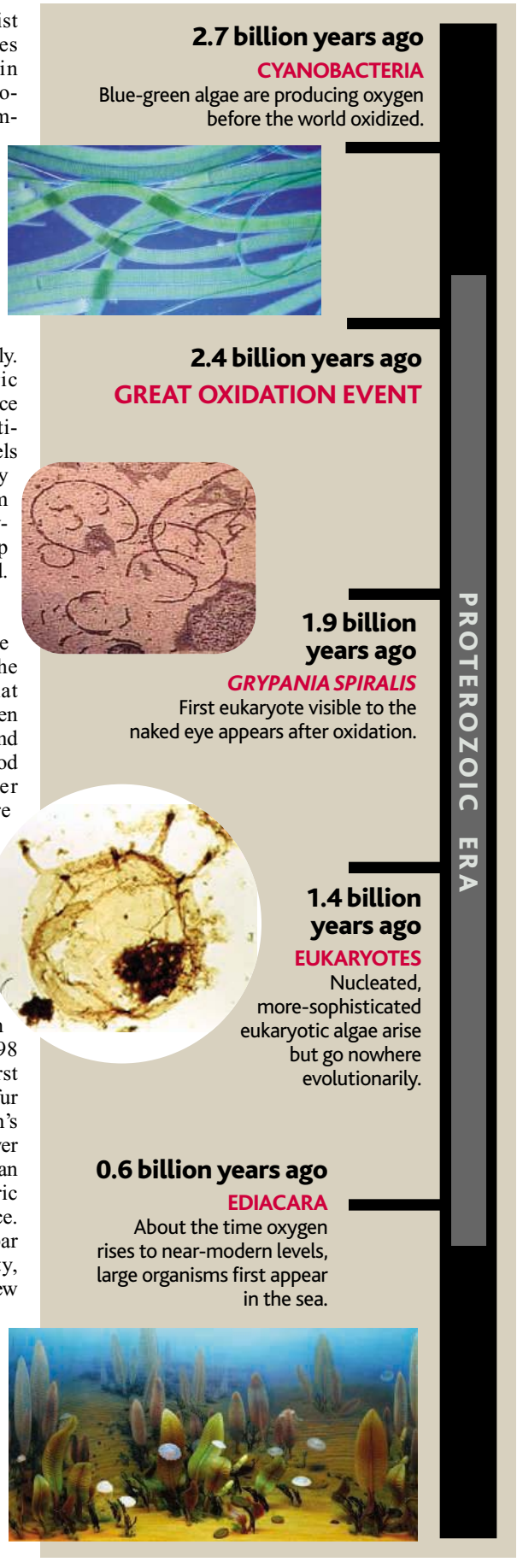

CREDITS (TOP TO BOTTOM): TOM ADAMS/VISUALS UNLIMITED; PAUL JANKE/PAN TERRA INC.; ANDREW KNOLL; CHASE STUDIO/PHOTO RESEARCHERS INC.

A Better Atmosphere for Life

Thirty years ago, geochemists took away the primordial soup that biologists thought they needed to cook up the first life on Earth. Now, some atmospheric chemists are trying to give it back. They're suggesting that the early Earth could have held onto much more of its volcanic hydrogen—a key ingredient in the recipe for making the organic compounds that may have led to the first life.

Creating the primordial organic goo used to be easy. If you combined the methane and ammonia seen in the still-primordial atmosphere of Jupiter, passed lightninglike sparks through the mixture, and added some water, voilà, complex organic compounds such as amino acids formed. But then in the 1970s geochemists spoiled the party by insisting that Earth's earliest atmosphere was nothing like Jupiter's. Earth's carbon would have been part of oxygen-rich carbon dioxide, and its nitrogen part of inert nitrogen gas, they said. And hydrogen seeping from the planet's interior would have quickly escaped to space. That left chemists with a thin gruel indeed. It had far too much oxygen, which destroys organics, and not enough of the hydrogen that enables carbon atoms to link up to form the complex polymers needed for life. In the lab, such mixtures yielded few organics, and simple compounds at that.

Now, atmospheric chemist Feng Tian of the University of Colorado, Boulder, and his colleagues argue that hydrogen on early Earth would have escaped much more slowly than has been assumed (*Science*, 13 May, p. 1014). Lacking the oxygen that absorbs solar energy, they point out, the outer fringes of the early atmosphere would have been far colder than they are today. With less energy jittering its atoms, much less lightweight hydrogen would have "boiled" away into space.

The researchers also figured out how to calculate the rate at which hydrogen would have been lost as wisps of the atmosphere flowed away into space. The mathematics of such supersonic flow had frustrated all previous attempts. Overall, hydrogen would have escaped at 1/100 the rate previously assumed, the group says. Rather than building to concentrations of just 0.1%, hydrogen might have reached 30%. That would make for a far more productive atmosphere than chemists have been coping with for 30 years. "The end result is you drop vast amounts of organic compounds into the ocean to make a soup," says the group's Brian Toon of the University of Colorado, Boulder.

Deep roots. A buildup of volcanic hydrogen may have helped form life's ingredients.

"On the face of it, what they have produced is quite reasonable," says atmospheric chemist Yuk Yung of the California Institute of Technology in Pasadena. "It's a nice piece of work. It's going to make the biologists a lot happier." Astrobiologist David Catling of the University of Bristol, U.K., isn't so sure. "It would be rather premature," he says, to shift emphasis back to the prebiotic chemistry of a hydrogen-rich atmosphere and organic-goo–laced ocean. Tian and his colleagues "haven't dealt with all the factors that lead to hydrogen escape," says Catling. He suspects that a more sophisticated model would show that hydrogen escaped the early Earth at least as fast as it does today. Time will tell whether too many cooks spoil the primordial broth. **–R.A.K.**

p. 1104). The atmospheric oxygen, they noted, would have weathered sulfur off the land, dosing the ocean with deadly sulfides, which would have chemically removed the iron and molybdenum from seawater. The algae needed these elements to form enzymes essential to taking up nutrients; without them, they were malnourished and therefore evolutionarily listless.

The Canfield Ocean, and thus the Malnourished Earth hypothesis, has since gained ground. Several groups have extended Canfield's sulfur isotope analysis across the midsection of the Proterozoic era (2.5 billion to 0.54 billion years ago), confirming signs of anoxia. But those studies drew on marine rocks deposited from waters that were at least partially isolated from the open ocean, like today's Red Sea. Perhaps their anoxia was not typical of the ocean at large.

Last year Anbar, geochemist Gail Arnold, then at the University of Rochester, New York, and colleagues allayed many of those doubts. In *Science* (2 April 2004, p. 87), they reported on their analysis of molybdenum isotopes preserved in mid-Proterozoic rocks. The ratio of two molybdenum isotopes depends on the amount of oxygen in the ocean. And unlike many other dissolved elements, molybdenum remains in seawater so long before being removed to the sediment that it has a chance to mix throughout the ocean, even its backwaters. Samples from one place in the Proterozoic ocean, then, should reflect the amount of oxygen in the ocean as a whole. Arnold and colleagues found signs that far more of the ocean floor was anoxic 1.4 billion and 1.7 billion years ago than today. So, almost 4 billion years after the world began, the team of life and Earth that boosted oxygen from nothing to detectable levels still had a ways to go.

Breakout

What locked a billion years of the Proterozoic in geochemical and evolutionary stasis remains a mystery. But the bigger, more enticing mystery may be how oxygen finally rose to something like modern levels toward the end of the Proterozoic, 0.6 billion or 0.7 billion years ago. That's when multicellular animals first appeared, and then large animals such as the enigmatic Ediacara, creatures that must have required higher levels of oxygen. Canfield's sulfur isotopes hint that oxygen levels did in fact rise about then.

This second oxidation event is proving far more elusive than the great one. Most scientists agree that it hinged on some major change that started locking up more organic matter in sediments before it could decay. Instead of being consumed in the chemistry of decomposition, oxygen built up in the atmosphere and ocean. As to what triggered the mass carbon burial, explanations fall into two camps: geological and biological.

Proposed geological shifts capable of driving up oxygen levels include a jump in the production of clays able to adsorb organic matter and preserve it beneath the sea floor, and the assembly of a supercontinent whose weathering could stimulate ocean life and subsequent carbon burial by adding nutrients to the seas. Biological shifts include the arrival of lichens on land, which would have accelerated rock weathering as well, and the evolutionary innovation among zooplankton that produced dense, organics-laden fecal pellets able to sink into the deep sea.

Before the oxygen historians can sort out the truth from the just-so stories, they'll have to come to grips with the nature of the ancient record of life as well as oxygen. "There's less data the older you go [in the geologic record]," says Kirschvink, "so there's less chance of being proven wrong right off" if you're working 2 billion or 3 billion years in the past. That can make spinning yarns about the early days more fun, but it puts a premium on collecting what data can be retrieved from the oldest rocks. **–RICHARD A. KERR**

A Sprawling Andromeda Galaxy Startles and Puzzles Observers

MINNEAPOLIS, MINNESOTA—A small meeting of about 680 astronomers here 29 May to 2 June featured some big claims about the Andromeda Galaxy and the ingredients of comets.

Skywatchers in the Northern Hemisphere can perceive the Andromeda Galaxy, our closest major galactic neighbor, as a faint fuzzy patch. But if our eyes could see the full extent of Andromeda's starry disk, it would span a startling 12 times the width of the full moon on the sky—triple the size of previous estimates. That result, presented at the meeting, throws a spanner into the works of galaxy formation theories. "This gigantic disk certainly came as a bolt from the blue," says study co-author Nial Tanvir of the University of Hertfordshire, U.K.

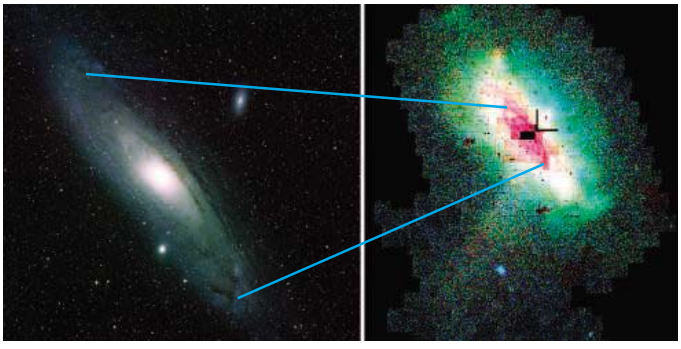

Growing galaxy. The classic starry disk of Andromeda (*left*) extends far deeper into space than astronomers thought (yellow and green, *right*).

Tanvir and his colleagues, led by astronomer Rodrigo Ibata of the Strasbourg Observatory in France, based their work on a sweeping scan of Andromeda's outskirts with the 2.5-meter Isaac Newton Telescope on the Canary Islands. The survey unveiled swarms of faint stars around the galaxy's graceful central spiral, a flattened disk that seemed about 50,000 light-years in radius. As in our Milky Way, this stellar disk revolves in a calm and orderly fashion. The team expected that the outlying stars would swoop randomly around the disk in a huge spherical "halo," as probable remnants of smaller galaxies that Andromeda has devoured.

The survey does reveal clumps and messy patterns of stars, some of which clearly belong to disrupted dwarf galaxies (*Science*, 20 May, p. 1104). But to the team's amazement, most of the far-flung stars revolve smoothly as a giant extension of Andromeda's classic disk—out to a distance of at least 150,000 light-years. The astronomers traced those motions by analyzing light from about 5000 stars with the 10-meter Keck II Telescope at Mauna Kea, Hawaii. "This is really impressive work, and the evidence of a rotating disk is convincing," comments astronomer Puragra Guhathakurta of the University of California, Santa Cruz.

The disk is no mere sprinkle. It may produce 1/10 of Andromeda's light, says postdoctoral researcher Scott Chapman of the California Institute of Technology (Caltech) in Pasadena, who led the Keck effort. Moreover, because of its vast breadth, the extended disk could account for 30% of the galaxy's angular momentum. "It's a real puzzle why this thing is there," Chapman says. The gravitational influence of Andromeda's hidden cocoon of dark matter—which probably reaches far beyond the newfound disk—undoubtedly played a role in dictating its shape, he notes.

Even so, tiny incoming galaxies should scatter stars in all directions rather than confining them in a thin plane. A single large merger long ago might have spread stars into a disk. Alternatively, shock waves from the merger could have induced stars to form within a preexisting flat whorl of gas around Andromeda. Each scenario has trouble creating a structure as wide and coherent as Ibata's team has found. "I still haven't digested the result," said Caltech astronomer Wallace Sargent after Chapman's talk. "I didn't expect to see ordered motion so far out."

Andromeda may spring more surprises. In a new paper under review, Guhathakurta and colleagues identify stars in the galaxy's halo as far as 500,000 light-years from Andromeda's core—fully 1/5 of the distance to the Milky Way. Our grand neighbor, it seems, is just a star's throw away. **–ROBERT IRION**

Snapshots From the Meeting

Future crash. Two white dwarfs locked in the closest known binary system (*Science*, 15 March 2002, p. 1997) are spiraling toward each other faster than any other pair of stars. Energy modulations measured by the Chandra X-ray Observatory show that the system's 321-second period is speeding up by 0.012 seconds annually, reported astrophysicist Tod Strohmayer of NASA's Goddard Space Flight Center in Greenbelt, Maryland. With that rapid approach—roughly 2.5 centimeters per hour—the dwarfs will merge about 500,000 years from now. But even today, the binary churns space with gravitational waves that an orbiting mission next decade should spot easily.

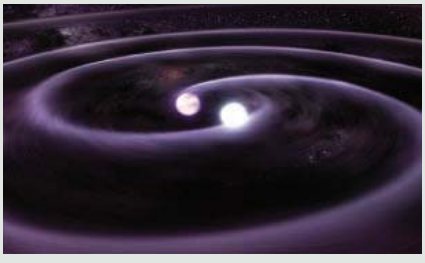

Doomed. These inspiraling white dwarfs should emit regular gravitational waves.

Probing Pluto's past. A college sophomore has helped retrace variations in the brightness of Pluto soon after the planet's discovery in 1930. Luke Smith of Louisiana State University in Baton Rouge and colleagues obtained 30 glass photographic plates taken in 1933 and 1934, when astronomers lacked the tools to gauge subtle trends in Pluto's light. The team's analysis—including new images of comparison stars close to Pluto at the time—suggests that the planet was slightly brighter than expected. The extra light may have reflected off frosts that slowly melted as Pluto edged closer to the sun later in the century, Smith reported.

SNEWS button. Astronomers are ready to catch an exploding star in our galaxy. The Supernova Early Warning System (SNEWS) looks for neutrinos—ghostly particles unleashed in torrents by stars when they blow up—spotted simultaneously by four detectors around the globe. Neutrinos would herald a supernova's blast of light by a few hours, because the shock wave takes time to break free of the collapsing star. SNEWS is patient: It may take several decades to trigger on a supernova, but it should produce less than one false alarm per century, reported Alec Habig of the University of Minnesota, Duluth. **–R.I.**

CREDITS (TOP, LEFT TO RIGHT): NOAO/AURA/NSF; R. IBATA *ET AL.*/ISAAC NEWTON TELESCOPE; (BOTTOM) D. BERRY/NASA/GSFC

Customize.
Exactly what you want.

Enhance your research success with custom products designed just for you. You specify what you want...volume, concentration, even formulation. Together, we make it happen. You spend more time with your research and less time preparing. When you need innovation and creativity, look to Promega.

For more information about Promega Custom, visit **www.promega.com/myway**

CERTIFIED ISO 9001 QUALITY SYSTEM

PROMEGA CORPORATION • www.promega.com

Promega

A Rocky Landing for Deep Impact?

Each time a comet rounds the sun, its body erodes. But a comet's glorious tails of dust and gas are like banks of fog: lots of surface area and little matter. Comets shed much more mass when larger particles sputter away into narrow "debris trails" along their orbits. A new survey of these trails has solidified a growing view that comets consist mainly of rock rather than ice. NASA will put that notion to a stiff test on 4 July when it plows a projectile into a comet for the first time.

Pressures from sunlight and the solar wind puff a comet's tiny particles into wide fans. Bigger fragments—millimeters to centimeters across—resist those forces. Instead, they remain in linear tracks in the comet's orbital path "like a line of boxcars," says doctoral student Michael Kelley of the University of Minnesota, Twin Cities. "The particles drift so slowly away from the nucleus that they take hundreds of years to fill a trail around the sun."

The debris trails pop out in infrared images, because the particles reradiate warmth from the sun. Astronomers first spied a handful of trails in images from the Infrared Astronomy Satellite, which flew in the 1980s. Their abundance led Mark Sykes of the Planetary Science Institute in Tucson, Arizona, to describe comets as "icy mudballs" of mostly rocky material—a twist on the canonical "dirty snowballs" picture of mostly ice.

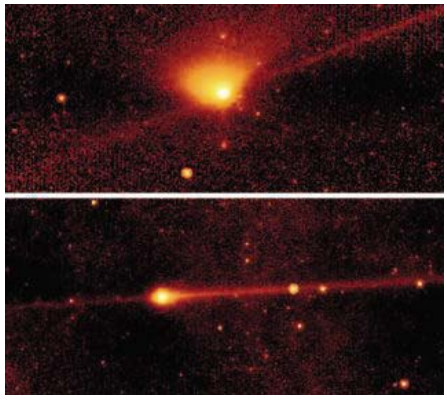

Space pebbles. Big particles form trails near comets Johnson (*top*) and Shoemaker-Levy 3.

Now, a team including Sykes, Kelley, and William Reach of the Spitzer Science Center in Pasadena, California, has taken a far more thorough look at debris trails with NASA's Spitzer Space Telescope. Their analysis reveals 21 debris trails out of 29 short-period comets, which loop around the sun in decades or less. The trails are all narrow, including seven extremely fine ribbons that only Spitzer could have detected. To trundle along such confined paths for years, the particles must be "miniasteroids" the size of small pebbles, Reach reported at the meeting.

The wispy sprays of fine particles in comet tails don't hold a candle to the mass contained in the bands of pebbles, models indicate. "It's clear that [debris trails are] the main mass-loss mechanism for comets," Reach says. "Comets cannot be composed of particles with finer grain sizes than these."

Some observers disagree. "It's important to understand the meaning of the word 'rock,' " says Zdenek Sekanina of NASA's Jet Propulsion Laboratory in Pasadena, an expert on comets and meteoroids. Particles in debris trails probably are agglomerations of dusty grains that clump weakly together before being expelled from the comet rather than strong and coherent nuggets like pebbles, Sekanina says.

Even if the crusty surfaces of comets cast rocks into space, fluffier icy matter may lurk inside, says dust scientist Diane Wooden of NASA's Ames Research Center in Mountain View, California. Testing that idea is a prime objective of Deep Impact, now on a collision course with Comet Tempel 1 (*Science*, 27 May, p. 1247). Reach ventures that the comet contains at least 10 times more rock than ice throughout its volume—and that Deep Impact will crash with a shallow, hard thud.

–ROBERT IRION

CREDITS (TOP TO BOTTOM): NASA/JPL-CALTECH/W. REACH, SPITZER SCIENCE CENTER; HUMPATH.COM

Meeting American Society of Gene Therapy

Retroviral Vectors: A Double-Edged Sword

ST. LOUIS, MISSOURI—The 1 to 5 June 8th annual meeting of the American Society of Gene Therapy attracted 1910 researchers who were abuzz over a possible third success for clinical gene therapy.

Gene therapy has entered a painful adolescence. In the past 6 years, the technique has restored the immune systems of 22 children with two types of severe combined immunodeficiency disease (SCID), marking the first clear success in the clinic. But these victories were bittersweet: Three of the children in a SCID trial in France later developed leukemia, and one died last year. At the meeting and a satellite retreat,* researchers discussed mounting evidence that using retroviruses to fix broken genes can spur cell growth that may raise the risk of cancer. But this side effect could also explain a new gene-therapy success reported at the meeting, this time in adults.

The leukemia in the French trial involved children with SCID caused by the defective X chromosome gene for a protein called common gamma chain (gc). In two of these cases, the retrovirus that carried the corrective gene into the children's blood stem cells inserted its DNA into and activated an oncogene called *LMO2*, and a single T cell derived from such a stem cell multiplied out of control. In St. Louis, Marina Cavazzana-Calvo of the Necker Hospital in Paris reported that the third leukemia case, which was disclosed in January, appears to involve multiple insertions of the corrective gene, affecting four different oncogenes, including *LMO2*—suggesting that a similar mechanism is at work. The French group has halted its trial until it can design a safer viral vector. The leukemias also apparently stem from an interaction between *LMO2* and gc, so trials for ADA-SCID, which involves a different defective gene, are continuing.

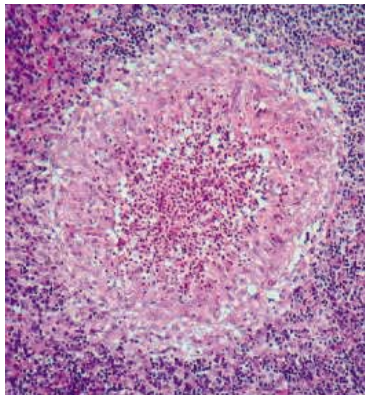

Good news. Gene therapy has cured two people of a disease in which phagocytes form areas of swollen tissue known as granulomas (*left*).

Researchers in St. Louis still had no definitive explanation for the mystery of why, so far, leukemias have not appeared in seven children treated in an X-SCID trial at the Institute of Child Health in London. That gene therapy protocol differed in subtle ways from the French group's. Adrian Thrasher, the leader of

*2nd Stem Cell Clonality & Genotoxicity Retreat, 1 June 2005.

the U.K. study, noted that "marked" T cell counts in the French patients rose steeply after they received corrected cells, whereas in the U.K. trial, the rise has been more gradual. "I don't know what it means," he acknowledged.

Several gene therapists, including Frederic Bushman of the Salk Institute for Biological Studies in San Diego, California, described evidence that retroviruses tend to insert in active genes, perhaps because the condensed DNA-containing chromatin opens up in these regions. And Christopher Baum of Hannover Medical School in Germany and Cincinnati Children's Hospital Medical Center in Ohio presented his group's recently published mouse study, which found that stem cells containing insertions near genes involved in cell proliferation keep multiplying until these clones far outnumber other cells (*Science*, 20 May, p. 1171).

Still, promoting cell proliferation might sometimes be a good talent for a retroviral vector. Describing gene therapy's latest success, a German-Swiss team reported that they used such a virus to restore the health of two adults with the rare inherited disorder chronic granulomatous disease (CGD). People born with CGD lack an enzyme complex, called phagocyte NADPH oxidase, which white blood cells use to make the hydrogen peroxide needed to kill microbial invaders. People with CGD usually die from fungal and bacterial infections by age 30.

In an attempt to correct the defect, molecular virologist Manuel Grez of the Georg-Speyer-Haus Institute for Biomedical Research in Frankfurt and collaborators in Germany and Switzerland extracted blood stem cells from two CGD patients in their mid-20s and, using a vector similar to that used in the X-SCID trials, inserted a good copy of one gene needed to make NADPH oxidase. Before putting the cells back, they gave the patients chemotherapy to kill some of their bone marrow and allow the corrected cells more room to grow. This step once seemed risky in already-sick patients but has proved crucial to the success of ADA-SCID trials, notes Donald Kohn of Children's Hospital in Los Angeles, California.

Unlike in previous CGD trials, 3 weeks after the cells were put back into the patients, a surprisingly large fraction, more than 20%, of their circulating white blood cells carried the corrected gene. The big surprise, however, was that after 4 months, a few cells in each patient went through an "unexpected expansion" in number so that up to 60% of their white blood cells contained the gene, Grez reported. Both patients now produce significant amounts of functional NADPH oxidase. And they are much healthier: A lung lesion in one has healed, and two liver abscesses have disappeared in the other. One has even been able to stop taking prophylactic antibiotics.

"There's no question that [the trial has] provided benefit to the patients," says Harry Malech of the U.S. National Institute of Allergy and Infectious Diseases in Bethesda, Maryland, who conducted two previous CGD trials. Malech and others add a note of caution, however. The clones that multiplied in these CGD patients had the corrected gene inserted in one of three locations near genes involved in cell proliferation. Although that could help explain the unexpected expansions and why the treatment worked so well, it also raises the risk of leukemia. Grez suggests that's unlikely because the growth of the stem cells eventually leveled off. Still, says Kohn, "it needs to be watched."

Smart Vector Restores Liver Enzyme

Stealing from the tool kit of viruses that infect bacteria, researchers have used a new gene-therapy method to cure the metabolic disorder phenylketonuria in mice. The method uses a viral enzyme, rather than a virus itself, to insert a corrective gene into a specific location in a mouse's DNA, making it a potentially safer way of delivering new genes.

Many gene-therapy efforts employ a retrovirus to deliver working copies of genes into a subject's body. But because these viruses integrate DNA into a host's genome at many locations, the approach can disrupt existing genes, like those implicated in cancer. The danger of that recently became clear when three patients in a seemingly successful gene therapy trial in France later developed leukemia (see previous story).

Ideally, researchers would like to place a corrective gene in a specific location, safely away from other genes. Back in 2001, geneticist Michele Calos's group at Stanford University in California invented such a method by turning to a smarter-than-average version of an enzyme called an integrase, which some viruses use to insert their DNA into a host's genome. Retroviruses, such as HIV, have integrases of their own, but they can insert DNA at locations that alter gene expression. Calos, however, found that an integrase from a bacteriophage, a virus that infects bacteria, only latches onto a specific DNA sequence within bacteria—one that is also found in a few places within mammalian genomes—and is considered low risk. She and her colleagues have recently had some success treating mouse models of hemophilia and other diseases by injecting rodents with a corrective gene and the gene for this phage integrase.

Li Chen in Savio Woo's lab at Mount Sinai School of Medicine in New York City has now used a similar strategy to treat a mouse version of phenylketonuria, a disease in which people don't make enough of the liver enzyme phenylalanine hydroxylase (PAH). In such cases, the body cannot convert the amino acid phenylalanine to tyrosine, and its buildup leads to severe mental retardation. Currently, the main treatment for the condition is a strict diet low in phenylalanine, one that must be started soon after birth.

Chen made plasmid loops of DNA containing a gene for a phage integrase and a good copy of the *PAH* gene and then injected these plasmids into the tail veins of mice with a defect in their *PAH* genes. After three injections, the mice made more PAH enzyme, and their blood levels of phenylalanine fell to within the normal range—and stayed there for more than 6 weeks, Chen reported at the meeting. Another sign that the gene therapy worked: The mice's fur turned from gray to black because they now had the tyrosine needed to make the pigment melatonin.

Colorful success. Gene therapy for phenylketonuria turned gray mice black.

The phage integrase used by Woo's team differs from that chosen by the Stanford group, and it targets different points on chromosomes. It may work better in certain tissues because, depending on the genes expressed in that tissue, different sites may be open or closed to a particular integrase, notes Barrie Carter of Targeted Genetics in Seattle, Washington. However, both groups of researchers still need to find more efficient ways of getting the genes into cells. The phage-integrase strategy "is not yet ready for prime time," says Woo.

—JOCELYN KAISER

CREDITS: LI CHEN

Private Mission Aims to Give Solar Sails Their Day in the Sun

Assembled by enthusiasts on a shoestring budget, Cosmos 1 could spearhead a new generation of photon-powered spacecraft

In the *Star Wars* movie *Attack of the Clones*, the villainous Count Dooku escapes the clutches of the Jedi in a spaceship that unfurls a vast, shiny solar sail to speed its way across space powered by starlight. Next week, something akin to this science-fiction fantasy will take to the skies above Earth.

The spacecraft, called Cosmos 1, aims to show that solar sailing is practical in our solar system and beyond. "This is the only technology that can do interstellar flight," says project director Louis Friedman, who is executive director of the Planetary Society, the nonprofit organization running the mission. Cosmos Studios, a U.S. science entertainment company run by Ann Druyan, widow of Carl Sagan, put up $4 million to bankroll the mission. Russian researchers at the Lavochkin Association and the Space Research Institute in Moscow built the spacecraft, which will be launched from a Russian naval submarine aboard a Volna rocket, a converted ICBM from the Cold War.

"Solar sails have come a long way in the last few years," says engineer Colin McInnes, a solar sail expert at the University of Strathclyde, U.K. At all the major space agencies, he says, scientists are pushing the technology as the only feasible form of propulsion for certain niche missions. "Now it needs the commitment to go to the next step," McInnes says. "Cosmos 1 can only do good."

Friedman got hooked on sails in the 1970s, while working on a team at NASA's Jet Propulsion Laboratory designing a solar sail mission to rendezvous with Halley's comet. That mission never got off the drawing board. But after co-founding the Planetary Society in 1980 with fellow space scientists Sagan and Bruce Murray to promote space exploration, Friedman got a second chance in 2000 thanks to Druyan, a member of the Planetary Society's board of directors. With money from Joe Firmage, a philanthropist who made a fortune in the 1990s Internet boom, Druyan formed Cosmos Studios and made Cosmos 1 its first project. "We could have a real launch, a place in the history of aeronautics, all for the cost of a Manhattan apartment," she says. Additional funding came from Peter Lewis, an insurance millionaire, and from the society's 100,000 members.

The society suffered a setback in 2001 when a practice run aboard a Volna, designed to test unfurling a sail, failed. The current launch date is 21 June, the summer solstice. If Cosmos 1 reaches its intended 825-kilometer orbit intact and is working properly, ground controllers in Moscow and at the society's headquarters in Pasadena, California, will start the mission. On command, inflatable booms will unfurl eight 15-meter-long triangular sails made of highly reflective Mylar plastic, creating a sail area of 600 square meters—some 1.5 times the size of a basketball court. The team hopes to see whether the pressure of photons bouncing off the sails will boost the craft to a higher orbit. "This has never before been done in controlled flight," says Friedman.

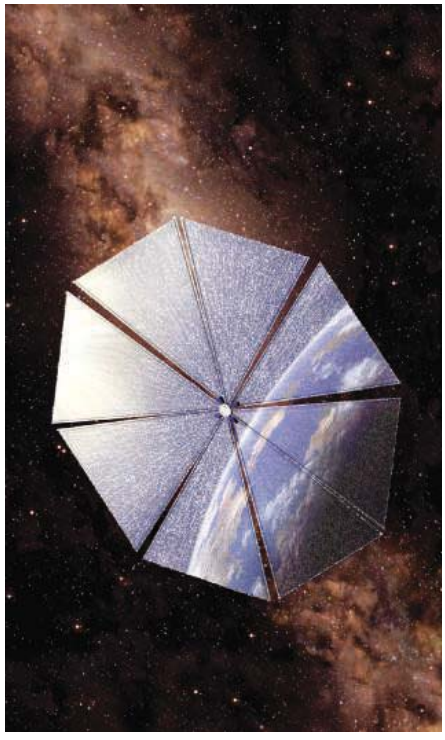

Sunny side up. Solar light pressure will push Cosmos 1 into a higher orbit and could propel future sail craft into interstellar space.

CREDIT: RICK STERNBACH/THE PLANETARY SOCIETY

Researchers at several space agencies are eager to follow in Cosmos's wake. In April, NASA and contractor ATK Space Systems tested a 20-meter solar sail in a huge vacuum chamber at NASA's Plum Brook facility in Sandusky, Ohio, and a second design from the company L'Garde will be tested later this month. A team led by Timothy Van Sant at NASA's Goddard Space Flight Center in Greenbelt, Maryland, is designing a demonstrator mission of a square sail 100 meters across that will compete for a launch slot in 2010.

The European Space Agency (ESA) is also banking on the technology in collaboration with DLR, Germany's space agency. Manfred Leipold of German contractor Kayser-Threde says that the agencies carried out a ground test of a 20-meter sail in 1999, and Leipold has since led a team that completed a design last year for a demonstrator mission in space. The mission is now awaiting a funding decision.

How did solar sails go from science-fiction favorite to must-have technology? The answer is thrust. Conventional spacecraft must carry all their fuel with them, and some missions are just too fuel-hungry. Although solar sails get only a feeble push from photons, it is unremitting and over time can build up to very high velocities. Researchers say sails are ideal for station-keeping: putting a satellite in one spot and using the sail's thrust to keep it in position. The National Oceanic and Atmospheric Administration is interested in using sails to station satellites above Earth's poles, where they can monitor the poorly understood polar climate, watch the moon and auroras around the clock, and even provide a phone link to researchers at the South Pole.

Other tempting applications include sending a probe to the sun and then pushing it into a polar orbit to observe the sun's higher regions. "This is very hard to do with conventional propulsion" because getting into a highly inclined orbit requires so much energy, says McInnes. A solar sail also may be the only way to travel for spacecraft headed far in the opposite direction, to the outer reaches of the solar system and into interstellar space. Leipold says ESA is studying such a mission to the heliopause, where the solar wind gives way to interstellar space. Its 250-meter-wide solar sail would boost its velocity to 50 kilometers/second, three times the speed of Voyager 1. NASA too would love to send a craft to deep space; its plans envisage a huge 400-meter-wide sail.

Such grand schemes may hinge on the small group of enthusiasts from the Planetary Society. Cosmos Studios has not been able to attract funding to film the preparations or launch, meaning that, as Druyan notes, "we haven't been able to make a dime off it." But McInnes says that solar sails should get a huge jump in credibility from the mission. "At meetings I can now put up slides with some real hardware," he says.

–DANIEL CLERY

Random Samples

Edited by Constance Holden

Bank on These Stamps

Some may be cautious about the promise of stem cell research, but not the South Korean post office. Even before Woo Suk Hwang and his team at Seoul National University announced the establishment of cell lines from cloned human embryos (*Science*, 20 May, p. 1096), the post office issued this stamp to celebrate his achievements. Last month Hwang said that by the end of the year he plans to set up a new stem cell bank in his country, one that would provide cells to researchers around the world.

A Boost for Aquaculture?

Submerged cages tethered to the sea floor house millions of fish.

The Bush Administration sent proposed legislation to Congress last week that would allow fish farmers to operate as far as 320 kilometers offshore, the boundary of the U.S. exclusive economic zone. Currently they are limited to state waters, which only extend to about 5 km from land.

"Nearly 70% of our seafood is imported, costing us about $40 billion," NOAA Administrator Conrad Lautenbacher noted at a press conference announcing the proposal. If the United States encourages large offshore aquaculture operations, which consist of gigantic submerged cages, it may help reduce this deficit and meet a growing global demand for seafood, which is projected to more than triple by 2025, he said.

Soul-Stirring Shales

Evolution seems to inspire the scientific soul, judging by entries in the "first annual evolution poetry contest" at the Society for the Study of Evolution (SSE). The winning poems, announced last week at a banquet at the SSE annual meeting in Fairbanks, Alaska, were selected from among 85 from seven countries, says SSE vice president Jessica Gurevitch of Stony Brook University in New York. One of the winners was Stanley Salthe of the University of Binghamton in New York, who composed:

Flat in the Wardie Shales

Flat in the Wardie Shales,
the Burdiehouse limestones,
pressed beneath the Pentland Oil Works and
in Pitcorthie in Fifeshire,
we have learned there lurk still
some of the first ones of us to come ashore on fours.

In stony waters, crumbling slabs of
frozen ripples near surfs
long extended in time as tunnels—
the roar of them unheard because uncompleted—
dainty Dolichopareias *was, and is, still,*
making a moveless step.
Also here in the measured coal swims Adelogyrinus,
its motion now too that of the earth itself only.

See how they have found the lower levels of energy
that fit them for the grander equations!

Computing: The Ultimate Challenge

Swiss researchers have teamed up with IBM to create the first computer model of the mammalian cerebral cortex.

It's a daunting task: Each of our 100 billion neurons can share synapses with as many as 10,000 others. But there's hope, believes Henry Markram, a neuroscientist at the École Polytechnique Fédérale in Lausanne, because of the uniformity of the brain's cortical architecture.

The neocortex, seat of higher cognitive functions, is built from about 1 million parallel columns of neurons. By modeling one of these cerebral building blocks, Markram's team hopes to scale up eventually to the entire cortex. "We are now at a crucial moment in the history of neuroscience where we can bring together 100 years of research into a single model," says Markram. He plans to do comparisons with rat brains to test the accuracy of the simulation.

Pyramidal neuron.

The project, dubbed "Blue Brain," will run on a superfast IBM machine about the size of four large refrigerators. The researchers are shooting for a model of a single cortical column within 3 years. Adding more will require either more computing power or finding a way to simplify the columns before duplication, says Markram.

"I worry that we might not yet understand the cortex well enough to make this work," says neuroscientist Colin Blakemore, chief of the U.K. Medical Research Council, but "it will be a success if it generates predictions [for] neurophysiology." In addition to modeling cortical functions, Blue Brain's designers envision it as an animal-free medical model—for example, to test new epilepsy drugs.

CREDITS (TOP TO BOTTOM): NOAA; IBM CORP.

PEOPLE

Edited by Yudhijit Bhattacharjee

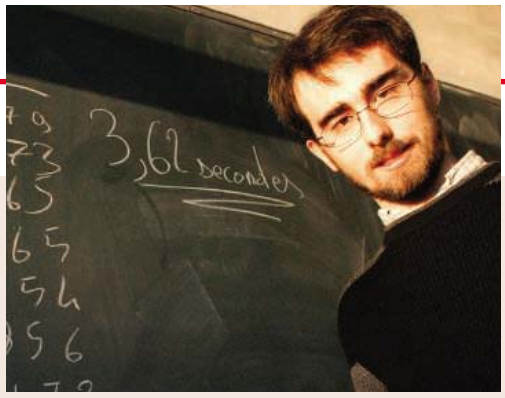

MILESTONES

Trade secret. A 24-year-old French informatics student has broken his own world record in mental calculation by extracting the 13th root of a 200-digit number. Alexis Lemaire of Reims performed the feat in 4:28 at a mathematics festival in Paris earlier this month. He broke his old record, set in April, by more than 4 minutes.

Aside from the obvious talent for rapid computation and an amazing memory, Lemaire uses an algorithm he developed but has only partially disclosed, says mathematician Jean-Paul Delahaye of Lille Science and Technology University, who was a witness at both events. "It would be very interesting to know how that works," says Delahaye, "because it is adapted to the human brain instead of a computer." Lemaire says he would like to set his next record in the United States. "In France almost everybody knows me now," he says. His winning answer: 2396280083911011.

AWARDS

Bountiful harvest. Indian fisheries scientist Modadugu Gupta, whose innovations have helped fuel fish production in developing countries, has won the $250,000 World Food Prize. The prize, founded by Nobelist Norman Borlaug, is awarded annually by the Des Moines, Iowa–based World Food Prize Foundation.

Responding to declining harvests due to pollution and overfishing, Gupta crossbred species with different feeding habits to create strains that could feed on all natural products, including farm waste such as chicken manure and rice bran. Raising these all-feeding varieties of fish in ponds has helped increase yields across India, Laos, Vietnam, and China.

The research coordinator for the World Fish Center in Penang, Malaysia, the 66-year-old Gupta is now studying the ecological impact of introducing his strains.

Got any tips for this page? E-mail people@aaas.org

Cancer Prizes. Pharmacologist Angela Brodie of the University of Maryland School of Medicine in Baltimore, biochemist Gerald Wogan of the Massachusetts Institute of Technology in Cambridge, and structural biologist Roger Kornberg of the Stanford School of Medicine in California are the winners of the 2005 General Motors Cancer Research Awards. Each will receive $250,000.

Shaw Prizes. A cell biologist, a mathematician, and two astronomers are the recipients of the $1 million Shaw Prizes awarded by the Hong Kong–based Shaw Prize Foundation. Michael Berridge of the Babraham Institute in Cambridge, U.K., receives the award for investigating the role of calcium signaling in regulating cellular activity. Andrew Wiles of Princeton University in New Jersey wins for his proof of Fermat's Last Theorem, and Geoffrey Marcy of the University of California, Berkeley, and Michel Mayor of the University of Geneva in Switzerland share $1 million for finding and characterizing the orbits and masses of extrasolar planets.

JOBS

Firm offer. Boston University has raided neighboring Massachusetts Institute of Technology (MIT) for its new president. The appointment of chemical engineer Robert Brown is aimed at calming the tumultuous leadership waters at the nation's fourth-largest private campus since longtime president John Silber retired in 2001. Silber's successor, Jon Westling, served only 18 months, and the trustees' next choice, former NASA Administrator Daniel Goldin, triggered such a row that he was asked to withdraw the day before he was to take office.

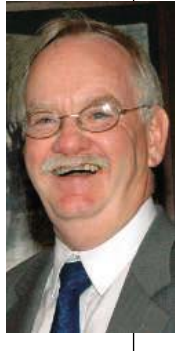

Brown, who has been MIT provost for 7 years, is unlikely to generate controversy. He was the search committee's only choice, says a BU press release, and his deep understanding of academia makes him "wonderfully suited to lead [BU's] broad community of scholars," says electrical engineer Roscoe Giles, chair of BU's faculty council. He takes office 1 September.

DATA POINT

Spreading the wealth. All boats were lifted by the recent doubling of the budget for the National Institutes of Health, new NIH data suggest.

Some observers had worried that the 1999–2003 doubling might have simply allowed an elite cadre of principal investigators (PIs) to expand their already large labs. But the new data show that the number of PIs rose steadily over the period, and the number of awards per PI barely changed (it went from 1.07 to 1.10). "There was a broader distribution of the funds than some might have imagined," says Howard Garrison, head of public affairs for the Federation of American Societies for Experimental Biology.

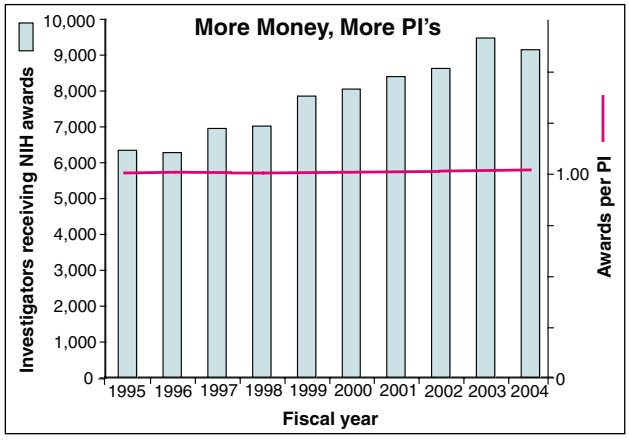

NIH's numbers also show that application success rates may be misleading. Although that rate dropped from more than 30% (during the doubling) to 25% in 2004, the success rate for grantees was 4 to 6 percentage points higher in each year. For more details, see table at www.sciencemag.org/sciext/news/061705.xls.

CREDITS (TOP TO BOTTOM): AFP/GETTY IMAGES; DONNA COVENEY/MIT

LETTERS

Retraction

THE REPORT "DEFECTIVE TRANSCRIPTION-coupled repair of oxidative base damage in Cockayne syndrome patients from XP group G" (*1*) is retracted. An ad hoc investigatory committee at the University of North Carolina at Chapel Hill has found that the last author (S.A.L.) of the paper "fabricated and falsified research findings" from an immunological assay for transcription-coupled repair. Three papers that were the subject of the investigation have been retracted. Although this paper was not implicated by the investigation, examination of the original data for Figs. 1 and 3 by P.K.C. indicates that the results of these experiments are not valid as reported in *Science*. Although some findings in the paper, notably those of Fig. 2, have been verified, the overall integrity of the paper cannot be supported by the presented results. We are therefore retracting the paper. The first three authors of the paper were not cognizant of any irregularities and were not involved in any wrongdoing. The fourth author (S.A.L.) declined to sign this retraction.

PRISCILLA K. COOPER,[1] THIERRY NOUSPIKEL,[2] STUART G. CLARKSON[3]

[1]Life Sciences Division, Lawrence Berkeley National Laboratory, Building 934, Berkeley, CA 94720, USA. [2]Department of Biological Sciences, Stanford University, Stanford, CA 94305, USA. [3]Department of Genetics and Microbiology, University Medical Center, 9 Avenue de Champel, 1211 Geneva 4, Switzerland.

Reference

1. P. K. Cooper, T. Nouspikel, S. G. Clarkson, S. A. Leadon, *Science* **275**, 990 (1997).

Reassessing U.S. Coral Reefs

ALTHOUGH WE AGREE WITH J. M. PANDOLFI *et al.*'s ("Are U.S. coral reefs on the slippery slope to slime?", Policy Forum, 18 Mar., p. 1725) vision of reversing coral reef declines where they exist (*1*), they have stretched the facts beyond reason in making their case. Certainly not all U.S. coral reefs are on a slippery slope to decline (*2*).

The claim that Hawaiian reefs are seriously degraded is misleading. Actually, a large majority of Hawaiian reefs are surprisingly healthy. Results have shown that over the last 30 years, open coastal reefs in Hawaii show essentially no effect of pollution (*3*). In addition, the $9-million "Mamala Bay Study" completed several years ago showed no impacts to reefs on the southern shore of Oahu, Hawaii's most populated island (*4*). Even though most of the Main Hawaiian Island reefs are overfished (*5*), the vast majority of these have not been replaced by algal communities (algal phase shifts) as purported by these authors (*6*).

In addition, many of the authors' comments on the Northwestern Hawaiian Islands (NWHI) are simply wrong. Green turtles have increased about 500% in recent decades, and monk seals are starting to invade the high Hawaiian Islands (*7*). Also, marine debris, although abundant and unsightly, has little overall impact on the corals themselves. Lead and PCB contaminants may exist in a few locales [at Midway Atoll (the Harbor and some debris left over from World War II)], but their impact on the reefs is negligible. With the exception of some selected fisheries, the reefs in the NWHI remain relatively pristine (*8*).

Yes, we can do a far better job of protecting our reefs, but let's focus our energy where it is needed most, on those reefs that are actually in trouble (*9*).

RICHARD W. GRIGG* AND STEVEN J. DOLLAR

Department of Oceanography, University of Hawai`i at Manoa, Marine Sciences Building, 1000 Pope Road, Honolulu, HI 96822, USA.

*To whom correspondence should be addressed. Email: rgrigg@soest.hawaii.edu

References

1. R. W. Grigg, S. J. Dollar, in *Coral Reefs*, vol. 25, *Ecosystems of the World*, Z. Dubinsky, Ed. (Elsevier, Amsterdam, 1990), pp. 439–452.
2. S. L. Miller, M. P. Crosby, in *NOAA's State of the Coast Report* (National Oceanic and Atmospheric Administration, Silver Spring, MD, 1999), pp. 1–34.
3. S. J. Dollar, R. W. Grigg, *Pac. Sci.* **58** (no. 2), 281 (2004).
4. Environment Hawai'i, Mamala Bay Study Commission Issues Draft Report on Coastal Pollution, www.environment-hawaii.org/1295cov.htm (1995).
5. A. M. Friedlander, E. E. DeMartini, *Mar. Ecol. Prog. Ser.* **230**, 253 (2002).
6. R. W. Grigg, in *Status of Coral Reefs of the Pacific*, R. W. Grigg, C. Birkeland, Eds. (University of Hawaii Sea Grant College Program, Honolulu, HI, 1997), pp. 61–72.
7. J. D. Baker, T. C. Johanos, *Biol. Conserv.* **116**, 103 (2004).
8. J. Maragos, D. Gulko, in *Coral Reef Ecosystems of the Northwestern Hawaiian Islands* (U.S. Fish and Wildlife Service and Hawai'i Department of Land and Natural Resources, Honolulu, HI, 2002), pp. 38–42.
9. R. W. Grigg, *Coral Reefs* **11**, 183 (1992).

LIKE J. M. PANDOLFI *ET AL.*, WE BELIEVE THAT coral reefs in the United States and elsewhere are facing serious threats and that it is in society's interest to protect them ("Are U.S. coral reefs on the slippery slope to slime?", by J. M. Pandolfi *et al.*, Policy Forum, 18 Mar., p. 1725). However, we were struck by the admonition that "scientists should stop arguing about the relative importance of different causes of coral reef decline." Although we agree that arguing is unproductive, it is surely the case that effective conservation requires an understanding of the relative importance of different causes of decline. A reef threatened by fishing requires different protective measures than a reef threatened by eutrophication, and there is clear value in understanding the nature of the threat. "Don't just stand there, do something" is not a prescription for conservation success.

A brown spotted eel hides in the coral reef of Kealakekua Bay on the Kona coast of the island of Hawaii.

CREDIT: JAY SYVERSON/CORBIS

AMIT HUPPERT

Department of Zoology, Tel-Aviv University, Tel Aviv 69978, Israel.

THE POLICY FORUM "ARE U.S. CORAL REEFS on the slippery slope to slime?" by J. M. Pandolfi *et al.* inaccurately characterizes the management approach of Florida Keys National Marine Sanctuary (FKNMS) and contains factual errors.

The Policy Forum states that managers must address multiple threats and employ an ecosystem management approach if we are to halt coral reef decline. For over 10 years, the FKNMS has employed just such an approach through a management plan that addresses local and regional threats ranging from poor water quality to direct damage from vessel groundings and anchors.

Part of the plan involves marine zoning that sets aside 6% of the FKNMS as no-take and is showing successes for spiny lobster,

snapper, and grouper. Contrary to the authors' assertions, these zones are strategically located. The 18 Sanctuary Preservation Areas protect more than 65% of the shallow spur and groove formations or bank reef formations. The two Ecological Reserves protect a variety of habitats, chosen to include spawning sites, current patterns, and other desirable ecological characteristics.

Water quality protection is an essential component of FKNMS management, and improvements to wastewater and stormwater treatment are progressing steadily. The authors ignore these advancements, which include deep well injection of highly treated wastewater in Key West, a Keys-wide no-discharge zone, and continuing replacement of substandard on-site systems.

We agree that we must review the full suite of issues in developing research and management plans. In fact, lessons learned within the Florida Keys National Marine Sanctuary are now serving as a larger model for ecosystem-based approaches within the National Oceanic and Atmospheric Administration.

BILLY D. CAUSEY[1] AND KATHERINE ANDREWS[2]*

[1]Superintendent, Florida Keys National Marine Sanctuary, National Oceanic and Atmospheric Administration, Post Office Box 500368, Marathon, FL 33050, USA. [2]Florida Department of Environmental Protection, Majory Stoneman Douglas Building, 3900 Commonwealth Boulevard, Tallahassee, FL 32399–3000, USA.

*Co-Trustee, Florida Keys National Marine Sanctuary

THE POLICY FORUM "ARE U.S. CORAL REEFS on the slippery slope to slime?" by J. M. Pandolfi *et al.* (18 Mar., p. 1725) stresses that the decline of coral reefs worldwide is due to multiple stresses that must be simultaneously reduced and that poor water quality is a contributing factor. There are mistakes and serious omissions that may lead readers to believe that very little is being done to correct water quality problems in the Florida Keys.

As required by the Florida Keys National Marine Sanctuary and Protection Act, a Water Quality Protection Program was developed that includes a comprehensive action plan. Since 1997, 26 of 49 high-priority activities have been fully implemented, including establishment of a long-term monitoring program on water quality, seagrass, and corals. Sanitary Wastewater and Storm Water Master Plans have been completed for Monroe County, and wastewater facility plans have been completed for Marathon and other municipalities.

State Law 99-395 requires all wastewater facilities in the Keys, including on-site systems, to upgrade treatment by 2010. Much progress has been made to achieve that requirement. The City of Key West has upgraded its sewage treatment plant to advanced wastewater treatment (AWT) standards and has replaced old, leaky collection pipes. A new neighborhood AWT plant is operating in the City of Marathon and treats wastes from approximately 500 homes previously "served" by cesspools or septic tanks. (Approximately 4000 cesspools have been identified in the Keys, not 16,000, as stated by Pandolfi *et al.*) Four other municipalities have such facilities planned or under construction. Also, in 2002, all state waters in the Florida Keys were declared a no-discharge zone for boat-generated sewage.

The Florida Keys Water Quality Improvement Act authorized Congress to appropriate $100 million for the wastewater and storm water improvements in Monroe County, and last year the state provided approximately $12 million. Obviously, much more needs to be done, but stressing the real progress made thus far is critical to keeping the money flowing.

WILLIAM L. KRUCZYNSKI

Program Scientist, Florida Keys National Marine Sanctuary, Water Quality Protection Program, U.S. Environmental Protection Agency, Post Office Box 500368, Marathon, FL 33050, USA.

IN THEIR POLICY FORUM "ARE U.S. CORAL reefs on the slippery slope to slime?" (18 Mar., p. 1725), J. M. Pandolfi *et al.* conclude that all threats to coral reefs must be addressed simultaneously to reverse coral decline. This is not a new recommendation (*1*), nor is it particularly useful to managers who need more from scientists than a call to address everything, everywhere. The authors offer a remedy (*2*–*5*) by suggesting that corals become resilient when food webs are restored and eutrophication controlled. In fact, studies of marine protected areas offer conflicting results as to how corals respond to protection (*6*).

Florida's reefs are incorrectly characterized by the authors as so polluted and overfished that they cannot recover under current levels of protection. In reality, there is no compelling evidence that coral decline or recovery was caused or hindered by pollution and overfishing (*7*). The ongoing, catastrophic decline of corals in Florida has been the product of pandemic coral diseases, winter cold fronts, hurricanes, and coral bleaching (*7*).

The idea that we can somehow manage for resilience holds false promise against the ongoing threat of regional and global-scale stressors (*8*). There are sufficient ecologic and economic reasons to manage fisheries better (*9*), and likewise there are significant public-health and economic reasons to reduce pollution. Unfortunately, global-scale coral stressors, such as disease and global warming, still threaten our reefs (*10*).

Today's ecology matters just as much as history does, and Pandolfi *et al.*'s recommendation "that scientists should stop arguing about the relative importance of different causes of coral reef decline" is misguided. Debate over the mechanisms of coral decline and recovery is both healthy and critical to the success of management. We strongly agree with the authors that "slowing or reversing global warming trends is essential for the long-term health of all tropical coral reefs." Disagreement among coral reef scientists, however, is not what is holding governments back from taking steps to address global environmental problems.

WILLIAM F. PRECHT,[1]* STEVEN L. MILLER,[2] RICHARD B. ARONSON,[3] JOHN F. BRUNO,[4] LES KAUFMAN[5]

[1]Ecological Sciences Program, PBS&J, 2001 NW 107th Avenue, Miami, FL 33172, USA. [2]Center for Marine Science, University of North Carolina Wilmington, 5600 Marvin Moss Lane, Wilmington, NC 28409, USA. [3]Dauphin Island Sea Lab, 101 Bienville Boulevard, Dauphin Island, AL 36528, USA. [4]Department of Marine Sciences, University of North Carolina at Chapel Hill, CB #3300, 12-2 Venable Hall, Chapel Hill, NC 27599–3300, USA. [5]Department of Biology, Boston University, 5 Cummington Street, Boston, MA 02215, USA.

*To whom correspondence should be addressed. E-mail: Bprecht@pbsj.com

References

1. R. W. Grigg, S. J. Dollar, in *Coral Reefs*, vol. 25, *Ecosystems of the World*, Z. Dubinsky, Ed. (Elsevier, Amsterdam, 1990), pp. 439–452.
2. J. B. C. Jackson *et al.*, *Science* **293**, 629 (2001).
3. J. B. C. Jackson, E. Sala, *Sci. Mar.* **65** (no. 2), 273 (2001).
4. J. M. Pandolfi *et al.*, *Science* **301**, 955 (2003).
5. D. R. Bellwood *et al.*, *Nature* **429**, 827 (2004).
6. T. McClanahan *et al.*, *Conserv. Ecol.* **6** (no. 2), 18 (2002) (available at www.consecol.org/vol6/iss2/art18).
7. W. F. Precht, S. L. Miller, in *Geological Approaches to Coral Reef Ecology*, R. B. Aronson, Ed. (Springer Verlag, New York, in press).
8. G. P. Jones *et al.*, *Proc. Natl. Acad. Sci. U.S.A.* **101**, 8253 (2004).
9. E. K. Pikitch *et al.*, *Science* **305**, 346 (2004).
10. R. W. Buddemeier *et al.*, *Coral Reefs & Global Climate Change* (Pew Center on Global Climate Change, Arlington, VA, 2004).

Response

THE DECLINE OF U.S. CORAL REEFS IS A GROW- ing crisis that scientists have failed to communicate effectively to the public. For over 40 years, research has implicated four major human causes of coral reef decline—fishing, land-based pollution, coastal development, and global climate change—and has identified their debilitating effects, such as coral disease and coral bleaching (*1*–*4*). The relative importance of these different factors naturally varies from place to place, and we agree that this is sometimes not obvious and may be important to resolve. The precautionary principle clearly dictates that we should not wait for conclusive evidence as to which of the four human disturbances has the biggest impact before action is taken. We will not obtain that evi-

dence for many years or even decades. Nevertheless, we can immediately reduce fishing, land-based pollution, and coastal development; coping with climate change will require global action at the highest levels of government (*5*, *6*).

Historical analysis provides a compelling picture of the problem of shifting baselines (*7*, *8*) that lulls us into a false sense of security. Shifting baselines are especially problematic for places like the Northwest Hawaiian Islands and the Great Barrier Reef, where many reefs are in comparatively good shape but significant threats remain [(*9*); figure in our Policy Forum]. History also provides a clear roadmap for setting objective goals and criteria to assess the success of management options. The Florida Keys National Marine Sanctuary management plan contains comprehensive strategies for addressing fishing, land-based pollution, and coastal development (*10*). However, we need to remember that the goal is not the drafting of a plan, but rather the reversal of coral reef decline. Nearly 8 years after initiation of the plan, only 6% of the Florida Keys Sanctuary is fully protected from fishing and other extractive activities in marine reserves. This meager level of protection compares poorly with the 33% protection afforded to the entire Great Barrier Reef, which is in vastly better ecological condition [(*11*); our figure]. Moreover, with the notable exception of the Tortugas Ecological Reserve, reserves in the Keys are far too small to be effective.

Water quality controls are contentious, politically sensitive, and expensive, and the science concerning potential impacts of sewage-based nutrients on coral reefs is often equivocal. In the Keys, nutrient issues have been confounded by potential offshore nutrient sources due to upwelling (*12*). But upwelling, like hurricanes and cold fronts that are invoked as causes of degradation, are natural processes that reefs have survived for millions of years. What is different today is the ever-increasing and universal impact of people (*13*), as exemplified most recently by global climate change. A significant percentage of the more than 20,000 on-site wastewater systems in the Keys were permitted in the 1980s or earlier when there was little concern for water quality (*14*). Adequate funding to deal with this issue has not been appropriated, and the retrofit of these systems to alternative methods is proceeding inexcusably slowly.

No one likes to hear bad news, but it is a fact that the condition of most U.S. coral reefs is rapidly deteriorating and that nowhere remains pristine. We need to wake up fast to the true magnitude of the challenges we are facing to save our reefs by quickly following the Australian example of vastly increased protection and by implementing more comprehensive management. At the imminent risk of losing our reefs forever, how can we do otherwise?

JEREMY B. C. JACKSON,[1,2]* JOHN C. OGDEN,[3] JOHN M. PANDOLFI,[4] NANCY BARON,[6] ROGER H. BRADBURY,[7] HECTOR M. GUZMAN,[2] TERENCE P. HUGHES,[8] CARRIE V. KAPPEL,[9] FIORENZA MICHELI,[9] HUGH P. POSSINGHAM,[5] ENRIC SALA[1]

[1]Center for Marine Biodiversity and Conservation, Scripps Institution of Oceanography, La Jolla, CA, 92093, USA. [2]Smithsonian Tropical Research Institute, Box 2072, Balboa, Republic of Panama. [3]Florida Institute of Oceanography, St. Petersburg, FL 33701, USA. [4]Centre for Marine Studies and Department of Earth Sciences, [5]Department of Mathematics and School of Life Sciences, University of Queensland, St. Lucia, QLD 4072, Australia. [6]National Center for Ecological Analysis and Synthesis, Santa Barbara, CA 93101, USA. [7]Australian National University, Canberra, ACT 0200, Australia. [8]Centre for Coral Reef Biodiversity, School of Marine Biology, James Cook University, Townsville, QLD 4811, Australia. [9]Hopkins Marine Station, Stanford University, Stanford, CA 93950–3094, USA.

References

1. D. Bryant *et al.*, *Reefs at Risk. A Map-Based Indicator of Threats to the World's Coral Reefs* (World Resources Institute, Washington, DC, 1998).
2. C. R. Wilkinson, *Status of Coral Reefs of the World: 2004* (Global Coral Reef Monitoring Network and Australian Institute of Marine Science, Townsville, Australia, in press) (vol. 1 is available at www.gcrmn.org/status2004.asp).
3. T. A. Gardner *et al.*, *Science* **301**, 958 (2003).
4. D. R. Bellwood, T. P. Hughes, C. Folke, M. Nyström, *Nature* **429**, 827 (2004).
5. N. Knowlton, *Proc. Natl. Acad. Sci. U.S.A.* **98**, 5419 (2001).
6. T. P. Hughes *et al.*, *Science* **301**, 929 (2003).
7. D. Pauly, *Trends Ecol. Evol.* **10**, 430 (1995).
8. J. B. C. Jackson *et al.*, *Science* **293**, 629 (2001).
9. C. Safina, *Eye of the Albatross* (Holt, New York, 2003).
10. Florida Keys National Marine Sanctuary, Draft Revised Management Plan (Department of Commerce, National Oceanic and Atmospheric Administration, National Marine Sanctuary Program, Washington, DC, Feb. 2005), pp. 1–361.
11. Great Barrier Reef Marine Park Authority, New Policy Web Site, www.gbrmpa.gov.au/corp_site/management/zoning/zoning_publications.html.
12. J. J. Leichter, H. L. Stewart, S. L. Miller, *Limnol. Oceanogr.* **48**, 1394 (2003).
13. S. R. Palumbi, *Nature* **434**, 713 (2005).
14. G. Garrett, Director, Monroe County Marine Resources Department, personal communication.

Written in Our Genes?

IN 1983, LANGSTON AND COLLEAGUES reported that accidental exposure of humans to 1-methyl-4-phenyl-1,2,3,6-tetrahydropyridine (MPTP) induces a Parkinsonian state (*1*, *2*). The authors hypothesized that damage to the substantia nigra might reflect a selective toxicity of MPTP for dopaminergic neurons. In the two decades since that initial report, a large body of evidence has accumulated to support this hypothesis. The mechanism of cell death appears to involve the selective uptake by dopaminergic neurons of the toxic MPTP metabolite 1-methyl-4-phenylpyridinium (MPP+). Dopaminergic neurons, such as the ones that populate the substantia nigra, are generally identified by the presence of tyrosine hydroxylase, the enzyme that catalyzes the first and rate-limiting step in the conversion of tyrosine to dopamine. Remarkably, the intimate connection between MPTP and dopaminergic neurons is immediately evident from a cursory perusal of the primary sequences of human, mouse, or rat tyrosine hydroxylase, each of which begins with the NH_2-terminal sequence methionine-proline-threonine-proline… (MPTP… in the single letter amino acid code) (*3*). Once again, an answer appears to be written in our genes—in this case, with unusual clarity.

JEREMY NATHANS

Howard Hughes Medical Institute, Department of Molecular Biology and Genetics, Johns Hopkins Medical School, 735 North Wolfe Street, Room 805 PCTB, Baltimore, MD 21205–2185, USA.

References

1. J. W. Langston, P. Ballard, J. W. Tetrud, I. Irwin, *Science* **219**, 979 (1983).
2. J. W. Langston, P. Ballard, *N. Eng. J. Med.* **309**, 310 (1983).
3. S. Ichikawa, T. Sasaoka, T. Nagatsu, *Biochem. Biophys. Res. Commun.* **176**, 1610 (1991).

Letters to the Editor

Letters (~300 words) discuss material published in *Science* in the previous 6 months or issues of general interest. They can be submitted through the Web (www.submit2science.org) or by regular mail (1200 New York Ave., NW, Washington, DC 20005, USA). Letters are not acknowledged upon receipt, nor are authors generally consulted before publication. Whether published in full or in part, letters are subject to editing for clarity and space.

CORRECTIONS AND CLARIFICATIONS

Random Samples: "Skyward" (6 May, p. 789). Due to a reporting error, Faith Vilas was incorrectly described as having been a high school science teacher earlier in her career. Also, Vilas has had extensive experience with telescopes in recent years.

Editors' Choice: "Food preservative" (1 Apr., p. 19). The *Streptomyces* bacteria supplied by the female beewolf protects its larva, and not the immobilized honeybee, from infection by fungi.

Essays: "When science is not enough: fighting genetic disease in Brazil" by M. Zatz (1 Apr., p. 55). The first sentence of the Essay is incorrect. It should read, "In my country, Brazil, one among five babies who die in the first year of life have a gene-related disorder."

Policy Forum: "Are U.S. coral reefs on the slippery slope to slime?" by J. M. Pandolfi *et al.* (18 Mar., p. 1725). In the bottom figure on p. 1725, Caribbean sites are purple (not green, as described in the legend), and some data points are not seen because of superimposed dots. Otherwise, the labels point to the dots in order. For example, the Bahamas and

eastern Panamá are represented by the purple dot partly showing above the red dot for the Main Hawaiian islands and Florida Keys. The lettering for the Outer Great Barrier Reef (Outer GBR) should be black.

Reports: "BZR1 is a trancriptional repressor with dual roles in brassinosteroid homeostasis and growth responses" by J.-X. He *et al.* (11 Mar., p. 1634). There was an error in the Fig. 3C legend. The sentence that reads, "Dots indicate BR-induced genes and crosses indicate BR-repressed genes" is incorrect. It should read, "Crosses indicate BR-induced genes, and dots indicate BR-repressed genes."

Reports: "The geometric distance and proper motion of the Triangulum Galaxy (M33)" by A. Brunthaler *et al.* (4 Mar., p. 1440). The credit in the legend for Fig. 1 should read "{Image courtesy of T. A. Rector [National Radio Astronomy Observatory (NRAO)/Associated Universities, Inc. (AUI)/NSF and National Optical Astronomy Observatory/Association of Universities for Research in Astronomy/NSF], D. Thilker (NRAO/AUI/NSF), and R. Braun (ASTRON).}" In addition, the second-last sentence of the first paragraph of the paper (p. 1440) ("This pushed…") should have been deleted.

Brevia: "Membrane insertion of a potassium-channel voltage sensor" by T. Hessa *et al.* (4 Mar., p. 1427). The correct URL for the supporting online material is www.sciencemag.org/cgi/content/full/1109176/DC1.

TECHNICAL COMMENT ABSTRACTS

COMMENT ON "The Oceanic Sink for Anthropogenic CO_2"

Ralph F. Keeling

The inventory of anthropogenic CO_2 in the ocean, estimated by Sabine *et al.* (Research Articles, 16 July 2004, p. 367), is an imperfect measure of the change in ocean carbon because it neglects the impact of recent warming on ocean chemistry and circulation. Allowing for warming, the change in ocean carbon is likely ~6% smaller than estimated, although uncertainties in the correction are large.
Full text at
www.sciencemag.org/cgi/content/full/308/5729/1743a

RESPONSE TO COMMENT ON "The Oceanic Sink for Anthropogenic CO_2"

Christopher Sabine, Nicolas Gruber

We argue that our estimate of anthropogenic CO_2 inventory is insensitive to changes in ocean circulation and heat content and warrants no adjustments. Carbon-climate feedbacks may have also altered ocean carbon content, but the proposed correction is too tentative and within the published uncertainty of the current estimate. Nevertheless, this discussion highlights the need for continuing oceanic observations.
Full text at
www.sciencemag.org/cgi/content/full/308/5729/1743b

COMMENT ON "Inflammatory Exposure and Historical Changes in Human Life-Spans"

Elisabetta Barbi and James W. Vaupel

Finch and Crimmins (Reviews, 17 Sep. 2004, p.1736) claim that analysis of Swedish data "reveals strong associations between early-age mortality and subsequent mortality in the same cohorts." However, these associations are modest and period effects have generally been more important than cohort effects. Future trends in life expectancy are unlikely to be slow merely because early-life mortality is now low.
Full text at
www.sciencemag.org/cgi/content/full/308/5729/1743c

RESPONSE TO COMMENT ON "Inflammatory Exposure and Historical Changes in Human Life-Spans"

Caleb E. Finch and Eileen M. Crimmins

In environments with high levels of infection, we hypothesize that inflammatory pathophysiology is a strong mechanistic link between early and later cohort mortality and morbidity. Using historical Swedish data, we show that cohort effects are stronger than period effects in associations of early and old age mortality. We argue that Barbi and Vaupel did not choose appropriate tests of our hypothesis.
Full text at
www.sciencemag.org/cgi/content/full/308/5729/1743d

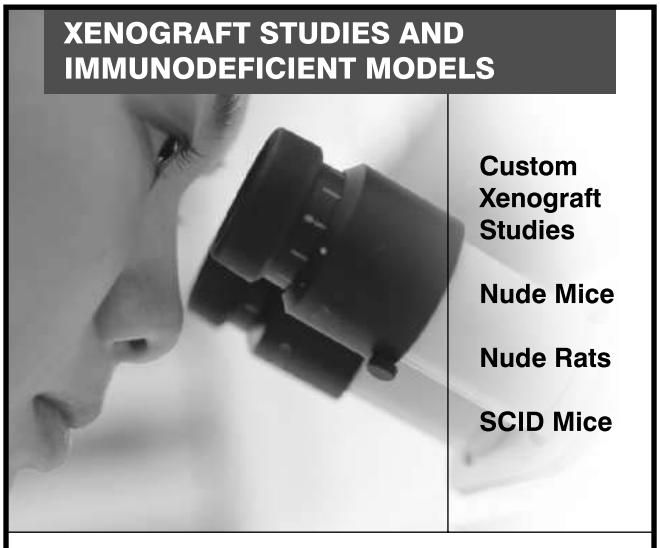

MEDICINE

Vanquishing the Terror of Poliomyelitis

Mark Pallansch

A half-century ago, on 12 April 1955, many in the United States paused to read the news out of Ann Arbor, Michigan, that a vaccine against polio developed in the laboratories of Jonas Salk had proved successful. The celebrations on that spring day have been recalled in commemorative ceremonies this year, and three recent books examine the very different country that then breathed a collective sigh of relief at the prospect that the seasonal fear of random affliction might soon end. Viewed in the global context, the story of polio's demise is in many ways unfinished. But these well-researched narratives demonstrate the extent of the changes since the first half of the 20th century, when fears of polio gripped the United States. The authors describe the suffering and determination of the paralyzed along with the efforts of the researchers, volunteers, and donors who fought against the disease. Although an entire generation still vividly remembers the dread of polio, younger people have only passing awareness of this viral plague.

Polio
An American Story
by David M. Oshinsky

Oxford University Press, New York, 2005. 340 pp. $30, £18.99. ISBN 0-19-515294-8.

Splendid Solution
Jonas Salk and the Conquest of Polio
by Jeffrey Kluger

Putnam, New York, 2004. 381 pp. $25.95, C$38. ISBN 0-399-15216-4.

Living with Polio
The Epidemic and Its Survivors
by Daniel J. Wilson

University of Chicago Press, Chicago, 2005. 300 pp. $29, £20.50. ISBN 0-226-90103-3.

In *Polio: An American Story*, David Oshinsky (a historian of modern U.S. politics and society at the University of Texas, Austin) offers an easily approachable yet factually rich narrative. Discussing the key events and characters that shaped the steady progression of the scientific search for a vaccine to vanquish polio, Oshinsky places them in the social context of the times. By weaving together the threads of stories of afflicted individuals, affected communities, and effective leaders while also chronicling the establishment of the organizations that championed the fight against the disease, he provides a solid backdrop for the philanthropic and scientific efforts. His portrait of the disease starts with a description of the impact a summer outbreak of polio had on the community of San Angelo, Texas, in 1949. Throughout the book, he emphasizes the burden polio placed on individuals and families. (For example, in the summer of 1952, polio infected 11 of the 14 children in the Thiel family of Mapleton, Iowa; none died, but two were left paralyzed.) Oshinsky also outlines the course of polio in the United States through the 20th century. He describes the increasing incidence of the disease from very low levels at the turn of the century, through the first notable outbreaks in 1907 and 1916, to the very large and widespread outbreaks in the 1940s and 1950s. And he records the decline and eventual disappearance of polio from the country following the introductions for routine use of first the Salk vaccine (in 1955) and then the Sabin vaccine (in 1962).

Using the building burdens of the disease as reference points, Oshinsky spends much of his book describing the intricate web of individuals behind the success of the polio vaccines. He does not ignore the big names, but far more interesting are the many lesser-known individuals who played important roles (both scientific and organizational) at critical junctures in the venture. The author traces the links that led from Franklin Roosevelt's affliction with polio in 1921 through a law partnership in New York; Democratic politics in that state; an ill-advised real estate investment in Warm Springs, Georgia; and ultimately to the creation of the National Foundation for Infantile Paralysis. Oshinsky highlights the stories of that foundation, its fund-raising arm (the March of Dimes), and the crucial leadership of its first director, Basil O'Connor—who welded quite disparate personalities to the common purpose of fighting polio. Relating the nearly constant tensions that affected the various participants, the author makes it clear that success was far from certain. Another major narrative thread in *Polio* concerns the scientific challenges faced by those trying to unravel the mysteries of the viruses. This account spares nonvirologists from intimidating scientific complexity while including enough details to successfully avoid the trap of oversimplification. Skillfully intertwining these multiple aspects of one of the 20th century's major medical successes, Oshinsky provides a very readable and enlightening history that also can be appreciated as good storytelling.

To stop transmission. During polio epidemics, communities attempted to deny entry to children who might have been exposed to the virus.

CREDIT: MARCH OF DIMES BIRTH DEFECTS FOUNDATION

In *Splendid Solution: Jonas Salk and the Conquest of Polio*, Jeffrey Kluger provides a distinctly biographical rendition of part of the same story. Through his focus on Salk's life, Kluger (a senior writer at *Time* magazine) reveals in more detail the individuals who most closely influenced and interacted with the scientist credited with the first licensed polio vaccine. The book stays close to the strand of the polio story that begins with Salk (not yet two years old) living through the New York polio outbreak of 1916 and continues until the use of his vaccine becomes routine, 40 years later. Kluger offers many fascinating details about the difficulties of Salk's childhood and schooling (which were probably not unusual for children of immigrant families in New York at the time) as well as some of the events that seemed to affect his life course, such as the shift to medicine after a brief dalliance with law. One point that surfaces in the author's account of Salk's professional life, and that is often forgotten today, is that Salk spent much of his early career as a distinct

The reviewer is in the Division of Viral and Rickettsial Diseases, Centers for Disease Control and Prevention, 1600 Clifton Road, NE, Mailstop G17, Atlanta, GA 30333, USA. E-mail: map1@cdc.gov

junior to many of his contemporaries who were working on the development of a polio vaccine. Kluger emphasizes the need for professional deference that he sees in Salk's writings to competitors and collaborators throughout the decade after he completed his medical internship in 1942. It is easy to conclude, as the author infers, that at least some of the disparagement Salk received from contemporaries derived from the appearance of impertinence from a junior scientist. However, the many anecdotes related in the book make it clear that, early in his career, Salk was fairly cautious and reluctant to deliberately create problems even if he was sometimes oblivious to the consequences of his actions.

Through the use of a variety of sources, including some from Salk's immediate family, Kluger attempts to provide some insight into the man behind the vaccine. This approach gives the reader much more understanding about the forces that affected Salk's life but almost increases the chasm between the accomplishments and the individual. Very few of the anecdotes actually help us to better understand the man. Instead, we are left wondering why the house in the country in Michigan was important. Why was professional independence so important to Salk in 1947 that he left a successful lab for a hospital basement and loose promises? Why did Salk fail to acknowledge the members of his own laboratory on that April day in 1955 when attention shown so brightly on him?

In contrast, the anecdotes and Kluger's account reveal one personality trait that was very evident in Salk—his conviction, particularly about the correctness of his professional judgment that an inactivated vaccine was not only possible but superior:

> For the rest of Salk's life, he would never see the argument between the live and killed factions fully settled. As he got older, he liked to say that when you're arguing for an unpopular idea, there are three stages of truth. First your opponents say it can't be true. Next they say if it's true, it can't be very important. Finally they say well, we've known it all along. Salk did not always make that point without anger, but in fact he came to long for stage three, if only because it would mean that his ideas had been universally accepted.

It is nearly certain that Salk's success can be largely credited to his unwavering belief that his vaccine would work. That Kluger chose to move rapidly through Salk's career after the acceptance of the killed vaccine in 1955 illustrates the perplexity of the story. The complex man at the center of the development of the first successful polio vaccine still elicits a diversity of opinions, many of them captured in *Splendid Solution*. Nevertheless, his accomplishments in the space of eight years after he arrived at the University of Pittsburgh are undeniable. Salk was at the center of the successful efforts—by him and his colleagues—that led to the rapid decline in the number of new polio cases arriving at hospitals. It is that change for which he will be remembered.

Complementing the accounts Oshinsky and Kluger provide of research on polio vaccines, Daniel J. Wilson paints a very personal portrait of the victims of poliovirus in the United States during the decades of the 1940s and 1950s in *Living with Polio*. Wilson, a historian at Muhlenberg College who was himself struck by the disease, has explored a large range of accounts by polio survivors: written narratives, oral histories, and Internet postings. Avoiding a mere compendium of such works, he instead creates a synthesis that reflects both the commonality and the variability of the experiences of polio victims during the height of the mid-century outbreaks in the United States.

Protecting Protection. In April 1957, people lined up at the Protection, Kansas, high school for inoculations with the Salk vaccine.

CREDIT: MARCH OF DIMES BIRTH DEFECTS FOUNDATION

The book overlooks very few aspects of the course of the disease. Wilson organizes the various narratives around a chronological progression of the disease and whatever recovery and rehabilitation were possible. He begins with the first onset of symptoms, including the fever, pain, and the earliest recognition that one's limbs are no longer functioning properly. Then he turns to the initial hospitalization and the time when the diagnosis of polio was made. The author examines these and the remaining experiences not only for the physical symptoms but also for the psychological impacts, particularly as affected by the victim's age, sex, and race. Wilson continues through stories of extended hospitalization and separation from family and of the extreme challenges of rehabilitation. He also documents the substantial effect the severity of paralysis had on the ability of patients and families to adjust when the patient returns home and attempts to reintegrate into the nonparalyzed world of family, friends, community, and work.

By interweaving the stories of specific individuals at comparable stages of their affliction, Wilson clarifies both the experiences shared by many victims and the differences—particularly in the consequences of polio and adaptations to it. By the end of the book, one has gained a vicarious acquaintance with those whose accounts the author has mined, and Wilson, in always referring to his sources by name, establishes personal connections with them while maintaining the objectivity of his work. For readers who (like me) did not live during the prevaccine period, *Living with Polio* provides an excellent survey of the stories of those who had the misfortune of being struck by the disease. The accounts also demonstrate that the effects of the virus extended well beyond the paralyzed victims. As Wilson comments on the experiences of Kathryn Black,

> It was "pointless to try to decide whether the agony of a child who loses her mother is worse than the devastation of a mother who loses her child." Black's story and the stories of those other spouses and children who lived with polio forcefully remind us that polio not only changed the lives of those who had the illness, it also affected the lives of all the family and friends who came in contact with the disease.

Much is gained when the tale of a disease and its control can be approached from several perspectives. Individually, these three books emphasize respectively the powerful individuals and institutions in American society that confronted the challenge of polio, the efforts of one researcher, and the points of view of the virus's victims. Together, they provide many insights into the eradication of poliovirus in the United States—the first step toward its subsequent elimination from much of the world.

10.1126/science.1111459

FILM: HISTORY OF SCIENCE

Nature's Beauty and Haeckel's Talents

Manfred Laubichler

All art should become science and all science art; poetry and philosophy should be made one. —Friedrich Schlegel (*1*)

Proteus, written and directed by award-winning documentary filmmaker David Lebrun, presents a 19th-century vision of the age-old quest to grasp nature and her creative powers. In the 19th century, with Earth's surface mostly mapped and the readily visible life forms largely described and cataloged, the quest to understand nature turned inward toward the depths of the sea, the psyche, and the smallest elements of organic forms. Aptly named after the shape-shifting ancient Greek god of the sea, the film follows these interconnecting lines of research at this mythical frontier that so preoccupied the imagination of artists, scientists, and explorers.

Proteus
A Nineteenth Century Vision
by David Lebrun
First Run/Icarus Films, New York, 2004. 61 minutes. www.frif.com/new2004/pro.html

In the life sciences, the main discoveries of the 19th century were all related to the idea of transformation. Beginning with Johann Wolfgang von Goethe's conceptions of morphology and metamorphosis, Jean Baptiste de Lamarck's theory of evolutionary transformations, and Karl Ernst von Baer's detailed descriptions of embryological sequences (Entwicklungsgeschichte), a dynamic and historical conception of life emerged—one that also resonated with the art of the romantics and the ideas of the Naturphilosophen (*2*). It was Charles Darwin, of course, who provided the basis for the explanatory unification of all these diverse ideas and observations. But for all his agonies about the social implications of his theory, Darwin was a deeply practical man. In many ways, he was the scientific archetype of the Victorian age of industrialism and empire: a solid defender of order and virtue, albeit of a new kind (*3*, *4*).

In that, Ernst Haeckel (1834–1919), the film's main protagonist, was quite different from Darwin. A generation younger, Haeckel was in many ways Darwin's "German Shepherd," playing a role similar to the one Thomas H. Huxley, Darwin's bulldog, played in England. But Haeckel, who was an equally talented artist and scientist, was torn between the scientific and romantic conceptions of nature. As a scientist, he would describe most of the known species of Radiolaria, develop (together with his friend Carl Gegenbaur) evolutionary morphology, formulate the "biogenetic law" ("ontogeny recapitulates phylogeny"), and coin many now-familiar concepts in biology (such as ecology). As an artist, he would produce numerous paintings and illustrations of many newly discovered creatures that populated the deep seas. His book *Art Forms in Nature* (*5*) is, to this day, a testament to both nature's beauty and Haeckel's talents. And as a philosopher and theorist, Haeckel would champion his own brand of monism, an idiosyncratic form of materialism that tried to overcome the divide between modern man and nature—a goal he shared with an earlier generation of romantic poets and artists (*6*, *7*).

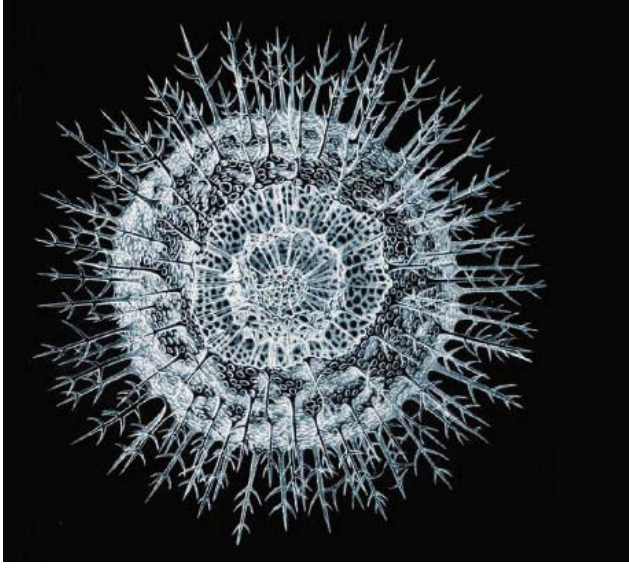

One among thousands. Haeckel described, classified, and painted over 3000 species of radiolarians.

The 19th-century vision of nature set forth in the film is, however, not just about the artist and the scientist each contemplating nature in their own way. Lebrun presents the whole nexus of interacting technological, scientific, artistic, and economic factors that together shaped the century as well as all perceptions of nature. These factors include technological accomplishments such as the first transatlantic cable, the cable's economic context, and the emerging fields of physical oceanography and marine biology. The film recounts the famed expedition of HMS *Challenger* (1872–1876) as well as its impact on science. The bounty of collected radiolarians alone would keep Haeckel busy for ten years, during which time he produced detailed descriptions of more than 3000 new species.

Ready for the field. Haeckel with his assistant Nicolaus von Miclucho-Maclay during their 1866 expedition to Lanzarote (Canary Islands).

What makes *Proteus* a truly stunning film—one that I highly recommend for a general audience, students, and scientists alike—is its creative use of montage and animation. Throughout the film, Lebrun relies exclusively on original 19th-century images. He presents drawings, historical photographs, and paintings along with animations of these images that highlight the stunning beauty of organic forms and of Haeckel's artistic representations. These animations (together with Yuval Ron's minimalist musical score) convey, through contemporary means, the sense of nature's creative and transformative powers that so fascinated 19th-century artists and scientists. Furthermore, Lebrun contrasts Haeckel's quest to understand nature with the inward journey of Samuel Coleridge's *Rime of the Ancient Mariner* (making effective use of Gustav Dore's illustrations). This juxtaposition further highlights the different roles of the sea in the 19th-century imagination.

The strength of the film stems from the combination of historical illustrations and quotes with a clear narrative. Lebrun successfully fuses his selection of images and text to bring to life the drama behind this 19th-century vision of nature. *Proteus* is thus a highly effective way to educate and entertain large audiences about science and its history. Today, especially, such works are truly needed.

The reviewer is at the School of Life Sciences and Center for Biology and Society, Arizona State University, Post Office Box 874501, Tempe, AZ 85287–4501, USA. E-mail: manfred.laubichler@asu.edu

References

1. F. Schlegel, *Kritische Fragmente*, no. 115, in *Kritische Schriften und Fragmente*, E. Behler, H. Eichner, Eds. (Ferdinand Schöningh, Paderborn, Germany, 1988).
2. R. Richards, *The Romantic Conception of Life: Science and Philosophy in the Age of Goethe* (Univ. Chicago Press, Chicago, 2002).
3. J. Browne, *Charles Darwin: Voyaging* (Pimlico, London, 1995).
4. J. Browne, *Charles Darwin: The Power of Place* (Knopf, New York, 2002).
5. E. Haeckel, *Kunstformen der Natur* (Verlag des Bibliographischen Instituts, Leipzig, Germany, 1899–1904).
6. M. D. Laubichler, *J. Exp. Zool. B Mol. Dev. Evol.* **300B**, 23 (2003).
7. L. K. Nyhart, *Biology Takes Form: Animal Morphology and the German Universities, 1800–1900* (Univ. Chicago Press, Chicago, 1995).

10.1126/science.1112998

ETHICS

Issues in Oocyte Donation for Stem Cell Research

David Magnus and Mildred K. Cho*

As described by Hwang *et al.* in *Science* (*1*), somatic cell nuclear transfer (SCNT) to create human embryonic stem cell (hESC) lines represents a step toward realizing the promise of stem cell research. They have shown the generalizability and efficiency of the approach in creating 11 cell lines from the nuclei of skin cells of individuals with serious diseases or disabilities and the oocytes of donors. This work raises ethical and policy questions. As hESC research proceeds internationally, these issues must be adequately addressed for public confidence to be maintained. We discuss three areas that particularly deserve attention: (i) ethical oversight of collaborations between scientists working in countries with different standards, (ii) protection of oocyte donors, and (iii) avoidance of unrealistic expectations.

International Oversight

The research described in Hwang *et al.* took place in South Korea. It was conducted with oversight and approval from Korean institutions required by South Korean law. However, one of the researchers is a U.S. scientist. No U.S. Federal funding was used, and the creation of human embryonic stem cells for research under these conditions is not prohibited in either country (*2*, *3*). This scientist obtained Institutional Review Board (IRB) review from his university, in which the IRB determined that the research did not involve human subjects on the basis of the Federal definition of human subjects research. These regulations exempt research from full IRB review if samples cannot be traced back to their donors (*4*). If this had been a clinical trial, his institution in the United States would have been mandated also to provide full IRB oversight for the research. Full IRB review might have been warranted in this case, because at least one of the researchers must be able to ascertain the identity of the donor from the clinician's encoded information if family members were to receive priority for future hESC transplants, in compliance with the Korean Network for Organ Sharing Regulation Code 18-1 [see SOM for (*1*)]. However, until recently, specific guidance to IRBs for review of procurement of oocytes for stem cell research has been minimal.

IRBs now can look to the new U.S. National Research Council—Institute of Medicine (NRC-IOM) report on stem cell research recommending that all such research have IRB approval and additional oversight by a special hESC research ethics oversight committee (*5*). If such oversight is not required by law, but is routine within the United States, should we expect that U.S. researchers working in other countries will voluntarily comply with these requirements? Or should they follow the laws and regulations of the country where the research is taking place unless mandated by U.S. law to do otherwise? This research was conducted before the NRC-IOM recommendations and at this point, it is not clear what the involvement of the U.S. IRB should have been.

Differing ethical standards in international collaborative research are not new, and solutions for reconciling differences have been proposed (*6*, *7*). Therefore, the evolving oversight of hESC research will require that, as new mechanisms are put in place [such as for research funded by the passage of the state's Proposition 71 (*8*) in 2004], U.S. researchers would be wise to seek approval from all relevant bodies and to ensure compatibility with the highest standards. This can help researchers obtain approval of the FDA or other similar bodies of clinical application of their research.

Nonmedical Oocyte Donation

A major challenge facing hESC research will be procurement of oocytes from "nonmedical" donors, meaning those who are donating oocytes neither for reproductive, nor medical purposes. The use of excess embryos and oocytes from in vitro fertilization procedures for research has a clear precedent. It uses a clinical informed consent process for women who are considering using assisted reproductive technology that includes discussion of the risks and benefits with the patient. In addition, there is a research informed consent process, as the patient (now a subject) agrees to allow her gametes to be used for research purposes (*9*, *10*). Agreement will be required on the confidentiality and the use of the material. In other words, for these patients, there is a two-part process—a clinical consent that covers the (not insignificant) risks and benefits of the procedure used to procure the oocytes for reproductive purposes (drugs for hyperstimulation, removal of the follicles, etc.) and then a research consent that focuses on the subject as a tissue donor. If cell lines derived from this material are eventually used in clinical trials, then the consent process for a new clinical trial comes into play.

The clinical consent model does not seem to fit women who agree to donate oocytes entirely for research purposes. These women are not pursuing the procedure for any reproductive or medical benefit to themselves; rather, they are exposing themselves to risk entirely for the benefit of others. If we were to think of them as simply clinical patients, their physician's fiduciary obligations would seem to require counsel against undergoing such a procedure for no benefit (*11*). Between 0.3 and 5% (*12*) or up to 10% (*13*) of women who undergo ovarian stimulation to procure oocytes experience severe ovarian hyperstimulation syndrome, which can cause pain, and occasionally leads to hospitalization, renal failure, potential future infertility, and even death.

Alternatively, these individuals can be viewed purely as research subjects. After all, research often requires individuals to expose themselves to risk for the benefit of others (albeit often with the possibility of direct benefit to themselves). This model may also be inadequate for addressing the status of these women, because the consent process is likely to focus on the post-procurement research risks and benefits. Thus, the risks of the actual procurement process may not be adequately highlighted. There is nothing experimental being tested on these women. The only research aspect of their experience is use of their tissues.

Finally, once current technical limits are overcome, cell lines derived from this research may actually be used in therapy. There may be very little difference for the oocyte donors between donating their

Stanford Center for Biomedical Ethics and Department of Pediatrics, Stanford University, Palo Alto, CA 94304, USA.

*Author for correspondence. E-mail: micho@stanford.edu

CREDIT: PRESTON HUEY/*SCIENCE*

gametes for research or for clinical purposes—yet the consent processes would seem to require different approaches. All of these factors doubtless contribute to the fact that Hwang and colleagues' discussion of the consent process and their consent forms (*1*) reveal little attention to the risks of the procedure and focus on the research aspects of their contribution.

We may need a new category to deal with this unusual class of participants who expose themselves to substantial risk only for the benefit of others, where the risk is incurred not in the actual research but in the procurement of materials for the research. When the oocytes that are donated are anonymized, current U.S. regulations no longer recognize these donors as research subjects. However, the donors are also not patients. We recommend use of the term "research donors" as distinct from "research subjects" to signify their dissimilar roles. This new category does not apply to donors of sperm used to create hESCs, because they are not exposed to similar risks. It also does not apply to donors of tissue for genetic research projects such as the HapMap (*14*), even though direct benefits do not accrue to those donors, because of the low physical risks involved.

When someone volunteers to donate an organ (such as a kidney or a liver lobe), there is a similar conceptual difficulty (*15*–*17*). These procedures are not now considered research, but it is difficult to see the donors truly as patients in the way that recipients are seen (*18*). Simply taking the best interests of the donor into account, it is hard to justify organ donation.

In dealing with the problem of benefit, the transplant community has moved fairly cautiously, and a great deal of conceptual and procedural work has gone into protecting the individuals who are making a sacrifice for others (*15*–*19*). In general, scrutiny of the motives for undergoing such donation is far greater than would normally be required for an elective procedure, and whole classes of potential live donors are ruled out on principle. For example, altruistic directed donation by live donors (i.e., to strangers) has generally been regarded as problematic, both ethically and practically (*16*, *20*). In general, it has been found that it is much easier to justify donation to close family members and friends.

However, it seems that clinicians and stem cell researchers envision this type of altruistic donation as the primary vehicle for generating hESC lines for research and eventual clinical application. Applying this model to the procurement of oocytes would mean that researchers would have to exercise a great deal of caution and to be rigorous in their assessment of whether someone is an appropriate donor as well as being clear about all of the risks.

Recruiting oocyte donors from families of afflicted patients would follow the pattern of justification typically cited in living organ donation. However, it does raise the question of whether oocyte donors feel coerced by their family situations into donating. Furthermore, there is one significant difference that leads to a final problem—organ donation has fairly clearly established benefits to the recipient; hESC research based on SCNT does not.

Misconception of Therapeutic Use

As the NRC-IOM report highlights, it is necessary that prospective donors recognize the large gap between research and therapy. This is particularly important in frontier areas of research where therapeutic impact in humans is unproven. Because it is likely that oocyte donors will be recruited from individuals with diseases and disabilities or their close family members, researchers must make every effort to communicate to these volunteers that it is extremely unlikely that their contributions will directly benefit themselves or their loved ones. Also, it is nearly certain that the clinical benefits of the research are years or maybe decades away. This is a message that desperate families and patients will not want to hear. Their vulnerability and the risks of oocyte donation make it imperative that prospective donors are adequately counseled and that risks are weighed carefully against a realistic assessment of benefits before allowing research to proceed. Donors who are family members or friends of patients hoping to benefit from downstream stem cell research are more vulnerable than the so-called altruistic donors who are strangers.

The language used to describe the research can reinforce the therapeutic misconception (*21*), misleading donors and subjects into believing that research is therapy. This was recognized as a serious problem in so-called "gene therapy" research (*20*, *22*, *23*) and has led to recommendations that this research should more accurately be described as "gene transfer research." Similarly, it is important not to use the term "therapy" when what is meant is "research" and not to refer to hESC research as "therapeutic cloning." There is currently no such thing as "therapeutic cloning" and this is not "therapeutic cloning research," nor can we say with any certainty that "cell therapy" is in the near future. Similarly, referring to research subjects as "patients" contributes to confusion (*2*). Introducing such terminology increases the likelihood that individuals have been or will be misled into exposing themselves to risk. It is permissible and perhaps even laudatory for women to contribute voluntarily to moving the field forward. But it would be a mistake to allow our language and the enthusiasm of researchers to allow that research to take place through exploitation of vulnerable patients and their friends and family members.

Responsibilities of Journals

Journals have an ethical obligation to publish research such as Hwang *et al*.'s if it is scientifically sound. However, journals must also be satisfied that the research was conducted ethically and must call attention to ethical issues raised by the work that they publish. Research that crosses the boundary into the illegal or clearly ethically unacceptable (e.g., if this research had been conducted without consent) should not be published. Although Hwang *et al*. did not cross those boundaries, their work is in such a novel and controversial area that it is unsurprising that it raises new ethical challenges, and is beset by some ambiguities. Journals are obligated to publish such research and to encourage ethical reflection on how future research should be conducted.

References and Notes

1. W. S. Hwang *et al.*, *Science* **308**, 1777 (2005); published online 12 May 2005 (10.1126/science.1112286).
2. Republic of Korea Bioethics and Biosafety Act No. 7150 (2005).
3. Executive Order by President G. W. Bush regarding federal funding of human stem cell research, 9 August 2001; www.whitehouse.gov/news/releases/2001/08/print/20010809-1.html
4. U.S. Code of Federal Regulations, 45 CFR 46, Subpart B, (1991).
5. Committee on Guidelines for Human Embryonic Stem Cell Research, Institute of Medicine and National Research Council, "Guidelines for human embryonic stem cell research" (National Academies Press, Washington, DC, 2005).
6. M. T. White, *J. Law Med. Ethics* **27**, 87 (1999).
7. R. Macklin, *Kennedy Inst. Ethics J.* **11**, 17 (2001).
8. California Health and Safety Code, Section 125291.10-125291.85., California Stem Cell Research and Cures Bond Act of 2004.
9. B. Lo *et al.*, *Science* **301**, 921 (2003).
10. B. Lo *et al.*, *Fertil. Steril.* **82**, 559 (2004).
11. M. Rimington *et al.*, *Reprod. Biomed. Online* **6**, 277 (2003).
12. J. Schenker, D. Weinstein, *Fertil. Steril.* **30**, 255 (1978).
13. A. Golan, R. Ron-El, A. Herman, *Obstet. Gynecol. Surv.* **44**, 430 (1989).
14. The International HapMap Consortium, *Nat. Rev. Genet.* **5**, 467 (2004).
15. The Authors for the Live Organ Donor Consensus Group, *JAMA* **284**, 2919 (2000).
16. P. Adams *et al.*, *Transplantation* **74**, 582 (2002).
17. N. Biller-Andorno, G. Agich, K. Doepkens, H. Schauenburg, *Theor. Med. Bioethics* **22**, 351 (2001).
18. F. Delmonico, O. Surman, *Transplantation* **76**, 1257 (2003).
19. American Society of Transplant Surgeons Statement on Solicitation of Donor Organs (2005); available at www.asts.org/donorsolicitation.cfm
20. S. Zink *et al.*, *Am. J. Bioethics* 5, 1 (2005).
21. P. Appelbaum, L. Roth, C. Lidz, *Int. J. Law Psychiatry* **5**, 319 (1982).
22. N. King, *Hum. Gene Ther.* **10**, 133 (1999).
23. G. Henderson *et al.*, *Mol. Ther.* **10**, 225 (2004).

10.1126/science.1114454

CREDIT: PRESTON HUEY/*SCIENCE*

PLANT SCIENCE

GRAS Genes and the Symbiotic Green Revolution

Michael K. Udvardi and Wolf-Rüdiger Scheible

Industrial nitrogen fixation, which annually converts 100 million metric tons of N_2 to NH_3, produced fertilizer that fueled the agricultural Green Revolution (*1*). A different Green Revolution occurred 65 million years earlier when some plants discovered a way to utilize atmospheric N_2 directly, through symbiosis with nitrogen-fixing bacteria. Evolution of symbiotic nitrogen fixation won these plants a competitive edge in natural environments with limited mineral- and organic-nitrogen. Nitrogen fixation by bacteria, called rhizobia, within legume plants now annually injects about 50 million metric tons of nitrogen into agricultural systems (*2*) in an environmentally friendly manner. The rhizobia reside in nodules that develop on the roots or stems of legumes in response to signaling between plant and bacteria. Both organisms reprogram their gene expression and metabolism in response to the interaction (*3*). Genetic analyses have revealed some of the plant genes and proteins essential for nodule development and function (*3*–*5*). In this issue, Kaló *et al*. on page 1786 (*6*) and Smit *et al*. on page 1789 (*7*) describe two putative transcription factors of the GRAS family that appear to link the initial rhizobial signaling molecule, Nod factor (modified oligosaccharide), to changes in plant gene expression that are required for nodule development (*6*, *7*). GRAS proteins are a recently discovered family of plant-specific proteins named after the three founding members: GAI, RGA, and SCR. Recruitment of the two legume GRAS proteins into the symbiotic program may have been key to the evolutionary success of this family of plants.

The recent adoption of *Medicago truncatula*, a relative of alfalfa, and *Lotus japonicus* as models for legume research has greatly accelerated the genetic mapping and isolation of genes required for nitrogen fixation, especially those involved in rhizobial-plant signaling and nodule development (*3*, *4*). Among the signaling components discovered in these two species are probable components of the Nod factor receptor (*8*–*10*); a leucine-rich repeat receptor–like kinase (*11*, *12*); a pair of putative plastid cation channels (*13*, *14*); and a calcium/calmodulin-dependent protein kinase (CCaMK) (*15*, *16*), which may decode a calcium oscillation signal (*17*). Each of these proteins is required for the initial burst of gene expression that occurs within hours of the plant perceiving Nod factor (*18*) (see the figure). Two mutants of *Medicago*, *nsp1* and *nsp2*, exhibit calcium spiking but fail to alter gene expression (*18*, *19*). Map-based cloning of mutant alleles identified the genes *NSP1* and *NSP2*, which encode putative transcription factors of the GRAS family.

Other evidence supports the proposed roles of NSP1 and NSP2 in transcriptional regulation. First, related GRAS family proteins regulate transcription in other plants, where they control diverse developmental and cellular processes (*20*). Second, GRAS proteins possess several structural features typical of transcriptional regulators, although direct DNA binding has not yet been shown. Third, both NSP1 and NSP2 are nuclear proteins. Each protein, when fused with green fluorescent protein (GFP) and expressed in plant root cells (*6*, *7*), translocated to the nucleus, where it rescued the nodulation defects of *nsp1* or *nsp2*. Although NSP1 is constitutively expressed in the nucleus (*7*), NSP2 relo-

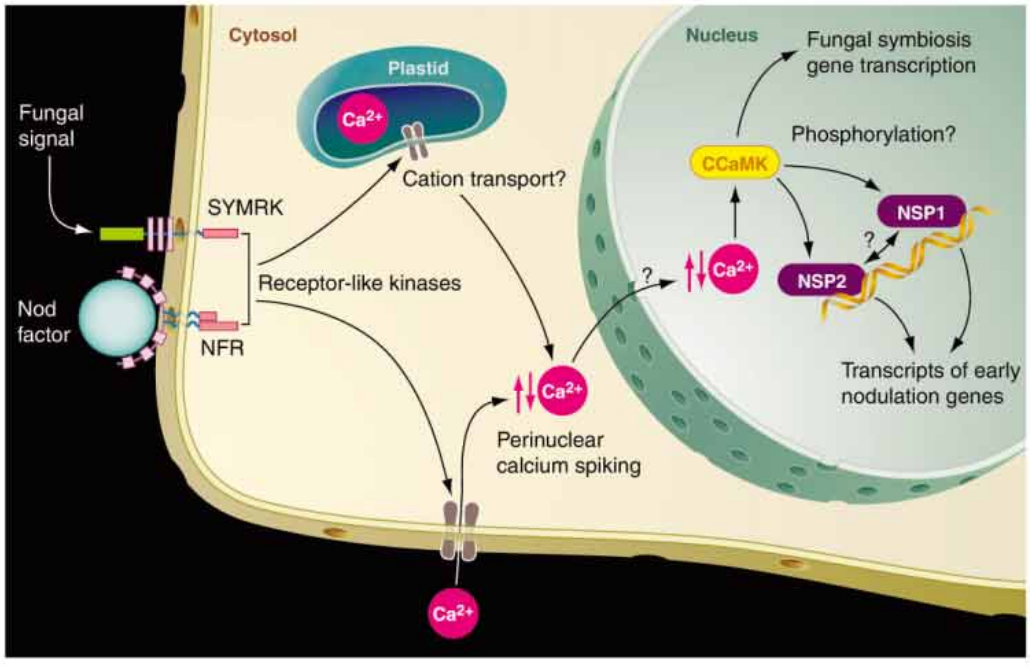

Possible signaling pathway triggered by bacterial Nod factor in plant root cells. Nod factors are perceived at the cell surface by receptor-like kinase proteins (NFR, Nod factor receptor complex, and SYMRK, symbiosis receptor kinase). Protein phosphorylation may then lead to influx of extracellular calcium (Ca^{2+}) and/or release of intracellular calcium stores by channel proteins into the cytoplasm. Rhythmic calcium spiking, especially around and possibly within the nucleus, may activate a nuclear calcium/calmodulin-dependent protein kinase (CCaMK), which in turn could activate the GRAS-type transcriptional regulators NSP1 and NSP2 by phosphorylation. NSP1 and NSP2 then induce transcription of early nodulation genes, leading to root hair deformation and formation of nodules. CCaMK probably also activates expression of genes required for fungal (mycorrhizal) symbiosis, through an independent pathway.

CREDIT: PRESTON HUEY/*SCIENCE*

The authors are at the Max-Planck Institute of Molecular Plant Physiology, Am Mühlenberg 1, 14476 Golm, Germany. E-mail: udvardi@mpimp-golm.mpg.de (M.K.U.), scheible@mpimp-golm.mpg.de (W.-R.S.)

cates from the nuclear envelope to the nuclear lumen in response to Nod factor detection by the cell (*6*). However, the NSP2-GFP localization studies were done with a gene construct driven by the strong constitutively active cauliflower mosaic virus (CaMV) 35*S* promoter, which the authors admit can lead to spurious localization results, so care must be exercised in interpreting the Nod factor–dependent relocation of the NSP2 fluorescence fusion protein. Expression of NSP1-GFP in transgenic roots was driven by the native *nsp1* promoter, which avoids this concern. The nuclear location of NSP1 and NSP2 is interesting, not only because this puts both proteins within easy reach of genes, but also because CCaMK, which acts upstream of NSP1 and NSP2 in the Nod factor signaling pathway (*18*), is located in the nucleus as well (*6*, *7*). Indeed, CCaMK may physically interact with either NSP1 or NSP2 (or both). Phosphorylation of the NSP proteins by this kinase may activate them, promoting transcription of target genes. The calcium-spiking signal that has been observed in cytoplasm following Nod factor perception (*4*) may propagate into the nucleus to be interpreted by CCaMK

A portion of the rhizobial signaling pathway in legumes does double duty. The components from downstream of the Nod factor receptor to just upstream of the NSP proteins (see the figure) are also used by mycorrhizal fungi to establish beneficial symbioses with legumes. Mycorrhizal symbioses, which provide plants with phosphorous and other nutrients, evolved ~460 million years ago when plants first colonized the land (*21*). In fact, such symbioses may have been a prerequisite for successful colonization. Mycorrhizal symbioses still exist in 90% of land plant species. Ancestral legumes may have coopted part of the signaling machinery of this ancient symbiosis to facilitate the more recent symbiosis with nitrogen-fixing rhizobia (*21*). NSP1 and NSP2 are not part of this shared portion of the signaling pathway; instead they act later to confer specificity, which enables the plant to respond appropriately to rhizobial infection alone.

Another transcription factor implicated in legume nodule development, NIN from *L. japonicus* (*22*), probably acts downstream of NSP1 and NSP2 and the early transcriptional responses in root cells. NSP1 and NSP2, however, are key links in the early Nod factor signaling chain, and their discovery will lead to a better understanding of the molecular interactions that make the pathway functional.

With this identification of NSP1 and NSP2, most of the proteins that are indispensable for early rhizobia-legume signaling are now known. However, many questions about the detailed workings of this pathway remain. Does CCaMK interact with and phosphorylate either NSP1 or NSP2? Do NSP1 and NSP2 interact physically? Do NSP1 or NSP2 bind directly to the promoters of genes that are activated by Nod factor signaling? Do NSP1 and NSP2 act cooperatively on the same target genes? The plethora of questions surrounding these and other Nod factor signaling components presage exciting times in symbiosis research.

References

1. V. Smil, *Nature* **400**, 415 (1999).
2. V. Smil, *Global Biogeochem. Cycles* **13**, 647 (1999).
3. G. E. D. Oldroyd, M. J. Harrison, M. Udvardi, *Plant Physiol.* **137**, 1205 (2005).
4. G. E. D. Oldroyd, J. A. Downie, *Nat. Rev. Mol. Cell Biol.* **5**, 566 (2004).
5. L. Krusell *et al.*, *Plant Cell* **17**, 1625 (2005).
6. P. Kaló *et al.*, *Science* **308**, 1786 (2005).
7. P. Smit *et al.*, *Science* **308**, 1789 (2005).
8. E. B. Madsen *et al.*, *Nature* **425**, 637 (2003).
9. S. Radutoiu *et al.*, *Nature* **425**, 585 (2003).
10. E. Limpens *et al.*, *Science* **302**, 630 (2003).
11. S. Stracke *et al.*, *Nature* **417**, 959 (2002).
12. G. Endre *et al.*, *Nature* **417**, 962 (2002).
13. J. M. Ana *et al.*, *Science* **303**, 1364 (2004).
14. H. Imaizumi-Anraku *et al.*, *Nature* **433**, 527 (2005).
15. J. Levy *et al.*, *Science* **303**, 1361 (2004).
16. R. M. Mitra *et al.*, *Proc. Natl. Acad. Sci. U.S.A.* **101**, 4701 (2004).
17. D. W. Ehrhardt, R. Wais, S. R. Long, *Cell* **85**, 673 (1996).
18. R. Catoira *et al.*, *Plant Cell* **12**, 1647 (2000).
19. G. E. D. Oldroyd, S. R. Long, *Plant Physiol.* **131**, 1027 (2003).
20. C. Bolle, *Planta* **218**, 683 (2004).
21. C. Kistner, M. Parniske, *Trends Plant Sci.* **7**, 511 (2002).
22. L. Schauser, A. Roussis, J. Stiller, J. Stougaard, *Nature* **402**, 191 (1999).

10.1126/science.1114217

ARCHAEOLOGY

Glassmaking in Bronze-Age Egypt

Caroline M. Jackson

Ever since Sir Flinders Petrie discovered evidence for Bronze-Age glass production in Tell el-Amarna, Egypt, in the late 19th century (*1*), controversy has surrounded his findings. Does the evidence represent primary glass production (raw materials were mixed to produce glass) or secondary working (ready-made glass was imported and reworked into artifacts)? The answer has important implications for understanding trade and exchange in the Mediterranean during the late second millennium B.C. On page 1756 of this issue, Rehren and Pusch (*2*) provide evidence in favor of primary production in Egypt.

Enhanced online at www.sciencemag.org/cgi/content/full/308/5729/1750

In the Late Bronze Age, glass was a high-status commodity. Any group that controlled its production or consumption would have occupied a powerful position. Archaeological evidence of a rise in trade and consumption indicates that this was a period of political change throughout the Near and Middle East and the Mediterranean area. This transformation may be explained by the rise of elite groups who chose to express allegiances through competitive gift exchange of prestigious artifacts. Glass—being difficult to work, complicated to produce, and available in vivid, symbolically significant colors—was favored for use in such artifacts. Understanding the evidence from Amarna will help to define the role of prestige goods and how elites used them to enhance their position.

The first glass vessels found in Egypt were stylistically indistinguishable from the earlier Mesopotamian glasses. The only contemporary written accounts of glasses are from the Amarna tablets. These small, sun-dried clay tablets document dispatches to and from the Egyptian courts and, in the case of glass, record a request by the pharaoh Akhenaten (~14th century B.C.) for glass to be brought to Egypt. These strands of evidence suggest that glass was not produced in Egypt, but only reworked there.

However, stylistic analysis and analysis of textual accounts are not the only ways to understand the trade in, and manufacture of, glass. The composition of a glass will vary when different raw materials and recipes are used, in principle allowing both technology and provenance to be investigated with chemical fingerprinting. Egyptian glasses were produced from silica (probably from quartz pebbles) and a soda-rich plant ash flux, which should vary in composition depending on where the raw materials were procured. Therefore, glasses with similar compositions would suggest that they were produced with similar raw materials and technology and were made at the same production center. Ideally, we may expect to see different chemical fingerprints of glasses made at different factories, or at least differentiate glasses with respect

The author is in the Department of Archaeology, University of Sheffield, Sheffield S1 4ET, UK. E-mail: c.m.jackson@sheffield.ac.uk

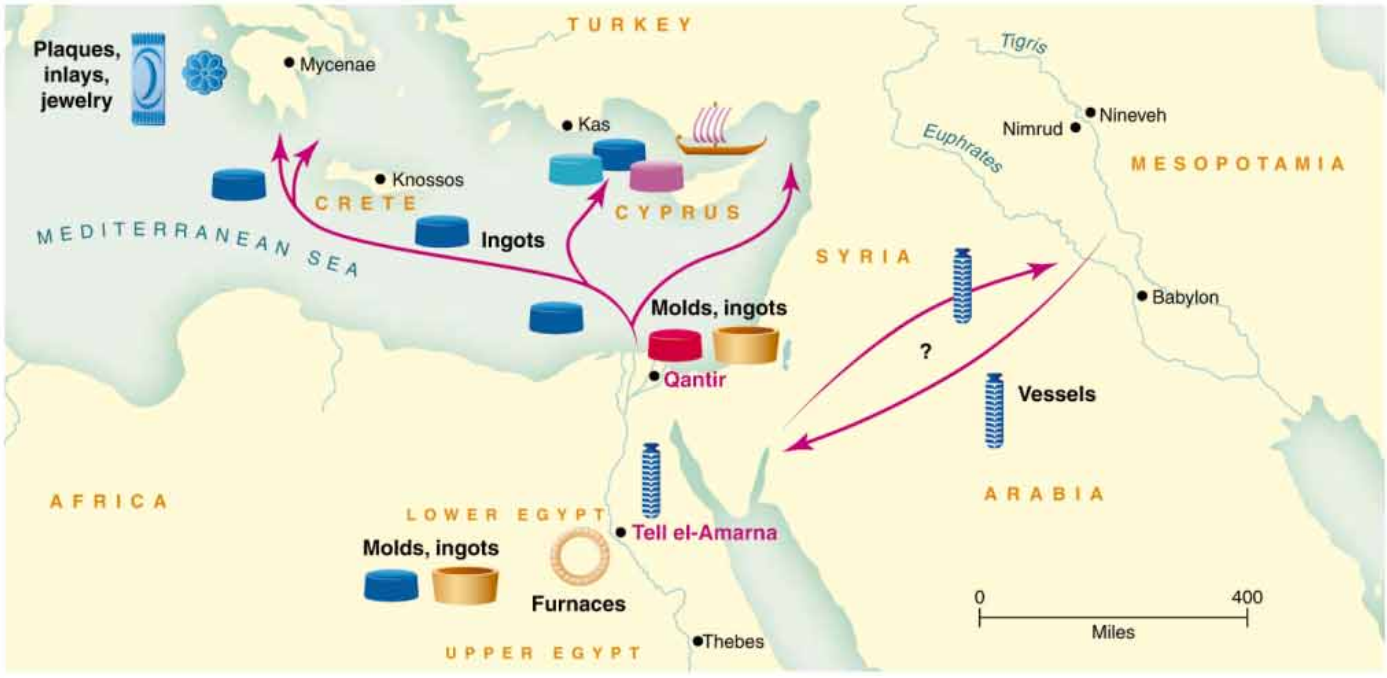

Trade in glass. This map shows the location of sites discussed in the text in the context of glass production and trade around the Mediterranean in the Late Bronze Age. Evidence presented by Rehren and Pusch strengthens the case for primary glass production in Egypt.

to broad geographical areas such as Egypt and Mesopotamia.

This concept can be applied to the Amarna controversy. If the chemical fingerprint of glass production debris found by Petrie at Amarna differed from that of Mesopotamian glasses, then, with the support of secure archaeological evidence, we could suggest that Amarna was a primary production center.

In practice, chemical analysis of artifacts has both expanded and complicated our knowledge in this area. For example, such analysis has shown that contemporary glasses from Egypt and Mesopotamia cannot be unequivocally distinguished on the basis of their chemistry (*3*), giving no real clue as to possible provenance. Rehren (*4*) has attributed this finding to the method by which the glass was produced, rather than to the use of raw materials with a similar composition or adherence to a strict recipe. By only partially melting the glass, the glass composition with the lowest melting point would be obtained; any unfused raw material would be removed from the melt. This approach would produce glasses of similar compositions, irrespective of slight differences in the raw materials, because it depends on temperature rather than raw material composition.

This partial-melting model is not contradicted by compositional differences observed between glasses of differing colors. Different concentrations of potassium in cobalt- and copper-colored blue glasses are attributed to the use of different plant ashes in their production (*3*, *5*). This observation has led Rehren to propose that Egyptian glasses were made at a few large glassmaking centers, each specializing in a particular color (*4*).

These ideas can only really be tested against archaeological evidence. In the 1990s, excavations were undertaken at Amarna, the royal city of Akhenaten, to locate Petrie's glass-production site (*6*). Two large circular furnaces were discovered, and the associated vitrified mud brick suggested that they had reached temperatures adequate for primary glass production from raw materials. This interpretation was confirmed by experimental reconstruction (*7*). Supporting evidence that the furnaces were used for glassmaking rather than reworking comes in two forms: fragmentary lumps of deep-blue "frit," currently thought to be the remains of an intermediate, low-temperature stage of the glassmaking process (*5*), and fragments of cylindrical ceramic vessels, coated on the outside with drips of dark-blue cobalt glass and on the inside with a calcareous liner.

Our understanding of Egypt's role in glass production and trade at this time hinges on the function of these ceramic vessels. It is assumed that they were used as ingot molds, in which glass, produced from raw materials, was cast into ingots and traded around the Mediterranean (see the figure). Support for this interpretation comes from cobalt blue glass ingots fitting the dimensions of the cylindrical vessels from Amarna, which have been found in a Late Bronze Age shipwreck off the coast of Turkey at Uluburun, near Kas (*8*, *9*). Such evidence argues against the stylistic and documentary evidence referred to earlier.

This is where the report by Rehren and Pusch (*2*) becomes highly significant. They present evidence for primary glassmaking from the 19th-dynasty Ramesside capital at Qantir (~13th century B.C). This evidence is extremely important in two respects. First, it provides a key to glass technology at the site that is missing from other production centers. Evidence of cylindrical vessels filled with partially fused glasses and jars indicates a two-stage glassmaking process. The first stage involved heating the glass at low temperatures in ovoid jars. The resulting material was then removed from the jars, the nonfused insoluble material discarded, and more flux and a colorant added. The second stage involved melting these components to form glass ingots, in cylindrical molds similar to those found at Amarna.

Most of the glass found at Qantir is red, produced with copper in a reducing atmosphere. Red glasses are relatively difficult to produce, requiring a high level of technical know-how, whereas cobalt blue glasses, probably produced at Amarna, require no special regulation of redox conditions. Whether production of cobalt glasses follows a similar two-stage process remains to be seen, because evidence for filled ingot molds is absent from Amarna. Aside from the number of stages in glass production, both sites have yielded cylindrical vessels and semifused raw materials, implying that a similar technology was practiced at both centers.

CREDIT: PRESTON HUEY/*SCIENCE*

Second, these finds also address the question of provenance. Rehren and Pusch (*2*) convincingly show that the Egyptians were making their own glass in large specialized facilities that were under royal control. At Qantir, production was linked specifically to the use of copper to color the glasses either red or blue, and glass was manufactured in the form of ingots to be reworked elsewhere.

The production of ingots at Qantir, presumably for export, shows that at this period, Egypt exported rather than imported glass. The chemical composition of fully formed vessels, inlays, and plaques from other high-status sites throughout the Mediterranean and particularly the Aegean, at least in the case of cobalt blue glass, is indistinguishable from that of the ingots, indicating that it was produced from Egyptian glass (*10*). Hence, elites in other societies were supplied with raw glass from Egypt for reworking. The location of glass manufacturing at the royal sites of Amarna and Qantir suggests that it was a controlled activity, which is not surprising, because glass was a "royal" medium used to enhance power, status, and political allegiances.

The evidence from Amarna and Qantir suggests that in the Late Bronze Age there was an Egyptian monopoly not just on the exchange of luxury glass but also on the diplomatic currency that the control of such technologies offered the elite. The evidence from Qantir presented by Rehren and Pusch (*2*) reinforces and reappraises the role of glass both within Egyptian society and as an elite material that was exported from Egypt to the Mediterranean world.

References

1. W. M. F. Petrie, *Tell el-Amarna* (Methuen, London, 1894).
2. Th. Rehren, E. B. Pusch, *Science* **308**, 1756 (2005).
3. C. Lilyquist, R. H. Brill, *Studies in Early Egyptian Glass* (Metropolitan Museum of Art, New York, 1993).
4. Th. Rehren, *J. Glass Stud.* **42**, 13 (2000).
5. M. S. Tite, A. J. Shortland, *Archaeometry* **45**, 285 (2003).
6. P. T. Nicholson, *Glass Technol.* **37**, 11 (1995).
7. C. M. Jackson, P. T. Nicholson, W. Gneisinger, *J. Glass Stud.* **40**, 11 (1998).
8. G. Bass, *Natl. Geogr.* **172**, 692 (1987).
9. P. T. Nicholson, C. M. Jackson, K. M. Trott, *J. Egypt. Archaeol.* **83**, 143 (1997).
10. R. H. Brill, *Chemical Analyses of Early Glasses* (Corning Museum of Glass, Corning, 1999), vols. 1 and 2.

10.1126/science.1112553

MACROEVOLUTION

Seeds of Diversity

Douglas H. Erwin

In a simple logistic growth model, the size of a population expands until further growth is limited by resource availability and the population size reaches a plateau. Robert MacArthur and E. O. Wilson extended these ideas to account for the effect of resources on species diversity in their model of island biogeography (*1*). Over the short term, competition for resources generates an equilibrium level of species diversity through a balance between immigration and extirpation. Over the longer term, equilibrium diversity reflects a balance between speciation and extinction, but in all cases the available resources control the equilibrium diversity. Now, Emerson and Kolm, in a recent paper in *Nature*, suggest that species diversity itself plays an important role in species diversification. They considered patterns of species diversity among plants and arthropods in the Hawaiian and Canary islands (*2*) and, after carefully controlling for island age, area, altitude, and nearest neighbor proximity through multiple regression analysis, concluded that species diversity itself promotes speciation. Simply put, the reason the tropics have so many species is that they have so many species.

What processes drive this positive feedback, and is it congruent with the MacArthur and Wilson model? There are explanations in which resource availability still limits maximal diversity. Perhaps new species are continuing to subdivide resources as part of an adaptive radiation, or geographic differentiation is producing ecologically redundant species. A more interesting alternative is Emerson and Kolm's proposal that greater community structural complexity may drive greater diversity. Many organisms provide a habitat for a myriad of other species, either by serving as hosts for parasites or by modifying the environment through burrowing, nest building, or other activities. Issues of how species modify their own niche [niche construction (*3*)] and physically modify the environment to facilitate the production of niches for other species [ecosystem engineering (*4*, *5*)] have received growing attention. The genesis of these ideas extends back to Richard Dawkins' *The Extended Phenotype* (*6*) and a paper by Richard Lewontin (*7*), each of which argues for a more expansive view of the selective interplay between organisms and their environment.

Niche construction involves activities of organisms that modify their environment and consequently modify the selective forces they experience. Many of these modifications may last for generations (think of the burrowing of earthworms or the multiple generations that may use a beaver dam), and these have been described as ecological inheritance. Laland and colleagues (*3*) have suggested that ecological inheritance represents a challenge to natural selection as the major driver of evolution. In a recent criticism of niche construction, Dawkins (*8*) observed that the critical issue is the pattern of covariance between external, organismically induced factors and underlying genes: He would limit niche construction as a special case of the extended phenotype to settings where such covariance exists, a far more restricted view than that presented in (*3*). The by-products of life Dawkins calls "niche change," and he would include oxygenation of the atmosphere and soil formation. Ecosystem engineering is often lumped with niche construction, but this is not limited to a species modifying its own environment. Modifications of the physical environment by one species affect, either positively or negatively, resource availability for other species. A termite mound may modify the selective forces facing the termites, but it also creates habitats for other species.

Missing from these discussions has been a sense of time and scale—a recognition that the most important episodes of niche generation may be during major evolutionary transitions, or recoveries from mass extinctions. Some of these are probably analogous to adaptive radiations, where ecological release in the face of underused resources allows a clade to diversify into a variety of more specialized forms. But many paleontologists have long expressed the view that the opening of new niches is an important component of such transitions, invoking "new adaptive zones," "empty ecospace," and similar concepts. For example, the diversification of multiple class- and ordinal-level invertebrate clades during the Ordovician established the marine communities of the Paleozoic, dominated by such sessile, filter-feeding forms as articulate brachiopods, bryozoans, and stalked echinoderms (*9*). Here new resources were provided by an expansion of the plankton (*10*) and through increased community com-

The author is in the Department of Paleobiology, MRC-121, National Museum of Natural History, Post Office Box 37012, Washington, DC 20013, USA. E-mail: erwind@si.edu

plexity. The rapidity of the diversification and the ecological interactions between species suggests that, as in the plants and insects of the Hawaiian and Canary islands, species begat species. In terms of MacArthur and Wilson's model, these macroevolutionary events should be limited by the extent to which new resources increased the carrying capacity of the environment. But if there is feedback between diversifying species, and a total potential diversity that is not limited by resources, then we may need a class of models in which future diversity is a function of current diversity.

Diversity cannot continue to increase forever, and ultimately resource availability must play a role, but perhaps a smaller one over evolutionary time than has been thought. Paleontologists, taking their cue from ecologists, have generally assumed that resource limitation controls the diversity of a community, but some have wondered whether changes in diversity might come from periodic disturbance. There have been few explicit considerations of this possibility, but Stanley (*11*) suggested that the apparent periodicity of mass extinctions and biotic crises reflected prolonged environmental disturbance and lengthy rediversification, not a periodic external forcing factor (such as periodic meteor bombardment). If periodic disturbance does provide a major control on diversity, then niche generation may be an ongoing process, more rapid during macroevolutionary transitions, but providing a regular source of new adaptive possibility until the next crisis occurs.

References

1. R. H. MacArthur, E. O. Wilson, *The Theory of Island Biogeography* (Princeton Univ. Press, Princeton, NJ, 1967).
2. B. C. Emerson, N. Kolm, *Nature* **434**, 1015 (2005).
3. F. J. Odling-Smee, K. N. Laland, M. W. Feldman, *Niche Construction: The Neglected Process in Evolution* (Princeton Univ. Press, Princeton, NJ, 2003).
4. C. G. Jones, J. H. Lawton, M. Shachak, *Oikos* **69**, 373 (1994).
5. C. G. Jones, J. H. Lawton, M. Shachak, *Ecology* **78**, 1946 (1997).
6. R. Dawkins, *The Extended Phenotype* (Oxford Univ. Press, Oxford, 1982).
7. R. C. Lewontin, in *Evolution from Molecules to Men*, D. S. Bendall, Ed. (Cambridge Univ. Press, Cambridge, 1983), pp. 273–285.
8. R. Dawkins, *Biol. Philos.* **19**, 377 (2004).
9. B. D. Webby, F. Paris, M. L. Droser, I. G. Percival, *The Great Ordovician Biodiversification Event* (Columbia Univ. Press, New York, 2004).
10. P. W. Signor, G. J. Vermeij, *Paleobiology* **20**, 297 (1994).
11. S. M. Stanley, *Paleobiology* **16**, 401 (1990).

10.1126/science.1113416

CLIMATE

Uncertainty in Hurricanes and Global Warming

Kevin Trenberth

During the 2004 hurricane season in the North Atlantic, an unprecedented four hurricanes hit Florida; during the same season in the Pacific, 10 tropical cyclones or typhoons hit Japan (the previous record was six) (*1*). Some scientists say that this increase is related to global warming; others say that it is not. Can a trend in hurricane activity in the North Atlantic be detected? Can any such trend be attributed to human activity? Are we even asking the right questions?

In statistics, a null hypothesis—such as "there is no trend in hurricane activity"—may be formed, and it is common to reject the null hypothesis based on a 5% significance level. But accepting the null hypothesis does not mean that there is no trend, only that it cannot be proven from the particular sample and that more data may be required. This is frequently the case when the signal being sought is masked by large variability. If one instead formulates the inverse null hypothesis—"there is a trend in hurricane activity"—then the 5% significance level may bias results in favor of this hypothesis being accepted, given the variability. Acceptance of a false hypothesis (a "type II" error) is a common mistake. Rather than accept the hypothesis, one may be better off reserving judgment. Because of the weakness associated with statistical tests, it is vital to also gain a physical understanding of the changes in hurricane activity and their origins.

Hurricane activity generally occurs over the oceans in regions where sea surface temperatures (SSTs) exceed 26°C (*2*). In the Atlantic, SSTs and hurricane activity (see both figures) vary widely on interannual and multidecadal time scales. One factor in the year-to-year variability is El Niño: Atlantic hurricanes are suppressed when an El Niño is under way in the Pacific (*3*, *4*). The decadal variability is thought to be associated with the thermohaline circulation and is referred to as the Atlantic multidecadal oscillation. It affects the number of hurricanes and major hurricanes that form from tropical storms first named in the tropical Atlantic and the Caribbean Sea (*5*–*7*).

In addition to interannual and multidecadal variability, there is a nonlinear upward trend in SSTs over the 20th century. This trend is most pronounced in the past 35 years in the extratropical North Atlantic (see the first figure). It is associated with global warming and has been attributed to human activity (*8*). In the tropical North Atlantic—the region of most relevance to hurricane formation—multidecadal variability dominates SSTs (see the first figure), but the 1995–2004 decadal average is nonetheless the highest on record by >0.1°C. Hence, although the warming in the tropical North Atlantic is not as pronounced, it is probably related to that in the extratropical North Atlantic.

SSTs are not the only important variable affecting hurricanes (*2*, *9*, *10*). Other factors that have influenced the increase in hurricane activity in the past decade (*11*) include an amplified high-pressure ridge in the upper troposphere across the central and eastern North Atlantic; reduced vertical wind shear over the central North Atlantic [wind shear tends to inhibit the vortex from forming (*2*)]; and African easterly lower atmospheric winds that favor the development of hurricanes from tropical disturbances moving westward from the African coast. Atmospheric stability is also important (*4*).

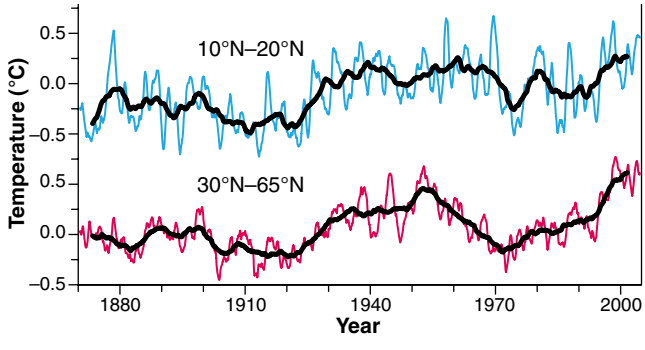

Getting warmer. Annual mean SST anomalies relative to 1961 to 1990 (*23*) for 1870 to 2004, averaged over the tropical Atlantic (10°N to 20°N, excluding the Caribbean west of 80°W) (**top**) and the extratropical North Atlantic (30°N to 65°N) (**bottom**). Heavy lines are 10-year running means.

The author is at the National Center for Atmospheric Research (NCAR), Boulder, CO 80307, USA. E-mail: trenbert@ucar.edu

Higher SSTs are associated with increased water vapor in the lower troposphere. Since 1988, the amount of total column water vapor over the global oceans has increased by 1.3% per decade (*12*); the variability and trends in water vapor are strongly related to SST anomalies. This behavior is similar to that expected theoretically (*13*) and supports model projections (*14*) suggesting that relative humidity remains about the same as temperatures increase. Both higher SSTs and increased water vapor tend to increase the energy available for atmospheric convection, such as thunderstorms, and for the development of tropical cyclones (*9*, *15*). However, the convective available potential energy (*15*) is also affected by large-scale subsiding air that increases the stability and dryness of the atmosphere, and is often associated with wind shear throughout the troposphere (*16*). The convective available potential energy appears to have increased in the tropics from 1958 to 1997 (*17*, *18*), which should increase the potential for enhanced moist convection, and thus—conceivably—for more hurricanes.

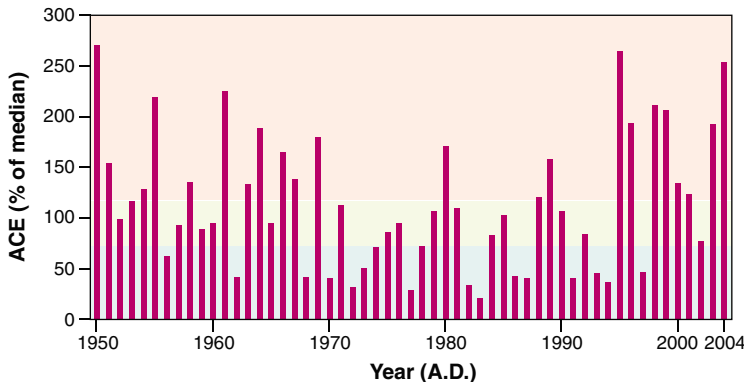

A measure of regional storm activity. The ACE index reflects the collective intensity and duration of tropical storms and hurricanes during a given hurricane season. Values are given as percentage of the median from 1951 to 2000; the white band indicates normal conditions, the blue is below normal, and the pink is above normal, according to NOAA. [Adapted from (*1*)]

An important measure of regional storm activity is the Accumulated Cyclone Energy (ACE) index (see the second figure) (*1*). Since 1995, the ACE indexes for all but two Atlantic hurricane seasons have been above normal; the exceptions are the El Niño years of 1997 and 2002. According to the National Oceanic and Atmospheric Administration (NOAA), the hurricane seasons from 1995 to 2004 averaged 13.6 tropical storms, 7.8 hurricanes, and 3.8 major hurricanes, and the ACE index was 169% of the median. In contrast, the hurricane seasons during the previous 25-year period (1970 to 1994) averaged 8.6 tropical storms, five hurricanes, and 1.5 major hurricanes, and the ACE index was 70% of the median. In 2004, ACE reached the third-highest value since 1950 (*1*); there were 15 named storms, including nine hurricanes.

Despite this enhanced activity, there is no sound theoretical basis for drawing any conclusions about how anthropogenic climate change affects hurricane numbers or tracks, and thus how many hit land. The environmental changes that are under way favor enhanced convection and thus more thunderstorms. But to get a hurricane, these thunderstorms must first be organized into a tropical storm (which is essentially a collection of thunderstorms that develops a vortex). Model projections of how wind shear in the hurricane region responds to global warming caused by increased carbon dioxide in the atmosphere tend to differ (*14*), and it is not yet possible to say how El Niño and other factors affecting hurricane formation may change as the world warms.

However, once a tropical storm has formed, the changing environmental conditions provide more energy to fuel the storm, which suggests that it will be more intense than it would otherwise have been, and that it will be associated with heavier rainfalls (*14*). Groisman *et al.* (*19*) found no statistically significant evidence that precipitation associated with hurricanes increased along the southeastern coast of the contiguous United States during the 20th century; however, their analysis did not include years after 2000, and there was a distinct increase in hurricane precipitation after 1995. Groisman *et al.* found a linear upward trend in precipitation amount by 7% in the 20th century in the contiguous United States; the increases in heavy precipitation (the heaviest 5%) and very heavy precipitation (the heaviest 1%) were much greater at 14% and 20%, respectively (*19*). Such trends are likely to continue (*20*).

Thus, although variability is large, trends associated with human influences are evident in the environment in which hurricanes form, and our physical understanding suggests that the intensity of and rainfalls from hurricanes are probably increasing (*8*), even if this increase cannot yet be proven with a formal statistical test. Model results (*14*) suggest a shift in hurricane intensities toward extreme hurricanes.

The fact that the numbers of hurricanes have increased in the Atlantic is no guarantee that this trend will continue, owing to the need for favorable conditions to allow a vortex to form while limiting stabilization of the atmosphere by convection. The ability to predict these aspects requires improved understanding and projections of regional climate change. In particular, the tropical ocean basins appear to compete to be most favorable for hurricanes to develop; more activity in the Pacific associated with El Niño is a recipe for less activity in the Atlantic. Moreover, the thermohaline circulation and other climate factors will continue to vary naturally.

Trends in human-influenced environmental changes are now evident in hurricane regions. These changes are expected to affect hurricane intensity and rainfall, but the effect on hurricane numbers remains unclear. The key scientific question is not whether there is a trend in hurricane numbers and tracks, but rather how hurricanes are changing.

References and Notes

1. D. H. Levinson, Ed., special issue on State of the Climate in 2004, *Bull. Am. Meteorol. Soc.* **86 (suppl.)** (2005).
2. A. Henderson-Sellers *et al.*, *Bull. Am. Meteorol. Soc.* **79**, 19 (1998).
3. W. M. Gray, *Mon. Weather Rev.* **112**, 1649 (1984).
4. B. H. Tang, J. D. Neelin, *Geophys. Res. Lett.* **31**, L24204 (2004).
5. M. E. Schlesinger, N. Ramankutty, *Nature* **367**, 723 (1994).
6. T. L. Delworth, M. E. Mann, *Clim. Dyn.* **16**, 661 (2000).
7. S. B. Goldenberg *et al.*, *Science* **293**, 474 (2001).
8. Intergovernmental Panel on Climate Change, *Climate Change 2001: The Scientific Basis*, J. T. Houghton *et al.*, Eds. (Cambridge Univ. Press, Cambridge, 2001).
9. G. J. Holland, *J. Atmos. Sci.* **54**, 2519 (1997).
10. K. A. Emanuel, *Nature* **401**, 665 (1999).
11. M. Chelliah, G. D. Bell, *J. Clim.* **17**, 1777 (2004).
12. K. E. Trenberth, J. Fasullo, L. Smith, *Clim. Dyn.*, 10.1007/s00382-005-0017-4 (25 March 2005).
13. The water-holding capacity of the atmosphere increases by ~7% per °C (*20*).
14. T. R. Knutson, R. E. Tuleya, *J. Clim.* **17**, 3477 (2004).
15. The convective available potential energy (CAPE) depends on the vertical profile of moist static energy (the combination of sensible heat, which is related to temperature, and potential and latent energy) and thus on moisture and temperature profiles.
16. J. C. L. Chan, K. S. Liu, *J. Clim.* **17**, 4590 (2004).
17. A. Gettelman *et al.*, *J. Geophys. Res.* **107**, 10.1029/2001JD001082 (2002).
18. Results based on more stations (*21*) may be compromised by uncertainties in changing instrumentation and adjustments to the data that were flawed (*22*).
19. P. Ya. Groisman *et al.*, *J. Hydrometeorol.* **5**, 64 (2004).
20. K. E. Trenberth, A. Dai, R. M. Rasmussen, D. B. Parsons, *Bull. Am. Meteorol. Soc.* **84**, 1205 (2003).
21. C. A. DeMott, D. A. Randall, *J. Geophys. Res.* **109**, D02102 (2004).
22. I. Durre, T. C. Peterson, R. S. Vose, *J. Clim.* **15**, 1335 (2002).
23. N. A. Rayner *et al.*, *J. Geophys. Res.* **108**, 10.1029/2002JD002670 (2003).
24. I thank J. Fasullo for generating the first figure, and R. Anthes, G. Holland, and S. Solomon for comments. NCAR is sponsored by the National Science Foundation.

10.1126/science.1112551

Energetics of Load Carrying in Nepalese Porters

Guillaume J. Bastien, Bénédicte Schepens, Patrick A. Willems, Norman C. Heglund*

Nepalese porters routinely carry head-supported loads exceeding their body weight (M_b) for many kilometers up and down steep mountain footpaths at high altitudes. Except in African women (*1*–*3*), virtually nothing is known about the energetic cost of carrying head-supported loads. We set out to determine the loads and distances carried by Nepalese porters, their metabolic cost for carrying the loads, and whether their optimal walking speed (as determined by the minimum cost for carrying a load) changed as a function of load.

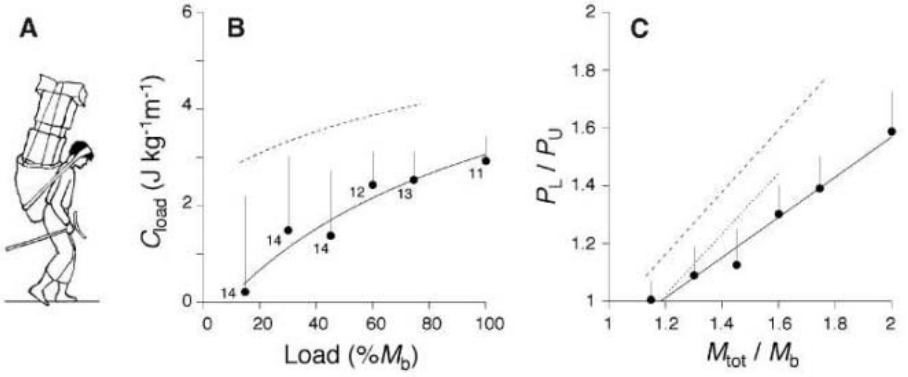

Fig. 1. (**A**) Method of load carriage in Nepal. Porters use a head strap (namlo) to support a basket (doko) containing the load. The T-shaped stick (tokma) is used to support the basket during the frequent rest periods taken by the porters. (**B**) Metabolic cost of carrying 1 kg of load over a distance of 1 m. C_{load} is shown as a function of the load in Nepalese porters (symbols and continuous line). The dashed line represents the C_{load} of control subjects using backpacks (*5*). (**C**) Gross metabolic power increase (power loaded, P_L, divided by power unloaded, P_U) due to carrying a load as a function of the increase in load (total weight, M_{tot}, divided by body weight, M_b). Nepalese porters (symbols and continuous line), carrying head-supported loads, are the most economical, particularly at high loads. African women (dotted line) (*1*), also carrying head-supported loads, equal the Nepalese at low loads. Control subjects (dashed line) (*5*) are close to the proportionality line. The number of data points averaged is indicated near the symbols in (B) and is the same in (C); the bars indicate the standard deviation. All measurements were near the optimal walking speed (0.8 to 1.4 m s^{-1}).

The town of Namche (at an altitude of 3500 m) near Mount Everest hosts a weekly bazaar. Porters (Fig. 1A), predominantly ethnic Rai, Sherpa, or Tamang, typically take 7 to 9 days to travel to Namche from the Kathmandu valley. The route, no more than a dirt footpath, covers a horizontal distance of ~100 km, with total ascents (river crossings to mountain passes) of ~8000 m and total descents of ~6300 m.

One day before the bazaar, we counted 545 male and 97 female porters (and 32 yaks) en route to Namche; others passed by earlier and later in the darkness. We weighed randomly selected porters and their loads (*4*). The men carried loads of 93 ± 36% of their M_b (mean ± SD, n = 96 male porters), whereas the women carried 66 ± 21% of their M_b (n = 17 female porters). The youngest porter was 11 years old, and the oldest 68; the greatest load measured was 183% of M_b, and 20% of the men carried >125% of their M_b. More than 30 tons of material were ported to Namche that day.

We asked eight Nepalese porters to walk around a 51-m flat track at five speeds, carrying six or seven different loads, according to their ability. The energy costs of loaded and unloaded walking were determined from their oxygen consumption and carbon dioxide production (*4*). Control experiments on European subjects carrying backpacks have been reported separately (*5*).

For all loads, the weight-specific cost of carriage C_{load} (i.e., the energetic cost loaded minus the cost unloaded at the same speed, divided by the load weight, given in J kg^{-1} m^{-1}) as a function of speed presented a minimum at ~1.1 m s^{-1}, both in Nepalese porters and in control subjects. However, at all speeds and loads, the porters had a smaller C_{load} than the controls. The average C_{load} near the optimal walking speed can be shown as a function of load (Fig. 1B). C_{load} increased from 0 J kg^{-1} m^{-1} at 15% of M_b to ~3 J kg^{-1} m^{-1} at 100% of M_b in the Nepalese porters, whereas it was always >3 J kg^{-1} m^{-1} in the controls (*5*).

The increase in metabolic power while carrying a load (the loaded oxygen consumption rate divided by the unloaded oxygen consumption rate at the same speed) as a function of the total weight M_{tot} (M_b plus the load) is shown in Fig. 1C for the Nepalese porters, control subjects (*5*), and African women (*1*) at about the optimal speed. The Nepalese porters were far more economical than the control subjects at all loads and more economical than the African women at all except the lightest loads. Loads lighter than ~20% of M_b are carried "for free." Above 20% of M_b, the Nepalese porters' advantage increases with increasing loads. The Nepalese porters' economy allows them to carry loads that are on average 30% of M_b heavier than the maximum loads carried by the African women, for the same increase in metabolic rate.

The load versus speed versus energy-cost trade-off chosen by these porters is to walk slowly for many hours each day, take frequent rests, and carry the greatest loads possible. We observed, for example, a group of heavily loaded porters making slow headway up a steep ascent out of a river gorge. Following whistled commands from their leader, they would take up their loads and labor uphill for no more than ~15 s at a time, followed by a ~45-s period of rest. Incredibly, this group of barefoot porters was headed for Tibet, across the Nangpa glacier (altitude 5716 m), about another week's travel beyond Namche.

So how do they do it? They might reduce the muscular work required to carry a load or increase their overall efficiency. The actual mechanism is unknown at this time.

References and Notes

1. G. M. O. Maloiy, N. C. Heglund, L. M. Prager, G. A. Cavagna, C. R. Taylor, *Nature* **319**, 668 (1986).
2. N. C. Heglund, P. A. Willems, M. Penta, G. A. Cavagna, *Nature* **375**, 52 (1995).
3. G. A. Cavagna, P. A. Willems, M. A. Legrammandi, N. C. Heglund, *J. Exp. Biol.* **205**, 3413 (2002).
4. Materials and methods are available as supporting material on *Science* Online.
5. G. J. Bastien, P. A. Willems, B. Schepens, N. C. Heglund, *Eur. J. Appl. Physiol.* **94**, 76 (2005); published online 14 January 2005.
6. We thank B. Basnyat of the Nepal International Clinic and Himalayan Rescue Association, M. Penta of the Université catholique de Louvain, and A. de Vinck. Supported by the National Geographic Society and the Belgian Fonds National de la Recherche Scientifique.

Supporting Online Material
www.sciencemag.org/cgi/content/full/308/5729/1755/DC1
Materials and Methods

25 February 2005; accepted 13 April 2005
10.1126/science.1111513

Unité de Physiologie et Biomécanique de la Locomotion, Faculté de Médecine, Université catholique de Louvain, Belgium.

*To whom correspondence should be addressed. E-mail: norman.heglund@loco.ucl.ac.be

Late Bronze Age Glass Production at Qantir-Piramesses, Egypt

Thilo Rehren[1]* and Edgar B. Pusch[2]

It has been uncertain whether the glass produced during the Late Bronze Age (LBA) originated in Egypt or Mesopotamia. Here we present evidence for the production of glass from its raw materials in the eastern Nile Delta during the LBA. Glass was made in workshops that were separate from where the production of objects took place. The initial melting of the raw materials to semi-finished glass was done at temperatures of 900° to 950°C, followed by coloration and ingot production at 1000° to 1100°C.

Large numbers of Late Bronze Age (LBA) glass artifacts are known from Mesopotamia and Egypt, roughly dating between 1500 and 1000 B.C. They are made from soda-lime-silica glass with elevated levels of potash and magnesia, and are intensively colored and opacified by metal oxides to emulate precious stones, notably turquoise and lapis lazuli. Although several archaeological sites in western Asia and Egypt show evidence of the production of glass vessels in artistic or secondary glass workshops (*1*), the location of primary glass production sites has been enigmatic. Here we describe evidence for glassmaking found in recent excavations at Qantir-Piramesses in the eastern Nile Delta (*2*). Several fragments of worked glass are known from Qantir, but not the debris that is typical of secondary glass workshops. Instead, ceramic fragments with glass attached on the inside abound, ranging from almost-complete vessels to tiny fragments; other evidence includes the presence of glass-related slag and unshaped glass fragments.

Glassmaking vessels or archaeological finds. The most diagnostic elements of the glass works at Qantir are cylindrical vessels or glass-coloring crucibles (*3*, *4*), for which no domestic parallel is known. So far, about 1100 fragments have been recovered, representing a minimum of 250 to 300 vessels. About 90% of these have external base diameters between 12 and 20 cm. They taper slightly and have rim diameters that are about 2 cm larger than that of the base (Fig. 1). The wall ranges from about 2 cm thick near the base to 0.6 to 1.3 cm near the rim. The average height of the vessels is 15 cm, based on the few complete profiles known. The fabric fits into Vienna System I.E.01 (*5*). Almost all fragments have a thin layer of lime on their inner side, thought to be a parting layer, which prevented the liquid glass from being contaminated by the ferruginous clay and sticking to the ceramic of the vessels, thus facilitating the release of the finished glass ingot from the crucible (*6*, *7*). In addition to this internal lime layer, many fragments show an outer layer of a different ceramic fabric, typically several millimeters thick. This is mostly a mixture of crushed lime and quartz sand, with some clay as a binder, or Nile clay tempered with lime and chaff. This outer wrap is not strongly bonded to the vessels and is often rather fragile. Most fragments show evidence of being "hot" or "very hot"; very few are "cold" (*8*, *9*). Many larger pieces show two or three temperature grades in different locations, indicating that they were heated unevenly. In hot vessels, the lime layer has reacted with the ceramic body to form a bottle-green interface glass layer.

A key find is object 00/0344, inventory number 3108, a substantially preserved crucible filled with a heavily corroded block of raw glass (Fig. 2). This glass contains abundant quartz grains in two distinct groups of shape and size: A few relatively large and rounded sand grains are mixed with large quantities of highly angular, very fine quartz dust. The sand grains include rare dark minerals and may represent contamination. The quartz dust is similar to crushed quartz, thought to be the main silica source of LBA glassmaking. For some reason, the processing of this charge was abandoned before the batch material had fused completely, in effect preserving much of the original raw material.

A second type of fragment with attached glass is most likely a variant of the common ovoid jar (*10*), adapted for use in the glassworks by the addition of a lime-rich layer on the inside, similar to the parting layer in the cylindrical vessels. Only one fragment has evidence of an outer ceramic layer, and none show any indication of localized heating. Most fragments fall in the thermal group "warm" or just about "hot"; heavily vitrified examples are absent.

Nine fragments are purpose-made funnel-shaped rim extensions. They form a right-angle triangle in cross section and have a groove in the short side that fits over the rims of the crucibles and a protrusion on the long side that reaches into the crucibles (Fig. 3). They were not prefired and were most likely fitted in their unfired state to the crucibles. The protrusion was luted to the upper inside of the vessels for a tight fit, enabling the long side to act as a slope or funnel leading into the crucible. The surface of the long side is now covered by a thin corroded glass film, indicating that glass, probably as crushed powder, was added into the hot crucibles, using the rim extension as a funnel. Many rim shards have diagnostic ruptures and the remains of a lute running parallel to the rim at a distance of between 1 and 2 cm, indicating that such extensions were much more frequent than the small number of identified fragments indicates.

Several "cold" jar fragments were found without the characteristic lime layer, containing

Fig. 1. Glass crucible 84/0088. The scale is in centimeters. Note the area of intense vitrification at the front left-hand side (a hot spot) and the lime-rich parting layer on the inside.

[1]Institute of Archaeology, University College London, 31-34 Gordon Square, London WC1H 0PY, UK. [2]Pelizaeus-Museum Hildesheim, Am Steine 1-2, D-31134, Hildesheim, Germany.

*To whom correspondence should be addressed. E-mail: th.rehren@ucl.ac.uk

remains of white powders. These powders were mostly lime and occasionally finely crushed pure quartz dust, probably stored in these vessels for later use.

The white material attached to the inside of many jar fragments is incompletely melted and corroded semi-finished glass. Most samples contain abundant quartz inclusions in an uncolored glass matrix (Fig. 4) with a very high porosity of >30% by volume (Fig. 5). Almost all of these samples were heavily corroded; they disintegrated quickly in hydrochloric acid, releasing clouds of silica gel, a scatter of finely ground quartz dust, and a few sand grains. In a few remains, we identified freshly formed platelike crystals, probably wollastonite ($CaSiO_3$).

Overall, we could identify several hundred individual vessels used in glassmaking and coloring; more than 90% of these are crucibles, the rest being jars. Of the crucibles, about one-quarter have remains of red glass attached; slightly more have traces of glass of unidentifiable or no color (*8*). About 1-10th have remains of semi-finished glass, four or five fragments have blue glass, and a single one has transparent purple glass attached. The remainder have no visible traces of glass but are identified as glass-working vessels by their diagnostic shape, internal lining, and evidence of temperature effects on the fabric.

The adapted domestic jars form a distinct group; they exclusively contain either semi-finished glass or glass of unidentifiable color, and traces of colored glass are absent. The estimated temperatures of these vessels are virtually all "cold," "warm," or just about "hot." Remains of colored glass are restricted to crucibles, although there are also several crucibles containing semi-finished glass. The temperature range of the crucible fragments is mostly "hot" and "very hot."

Ramesside glassmaking. The finds from Qantir indicate that glass was made locally here, using finely crushed quartz powder. The actual glassmaking probably began with a first melting (*11*) at about 900°C, apparently in domestic vessels such as beer jars adapted for the purpose. The resulting semi-finished glass may still have been rich in residual quartz grains and air bubbles, requiring refining before it could be worked into objects. It was probably first crushed and washed to homogenize the material and to remove nonreactive but water-soluble components of the plant ash, primarily chlorides and sulfates (*12*). The glass powder was then transferred to the cylindrical crucibles for melting, refining, and coloration to produce ingots; we assume that the crushed semi-finished glass was added in portions into the hot crucibles, aided by funnel-shaped tops. The degree of vitrification of the crucibles indicates that this second melting took place at 1000°C or more. Stepwise charging not only facilitated fusion and melting through an increased heat uptake of the batch, resulting in better-quality glass, but also enabled the production of thicker ingots. Both the making of semi-finished glass and the production of glass ingots may have required repeated melting to reach the necessary quality and homogeneity. Visual inspection of semi-finished material for transparency and color would have been sufficient to govern this (*13*), but such an iterative practice is impossible to prove archaeologically. The crucibles were eventually broken to remove the finished ingots. These would then have been transported to other, artistic, workshops where they were re-melted and worked into objects.

The shape of the domestic jars was beneficial for glassmaking: The narrow neck would avoid loss of material during the initial foaming of the batch, which occurs when the alkali carbonates of the plant ash decompose and react with the silica of the quartz, and would also reduce the danger of contamination. The oblong shape of the vessels would provide a large surface area relative to their volume, improving heat uptake. The relatively low temperature required for this step was easily provided through indirect heating of the vessels, possibly in an installation similar to a pottery kiln.

The final ingot production required a higher temperature to produce a homogenously colored and fully molten glass; these temperatures were close to the thermal limit of the ceramic material available (*7*). The complex pattern of localized heating, regularly reaching the point of ceramic bloating and fusion at selected hot spots near the base, in combination with an outer packing elsewhere of a cooler and inert material to provide additional mechanical stability to the vessels, indicate an elaborate and carefully controlled heating regime. The use of comparatively shallow, wide, and open cylindrical crucibles for this step improves heat transfer into the batch through a combination of radiant heat from above and heat transfer through the ceramic body from near

Fig. 2. Top view of crucible 00/0344, filled with corroded and half-reacted glass charge. The trench in the lower right quarter serves to study the internal structure of the filling. The diameter of the crucible is ~15 cm.

Fig. 3. Funnel fragment 00/0166 mounted on a crucible rim fragment to illustrate the supposed reconstruction. The total height of the assemblage is ~11 cm.

Fig. 4. Find 00/0618.0004: jar fragment with raw glass. The width of of the object is ~3 cm. Note the thin yellow parting layer between the ceramic and the glass. The black lines in the glass are a corrosion phenomenon.

Fig. 5. Find 02/0339.0022: jar fragment with semi-reacted raw glass. The width of the object is ~4 cm. Note the residual quartz grains trapped in the fused glass and the limited wetting of the underlying parting layer by the glass.

the base. The hearth or furnace type used for this step is unknown.

Glass ingots. Large numbers of colored glass ingots matching the internal size and shape of these crucibles were found as part of the cargo of the LBA Uluburun shipwreck (*14*, *15*), demonstrating the important role that these ingots played in the international glass trade. Crucible fragments almost identical to those from Qantir, with adhering glass and lime-rich parting layers, are known from el-Amarna (*6*, *7*) and Lisht. No comparative material is known for the jar fragments with attached semi-finished glass. However, they are inconspicuous and may have been overlooked. It is possible that the use of funnel-shaped extensions was a uniquely Ramesside feature; there is no evidence for them at Amarna, and the Uluburun glass ingots, which pre-date the evidence from Qantir by about 50 to 100 years, are significantly thinner than the one known Qantir ingot, which is 10 cm thick (*14*, *16*). Their limited thickness may be related to the charging of the crucible with a single installment of crushed glass, which upon fusion shrank to form an ingot ~3.5 to 7 cm thick. Only the further addition of crushed glass, using the rim extensions, would have enabled the production of much thicker ingots, approaching the depth of the crucibles.

Summary. The LBA glass industry included several distinct technological steps. After the procurement of plant ash and crushed quartz, the initial semi-finished glass was produced in ovoid jars at a relatively low temperature. The incompatible salt component of the plant ash was then probably removed by washing the crushed semi-finished glass with water. Insufficiently fused material might have been returned for renewed melting with more flux. The semi-finished glass powder was then mixed with a colorant and charged into a cylindrical crucible for the production of colored ingots. The evidence from Qantir suggest that some workshops specialized in specific colors. The colored glass ingots were then transferred to artistic workshops specializing in the production of polychrome glass vessels from a range of monochrome glass ingots, possibly obtained from different glassmaking centers. No close geographical relation is needed between the primary glassmaking and ingot production, and the secondary glass-working workshops.

References and Notes

1. These artistic workshops have been found at Tell Brak, Amarna, and Malkata, among other sites. Typical debris from secondary glass-working includes ingot fragments, monochrome glass rods in a range of colors used for making core-formed vessels, and malformed vessel fragments.
2. Excavations at Qantir first took place in 1929 by Mahmoud Hamza of the Egyptian Antiquities Service; since 1984, excavation has been done by E. B. Pusch as part of a joint Austrian-German mission, on behalf of the Pelizaeus-Museum in Hildesheim. The site is ancient Piramesses, northern capital of Egypt under Ramesses II; the material discussed here dates mostly to around 1250 to 1200 B.C. The village of Qantir is in Faquz district, province Sharkijah, some 30 km north of its capital Zaggazig in the eastern Nile delta. See (*3*) (p. 130) and (*17*) (p. 127) for maps of excavation sites within Qantir-Piramesses.
3. Th. Rehren, E. B. Pusch, *J. Egypt. Archaeol.* **83**, 127 (1997).
4. Th. Rehren, *Archaeometry* **39**, 355 (1997).
5. D. Aston, *Die Keramik des Grabungsplatzes Q I. Teil 1, Corpus of Fabrics, Wares and Shapes* (Zabern, Mainz, Germany, 1998).
6. Sir W. M. F. Petrie was the first to identify this vessel type at the glassworks in Amarna and to link these vessels to glassmaking. For a reassessment of their function, see (*7*, *18*).
7. W. E. S. Turner, *J. Soc. Glass Technol.* **38**, 436 (1954).
8. Materials and methods are available as supporting material on *Science* Online.
9. Working temperatures were estimated on the basis of fabric color: Normal red equals "cold"; darker red to purple equals "warm"; dark red is termed "hot"; and dark red to black vitrified fabric and bloating of the interface is called "very hot." An absolute temperature of about 900°C is estimated as the lower limit of "hot," based on the survival of calcite in the "warm" samples. The temperature above which samples appear "very hot" is estimated to be around 1050°C [see also (*8*)].
10. These ovoid vessels with straight rims (beer jars) or funnel-shaped necks (funnel-necked jars) were originally between 20 and 30 cm tall and had a maximum diameter of 15 to 20 cm. Their typical volume is between 2 and 3 liters [see (*5*), drawings 904–906 and 917–924].
11. We avoid the term "fritting," which is a solid-state reaction of the raw material without the formation of a continuous glass phase, or frit, which as a material has a different meaning in Egyptology than in glassmaking.
12. Published analyses of halophytic plant ashes give between 10 and 50 weight % of these salts (*19*).
13. A. Shugar, Th. Rehren, *Glass Technol.* **43C**, 145 (2002).
14. C. Pulak, in *Res Maritimae*, S. Swiny, R. Hohlfelder, H. Swiny, Eds. (Scholars Press, Atlanta, GA, 1997), pp. 233–262.
15. P. Nicholson, C. Jackson, K. Trott, *J. Egypt. Archaeol.* **83**, 143 (1997).
16. Th. Rehren, E. B. Pusch, A. Herold, in *The History and Prehistory of Glassmaking Technology*, P. McCray, Ed., vol. 8 of *Ceramics and Civilization* (American Ceramics Society, Westerville, OH, 1998), pp. 227–250.
17. E. B. Pusch, in *Pelizaeus-Museum Hildesheim Guidebook*, A. Eggebrecht, Ed. (Zabern, Mainz, Germany, 1996), 126–144.
18. P. Nicholson, *Egyptian Faience and Glass* (Shire Egyptology Series, Princes Risborough, UK, 1993).
19. R. Brill, *Chemical Analyses of Early Glasses* (Corning, New York, 1999).

20. We acknowledge the long-term funding of the excavations at Qantir through the Deutsche Forschungsgemeinschaft and additional funding for the study of the glass workshop from the British Academy and individual sponsors.

Supporting Online Material
www.sciencemag.org/cgi/content/full/308/5729/1756/DC1
Materials and Methods
References and Notes

31 January 2005; accepted 20 April 2005
10.1126/science.1110466

Tubulin Polyglutamylase Enzymes Are Members of the TTL Domain Protein Family

Carsten Janke,[1]* Krzysztof Rogowski,[2]* Dorota Wloga,[2]* Catherine Regnard,[3] Andrey V. Kajava,[1] Jean-Marc Strub,[4] Nevzat Temurak,[1] Juliette van Dijk,[1] Dominique Boucher,[5] Alain van Dorsselaer,[4] Swati Suryavanshi,[2] Jacek Gaertig,[2]† Bernard Eddé[1,6]†

Polyglutamylation of tubulin has been implicated in several functions of microtubules, but the identification of the responsible enzyme(s) has been challenging. We found that the neuronal tubulin polyglutamylase is a protein complex containing a tubulin tyrosine ligase–like (TTLL) protein, TTLL1. TTLL1 is a member of a large family of proteins with a TTL homology domain, whose members could catalyze ligations of diverse amino acids to tubulins or other substrates. In the model protist *Tetrahymena thermophila*, two conserved types of polyglutamylases were characterized that differ in substrate preference and subcellular localization.

Polyglutamylation is an uncommon type of post-translational modification that adds multiple glutamic acids to a γ-carboxyl group of a glutamate residue of target proteins, including tubulin and nucleosome assembly proteins NAP1 and NAP2 (*1*–*4*). The resulting polyglutamate side chains are of variable length, allowing for a graded regulation of protein-protein interactions. Polyglutamylation regulates the binding of neuronal microtubule (MT)–associated proteins as a function of the length of the polyglutamate chain, which suggests that the modification is important for the organization of the neuronal MT network (*5*). Tubulin polyglutamylation may also play a role in centriole stability (*6*), axoneme motility (*7*, *8*), and mitosis (*9*, *10*).

Identification of mouse brain polyglutamylase. Monoclonal antibody (mAb) 206, raised against a partially purified brain tubulin polyglutamylase fraction, immunoprecipitates the enzyme complex, including the PGs1 (polyglutamylase subunit 1) protein p32 (*11*).

[1]Centre de Recherches de Biochimie Macromoléculaire, CNRS, 34293 Montpellier, France. [2]Department of Cellular Biology, University of Georgia, Athens, GA 30602, USA. [3]Department of Molecular Biology, Adolf Butenandt Institute, 80336 Munich, Germany. [4]Université Louis Pasteur, 67087 Strasbourg, France. [5]Laboratoire de Biochimie Cellulaire, CNRS, Université Paris 6, 75252 Paris, France. [6]Université Paris 6, 75252 Paris, France.

*These authors contributed equally to this work.
†To whom correspondence should be addressed. E-mail: jgaertig@cb.uga.edu; bernard.edde@crbm.cnrs.fr

We used two-dimensional (2D) gel electrophoresis followed by nano-LC-MS-MS (liquid chromatography–mass spectrometry) to identify four additional protein components of the same complex: p24, p33, p49, and p79 (Fig. 1A) (table S1). Polyclonal antibodies were raised against recombinant proteins or peptides of p24, p32, p33, p49, and p79 and used for coimmunoprecipitation analyses; mAb 206, polyclonal antibody to p32 (L83), and polyclonal antibody to p79 (L80) precipitated ≥80% of the polyglutamylase activity (Fig. 1B) along with all five proteins (Fig. 1C). These five proteins also consistently copurified with the polyglutamylase activity during several purification steps (fig. S1); therefore, p33, p49, p79, and p24 were named PGs2, PGs3, PGs4, and PGs5, respectively. Additional proteins were found in the mAb 206–immunoprecipitated fraction, including Arp1 and CF Im25 (table S1), but these did not consistently copurify with the enzyme activity.

The apparent size of the neuronal polyglutamylase complex, 360 kD (*12*), is greater than the theoretical sum of the predicted molecular masses of all five subunits (217 kD), which implies that the complex contains multiple copies of one or more subunits. Because some of the components appear on 2D gels as multiple spots at different isoelectric points, they may themselves be subject to charge-altering post-translational modifications (Fig. 1A). Indeed, PGs1 was phosphorylated on Ser^{279} (*13*).

PGs1 (a product of the mouse gene *GTRGEO22*) is required for sperm axoneme assembly and normal animal behavior (*14*) and may act in the intracellular targeting of the polyglutamylase complex (*11*). PGs3 is an ortholog of the human TTLL1 protein (*15*). The amino acid sequence of TTLL1 exhibits 17% identity with tubulin tyrosine ligase (TTL), which catalyzes the addition of tyrosine to the C-terminal glutamate of detyrosinated α-tubulin (*16*). Despite obvious differences, both polyglutamylation and tyrosination reactions involve an amino acid addition to a glutamate residue through the formation of an amide bond. Thus, we examined the possibility that TTLL1 is the catalytic subunit of neural tubulin polyglutamylase.

A structural model for TTLL1. The amino acid sequence of TTLL1 (PGs3) contains three conserved motifs that correspond to the adenosine triphosphate (ATP)/Mg^{2+}-binding site typical of enzymes with a carboxylate-amine/thiol ligase activity, such as glutathione synthetase (*17*). Although the overall sequence similarity between TTLL1 and the known carboxylate-amine/thiol ligase enzymes is low, we could align the ATP-binding regions as well as all major parts of TTLL1. Using glutathione synthetase from *Escherichia coli* as a template, we obtained a structural model of TTLL1 by homology-based modeling (Fig. 2, A and B). Docking of ATP and Mg^{2+} into the model supports the localization of the ATP/Mg^{2+}-binding site (Fig. 2, B and C) (fig. S2). We were also

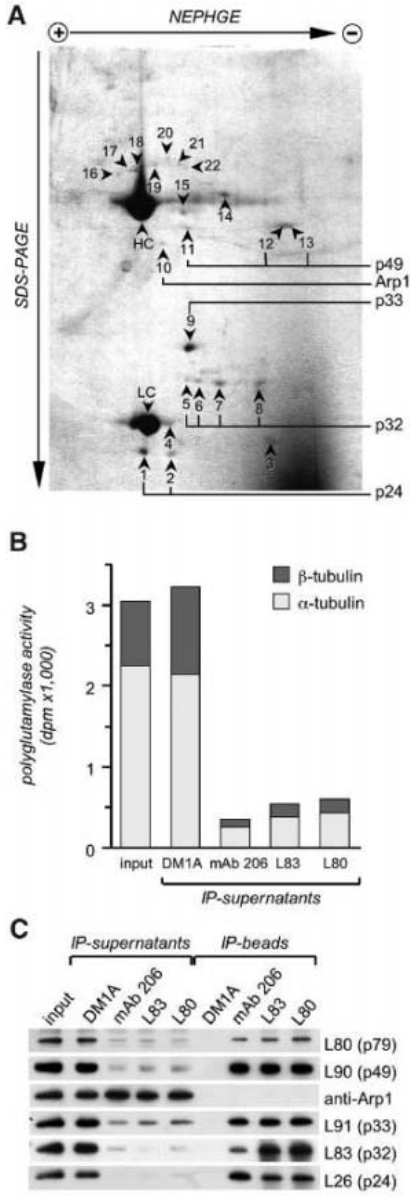

Fig. 1. Characterization of the neuronal polyglutamylase. (**A**) Coomassie Brilliant Blue–stained nonequilibrium pH gradient electrophoresis (NEPHGE)/SDS–polyacrylamide gel electrophoresis (PAGE) 2D gel of a purified polyglutamylase fraction, immunoprecipitated from 200 3-day-old mouse brains with mAb 206. All numbered protein spots were identified by nano-LC-MS-MS (table S1). HC and LC mark the positions of heavy and light chains of mAb 206. (**B**) Immunoprecipitations with mAb 206, L83 [antibody to p32 (*11*)], L80 (antibody to p79), and DM1A (α-tubulin mAb) used as a control. Equal proportions of input and supernatants were assayed for polyglutamylase activity. (**C**) Input, supernatants, and beads (equal proportions) were analyzed by immunoblotting with antibodies L26, L80, L83, L90, and L91 and antibody to Arp1. The polyglutamylase activity and all five polyglutamylase complex subunits were strongly depleted from the supernatants. The proteins were quantitatively recovered with the beads of mAb 206, L83, and L80, but not of DM1A. Arp1 did not quantitatively copurify with the enzyme.

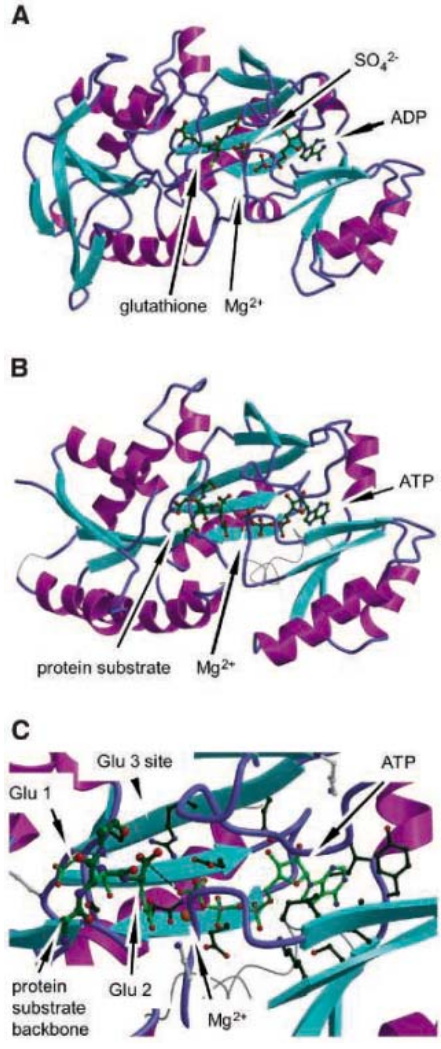

Fig. 2. A structural model of TTLL1. Cyan arrows represent β sheets, α helices are magenta, and loops are blue. (**A**) Crystal structure of glutathione synthetase from *E. coli* (PDB code 1GSA) in a complex with adenosine diphosphate (ADP), glutathione, Mg^{2+}, and sulfate (*27*). (**B**) A model of mouse TTLL1 (PGs3) in a complex with ATP, Mg^{2+}, and a protein substrate. The regions of TTLL1 that could not be modeled are drawn as thin lines. (**C**) A close-up view of the active center of TTLL1. The protein substrate is a three-residue peptide with a central modified glutamate (backbone in medium green). The flanking amino acids are drawn only with Cβ atoms for clarity. The glutamate side chain contains two additional glutamate residues (Glu 1, Glu 2). The putative site for the next glutamate residue to be added to the side chain is indicated (Glu 3 site). All residues of the active site that are conserved with other ATP-dependent carboxylate-amine ligases are shown in dark green (see fig. S2). Some positively charged amino acid residues (Lys^{13}, Lys^{142}, and Lys^{215} in light gray) that are specific to TTLL1 and close to the active site might be important for substrate binding. The proximity of the carboxyl group of Glu 2 and the phosphate of ATP could catalyze the formation of an acylphosphate intermediate (broken line). Oxygen, nitrogen, phosphate, and magnesium atoms are in red, blue, magenta, and orange, respectively.

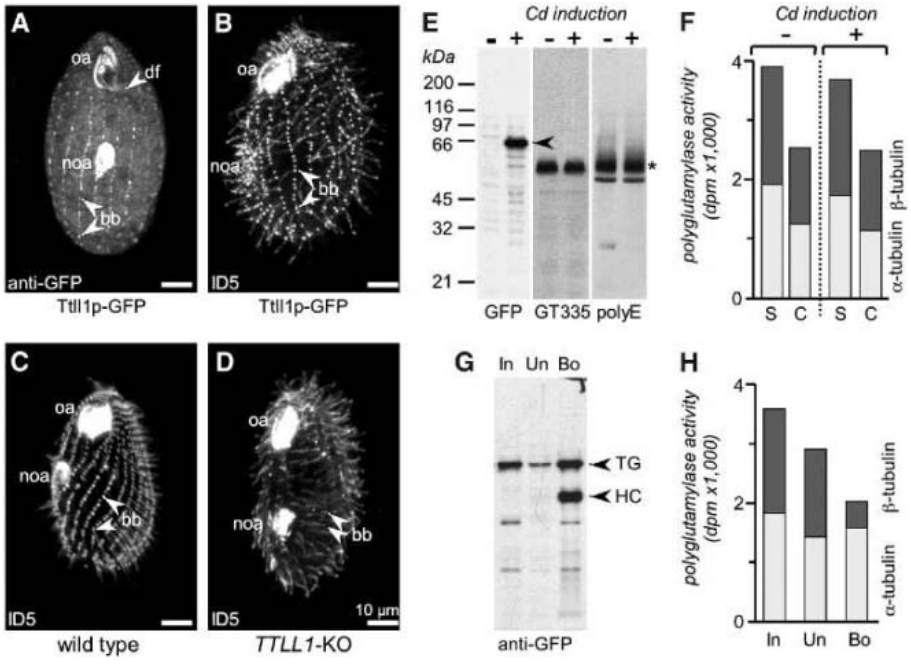

Fig. 3. Ttll1p of *Tetrahymena* is associated with tubulin glutamylation. (**A**) A cell expressing Ttll1p-GFP, labeled by immunofluorescence using antibody to GFP. (**B** to **D**) Polyglutamylated MTs labeled by mAb ID5 in a cell overproducing Ttll1p-GFP (B), a wild-type cell (C), and a *TTLL1*-null cell (D). Note a strong reduction in the labeling of rows of basal bodies in (D) relative to (C). Abbreviations: oa, oral apparatus; noa, new oral apparatus before cell division; df, deep fiber; bb, basal bodies. (**E**) Immunoblotting studies on total *Tetrahymena* cell extracts before (–) and after (+) 3 hours of cadmium induction of Ttll1p-GFP, analyzed with antibodies to GFP and to polyglutamylation (mAb GT335 and antibody polyE). An arrowhead points to Ttll1p-GFP; an asterisk marks the comigrating α- and β-tubulin bands. (**F**) Soluble (S) and cytoskeletal (C) fractions from cells overproducing Ttll1p-GFP (+) or noninduced controls (–) were analyzed for tubulin polyglutamylase activity in vitro. (**G** and **H**) Soluble fractions of cells overproducing Ttll1p-GFP were subjected to immunoprecipitation with antibody to GFP. The input (In), unbound (Un), and bound (Bo) fractions were analyzed by immunoblotting with antibody to GFP (arrowhead TG points to Ttll1p-GFP, HC to the antibody heavy chain) (G) and assayed for glutamylase activity in vitro (H). Equal volumes of input, unbound, and bead fractions were analyzed by immunoblotting; a volume of bead fraction 20 times this size was assayed for glutamylase activity.

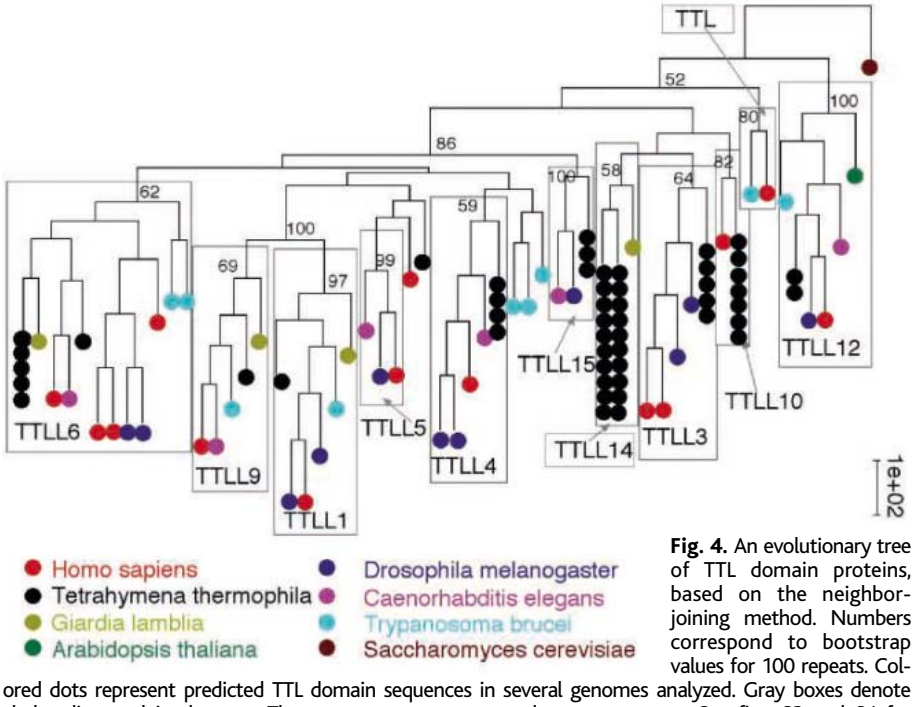

Fig. 4. An evolutionary tree of TTL domain proteins, based on the neighbor-joining method. Numbers correspond to bootstrap values for 100 repeats. Colored dots represent predicted TTL domain sequences in several genomes analyzed. Gray boxes denote clades discussed in the text. The yeast sequence was used as an outgroup. See figs. S3 and S4 for complete data.

able to fit a peptide with a polyglutamate side chain into the active site, which located a putative binding site for free glutamate (Fig. 2C). Thus, it is likely that TTLL1 protein is the catalytic subunit of neural tubulin polyglutamylase.

Ttll1p is associated with α-tubulin polyglutamylase activity in vivo. When expressed in bacteria or in various cell lines as well as in several heterologous systems, the murine TTLL1 had a strong tendency to precipitate and did not show polyglutamylase activity in vitro. We used a homologous protein expression system based on the ciliated protist *Tetrahymena thermophila* to assess the role of TTLL1-related proteins in polyglutamylation. *Tetrahymena* has a complex cytoskeleton with a large number of distinct types of MTs (*18*). Most types of MTs in *Tetrahymena* are monoglutamylated, although a small subset—including MTs of the basal bodies (BBs), cilia, contractile vacuole pore (CVP), and oral deep fiber (DF)—have side chains composed of two or more glutamates (*19*). Using the recently sequenced macronuclear genome of *Tetrahymena* (*20*), we identified the likely TTLL1 ortholog Ttll1p (54% amino acid sequence identity with TTLL1). Ttll1p with an N-terminal green fluorescent protein (GFP) was strongly overexpressed by means of a cadmium-inducible gene promoter (*21*). Ttll1p-GFP localized to a subset of polyglutamylated MT organelles including BBs, CVPs, and DF (Fig. 3A), but no increase in the level of MT polyglutamylation over normal levels was detected (Fig. 3, B, C, and E) and the phenotype appeared normal. Similar results were obtained for the hemagglutinin epitope C-terminally tagged protein (*22*). No change in tubulin polyglutamylation activity in vitro was detected in cell extracts despite the strong accumulation of Ttll1p-GFP (Fig. 3F). However, a polyglutamylase activity directed mostly toward α-tubulin was coimmunoprecipitated with antibody to GFP from extracts of overexpressing cells (Fig. 3, G and H). The overexpressed protein apparently could replace a part of the endogenous Ttll1p but could not function alone. On the basis of the data obtained for the murine homolog, it is likely that Ttll1p also acts in a complex and that other subunits are limiting.

We also used gene disruption to construct cells completely lacking the *TTLL1* gene. The *TTLL1*-null cells had a normal phenotype but showed a strong reduction in tubulin polyglutamylation in the BBs (Fig. 3, C and D). This result confirms that Ttll1p is involved in polyglutamylation but also suggests that there are additional polyglutamylase activities in this organism that do not require Ttll1p.

The TTLL family. TTLL1 and TTL are members of a large family of conserved eukaryotic proteins with a TTL homology domain, which raises the possibility that other members of this family are also involved in polyglutamylation or other types of posttranslational amino acid ligations. Phylogenetic analyses showed

that TTLLs of diverse eukaryotes belong to several conserved subtypes (Fig. 4) (figs. S3 and S4). We used the HsTTLL1 sequence (*15*) as a template for tBLASTn searches to identify all TTLL loci of *Tetrahymena* and several other model eukaryotes. Phylogenetic analyses revealed 10 clades of TTLLs, eight of which contain predicted mammalian proteins. *Tetrahymena* has one to seven sequences in most groups, as well as one clade of 20 ciliate-specific TTLLs. Among the genomes surveyed, only *Trypanosoma* has a close homolog of the mammalian TTL, which may be why an enzymatic activity of TTL was not detected in invertebrates (*23*) and *Tetrahymena* (*24*).

***Tetrahymena* Ttll6Ap is a β-tubulin–preferring polyglutamylase.** The *Tetrahymena TTLL6A* sequence belongs to a clade related to TTLL1 (Fig. 4) (fig. S3). Overproduced Ttll6Ap-GFP localized mainly to cilia, with a small amount associated with BBs and cell body MTs (Fig. 5A). Overproduction of Ttll6Ap-GFP led to a strong increase in polyglutamylation in cilia and on cell body MTs (Fig. 5C; compare with Fig. 3C). A strong increase in tubulin polyglutamylation (but not in polyglycylation) was also detected in whole cells by immunoblotting (Fig. 5F).

A truncated variant lacking the 286 C-terminal amino acids, Ttll6ApΔ_{710}-GFP, localized predominantly to the cell body with a strong preference for subcortical MTs that extend from the apical end of the cell and run below the BBs (Fig. 5B). Consistently, overexpression of Ttll6ApΔ_{710}-GFP led to a strong increase in polyglutamylation on MTs in the cell body and to a much lesser extent in cilia (Fig. 5D). Thus, the 286 C-terminal amino acids of Ttll6Ap are required for preferential targeting to cilia.

We used the truncated version of Ttll6Ap for biochemical studies because the proportion of this variant in the soluble/cytosolic pool is increased relative to the full-length protein. Extracts of cells overexpressing Ttll6ApΔ_{710}-GFP showed a 100-fold increase in polyglutamylase activity in vitro for β-tubulin and a 10-fold increase for α-tubulin relative to noninduced cells (Fig. 5E). This activity copurified with Ttll6ApΔ_{710}-GFP protein under all conditions tested (fig. S5, A to C). No in vitro activity toward NAP proteins was detected. Thus, Ttll6Ap is a tubulin polyglutamylase displaying a strong preference for the β-tubulin subunit.

Increased polyglutamylation affects cell growth and motility. *Tetrahymena* cells overexpressing Ttll6Ap-GFP ceased to multiply within a few hours after cadmium induction (Fig. 5G), and most had paralyzed cilia (Fig. 5I), indicating that excessive polyglutamylation inhibits cell proliferation and ciliary dynein-based motility. Cells overexpressing the truncated protein also ceased to proliferate, but the effect on ciliary motility was much weaker, in accordance with the altered protein localization pattern (Fig. 5, H and I). These effects did not occur when a mutation in the predicted ATP binding site of the TTL homology domain (Glu^{422} → Gly, E422G) was introduced (fig. S2). Relative to the ATPase-active protein, the inactive variant, Ttll6ApΔ_{710}-E422G-GFP, was expressed at a similar level (Fig. 5F) and localized to the same types of MT organelles (*22*). However, no increase in tubulin polyglutamylation was observed (Fig. 5F), nor were alterations of cell growth or motility observed (Fig. 5, H and I); these findings confirm that excessive polyglutamylation, not the overproduced protein, was responsible for the observed phenotypes.

Conclusion. The simplest interpretation of our data is that TTLL1/Ttll1p and Ttll6Ap are two types of tubulin polyglutamylase catalytic components with distinct tubulin subunit preferences. The neuronal TTLL1 as well as Ttll1p have a preference for α-tubulin, whereas Ttll6Ap preferentially polyglutamylates β-tubulin. Unlike Ttll6Ap, Ttll1p (and its murine ortholog) did not increase polyglutamylation in vitro and in vivo upon overproduction. However, TTLL1 exists in

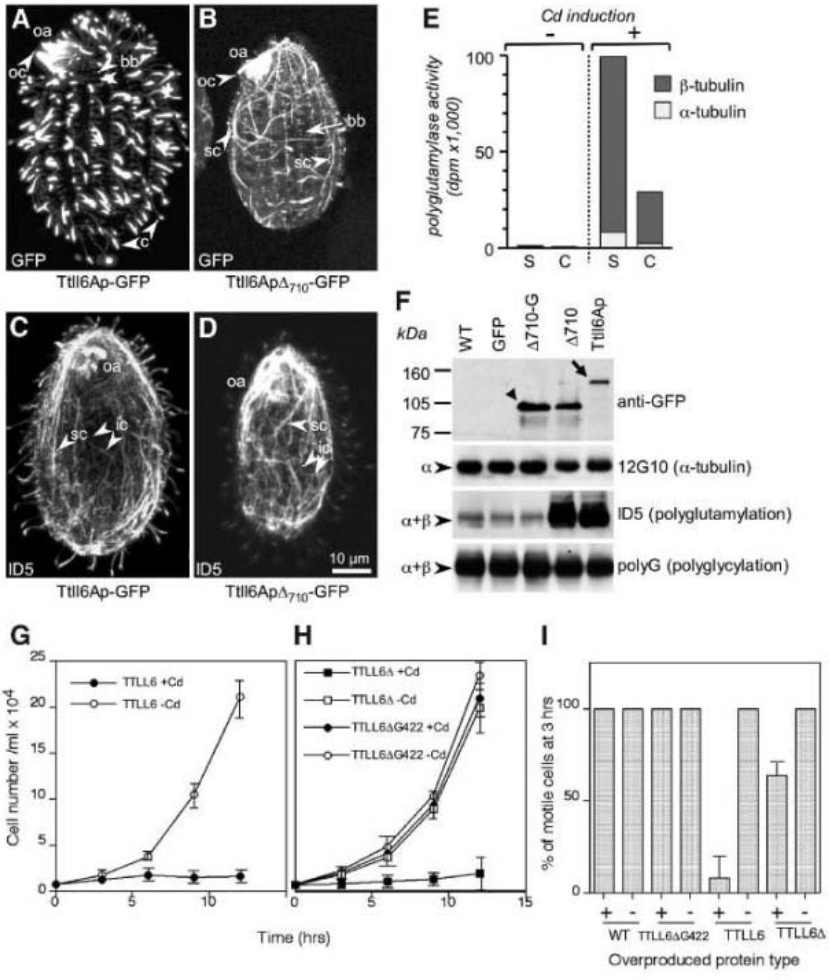

Fig. 5. Ttll6Ap-GFP is associated with strong tubulin polyglutamylation in vivo and in vitro. (**A** to **D**) GFP fluorescence [(A) and (B)] and immunofluorescence images with mAb ID5 [(C) and (D)] of cells overproducing Ttll6Ap-GFP [(A) and (C)] or Ttll6ApΔ_{710}-GFP [(B) and (D)]. The staining detected in (A) and (B) colocalized with MTs visualized by mAb 12G10 to α-tubulin (*22*). Strong polyglutamylation appears in the cell body in cells overproducing forms of Ttll6Ap, whereas polyglutamylation is restricted to cilia and basal bodies in control cells (compare with the wild-type cell in Fig. 3C). Abbreviations: c, cilia; oc, oral cilia; oa, oral apparatus; bb, basal bodies; sc, subcortical MTs; ic, intracytoplasmic MTs. (**E**) Tubulin polyglutamylase assays using soluble (S) and cytoskeletal (C) fractions from Ttll6ApΔ_{710}-GFP cells grown in the absence (–) and presence (+) of cadmium for 3 hours. (**F**) Immunoblots of total cells or cytoskeletons of the following strains after 3 hours of cadmium treatment: wild type (WT), cells overproducing GFP (GFP), Ttll6ApΔ_{710}-E422G-GFP (Δ710-G), Ttll6ApΔ_{710}-GFP (Δ710), and Ttll6Ap-GFP (Ttll6Ap). Antibodies used are shown at the right. (**G** to **I**) Cells overproducing an enzymatically active Ttll6Ap and not an ATPase-deficient form fail to multiply and undergo ciliary paralysis. Growth curves on SPP medium are shown for strains expressing Ttll6Ap-GFP (G), Ttll6ApΔ_{710}-GFP (H), or Ttll6ApΔ_{710}-E422G-GFP (H) with or without cadmium induction. Note that only the ATPase-capable proteins reduce the growth rate. (I) Percentage of motile cells in several overproducing strains. After 3 hours of cadmium induction, 100 to 200 cells were scored for vigorous motility. Either extremely sluggish (showing rotations but no directional movement) or completely paralyzed cells were counted as nonmotile. Data in (G) to (I) are mean values from three independent experiments.

a protein complex, and additional subunits may be required for its activity and could be limiting in vivo. Indeed, immunoprecipitation of Ttll1p-GFP from overproducing *Tetrahymena* cells led to a recovery of polyglutamylase activity.

Ttll6Ap is a much larger protein (116 kD) than TTLL1 (49 kD) and Ttll1p (42 kD), and it may contain all properties required for autonomous polyglutamylase activity. The four noncatalytic subunits identified in the neuronal TTLL1 complex may be involved in tubulin substrate recognition, regulation of enzymatic activity, or subcellular localization, as has been suggested for PGs1 (*11*). It is likely that Ttll1p is also in a complex, as is the murine homolog. Except for PGs4, we could not identify homologs of the other subunits of the neural complex (PGs1, PGs2, PGs5) outside of vertebrates, including *Tetrahymena*; therefore, variations in the composition of noncatalytic subunits likely occur across phyla. The unusually large number of TTLL genes in *Tetrahymena* and the lack of a detectable loss-of-function phenotype for *TTLL1* suggest functional redundancy. In contrast, a mutation in the PGs1 component of the murine TTLL1 complex led to defective sperm axonemes and changes in animal behavior (*14*). In *Caenorhabditis elegans*, RNA interference (RNAi) depletion of *C55A6.2* (a TTLL5 type) causes embryonic lethality and sterility (*25*). Depletion of TTLL1 mRNA in PC12-E2 cells inhibited neurite outgrowth, suggesting an essential function in neurogenesis (*22*).

The phylogenetic association of TTLL1, TTLL9, TTLL4, TTLL6, TTLL5, and TTLL15 protein types (86% bootstrap value; Fig. 4) suggests that these protein types are all involved in glutamylation of tubulin or possibly of other proteins such as NAPs (*4*). Other members of the TTLL family may catalyze different types of posttranslational addition of an amino acid, such as polyglycylation (*26*).

References and Notes

1. B. Eddé *et al.*, *Science* **247**, 83 (1990).
2. M. Rüdiger, U. Plessman, K. D. Kloppel, J. Wehland, K. Weber, *FEBS Lett.* **308**, 101 (1992).
3. V. Redeker, R. Melki, D. Prome, J. P. Le Caer, J. Rossier, *FEBS Lett.* **313**, 185 (1992).
4. C. Regnard *et al.*, *J. Biol. Chem.* **275**, 15969 (2000).
5. C. Bonnet *et al.*, *J. Biol. Chem.* **276**, 12839 (2001).
6. Y. Bobinnec *et al.*, *J. Cell Biol.* **143**, 1575 (1998).
7. C. Gagnon *et al.*, *J. Cell Sci.* **109**, 1545 (1996).
8. K. Million *et al.*, *J. Cell Sci.* **112**, 4357 (1999).
9. Y. Bobinnec *et al.*, *Cell Motil. Cytoskeleton* **39**, 223 (1998).
10. C. Regnard, E. Desbruyères, P. Denoulet, B. Eddé, *J. Cell Sci.* **112**, 4281 (1999).
11. C. Regnard *et al.*, *J. Cell Sci.* **116**, 4181 (2003).
12. C. Regnard, S. Audebert, E. Desbruyères, P. Denoulet, B. Eddé, *Biochemistry* **37**, 8395 (1998).
13. The three more acidic spots of p32 contain phosphorylated peptides 277 to 284 (Arg-Pro-Ser-Val-Pro-Met-Ala-Arg) (Fig. 1A, spots 5 to 7). Phosphorylation site prediction (ExPASy Proteomics Server, www.expasy.org) indicates that Ser^{279} can be phosphorylated by cAMP- or cGMP-dependent protein kinases.
14. P. K. Campbell *et al.*, *Genetics* **162**, 307 (2002).
15. V. Trichet, M. Ruault, G. Roizes, A. De Sario, *Gene* **257**, 109 (2000).
16. K. Ersfeld *et al.*, *J. Cell Biol.* **120**, 725 (1993).
17. M. Y. Galperin, E. V. Koonin, *Protein Sci.* **6**, 2639 (1997).
18. J. Gaertig, *J. Eukaryot. Microbiol.* **47**, 185 (2000).
19. K. Rogowski, J. Gaertig, unpublished data.
20. The Institute for Genomic Research, *Tetrahymena thermophila* Sequence BLAST Search (http://tigrblast.tigr.org/er-blast/index.cgi?project=ttg).
21. Y. Shang *et al.*, *Proc. Natl. Acad. Sci. U.S.A.* **99**, 3734 (2002).
22. C. Janke *et al.*, data not shown.
23. S. F. Preston, G. G. Deanin, R. K. Hanson, M. W. Gordon, *J. Mol. Evol.* **13**, 233 (1979).
24. D. Raybin, M. Flavin, *J. Cell Biol.* **73**, 492 (1977).
25. I. Maeda, Y. Kohara, M. Yamamoto, A. Sugimoto, *Curr. Biol.* **11**, 171 (2001).
26. V. Redeker *et al.*, *Science* **266**, 1688 (1994).
27. T. Hara, H. Kato, Y. Katsube, J. Oda, *Biochemistry* **35**, 11967 (1996).

28. Supported by Association de la Recherche contre le Cancer award ARC 5859 (B.E.), Fondation pour la Recherche Médicale award INE20021108027/1 (C.J.), NSF award MBC-0235826 (J.G.), and EMBO long-term fellowship ALTF 387-2001 (C.J.). Preliminary sequence data for *Tetrahymena thermophila* were obtained from The Institute for Genomic Research. We thank E. Desbruyères, G. Herrada-Aldrian, J. M. Donnay, A. Bernet, and G. Rabeharivelo for technical assistance; P. Chaussepied, J. Frankel, M. Gorovsky, E. Kipreos, and M. Fechheimer for helpful comments; R. Melki for antibody to Arp1; S. Dettwiler and W. Keller for antibody to CF Im25; M. Gorovsky for antibodies polyG and polyE; K. Weber and S. Westermann for mAb ID5; and J. Frankel for mAb 12G10. Molecular interaction data have been deposited in the Biomolecular Interaction Network Database with accession code 295280.

Supporting Online Material
www.sciencemag.org/cgi/content/full/1113010/DC1
Materials and Methods
Figs. S1 to S5
Table S1
References

31 March 2005; accepted 28 April 2005
Published online 12 May 2005;
10.1126/science.1113010
Include this information when citing this paper.

REPORTS

Quantum Interference Device Made by DNA Templating of Superconducting Nanowires

David S. Hopkins, David Pekker, Paul M. Goldbart, Alexey Bezryadin*

The application of single molecules as templates for nanodevices is a promising direction for nanotechnology. We used a pair of suspended DNA molecules as templates for superconducting two-nanowire devices. Because the resulting wires are very thin, comparable to the DNA molecules themselves, they are susceptible to thermal fluctuations typical for one-dimensional superconductors and exhibit a nonzero resistance over a broad temperature range. We observed resistance oscillations in these two-nanowire structures that are different from the usual Little-Parks oscillations. Here, we provide a quantitative explanation for the observed quantum interference phenomenon, which takes into account strong phase gradients created in the leads by the applied magnetic field.

DNA has recently been considered as a "backbone" for the fabrication of information-processing devices, chemical and biological sensors, and molecular transistors at the nanometer-size scale (*1*, *2*). By taking advantage of DNA self-assembly possibilities (*3*), one can envision using single DNA and self-assembled DNA constructs as scaffolds for precise nanometer-scale positioning of other molecules and nanoscale objects. Recently, electronic devices with features that have molecular-scale dimensions have been assembled on such molecular-scale scaffolds (*4*). One of the simplest practical realizations of this approach lies in the metallization of DNA molecules (*5*). Previously, a wet-chemistry approach was used to metallize DNA (*5*–*8*), which tends to yield rather granular wires that become highly resistive at low temperatures.

We used a physical method of metallization [analogous to (*9*)] that involves sputter deposition of metallic films over suspended DNA molecules to fabricate wires as thin as 3 to 4 molecular diameters (as thin as 5 to 15 nm). Our nanowires are homogeneous, make seamless contacts with the leads, and become superconducting at low temperatures. We

Department of Physics and Frederick Seitz Materials Research Laboratory, University of Illinois at Urbana-Champaign, Urbana, IL 61801, USA.

*To whom correspondence should be addressed. E-mail: bezryadi@uiuc.edu

fabricated structures with pairs of such DNA-templated nanowires (Fig. 1) (*10*) to study quantum interference effects and the effect of thermal fluctuations at the nanoscale. Well-known examples of quantum interference include critical-current oscillations in conventional superconducting quantum interference devices (SQUIDs) (*11*, *12*) and Little-Parks resistance oscillations in thin-walled cylinders (*13*). In these examples, the periods of the oscillations are controlled by the superconducting flux quantum $\Phi_0(\equiv h/2e)$ where h is Planck's constant and $-e$ is the electronic charge, divided by the geometrical area enclosing the magnetic field. Our measurements on two-nanowire devices show a strong discrepancy with the usual behavior, and we provide a quantitative theoretical explanation for the observed period and amplitude of the oscillations.

Transport measurements at temperatures as low as 0.3 K at various magnetic fields (*10*) reveal a resistive transition, associated with the development of superconducting phase coherence throughout the nanowires, occurring over a broad temperature range in the absence of a magnetic field (Fig. 2A). This transition is found to broaden and narrow periodically with magnetic field. Consequently, at any temperature in the transition region, we see highly pronounced and very regular oscillations of the resistance with magnetic field (Fig. 2B). For higher temperatures in this region, the oscillation appears cosinusoidal, with a maximum in the amplitude at some intermediate temperature. For each sample, the observed period does not show any temperature or field dependence.

What distinguishes our resistance oscillations from those found, for example, by Little and Parks? First, the most notable aspect of these oscillations is the value of the measured period (456 μT in Fig. 2B), which is far shorter than one would estimate on the basis of the superconducting flux quantum divided by the area of the hole between the wires ($\Phi_0/2ab$ = 25 mT with dimensions a and b, defined in Fig. 1A, for sample 219-4 of Table 1). Thus, we see that the period of our oscillations is not controlled by the geometrical area defined by the nanowires and the edges of the leads. Instead, we find that in the low magnetic-field regime (when no vortices are present in the leads), the period is controlled by Φ_0 divided by a new quantity: the product of the lead width ($2l \sim$ 9 to 15 μm) and the interwire spacing ($2a \sim$ 0.3 to 4 μm). The reason for this is that the leads are mesoscopic—i.e., they are narrower than the perpendicular magnetic penetration depth ($\lambda_\perp \sim 70$ μm)—and therefore the magnetic field penetrates the leads with negligible attenuation. Second, because the resistance is caused by thermal phase fluctuations (i.e., phase slips) in very narrow wires, the oscillations are observable over a wide range of temperatures (~1 K). Third, the Little-Parks resistance is wholly ascribed to a rigid shift of the $R(T)$ curve with magnetic field as the critical temperature T_c oscillates. In contrast, in our system we find a much more substantial contribution to the resistance oscillations coming from the modulation of the barrier heights for phase slips.

Superconducting nanowires are unusual in that they never show zero resistance, although resistance does decrease exponentially upon cooling. As discussed by Little (*14*), Langer and Ambegaokar (LA) (*15*), and McCumber and Halperin (MH) (*16*), the origin of this resistive behavior lies in the occurrence of thermally activated slips of the phase of the Ginzburg-Landau (GL) order parameter $\psi(\vec{r})$. During a phase slip, a small normal segment appears on the nanowire for a short time, causing the loss of phase coherence between the leads. Resistance is then associated with a nonzero value of the average voltage, which matches the imbalance, due to the current, between forward and backward phase slips (*12*).

We developed an extension of LAMH theory that applies to devices containing two nanowires connected in parallel, including the effect of an applied magnetic field. The model accurately describes the period, magnitude, and temperature dependence of the observed magnetoresistance oscillations. The essential ingredients in our model are (i) leads, in which the applied magnetic field induces supercurrents and, hence, gradients in the phase of the order parameter and (ii) the two wires, whose behavior is controlled by the leads through the boundary conditions imposed by the leads on the phase of the order parameters in the wires. We assume that the wires have sufficiently small cross sections that the currents through them do not feed back on the order parameter in the leads.

In our model, thermally activated phase slips cause the superconducting order parameter to explore a discrete family of local minima of the free energy. These minima (and the saddle-point states connecting them) may be indexed by the net (i.e., forward minus reverse) number of phase slips that have occurred in each wire (n_1 and n_2) or, more usefully, by $n_s = \min(n_1, n_2)$ (i.e., the net number of phase slips that have passed through both wires) and $n_v = n_1 - n_2$ (i.e., the number of vortices accumulated in the loop, which is formed by the wires and the edges of the leads). Notably, two configurations with identical n_v but distinct n_s and n_s' have identical order parameters but differ in energy by $\Phi_0 I (n_s' - n_s)$, due to the work done by the current source supplying the current I.

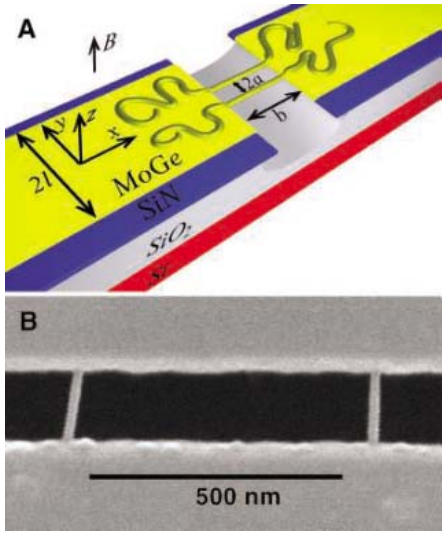

Fig. 1. (**A**) Schematic of the DNA-templated two-nanowire device. Two strands of DNA are stretched across a trench etched into SiN/SiO_2 on a Si chip (*6*). The molecules and the banks are coated with superconducting $Mo_{21}Ge_{79}$. The dimensions are indicated. (**B**) SEM micrograph of two metal-coated DNA molecules (sample 219-4).

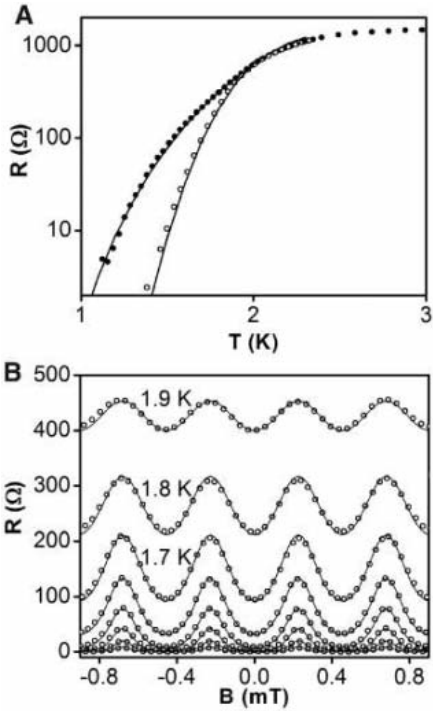

Fig. 2. (**A**) Resistance versus temperature measurements (sample 219-4) in zero magnetic field (open circles) and at a magnetic field of 228 μT (solid circles) corresponding to a maximum change in magnetoresistance. The lines are theoretical fits, based on the short-wire limit of our theory, with the following fitting parameters: J_{c1} = 639 nA, J_{c2} = 330 nA, T_{c1} = 2.98 K, and T_{c2} = 2.00 K, with corresponding coherence lengths $\xi_1(0)$ = 23 nm and $\xi_2(0)$ = 30 nm. (**B**) Resistance versus magnetic field measurements (sample 219-4) at temperatures from 1.2 to 1.9 K in 0.1 K increments. The lines are theoretical fits using the same fitting parameters as in (A) with the period set to 456 μT. Resistance is measured in ohms.

Table 1. A summary of the geometries (obtained from SEM), the theoretical predictions for the period of the magnetoresistance oscillations, and the measured periods for all of the two-wire devices. The geometry of 930-1 was changed by milling with a focused ion beam, and the magnetoresistance period was remeasured. Wire sep., wire separation; Th. per., theoretical period; Ex. per., experimental period, diff., difference.

Sample	Wire length b (nm)	Wire sep. $2a$ (nm)	Lead width $2l$ (nm)	Th. per. ΔB (μT)	Ex. per. (μT)	% diff.
205-4	121	265	11270	929	947	1.9
219-4	137	595	12060	389	456	14.8
930-1	141	2450	14480	78.4	77.5	–1.2
930-1 (FIB-narrowed leads)	141	2450	8930	127	128	0.9
205-2	134	4050	14520	47.4	48.9	3.0

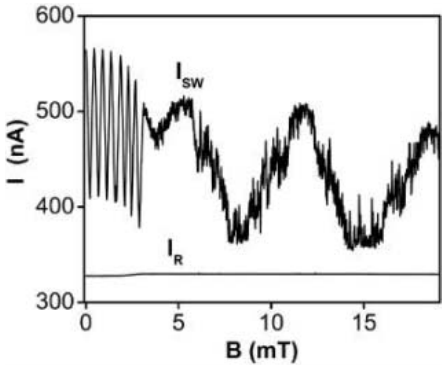

Fig. 3. Critical switching (I_{SW}) and retrapping (I_R) currents plotted versus magnetic field, measured at T = 285 mK (sample 219-4).

Due to the screening currents in the left lead (Fig. 1A), induced by the applied perpendicular magnetic field B (and independent of the wires), there is a field-dependent phase $\delta_{1\to2,L}(B) = \int_1^2 d\vec{r} \cdot \vec{\nabla}\varphi(B)$, where $\varphi(B)$ is the field-dependent phase of the order parameter, accumulated in passing from the point at which wire 1 (the back one) contacts the left (L) lead to the point at which wire 2 (the front one) contacts the left lead. Similarly, the field creates a phase accumulation $\delta_{1\to2,R}(B)$ between the contact points in the right (R) lead. Because leads are geometrically identical, the phase accumulations in them differ in sign only, $\delta_{1\to2,L}(B) = -\delta_{1\to2,R}(B)$. We define $\delta(B) = \delta_{1\to2,L}(B)$. In determining the local free-energy minima, we solve the GL equation for the wires for each vortex number n_v, imposing the single-valuedness condition on the order parameter, $\theta_{1,R\to L} - \theta_{2,R\to L} + 2\delta(B) = 2\pi n_v$. Here, $\theta_{1,R\to L} = \int_R^L d\vec{r} \cdot \vec{\nabla}\varphi$ is the phase accumulated along wire 1 in passing from the right to the left lead; $\theta_{2,R\to L}$ is similarly defined for wire 2. Because we can neglect the direct effect of the magnetic field on the wires, $\delta(B)$ is the only field-dependent parameter that affects the wires. The magnetic field increases $\delta(B)$ and imposes additional phase gradients in the wires, which, according to LAMH theory, decrease the barriers for phase slips and, hence, increase the resistance. The period of the observed oscillations is derived from the fact that whenever the magnetic field is such that $2\delta(B) = 2\pi m$ (where m is an integer, and the factor of 2 reflects the presence of two leads), the family of free-energy minima (all of which are statistically populated according to their energies) of the two-wire system is identical to the $B = 0$ case. The identity is established by redefining $n_v \to n_v - m$. Thus, the resistance of the device returns to the zero-field value each time the phase accumulation in the leads satisfies $\delta = \pi m$.

Next, we describe how $\delta = \delta(B)$ is calculated. Consider an infinitely long, thin-film, superconducting strip of width $2l$, much narrower than the perpendicular penetration depth and subject to a uniform, perpendicular magnetic field $B\hat{z}$, sufficiently weak that no vortices are present in the strip. The vector potential $\vec{A} = By\hat{x}$ is always in the plane of the strip with $\vec{A} = 0$ along the middle of the strip. Thus, for the infinite strip, we have the London gauge (*12*) and the two-dimensional current density is $\vec{J}(x,y) = -t_f\vec{A}(x,y)/\mu_0\lambda^2 = -(t_f By/\mu_0\lambda^2)\hat{x}$, where t_f is the film thickness and λ is the magnetic penetration depth. Then, $\vec{J}$ has magnitude $t_f Bl/\mu_0\lambda^2$ at the strip edges. In our experiment, the lengths of the two leads are much greater than their widths. Thus, the above estimate for the current density near the long edges continues to hold. By continuity, this edge current must sweep around at the short edges of the leads and, in so doing, must flow in the $\hat{y}$ direction as it passes the connection points of the wires. Owing to the finite length of the leads, our choice of gauge is not London type, given that the vector potential is perpendicular to the short edges of the leads. Thus, the supercurrent along the short edges is determined by the gradient of the phase, by $\vec{J}(x,y) = (t_{film}\Phi_0/2\pi\mu_0\lambda^2)(\nabla_y\varphi)\,\hat{y}$, which means that $\nabla_y\varphi \approx (2\pi/\Phi_0)Bl$. Correspondingly, the phase drop between the ends of the wires is approximately given by $\delta(B) = 2\pi(2alB/\Phi_0)$. It follows that the period of the resistance oscillations, ΔB, is given by $\Phi_0/4al$. A more precise analysis (valid for the case $a << l$) [supporting online material (SOM) text] yields $\Delta B = (\pi^2/8G)(\Phi_0/4al)$, where $G = 0.916\ldots$ is the Catalan number.

To test our prediction for the period, we measured five different samples (Table 1) and extracted the periods from the corresponding $R(B)$ curves. Table 1 shows the excellent agreement between the theoretically calculated and measured periods. Only one sample (219-4) showed a 15% deviation from the theoretical prediction. A scanning electron microscopy (SEM) inspection of the leads of this sample revealed that the lead shape was not precisely rectangular (fig. S1), in contrast with all other samples. Thus the current flow near the ends of the wires in 219-4 was distorted, explaining the observed deviation. A more stringent test of the formula for the period was obtained by narrowing the leads of one of the samples (930-1) with the use of a focused ion beam (FIB) milling and remeasuring the period and the lead width: The new period was larger and remained in excellent agreement with the new calculated value (Table 1). One can also account for an additional Aharonov-Bohm phase shift associated with the vector-potential integrated around the loop formed by the wires. In our geometry, this effect accounts for a ~1% correction to the calculated period, which is slightly below the accuracy of our measurements and was neglected (SOM text).

We now consider the question of the magnitude of the resistance oscillations. In our theory, the phase slip rate Γ between various local free-energy minima takes into account the response of one wire to any phase slip occurring in the other wire, and is determined by Arrhenius law $\Gamma = \Omega\exp[-\Delta F/k_B T]$, where Ω is the attempt frequency and k_B is the Boltzmann constant. The free-energy barrier ΔF for a phase slip depends on the initial and final configurations, each of which is defined by a pair of integers n_v and n_s. The zero-bias resistance is $R = V/I$, where the current I is small and fixed and the voltage is given by $V = (\hbar/2e)\dot{\varphi}$, where $\hbar$ is $h/2\pi$. The net phase slip velocity $\dot{\varphi} = 2\pi\dot{n}_s$ is determined by the net number of phase slips that pass through both wires per unit time, which in turn depends on Γ. For example, in the short-wire limit ($b < 4\xi$, where b is the wire length and ξ is the superconducting coherence length), we always have $n_v = 0$, and the resistance is $R = (\pi\hbar^2\Omega/2e^2\,k_B T)\exp[-\Delta F/k_B T]$. In the same limit, the barrier height is $\Delta F = (\hbar/e)$

$$\sqrt{(j_{c1}+j_{c2})^2\cos^2\delta(B) + (j_{c1}-j_{c2})^2\sin^2\delta(B)}.$$

Here, j_{c1} and j_{c2} are the critical currents for the wires, given by $j_c = [113\ \mu A][bT_c/R_N\xi(0)][1 - (T/T_c)]^{3/2}$, where T_c is the critical temperature of the corresponding wire, R_N is its normal state resistance, and ξ is its coherence length (*17*). The fit of the predictions of our model to the experimental data is shown as the solid curves in Fig. 2A (SOM text).

So far, we have concentrated on phenomena at magnetic fields below roughly 3 mT,

and for such fields we observed short-period, nonhysteretic resistance oscillations. Whenever fields larger than this scale have been applied, the magnetoresistance behavior becomes hysteretic, even if the field is swept back to the sub–3 mT regime. The most natural explanation for this transition follows from Likharev's threshold-field theory, according to which vortices start to enter the thin film leads at fields of this magnitude (*18–21*). Once present, some vortices remain in the leads and contribute the phase shifts experienced by the wires, and therefore can influence the measured resistance. To reduce the noise caused by the thermal motion of vortices, we measured (*10*) the switching and retrapping critical currents (instead of resistance) versus the magnetic field at $T = 0.3$ K (Fig. 3). It is clear that only the switching current shows oscillations, whereas the retrapping current is field independent. No detailed explanation for this interesting phenomenon is known to us at this point. Notably, the period of the switching current oscillation in the low-field regime coincides with that of the magnetoresistance (fig. S2). Two types of oscillatory behavior are observed (Fig. 3). The short-period oscillation corresponds to the fields at which no vortices are present and the large-period oscillation occurs when vortices have entered the leads. The large period changes with magnetic field and can be estimated as $\Delta B_{\mathrm{large}} \sim \Phi_0/2a(d + b)$, where d is the distance between the vortices.

We report a new class of metallic devices based on DNA molecules. Such an approach is promising, due to the self-assembly properties of DNA. As the resistance of the devices is controlled by the spatial profile of the superconducting phase within the leads, there is the potential for applications. These include local magnetometry (as is widely done with conventional SQUIDs) and the imaging of phase profiles created by supercurrents—in essence a superconducting phase gradiometer. Applications are not limited to a narrow range of temperatures; the ultranarrow widths of the wires ensure that the resistive transition occurs over a broad range of temperatures.

References and Notes

1. E. Braun, K. Keren, *Adv. Phys.* **53**, 441 (2004).
2. H. Watanabe, C. Manabe, T. Shigematsu, K. Shimotani, M. Shimizu, *Appl. Phys. Lett.* **79**, 2462 (2001).
3. N. C. Seeman, *Angew. Chem. Int. Ed.* **37**, 3220 (1998).
4. H. Yan, S. H. Park, G. Finkelstein, J. H. Reif, T. H. LaBean, *Science* **301**, 1882 (2003).
5. E. Braun, Y. Eichen, U. Sivan, G. Ben-Yoseph, *Nature* **391**, 775 (1998).
6. J. Richter, M. Mertig, W. Pompe, I. Monch, H. K. Schakert, *Appl. Phys. Lett.* **78**, 536 (2001).
7. J. Richter, M. Mertig, W. Pompe, H. Vinzelberg, *Appl. Phys. A* **74**, 725 (2002).
8. M. Mertig, L. C. Ciacchi, R. Seidel, W. Pompe, *Nano Lett.* **2**, 841 (2002).
9. A. Bezryadin, C. N. Lau, M. Tinkham, *Nature* **404**, 971 (2000).
10. Materials and Methods are available as supporting material on *Science* Online.
11. R. C. Jaklevic, J. Lambe, A. H. Silver, J. E. Mercereau, *Phys. Rev. Lett.* **12**, 159 (1964).
12. M. Tinkham, *Introduction to Superconductivity* (McGraw-Hill, New York, ed. 2, 1996).
13. W. A. Little, R. D. Parks, *Phys. Rev. Lett.* **9**, 9 (1962).
14. W. A. Little, *Phys. Rev.* **156**, 396 (1967).
15. J. S. Langer, V. Ambegaokar, *Phys. Rev.* **164**, 498 (1967).
16. D. E. McCumber, B. I. Halperin, *Phys. Rev. B* **1**, 1054 (1970).
17. M. Tinkham, C. N. Lau, *Appl. Phys. Lett.* **80**, 2946 (2002).
18. K. K. Likharev, *Sov. Radiophys.* **14**, 722 (1973).
19. J. R. Clem, *Bull. Am. Phys. Soc.* **43**, 411 (1972).
20. G. M. Maksimova, *Phys. Solid State* **40**, 1610 (1998).
21. G. Stan, S. B. Field, J. M. Martinis, *Phys. Rev. Lett.* **92**, 097003 (2004).

22. Supported by NSF CAREER grant no. DMR 01-34770, the A. P. Sloan Foundation (D.S.H. and A.B.), and the U.S. Department of Energy, Division of Materials Sciences under award no. DEFG02-91ER45439, through the Frederick Seitz Materials Research Laboratory at the University of Illinois at Urbana-Champaign, and the Center for Microanalysis of Materials Department of Energy grant no. DEFG02-96ER45439.

Supporting Online Material

www.sciencemag.org/cgi/content/full/308/5729/1762/DC1
Materials and Methods
SOM Text
Figs. S1 to S5
References

22 February 2005; accepted 28 April 2005
10.1126/science.1111307

Spectral Signatures of Hydrated Proton Vibrations in Water Clusters

Jeffrey M. Headrick,[1] Eric G. Diken,[1] Richard S. Walters,[2] Nathan I. Hammer,[1] Richard A. Christie,[3] Jun Cui,[3] Evgeniy M. Myshakin,[3] Michael A. Duncan,[2]* Mark A. Johnson,[1]* Kenneth D. Jordan[3]*

The ease with which the pH of water is measured obscures the fact that there is presently no clear molecular description for the hydrated proton. The mid-infrared spectrum of bulk aqueous acid, for example, is too diffuse to establish the roles of the putative Eigen (H_3O^+) and Zundel ($H_5O_2^+$) ion cores. To expose the local environment of the excess charge, we report how the vibrational spectrum of protonated water clusters evolves in the size range from 2 to 11 water molecules. Signature bands indicating embedded Eigen or Zundel limiting forms are observed in all of the spectra with the exception of the three- and five-membered clusters. These unique species display bands appearing at intermediate energies, reflecting asymmetric solvation of the core ion. Taken together, the data reveal the pronounced spectral impact of subtle changes in the hydration environment.

Despite the ubiquity of aqueous acids in chemical and biological systems (*1–7*), a molecular-level description of the hydrated proton remains elusive (*8–14*). The suggestion in introductory chemistry texts that the dominant speciation occurs as "hydronium" [H_3O^+, also called the Eigen (*9*) core] is too simplistic; an alternative limiting form proposed by Zundel (*10*) $(H_2O{\cdots}H{\cdots}OH_2)^+$ has long been thought to play an essential role, and the broad infrared absorptions of the aqueous proton at 1250, 1760, and 3020 cm^{-1} have been assigned in the context of both the Eigen and Zundel species (*15–17*). Here, we characterize the hydrated proton using a bottom-up approach. Through recent advances in laser generation of infrared light in the 1000- to 4000-cm^{-1} range, we directly monitor the spectral evolution of the proton accommodation motif as water molecules are sequentially added to the hydronium ion, up to an 11-membered cluster.

Infrared spectra of bare $H^+ \cdot (H_2O)_n$ clusters in the OH stretching region (2800 to 3900 cm^{-1}, with inconsistent coverage below 2800 cm^{-1}) have already been reported, and the observed bands are mostly attributed to water molecules remote from the proton (*18–23*). Dangling water molecules attached to the exterior of a hydrogen-bonded network, for example, produce sharp bands arising from the symmetric (υ_s) and asymmetric (υ_a) stretches of the nonbonded OH groups. Theoretical analysis of these spectra indicated a Zundel motif for the two-, six-, seven-, and eight-membered clusters, but an embedded Eigen core for the three- to five-membered clusters (Fig. 1).

[1]Sterling Chemistry Laboratory, Yale University, Post Office Box 208107, New Haven, CT 06520, USA. [2]Department of Chemistry, University of Georgia, Athens, GA 30602, USA. [3]Department of Chemistry, University of Pittsburgh, Pittsburgh, PA 15260, USA.

*To whom correspondence should be addressed. E-mail: maduncan@uga.edu (M.A.D.), mark.johnson@yale.edu (M.A.J.), jordan@pitt.edu (K.D.J.)

The vibrations associated with the excess charge in these structures occur at much lower energies than were accessible in the early experimental studies (*18*–*23*), and thus recent work has concentrated on extending the spectral range below 2100 cm^{-1}. Spectra in this lower energy region (600 to 1900 cm^{-1}) have already been obtained for the $H_5O_2^+$ ion (*24*–*27*). The patterns displayed by the bare complexes were quite complicated (*24*, *25*), but a much simpler spectrum was obtained when $H_5O_2^+$ was cooled by attachment of weakly bound Ar and, very recently, Ne atoms (*26*, *27*). Here, we extend the argon "messenger" (*18*) measurements to clusters with up to 11 water molecules and survey the critical low-energy region of the vibrational spectrum. This approach allows us to characterize most of the important vibrations associated with the excess positive charge.

The $H^+ \cdot (H_2O)_n$ vibrational spectra were obtained by photoevaporation of a weakly bound argon atom in a photofragmentation mass spectrometer (*28*, *29*). The enabling experimental advance was extension of the Yale infrared laser source (Laser Vision) down to 1000 cm^{-1} using parametric conversion in $AgGaSe_2$ (*30*). To aid in the interpretation of the spectra, we optimized the geometries of the clusters and calculated the harmonic frequencies at the MP2/aug-cc-pVDZ (*31*) level of theory using the Gaussian 03 program (*32*). For the two- to five-membered clusters, anharmonic spectra were calculated using the vibrational SCF (VSCF) method (*33*) as implemented in the GAMESS program (*34*).

We begin our discussion with the Eigen cation, $H^+ \cdot (H_2O)_4$, which has a minimum-energy structure well described as an H_3O^+ Eigen core, symmetrically solvated by three dangling water molecules (Fig. 1C) (*9*). The scaled harmonic frequencies calculated for this structure agree reasonably with the measured spectra (Fig. 2), where the outer water molecules contribute the two sharp OH stretching bands highest in energy. Most important is the strong band at 2665 cm^{-1}, which theory (red bars) matches to the degenerate asymmetric OH stretching vibration in an intact Eigen core. Thus, the first hydration shell acts to red-shift the intrinsic OH stretching motions of the isolated H_3O^+ ion (*35*) (blue arrows labeled H_3O^+ ν_{asym} at the bottom of Fig. 2) by more than 860 cm^{-1}, placing the band just below the range scanned in previous studies of this system (*18*–*20*).

Several transitions are also recovered in the lower energy region. The sharp feature (ν_b) at 1620 cm^{-1} can be readily assigned to the HOH intramolecular bends of the dangling water molecules, and the weak unresolved feature emerging at 1045 cm^{-1} is traced to the symmetric bending motion of the H_3O^+ ion core along its principle axis. The broader features near 1760 and 1900 cm^{-1} occur just above the equatorial bends in isolated H_3O^+ (*36*). It seems likely that these transitions are due to similar bending motions in the embedded H_3O^+ ion, although they are not anticipated at the harmonic level, and the 1760-cm^{-1} transition appears markedly similar to that displayed by the isolated Zundel ion (top trace in Fig. 3). Thus, even this simple, symmetrical cluster yields spectral complexity beyond that expected at the harmonic level.

Having established the spectral signature of the symmetrically hydrated Eigen core, we can interpret the evolution of the spectra as water molecules are removed from or added to this complete hydration shell, effectively mimicking rudimentary solvent fluctuations. The 2- to 11-membered cluster spectra (Fig. 3) persistently show sharp HOH intramolecular bending bands (ν_{bend} ~1620 cm^{-1}) (*37*), as well as two to four nonbonded OH stretches centered near 3695 cm^{-1}. The latter bands were analyzed previously (*18*–*21*). Here, we are primarily interested in the broader features (highlighted in red) associated with stretching motions of the H atoms bearing the excess charge. The frequency of these strong absorptions ranges from 1000 to 2700 cm^{-1} depending on the degree of excess charge localization.

To unravel the information contained in these spectra, we first consider removing a water molecule from the fully hydrated Eigen core to form $H^+ \cdot (H_2O)_3$. Although the resulting cluster is structurally characterized as an Eigen-based species (Fig. 1B), the 2665-cm^{-1} signature band of the Eigen cation is absent from its spectrum (Fig. 3). Instead, two strong bands emerge at 1880 and 3580 cm^{-1}. The calculations (Table 1) trace this pattern to a dramatic (~1700 cm^{-1}) splitting of the strong Eigen feature in $H^+ \cdot (H_2O)_4$ upon removal of a water molecule. Thus, the lowest of these transitions (highlighted in red in Fig. 3) arises from the asymmetric stretch of the two solvated protons, and the higher frequency 3580-cm^{-1} band involves the stretch of the unsolvated proton on the H_3O^+ core, which falls close to the OH stretch in bare H_3O^+. (*35*) Removal of one water molecule from the complete hydration shell around H_3O^+ thus leads to concentration of the excess charge onto two shared protons, pulling the two solvating water molecules closer to the

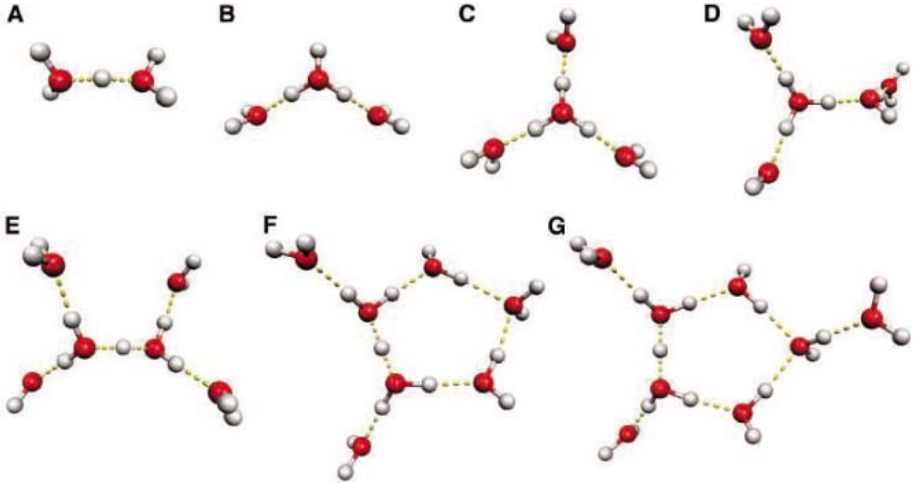

Fig. 1. (**A** to **G**) Minimum-energy structures of $H^+ \cdot (H_2O)_{2-8}$. Geometries were calculated at the MP2/aug-cc-pVDZ level of theory.

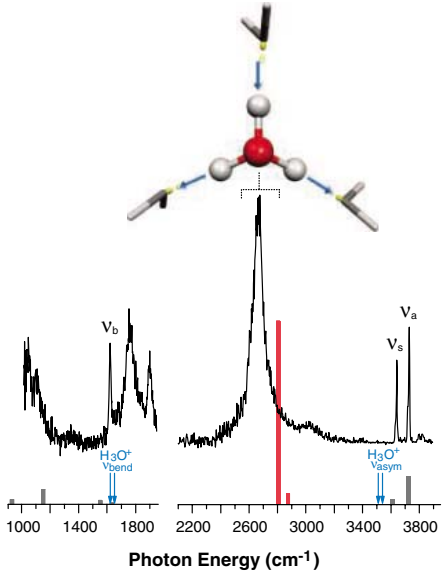

Fig. 2. Vibrational predissociation spectrum of the $H^+ \cdot (H_2O)_4 \cdot Ar$ complex. The OH asymmetric stretch (ν_{asym}) and asymmetric bending (ν_{bend}) bands of bare H_3O^+ are denoted by arrows (*35*, *36*), whereas the calculated harmonic spectrum (MP2/aug-cc-pVDZ level, 0.955 scaling) of $H^+ \cdot (H_2O)_4$ is displayed by bars. The Eigen core stretches are highlighted in red. The sharp bands highest in energy arise from the symmetric (ν_s) and asymmetric (ν_a) OH stretches of the dangling water molecules in the first hydration shell, with their associated intramolecular bending transitions (ν_b) at ~1600 cm^{-1}.

Eigen core and thereby red-shifting the associated OH stretch bands. In contrast to the behavior displayed by $H^+ \cdot (H_2O)_4$, anharmonic corrections (*33*) are required to qualitatively recover the large observed red-shifts in the lower energy $H^+ \cdot (H_2O)_3$ stretching transitions.

Removal of a second water molecule from $H^+ \cdot (H_2O)_4$ creates the isolated Zundel ion, $(H_2O{\cdots}H{\cdots}OH_2)^+$ (Fig. 1A), which has recently been reported and discussed in detail (*24*–*27*). Its infrared spectrum (top trace in Fig. 3) is dominated by a strong transition at 1085 cm^{-1}, arising from oscillation of the shared proton along the O–O axis, with a higher energy transition at 1770 cm^{-1} assigned to the out-of-phase bending vibrations of the flanking water molecules (*26*). The ~800-cm^{-1} incremental red-shift of the bands associated with the excess positive charge in going from $H^+ \cdot (H_2O)_3$ to $H_5O_2^+$ is about the same as that observed upon removal of the first water molecule from the fully hydrated Eigen core. Surprisingly large spectral shifts are thus driven by changes in the hydration environment.

We now turn to the systematic addition of water molecules to $H^+ \cdot (H_2O)_4$, nominally forming a second solvation shell. In the $H^+ \cdot (H_2O)_5$ spectrum (Fig. 3), three sharp bands appear in the high-energy nonbonded OH stretch region, consistent with the Eigen-like structure shown in Fig. 1D. Broader features also emerge that are unique to this cluster. In particular, an intense band (highlighted in purple in Fig. 3) appears ~200 cm^{-1} above the 2665-cm^{-1} signature absorption of the $H^+ \cdot (H_2O)_4$ Eigen ion. An unusual solvation-induced blue-shift seems unlikely, given that two new bands also appear at much lower energy (1490 and 1885 cm^{-1}). This pattern again raises the possibility that the degenerate Eigen vibrations are strongly split upon addition of the fourth water molecule, much as they were upon removal of a water molecule to form $H^+ \cdot (H_2O)_3$.

The harmonic frequency calculations (Table 1) for the $H^+ \cdot (H_2O)_5$ structure (Fig. 1D) anticipate a splitting of the Eigen vibrations, but severely underestimate the effect, with the three OH stretch vibrations of the Eigen core predicted to occur at 2344, 2942, and 2971 cm^{-1}. The two blue-shifted transitions are clearly derived primarily from the two protons of the Eigen core vibrating toward dangling water molecules in the first hydration shell. The calculated 2344-cm^{-1} OH stretch of the Eigen core, predicted to red-shift as the proton becomes solvated by a water dimer, still overshoots the experimental band at 1885 cm^{-1} by 459 cm^{-1}. The strong red-shift of this vibration is thus a consequence of excess charge concentration on the proton with two hydration shells coupled with pronounced vibrational anharmonicity. Vibrational self-consistent field calculations predict this stretch to resonate at 1852 cm^{-1}, close to the experimentally observed feature. This strong anharmonicity in the excess proton stretching vibration is analogous to that observed in the $H^+ \cdot (H_2O)_3$ cluster.

The addition of a second water molecule to $H^+ \cdot (H_2O)_4$ to give $H^+ \cdot (H_2O)_6$ creates a favorable geometry for capturing the symmetrical Zundel ion (Fig. 1E) within a complete first hydration shell. This arrangement has been identified previously (*38*) and is evidenced by the simple doublet in the free OH stretching region, similar to that found in the spectrum of the Eigen cation. This structure can be viewed as further stabilizing the preferentially hydrated proton in $H^+ \cdot (H_2O)_5$ such that it becomes equally shared between two oxygen atoms. The resulting $H^+ \cdot (H_2O)_6$ spectrum (Fig. 3) has a very strong transition at 1055 cm^{-1}, nearly the same frequency as the transition associated with oscillation of the bridging proton in the isolated Zundel ion. Thus, the characteristic signature of the local, shared proton motion is virtually unperturbed upon formation of a hydration shell, in strong contrast to the more charge-delocalized Eigen arrangement, where the H_3O^+ stretching bands shift by almost 860 cm^{-1} upon hydration [i.e., in going from H_3O^+ to $H^+ \cdot (H_2O)_4$].

The excess proton transitions in the spectra of the two- to six-membered clusters reveal an interesting progression in the distribution of excess charge with increasing size, first delocalizing over three protons in the Eigen cation then contracting back onto one proton in the six-membered cluster. Such oscillatory behavior naturally raises the question of whether this trend persists in the larger clusters. The spectra immediately establish that a simple repetition of the small-cluster evolution does not occur, because the 1055-cm^{-1} Zundel signature is maintained in the seven- and eight-membered clusters, even when strong variations in the higher energy OH stretching bands signal changes in the exterior network morphologies (Fig. 3). The calculated geometries anticipate this behavior, however, because the additional water molecules result in ring structures (Fig. 1, F and G) that preserve the quasi-symmetrical environment of the embedded Zundel motif. The character of these spectra is interesting in light of a recent paper reporting the OH stretching spectra of the bare

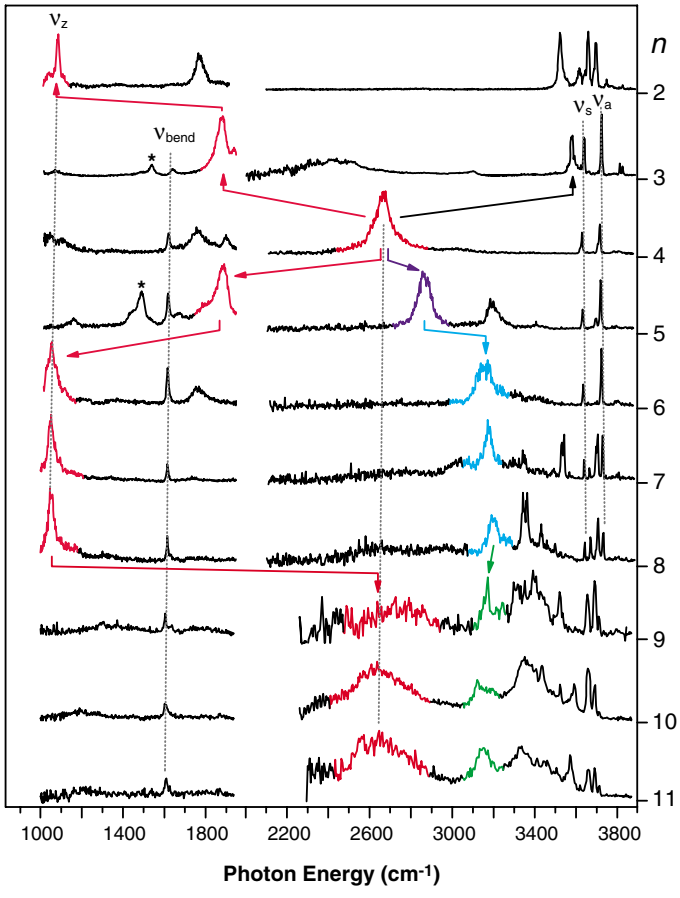

Fig. 3. Argon predissociation spectra of $H^+ \cdot (H_2O)_n$, n = 2 to 11, with n increasing down the figure. Dangling waters attached to the exterior of the cluster network are identified by sharp features assigned to the symmetric (ν_s) and asymmetric (ν_a) OH stretches. The sharp band near 1600 cm^{-1} arises from the bending modes of dangling OH groups. The bands most closely associated with the motions of H atoms bearing the excess charge are highlighted in red. This stretching feature first evolves toward higher energy as the excess charge approaches maximal delocalization at n = 4, but then returns to lower energy as more water molecules are added. The persistence of the intact Zundel signature (ν_z) in the six- to eight-membered cluster spectra indicates that the excess charge is preferentially retained on one strongly shared proton in this size range. Bands derived from the OH stretches bridging the Zundel ion to the first hydration shell are highlighted in blue, whereas the analogous bands involving the Eigen ion are indicated in green. The purple feature in the n = 5 spectrum is assigned to the OH stretches of the H_3O^+ ion bound to the two single acceptor water molecules (left side of Fig. 1D). Spectral features not readily recovered at the harmonic level are denoted with an asterisk (*).

clusters at temperature $T \approx 170$ K (*21*). In that study, the observed spectra of the six- and seven-membered clusters were assigned to a mixture of Eigen- and Zundel-based isomers, whereas the eight-membered cluster spectrum was attributed to a single Zundel-based isomer. The Ar-tagged six- to eight-membered clusters, in contrast, are all clearly dominated by Zundel-based isomers. Although the free OH stretches are similar in the three cases, notable differences arise in the lower energy H-bonded stretches in the 3200- to 3600-cm^{-1} range. The $H^+ \cdot (H_2O)_8$ spectrum actually appears quite similar in both the bare and Ar-tagged species, because the Ar predissociation spectrum displays sharper bands centered at almost the same locations. The bands in blue (Fig. 3) highlight the transitions associated with the OH stretches of the Zundel water molecules toward the second solvation shell, which shift toward higher energy with increasing cluster size. The isomers assigned to the observed spectra are shown in Fig. 1. These structures are also calculated to correspond to the minimum-energy isomers (after zero-point corrections).

Although previous work anticipated a change from Zundel to Eigen structures in progressing from eight to nine water molecules (*39*), the change in the low-energy bands here is pronounced. The nine-membered cluster spectrum displays very broad background absorption throughout the entire 2300- to 3000-cm^{-1} range, reminiscent of the excess proton spectrum in bulk water (*17*), whereas a distinct band near the Eigen signature at 2600 cm^{-1} is reestablished in the 10- and 11-membered clusters. None of the clusters in the size range from 9 to 11 display absorption near the Zundel band at 1000 cm^{-1}. The return of the embedded $H^+ \cdot (H_2O)_4$ Eigen cation is accompanied by a red-shift of the OH stretches bound to the first solvation shell (green). Notably, for nine or more water molecules, the free OH stretching bands appearing highest in energy are dominated by the doublet attributed to water molecules in AD and AAD (A is H-bond acceptor, D is H-bond donor) environments. Also noteworthy is the emergence of a relatively sharp feature near 3600 cm^{-1} in the spectrum of $H^+ \cdot (H_2O)_{10}$, which persists in the spectra of very large clusters and has been attributed to water molecules in a DDA site within the network (*21–23*).

The picture emerging from these cold cluster studies is that the excess proton transitions associated with the OH stretches of the Eigen cation occur highest in energy relative to the other accommodation motifs because it affords maximum charge delocalization (i.e., over three H atoms). Small asymmetries in the hydration structure around the H_3O^+ core result in preferential localization of the excess charge on one or two of the H atoms, as emphasized in the theoretical work by Parrinello (*13*) and Singer (*40*). This charge redistribution causes pronounced, size-dependent shifts of up to 1600 cm^{-1} in the characteristic absorptions nominally assigned to the excess proton. Such an extreme response to symmetry breaking would readily explain the lack of a sharp spectral signature of the hydrated proton in the bulk and would be consistent with Zundel's model of a highly polarizable excess proton (*10*).

Table 1. Comparison of the calculated and measured OH-stretch vibrational frequencies for the $H^+ \cdot (H_2O)_n$, $n = 2$ to 6 clusters. Calculated anharmonic (VSCF) frequencies, where available, are reported in parentheses. All other values are from harmonic calculations, unscaled in the case of the shared proton in the two Zundel ions and scaled by 0.955 to account approximately for vibrational anharmonicity in all other cases.

Description	ν_{calc} (cm^{-1})	ν_{expt} (cm^{-1})
	$n = 2$	
Proton oscillation	807 (1223)	1085
H_2O symmetric stretch	3552 (3546), 3558 (3538)	3520,* 3615*
H_2O asymmetric stretch	3660 (3594), 3661 (3585)	3660,* 3695*
	$n = 3$	
H_3O^+ asymmetric stretch	2381 (1984)	1880
H_3O^+ symmetric stretch	2509 (2363)	2420
H_2O symmetric stretch	3604 (3532), 3605 (3569)	3639
H_3O^+ free-OH stretch	3626 (3532)	3580
H_2O asymmetric stretch	3718 (3668), 3718 (3674)	3724
	$n = 4$	
H_3O^+ asymmetric stretch	2804	2665
H_3O^+ symmetric stretch	2874	
H_2O symmetric stretch	3612–3613	3644
H_2O asymmetric stretch	3725–3725	3730
	$n = 5$	
H_3O^+ stretch to AD-type† H_2O	2344 (1852)	1885
H_3O^+ asymmetric stretch	2942	2860
H_3O^+ symmetric stretch	2971	
AD-type H_2O H-bond stretch	3257	3195
H_2O symmetric stretch	3615–3623	3647
AD-type H_2O free-OH stretch	3695	3712
H_2O asymmetric stretch	3729–3741	3740
	$n = 6$	
Proton oscillation	1209	1055
H_2O in $H_5O_2^+$ symmetric stretch	3128	3160
H_2O in $H_5O_2^+$ asymmetric stretch	3143	
H_2O in $H_5O_2^+$ symmetric stretch	3274	
H_2O in $H_5O_2^+$ asymmetric stretch	3320	
H_2O symmetric stretch	3618–3625	3650
H_2O asymmetric stretch	3734–3744	3740

*The observed OH stretch splittings are induced by the argon "messenger" atom. Our results correlate well with those of (*19*), where the messenger was H_2. †AD-type H_2O molecules accept and donate a H-bond.

References and Notes

1. J. Heberle, J. Riesle, G. Thiedemann, D. Oesterhelt, N. A. Dencher, *Nature* **370**, 379 (1994).
2. D. Borgis, J. T. Hynes, *J. Phys. Chem.* **100**, 1118 (1996).
3. M. H. B. Stowell *et al.*, *Science* **276**, 812 (1997).
4. R. Waldmann, G. Champigny, F. Bassilana, C. Heurteaux, M. Lazdunski, *Nature* **386**, 173 (1997).
5. H. Luecke, H.-T. Richter, J. K. Lanyi, *Science* **280**, 1934 (1998).
6. K. Chen *et al.*, *Nature* **405**, 814 (2000).
7. M. Rini, B.-Z. Magnes, E. Pines, E. T. J. Nibbering, *Science* **301**, 349 (2003).
8. C. J. D. v. Grotthuss, *Ann. Chim.* **58**, 54 (1806).
9. M. Eigen, L. D. Maeyer, *Proc. R. Soc. London* **247**, 505 (1958).
10. P. Schuster, G. Zundel, C. Sandorfy, Eds. (North-Holland, Amsterdam, 1976).
11. M. Kunst, J. M. Warman, *Nature* **288**, 465 (1980).
12. N. Agmon, *Chem. Phys. Lett.* **244**, 456 (1995).
13. D. Marx, M. E. Tuckerman, J. Hutter, M. Parrinello, *Nature* **397**, 601 (1999).
14. A. L. Sobolewski, W. Domcke, *J. Phys. Chem. A* **106**, 4158 (2002).
15. M. Falk, P. A. Giguere, *Can. J. Chem.* **35**, 1195 (1957).
16. N. B. Librovich, V. P. Sakun, N. D. Sokolov, *Chem. Phys.* **39**, 351 (1979).
17. J. Kim, U. W. Schmitt, J. A. Gruetzmacher, G. A. Voth, N. E. Scherer, *J. Chem. Phys.* **115**, 737 (2002).
18. M. Okumura, L. I. Yeh, J. D. Myers, Y. T. Lee, *J. Chem. Phys.* **85**, 2328 (1986).
19. L. I. Yeh, M. Okumura, J. D. Myers, J. M. Price, Y. T. Lee, *J. Chem. Phys.* **91**, 7319 (1989).
20. L. I. Yeh, Y. T. Lee, J. T. Hougen, *J. Mol. Spectrosc.* **164**, 473 (1994).
21. J.-C. Jiang *et al.*, *J. Am. Chem. Soc.* **122**, 1398 (2000).
22. M. Miyazaki, A. Fujii, T. Ebata, N. Mikami, *Science* **304**, 1134 (2004).
23. J.-W. Shin *et al.*, *Science* **304**, 1137 (2004).
24. K. R. Asmis *et al.*, *Science* **299**, 1375 (2003).
25. T. D. Fridgen, T. B. McMahon, L. MacAleese, J. Lemaire, P. Maitre, *J. Phys. Chem. A* **108**, 9008 (2004).
26. J. M. Headrick, J. C. Bopp, M. A. Johnson, *J. Chem. Phys.* **121**, 11523 (2004).
27. N. I. Hammer *et al.*, *J. Chem. Phys.*, in press.
28. M. A. Johnson, W. C. Lineberger, in *Techniques for the Study of Ion-Molecule Reactions*, J. J. M. Farrar, W. H. Saunders, Eds. (Wiley, New York, 1988), vol. 20, p. 591.
29. M. A. Duncan, *Int. Rev. Phys. Chem.* **22**, 407 (2003).
30. M. Gerhards, C. Unterberg, A. Gerlach, *Phys. Chem. Chem. Phys.* **4**, 5563 (2002).
31. R. A. Kendall, T. H. Dunning Jr., R. J. Harrison, *J. Chem. Phys.* **96**, 6796 (1992).
32. M. J. Frisch *et al.*, *Gaussian 03* (Gaussian, Pittsburgh, PA, 2003).
33. G. M. Chaban, J. O. Jung, R. B. Gerber, *J. Chem. Phys.* **111**, 1823 (1999).
34. M. W. Schmidt *et al.*, *J. Comput. Chem.* **14**, 1347 (1993).

35. M. H. Begemann, R. J. Saykally, *J. Chem. Phys.* **82**, 3570 (1985).
36. M. Gruebele, M. Polak, R. J. Saykally, *J. Chem. Phys.* **87**, 3347 (1987).
37. That all of the larger clusters display sharp absorption near 1600 cm^{-1} demonstrates that the Ar atom is sufficiently weakly bound to enable action spectroscopy at this low excitation energy, thereby eliminating earlier uncertainties relating to photofragmentation kinetics.
38. Y.-S. Wang *et al.*, *J. Phys. Chem. A* **107**, 4217 (2003).
39. C.-K. Lin *et al.*, *Phys. Chem. Chem. Phys.* **7**, 938 (2005).
40. C. V. Ciobanu, L. Ojamae, I. Shavitt, S. J. Singer, *J. Chem. Phys.* **113**, 5321 (2000).

41. M.A.D., M.A.J., and K.D.J. thank the NSF for their support under grant numbers 0244143, 0111245, and 0078528.

4 April 2005; accepted 5 May 2005
10.1126/science.1113094

The Size and Duration of the Sumatra-Andaman Earthquake from Far-Field Static Offsets

P. Banerjee,[1] F. F. Pollitz,[2] R. Bürgmann[3]*

The 26 December 2004 Sumatra earthquake produced static offsets at continuously operating GPS stations at distances of up to 4500 kilometers from the epicenter. We used these displacements to model the earthquake and include consideration of the Earth's shape and depth-varying rigidity. The results imply that the average slip was >5 meters along the full length of the rupture, including the ~650-kilometer-long Andaman segment. Comparison of the source derived from the far-field static offsets with seismically derived estimates suggests that 25 to 35% of the total moment release occurred at periods greater than 1 hour. Taking into consideration the strong dip dependence of moment estimates, the magnitude of the earthquake did not exceed M_w = 9.2.

The 26 December 2004 Sumatra-Andaman earthquake was the largest seismic event to strike in the era of modern space geodesy. This event apparently ruptured a >1200-km section of the megathrust in a complex sequence of rapid and slow slip episodes that lasted for more than 1000 s (*1*, *2*). The estimates of the size of the earthquake from seismic data are highly sensitive to the method and frequency band used in the analysis and range from the initial Harvard CMT estimate of scalar seismic moment $M_0 = 4.0 \times 10^{22}$ Nm (M_w 9.0) to as much as three times that amount, as inferred from very-long-period data (>500 s) (*3*). Static surface offsets are caused by the elastic deformation of Earth in response to the earthquake. Geodetic measurements of these motions can be used to derive kinematic rupture models and calculate the size of the event, independent of the seismic energy released by the earthquake.

Here we use data from 41 continuously operating Global Positioning System (GPS) stations to calculate coseismic surface displacements throughout Southeast Asia (*4*). All but five of the stations are located at distances >1000 km from the earthquake epicenter (Fig. 1). We combined our own solutions with daily solutions of global International GNSS Service (IGS) stations (*5*). The GPS data were processed with the GAMIT/GLOBK software package to produce time series of station coordinates in the ITRF-2000 reference frame spanning at least 20 days before and after the earthquake (supporting online text and fig. S1). We estimated offsets at the time of the earthquake by differencing the mean positions in the 5 days before and after the earthquake, respectively. Data from the first 5 hours after the earthquake are not included in that day's solution. We used only the horizontal components in our analysis. We also used estimated offsets from campaign GPS measurements on the Andaman and Nicobar Islands (*6*). The GPS data show that there was a coherent surface motion roughly directed toward the earthquake rupture at distances up to 4500 km from the epicenter (Fig. 1 and table S1).

The standard approach of modeling the surface motions from an earthquake with an elastic half-space approximation of Earth (*7*) is inappropriate for an event of the magnitude and dimensions of the Sumatra earthquake. We model the event using PREM, a spherically layered elastic structure of the Earth determined from inversion of Earth's free-oscillation spectra (*8*, *9*). Static deformation in a spherical geometry is evaluated with the method described in (*10*, *11*). Forward model comparisons of the Sumatra earthquake show that surface motions calculated with a homogeneous spherical model greatly exceed surface motions of the layered spherical model at large distances (fig. S2).

We define the geometry of the earthquake rupture based on constraints provided by the distribution of aftershocks and independent seismic source studies (*1*). We subdivided the model geometry into three principal along-strike segments aligned with the strike of the megathrust from Sumatra to the northern Andaman Islands (table S2). The magnitudes of the far-field displacements are highly sensitive to fault dip (fig. S4), and we thus subdivided each segment in our model into two subsegments to simulate the dip increase with depth. This geometry is consistent with seismic constraints of depths to the top of the slab (*12*) and the ~30° nodal-plane dips of a large cluster of aftershocks at ~5°N and depths of 45 to 50 km (Fig. 2). Seismic source studies suggest that the rake of the rupture became more oblique toward the north (*2*). Little strike-slip motion on the southern segment is evident in the focal mechanism solutions of the aftershocks, but strike-slip motion appears likely on the Andaman and Nicobar segments (segments 1 and 2 in Fig. 2). The first-order models that we consider therefore involve uniform dip-slip and strike-slip components on the Andaman and Nicobar segments and uniform dip slip on the southern segment.

If we solve for the optimal uniform slip values on each rupture segment (Model M1 in Table 1), the slip averages more than 5 m on all segments. The displacement field predicted by this model (Fig. 1A) fits the GPS data set well at all distance ranges. A second case (Model M2), which does not allow for slip on the Andaman segment, results in a significantly worse fit (*13*) (Table 1). The predicted displacement field of Model M2 (Fig. 1B) fails particularly to predict the coseismic offsets of Indian sites, which moved up to 25 mm eastward. This confirms that the Andaman segment participated in the Sumatra-Andaman earthquake sequence and slipped by several meters predominantly as dip slip, but with a minor, right-lateral strike-slip component.

A variation of Model M1 in which the deeper subsegment of segment 3 is neglected leads to a significantly worse fit (reduced χ^2 = 1.63 versus 1.36 for Model M1). The sensitivity to fault dip around the southern part of the rupture arises from the large dependence of displacement azimuth on dip at Sumatran sites south of the equator (fig. S4). This result indicates that the deeper portion of the megathrust in the southernmost part of the rupture participated with several meters of slip, consistent with the occurrence of deeper aftershocks there (Fig. 2). If we restrict slip on the northern segments 1 and 2 to their shallowly dipping portions, the data set is fit nearly as well as that involving slip on the wider faults,

[1]Wadia Institute of Himalayan Geology, Dehra Dun, 248001, India. [2]U.S. Geological Survey, Menlo Park, CA 94025, USA. [3]Department of Earth and Planetary Science and Berkeley Seismological Laboratory, University of California, Berkeley, CA 94720, USA.

*To whom correspondence should be addressed. E-mail: burgmann@seismo.berkeley.edu

and estimated slip values nearly double (Model M3 in Table 1 and Fig. 1C).

These kinematic models may be compared with available horizontal movements determined from campaign GPS measurements of the Andaman and Nicobar Islands (*6*) (Fig. 2). Model M3 generally matches well the measured offsets, whereas Model M1 predicts offsets that are too small and predicts the incorrect sense of uplift at some of these sites. These comparisons indicate that most of the coseismic slip was shallow (less than ~30-km depth) in these regions. However, the actual slip distribution is expected to be more complex than predicted by our simple uniform slip models, consistent with substantial heterogeneity in the observed near-field uplift and subsidence patterns along the island chains (*14*).

The scalar seismic moment of the earthquake sequence calculated with Model M1 is $M_0 = 5.67 \times 10^{22}$ Nm, corresponding to a moment magnitude of $M_w = 9.14$. This value is 40% larger than the seismic moment determined in the Harvard CMT solution using long-period body waves and surface waves up to 300-s period. It is about one-half of that determined by (*3*) using free oscillations up to 1-hour period, which corresponds to $M_w = 9.30$. We note that source excitation of very-long-period fundamental spheroidal modes (*15*) is primarily through the moment tensor components M_{rr} and $(M_{tt} + M_{pp})$, which are proportional to $slip \times \sin(\lambda) \times \sin(2\delta)$, where λ is fault rake and δ is dip, and subscripts r, t, and p refer to the local vectors $\hat{\mathbf{r}}$, $\hat{\boldsymbol{\theta}}$, and $\hat{\boldsymbol{\phi}}$ in a spherical coordinate system. With moderate dips of $\delta = 35°$ used here on the deeper portions of the various segments, the contribution to the free-oscillation excitation is equivalent to that produced by a 15°-dipping fault with twice the slip. An increase in seismic moment will therefore result if slip is constrained to be on the shallowly dipping portions of the fault segments. This prediction is verified by Model M3, which is identical to Model M1 except that slip on segments 1 and 2 is restricted to their shallowly dipping portions and has an increased $M_w = 9.17$. The best-fitting point source constrained to the CMT source depth of 28.4 km and dip of 8° [i.e., the source depth and dip assumed by (*3*)] results in $M_w = 9.37$ (Model P in Table 1) and a scalar moment M_0 that is 27% greater than that estimated by (*3*). The sensitivity of the scalar moment to fault dip is directly illustrated in Fig. 3A, where M_0 estimated from inversion for the best-fitting point source exhibits a $\sim(\sin 2\delta)^{-1}$ dependence, whereas the estimated moment tensor component M_{rr} varies little with changing dip. Thus, once the steeper average dip of the Sumatra rupture is taken into consideration, the estimated moment magnitude does not exceed $M_w = 9.2$.

The static displacement field measures earthquake size at periods far greater than the ~1-hour period measured by Earth's free oscillations (*3*). A useful measure of the earthquake size is the combination of moment tensor components M_{rr} and $(M_{tt} + M_{pp})$, which dominate the excitation of both the

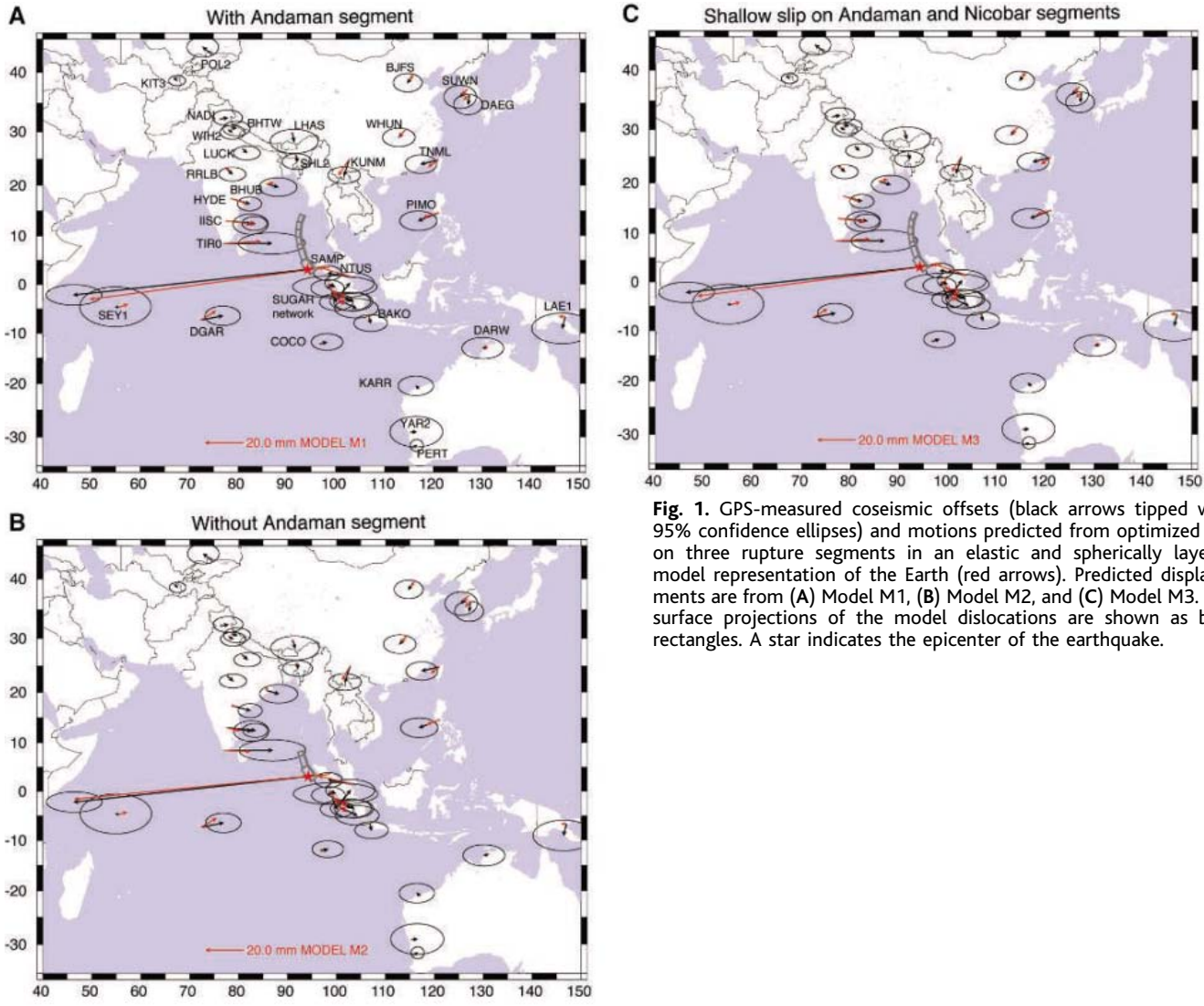

Fig. 1. GPS-measured coseismic offsets (black arrows tipped with 95% confidence ellipses) and motions predicted from optimized slip on three rupture segments in an elastic and spherically layered model representation of the Earth (red arrows). Predicted displacements are from (**A**) Model M1, (**B**) Model M2, and (**C**) Model M3. The surface projections of the model dislocations are shown as bold rectangles. A star indicates the epicenter of the earthquake.

low-degree fundamental spheroidal modes and the static displacements. Because $M_{rr} = -(M_{tt} + M_{pp})$ for a shear dislocation, we consider the single measure M_{rr}, which has the advantage of being nearly geometry independent (Fig. 3A). The model of (*3*) corresponds to $M_{rr} = 2.59 \times 10^{22}$ Nm. Our finite source models yield $M_{rr} = 3.26 \times 10^{22}$ to 3.61×10^{22} Nm (Table 1). Figure 3B demonstrates a systematic increase in M_{rr} with period, including the CMT solution involving periods <300 s and the seismic slip inversion of (*1*) at periods up to 2000 s. This trend, first noted by (*3*), implies that about 25 to 35% of the total seismic moment release occurred beyond the ~1-hour time scale that is directly detectable with seismic waves.

The precise time of cessation of substantial moment release is uncertain. The GPS time series (fig. S1) qualitatively suggest an upper bound of 1 day. If most or all of the post-1-hour slip were confined to the Andaman segment, then the evolution of aftershocks may provide guidance. Moderate-sized earthquakes on the Andaman segment may have occurred on localized asperities simultaneously with predominantly aseismic slip. The rate of moderate earthquakes on the Andaman segment (Fig. 3B) suggests that a large part of the slip occurred between 40 min after the mainshock, coinciding approximately with the initiation of coseismic subsidence of Port Blair (*14*), and 2.5 hours after the mainshock.

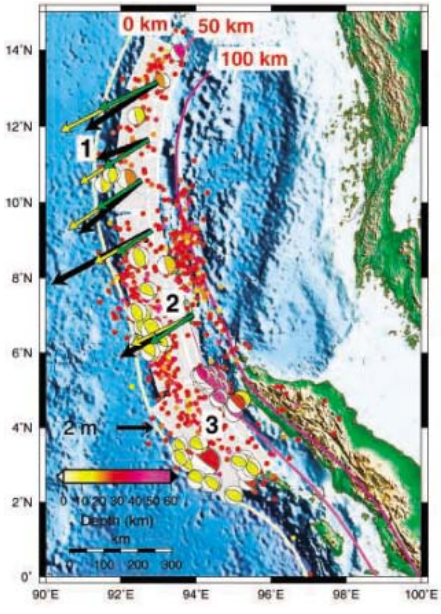

Fig. 2. Three-segment fault geometry of the Sumatra-Andaman Islands earthquake. Superimposed are the hypocenters of $M > 4$ earthquakes occurring from 26 December 2004 to 5 January 2005 from the National Earthquake Information Center (NEIC) catalog, the subset of CMT aftershock focal mechanisms with reverse slip (plunge of tension axis > 45°), and the 0-, 50-, and 100-km isocontours of the slab-top depth from (*12*). Fault geometry parameters are in table S2. Also shown are horizontal GPS offsets (solid black arrows) from the Andaman and Nicobar Islands from (*6*) compared with the predictions of Models M1 (green) and M3 (yellow).

References and Notes

1. T. Lay *et al.*, *Science* **308**, 1127 (2005).
2. C. J. Ammon *et al.*, *Science* **308**, 1133 (2005).
3. S. Stein, E. Okal, *Nature* **434**, 581 (2005).
4. The GPS data are from stations belonging to the IGS global network, the BAKOSURTANAL Indonesian network, the Sumatran GPS Array operated by the Tectonic Observatory at Caltech and the Indonesian Institute of Science (LIPI), and the Indian "National Program on GPS" Network of the Department of Science and Technology made available by the Survey of India GPS Data Centre.
5. We use daily solutions of global GPS stations processed and archived at the Scripps Orbital and Permanent Array Center (http://sopac.ucsd.edu). Eighteen IGS stations located >5000 km from the rupture are used in the ITRF-2000 reference frame realization. Our regional solution includes 25 stations, 9 of which are in common with the SOPAC solution (table S1).
6. C. P. Rajendran, A. Earnest, K. Rajendran, R. Bilham, J. T. Freymueller, in preparation.
7. Y. Okada, *Bull. Seismol. Soc. Am.* **75**, 1135 (1985).
8. A. M. Dziewonski, D. L. Anderson, *Phys. Earth Planet. Int.* **25**, 297 (1981).
9. The PREM model contains large increases in rigidity at major discontinuities at depths of 25 km (Mohorovocic discontinuity), 220 km (base of asthenosphere), 400 km, and 670 km (upper mantle–lower mantle boundary), followed by a decrease to zero rigidity at 2891 km (core-mantle boundary). Our modeling includes the fluid outer core but not the solid inner core.
10. F. F. Pollitz, *Geophys. J. Int.* **125**, 1 (1996).
11. A spherical harmonic expansion from l=1 to l=1500 is used to represent the spherical displacement fields. The l=1 component is found to be very important for correctly synthesizing far-field displacements. For typical Sumatra slip models, the predicted displacement at the farthest (Korean) sites amounts to several mm and arises almost entirely from the l=1 component of the displacement field.

Table 1. Fit of Sumatra slip models to far-field GPS. u_i and λ_i denote, respectively, slip and rake on fault *i*. We hold fixed $\lambda_3 = 90°$. Inversions are subjected to the constraint $90° = \lambda_3 \leq \lambda_2 \leq \lambda_1$. Variable rake on fault-1 subsegments is described in table S2.

Model	u_1 (m)	λ_1 (°)	u_2 (m)	λ_2 (°)	u_3 (m)	χ^{2*}	M_0 (10^{22} Nm)	M_{rr} (10^{22} Nm)	M_w
M1	5.3 ± 0.8	104 ± 5	9.2 ± 1.6	104 ± 7	6.0 ± 0.3	1.36	5.93	3.61	9.15
M2	0†	0†	14.4 ± 1.4	105 ± 7	5.8 ± 0.3	1.70	4.85	3.26	9.09
M3‡	10.5 ± 1.6	105 ± 5	14.1 ± 2.2	105 ± 8	6.6 ± 0.3	1.42	6.42	3.26	9.17
P‖						1.52	12.66	3.43	9.37

*Reduced χ^2, equal to the full χ^2 divided by $N - n$, where $N = 82$ is the number of data constraints and n is the number of independent parameters ($n = 5$ for Models M1 and M3, $n = 3$ for Model M2, $n = 5$ for Model P). †Value fixed in inversion. ‡Uniform slip on segments 1 and 2 is restricted to their respective shallow portions, i.e., only from 0- to 30-km depth. ‖Best-fitting point source constrained to CMT depth of 28.4 km and dip of 8°. Point source location and geometry: 8.0°N, 93.3°E, strike = 340°, rake = 102°. $\chi^2 = 1.52$ excluding SAMP, $\chi^2 = 6.19$ with SAMP.

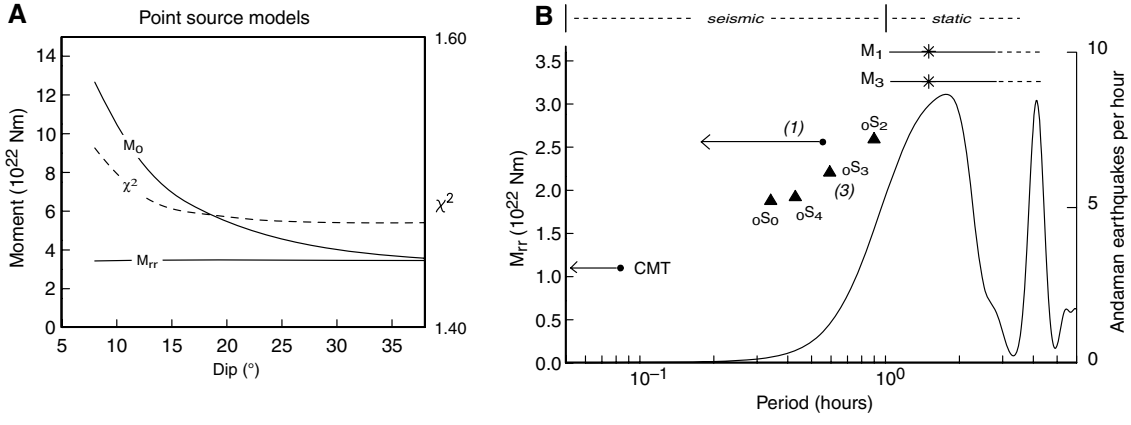

Fig. 3. (**A**) Scalar seismic moment M_0 and moment tensor component M_{rr} derived from inversion of GPS data set for best-fitting point source subject to fixed position at 8.0°N, 93.3°E, strike 340°, and CMT source depth of 28.4 km. Right-hand axis displays the corresponding reduced χ^2 excluding SAMP. (All static point source models yield a poor fit to SAMP.) (**B**) Moment tensor component M_{rr} derived from the CMT solution (periods <300 s), the seismic slip inversion of (*1*) (periods <2000 s), and free oscillations (*3*) compared with that of Models M1 and M3 derived from the far-field static offset. An average rake of 110° and average fault dip of 13.5° were assumed to convert scalar seismic moment of 6.0×10^{22} Nm estimated in (*1*) to the corresponding M_{rr}. Black curve is the rate of $M \geq 5$ earthquakes (from NEIC catalog) that occurred on the Andaman segment as a function of time after the mainshock, smoothed using a Gaussian scaling time of 0.25 hours. Shallow aftershocks in the back-arc region (8°N to 10°N and east of ~93.5°E) (Fig. 2) are excluded.

12. O. Gudmundsson, M. Sambridge, *J. Geophys. Res.* **103**, 7121 (1998).
13. A statistical F-test shows that the improvement in data fit with respect to Model M2 by including the additional two parameters of the Andaman segment is significant at 99.93% confidence (Model M1) or 99.76% confidence (Model M3).
14. R. G. Bilham, E. R. Engdahl, N. Feldl, S. P. Satyabala, *Seismol. Res. Lett.*, in press.
15. F. Gilbert, A. M. Dziewonski, *Philos. Trans. R. Soc. London Ser. A* **278**, 187 (1975).
16. We thank C. P. Rajendran and R. Bilham for providing results before publication. GPS data processing was carried out under a Department of Science and Technology, Government of India–sponsored project (to P.B.).

Supporting Online Material
www.sciencemag.org/cgi/content/full/1113746/DC1

SOM Text
Figs. S1 to S4
Tables S1 and S2
References and Notes

18 April 2005; accepted 10 May 2005
Published online 19 May 2005;
10.1126/science.1113746
Include this information when citing this paper.

Dilution of the Northern North Atlantic Ocean in Recent Decades

Ruth Curry[1]* and Cecilie Mauritzen[2]

Declining salinities signify that large amounts of fresh water have been added to the northern North Atlantic Ocean since the mid-1960s. We estimate that the Nordic Seas and Subpolar Basins were diluted by an extra 19,000 ± 5000 cubic kilometers of freshwater input between 1965 and 1995. Fully half of that additional fresh water—about 10,000 cubic kilometers—infiltrated the system in the late 1960s at an approximate rate of 2000 cubic kilometers per year. Patterns of freshwater accumulation observed in the Nordic Seas suggest a century time scale to reach freshening thresholds critical to that portion of the Atlantic meridional overturning circulation.

The salinities of water masses originating in the high-latitude North Atlantic Ocean have been cascading downward since the early 1970s (*1*–*4*). This region has climatic importance because the Nordic Seas and the Labrador and Irminger basins are sites where cold, dense waters are formed—an integral component of what is often termed the meridional overturning circulation (MOC). The Atlantic MOC involves a northward flow of warm surface waters in exchange for a southward flow of cold, dense waters in the deep ocean along the pathways shown in Fig. 1. This component of circulation transports heat northward and thus contributes to moderating the cold-season climate at high northern latitudes. Excessive amounts of fresh water could alter the ocean density contrasts that drive the northernmost extension of the Atlantic MOC, diminish its northward heat transport, and substantially cool some regions of the North Atlantic (*5*–*10*). The MOC's sensitivity to greenhouse warming remains a subject of much scientific debate (*10*). The observed freshening does not yet appear to have substantially altered the MOC and its northward heat transport (*11*, *12*). But uncertainties regarding the rates of future greenhouse warming and glacial melting limit the predictability of their impact on ocean circulation (*8*, *10*).

What has been missing from the evolving picture thus far is an explicit quantification of how much additional fresh water it took to cause the observed salinity changes, how fast it entered the sub-Arctic ocean circulation, and where that fresh water had been stored. All three factors are important for assessing the present and future impacts of freshening on the Atlantic MOC, and provide the types of information that facilitate climate model validation studies. To address these issues, we reconstructed the history of volumetric changes in ocean temperature, salinity, and density in the Nordic Seas and Subpolar Basins and estimated the magnitude of freshwater storage and net volume flux anomalies required to account for the observed dilution over the past 50 years. We then examined the degree to which density has responded to this freshening, as a means of gaining perspective on its seemingly negligible MOC impact. Finally, we used this perspective to estimate how much additional fresh water might be required to equalize the density contrast that contributes to the exchange of mass and heat between the Nordic Seas and the subpolar North Atlantic.

Extensive amounts of hydrographic data have been collected in the seas between Labrador and northern Europe in the past 50 years. We used these data to construct well-constrained, three-dimensional representations of ocean properties for successive 5-year time frames spanning the years 1953 to 2002 (*13*). Because salinity is approximately conserved in the ocean, salinity anomaly fields can be used to quantify the volume of additional fresh water that had to be added or removed to account for salinity changes accumulated through the entire water column (*13*). Mapping this quantity, layer by layer, time frame by time frame, throughout the domain describes the evolution of freshwater storage in space and time. Integrating it over a geographic area provides a history of the volumetric freshwater storage anomaly in cubic kilometers, and differencing this storage anomaly in consecutive time frames implies a rate of change—the net freshwater flux anomaly—in sverdrups (1 Sv = 10^6 m^3 s^{-1}).

Time series of freshwater storage anomaly and net flux anomaly for the Nordic Seas and Subpolar Basins were considered separately and as a whole (Fig. 2) (table S1). From the earliest part of the record through the mid-1960s, salinities increased in the upper 2000 m of all the Subpolar Basins. Its volumetric expression was a net loss in subpolar freshwater storage of ~5000 km^3 between 1955 and 1965. By contrast, the net change in the Nordic Seas was comparatively small at that time. Between 1965 and 1990, however, both the Nordic Seas and Subpolar Basins became increasingly freshened. Net freshwater storage increased by ~19,000 km^3, of which ~4000 km^3 spread into the Nordic Seas and ~15,000 km^3 accumulated in the Subpolar Basins. A recovery from the early 1990s peak of freshwater storage in the Subpolar Basins occurred in the mid-1990s, but our volumetric analysis falters for the last time frame (1998 to 2002) because of inadequate data coverage (*14*). For the Nordic Seas, an approximate balance between import and export of fresh and saline waters resulted in little net volumetric change in the late 1990s.

The most striking event of the time series occurred in the early 1970s. During the late 1960s, a large pulse of fresh water entered the Nordic Seas through Fram Strait and rapidly moved southward along the western boundary in the East Greenland Current. This event has been labeled the Great Salinity Anomaly (GSA) (*15*), and we can here confirm that the name is appropriate, for it contributed an extra ~10,000 km^3 of fresh water to the sub-Arctic seas in the late 1960s and early 1970s, implying a net flux anomaly of ~0.07 Sv during a 5-year period. The GSA was previously thought to be equivalent to ~2000 km^3 of excess fresh water (*15*) and has been attributed to several years of anomalously large sea ice export from the Arctic (*16*, *17*). The Arctic freshwater budget includes inflows from the Pacific (~1600 km^3 year^{-1}) and rivers (~3500 km^3 year^{-1}) that are mainly balanced by annual exports of fresh water and sea ice through Fram Strait and the Canadian

[1]Woods Hole Oceanographic Institution (WHOI), Woods Hole, MA 02543, USA. [2]Norwegian Meteorological Institute, 0313 Oslo, Norway.

*To whom correspondence should be addressed. E-mail: rcurry@whoi.edu

Archipelago of ~5000 km^3 year^{-1} (*16*). Thus, volumetric changes in freshwater storage suggest that exports associated with the GSA ran ~40% above normal on average during that 5-year time frame.

Only a fraction of the GSA's fresh water remained in the Nordic Seas. The East Greenland Current provides a direct transport route from the Arctic to the Subpolar Basins, and the ocean circulation at that time sent the majority south of Denmark Strait. A small portion of fresh water did quickly spread across the surface of the western Nordic Seas in the early 1960s (fig. S3), but only subsequently was additional fresh water mixed into the subsurface layers. Salinities in the dense overflow waters from the Nordic Seas to the North Atlantic began to decline only in the early 1970s (*4*). Similarly, freshening in the Subpolar Basins first spread across the surface layer in the late 1960s. During the 1970s, the bulk of the GSA's fresh water was vertically mixed downward in the Labrador and Irminger basins and then horizontally circulated at mid-depths around the Subpolar Basins.

Pulses of excess fresh water and ice also appear to have been emitted from the Arctic in the 1980s and 1990s (*18*), and freshening of the Subpolar Basins and Nordic Seas continued from the GSA period into the early 1990s. Of the estimated 19,000 km^3 of anomalous freshwater influx between 1965 and 1995, nearly 80% ended up in the Subpolar Basins, whose geographic area is slightly more than twice that of the Nordic Seas. Normalized for this difference, the subpolar storage anomaly amounted to an equivalent freshwater layer ~3.0 m thick spread evenly over its total area, compared to ~1.8 m for the Nordic Seas.

Although not statistically well quantified in our volumetric analysis (and thus not plotted in Fig. 2), warm, saline influences were clearly building in the eastern Subpolar Basins in our last time frame (1998 to 2002; fig. S3). There were also indications of higher salinities in the Atlantic inflow to the eastern Nordic Seas, but the most striking feature there is the accumulation of fresh water, since the 1980s, in the upper 1000 m (fig. S3, left and middle columns). In the 1990s, freshening spread ubiquitously in this layer across the Nordic Seas. By contrast, fresh water accumulated in the entire water column of the Subpolar Basins (fig. S3, right column), but most conspicuously in the intermediate layers—the depths reached by vertical wintertime mixing in the Labrador Basin.

About 6 Sv—or one-third of the Atlantic MOC—crosses the Greenland-Scotland Ridge, which separates the Nordic Seas from the North Atlantic (*19*). A pressure gradient between the waters north and south of the ridge causes dense waters from the Nordic Seas to flow southward across the ridge and spill downward into the depths of the Subpolar Basins. These southward-exiting waters, collectively called Nordic Seas Overflow Waters (NSOW), are replaced by warm, salty surface waters flowing northward via the Norwegian Atlantic Current. The rate of dense water export across the Greenland-Scotland Ridge is roughly proportional to the density contrast in the layers (200 to 900 m) that feed the overflows (*20*). This exchange has been monitored directly for more than a decade: Arrays of instruments have been maintained in key locations south of Denmark Strait (DS) since about 1986 and in the Faroe Bank Channel (FBC) since 1995. During this time, the flow has been measured to be ~3 Sv at each location, with little indication of sustained changes despite steadily declining salinities in the NSOW (*11*, *21*). This reflects the fact that the amount of fresh water thus far accumulated has not had a substantial impact on the density contrast that drives the overflows.

Although immediately adjacent to one another, the Nordic Seas and Subpolar Basins exhibit distinctly independent salinity, temperature, and density trends. Salinity and density evolution are described by a time series of 5-year-average salinity and density values at DS sill depth (~550 m) both upstream and downstream (Fig. 3); a more complete view is obtained from vertical property sections running perpendicular to the sill (fig. S4). Downstream in the Irminger Basin, the upper waters are less dense and are alternately influenced by subtropical warm and saline waters (e.g.,

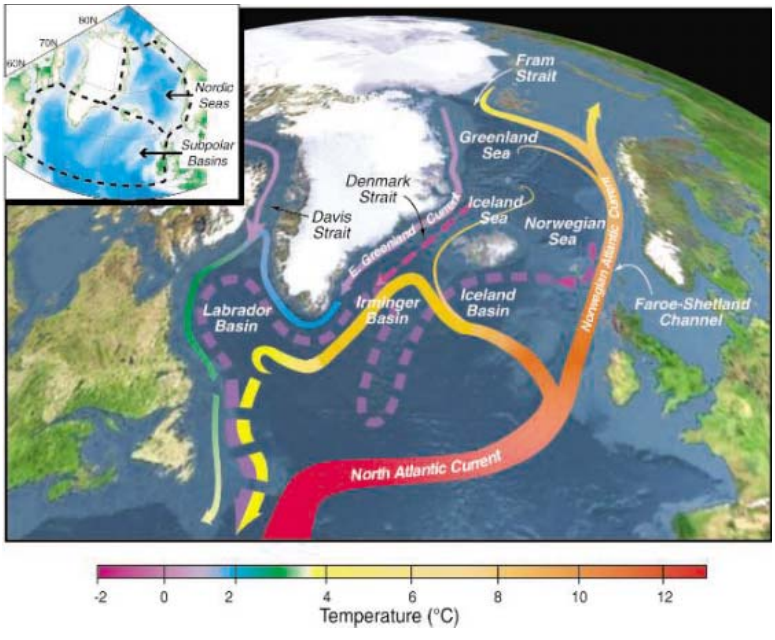

Fig. 1. Topographic map of Nordic Seas and Subpolar Basins with schematic circulation of surface currents (solid curves) and deep currents (dashed curves) that form a portion of the Atlantic MOC. Colors of curves indicate approximate temperatures. Map inset delineates the boundaries of the Nordic Seas and Subpolar Basins used in the volumetric analysis (dashed black lines).

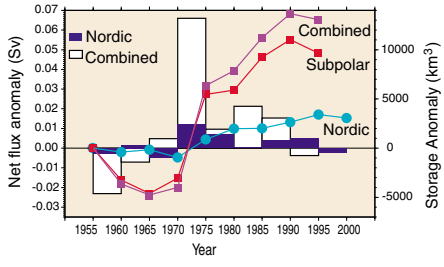

Fig. 2. Time series of freshwater storage anomaly (symbols, scale on right axis) for Nordic Seas (cyan circles), Subpolar Basins down to 50°N (red squares), and both regions combined (purple squares). The net freshwater flux anomaly (difference in storage anomaly between successive 5-year time frames) is shown as bars with scale on left axis (blue, Nordic Seas component; white, total freshwater flux anomaly including Subpolar Basins component).

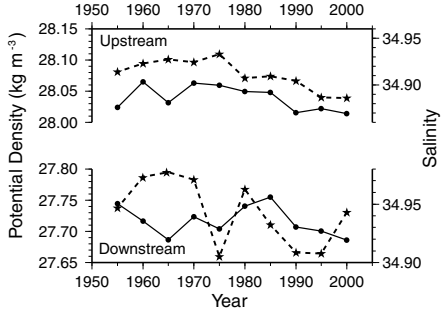

Fig. 3. Time series of 5-year-average density (solid lines, circles) and salinity (dashed lines, stars) at the sill depth of Denmark Strait (550 m). The upstream profiles are taken from the Iceland Sea at 68.5°N, 23.5°W; the downstream profiles are in the Irminger Basin at 64.5°N, 31.5°W.

1960s) and by colder, fresher subpolar waters (e.g., 1985 to 1995) (*22*). At sill depth, the downstream salinity jumped ±0.05 at several points in the time series, whereas density variations, moderated by temperature, ranged between 27.68 and 27.75 kg m^{-3}, although not monotonically through time. Upstream in the western Iceland Sea, by contrast, salinity at sill depth began a persistent decline of –0.05 in the mid-1970s, which contributed to the decline in density from a high of ~28.06 kg m^{-3} around 1970 to ~28.01 kg m^{-3} in the 1990s.

Vertical profiles of density contrast and hydraulic theory provide a basis for calculating the volume transport over the sill (*13*). Using this method, we find that the overflow rates in each time frame varied only slightly (3.0 ± 0.2 Sv at DS, 3.5 ± 0.1 Sv for FBC) and did not vary in any persistent manner during the past 50 years (figs. S5 and S6). Thus, the observed freshening did not sufficiently lower the Nordic Seas density—and hence the density contrast across the ridge—to have an enduring impact on the intensity of the overflows.

Because the overflow rates depend on this north-south density contrast, we address the question of how much additional fresh water would be required to reduce the present upstream density (~28.00 kg m^{-3}) to values found downstream in the Subpolar Basins (~27.70 kg m^{-3}). The observational record indicates that fresh water has been accumulating in the upper 1000 m everywhere across the Nordic Seas for the past 30 years (fig. S3), and we have extrapolated this pattern of dilution forward to gain perspective on our question (*13*). We find that a volume of ~9000 km^3—roughly equivalent to one GSA—mixed into the upper 1000 m of the Nordic Seas would be required to substantially reduce the overflows; two GSAs (~18,000 km^3) could essentially shut them down. We emphasize that these are not predictions, but merely a process to better understand what magnitude of changes would be involved.

Of the total 19,000 km^3 of additional fresh water that diluted the northern Atlantic since the 1960s, only 4000 km^3 remained in the Nordic Seas. Of this latter volume, our analysis indicates that ~2500 km^3 accumulated in the layer 200 to 1000 m between 1970 and 1995. This observed rate of net accumulation (~100 km^3 $year^{-1}$) integrates various dynamical processes controlling the mixing of fresh water into this layer and provides a basis for estimating future dilution. At the observed rate, it would take about a century to accumulate enough fresh water (e.g., 9000 km^3) to substantially affect the ocean exchanges across the Greenland-Scotland Ridge, and nearly two centuries of continuous dilution to stop them. In this context, abrupt changes in ocean circulation do not appear imminent.

Uncertainties remain in assessing the possibility of such disruptions. A weakened Atlantic MOC in the 21st century is a feature of numerous climate simulations of greenhouse warming (*5–9*, *23–27*). The cause is similar in all the models: glacial melting, enhanced precipitation, and continental runoff, which are projected to increase freshwater input to the Arctic and sub-Arctic seas (*26*, *27*). Pooling and sudden release of glacial meltwater, disintegration of shelf ice followed by a surge in glacier movement, and lubrication of the glacier base by increased melting are all possible mechanisms that could inject large amounts of fresh water from Greenland's ice sheet into the upper layers of the Nordic Seas (*28*). The possibility of such events precludes ruling out a substantial slowing or shutdown of the overflows as a result of greenhouse warming.

References and Notes

1. J. R. N. Lazier, in *Natural Climate Variability on Decade-to-Century Time Scales*, D. G. Martinson *et al.*, Eds. (National Academy Press, Washington, DC, 1995), pp. 295–302.
2. W. R. Turrell, G. Slesser, R. D. Adams, R. Payne, P. A. Gillibrand, *Deep Sea Res. I* **46**, 1 (1999).
3. J. Blindheim *et al.*, *Deep Sea Res. I* **47**, 655 (2000).
4. R. R. Dickson *et al.*, *Nature* **416**, 832 (2002).
5. S. Manabe, R. J. Stouffer, *J. Clim.* **7**, 5 (1994).
6. S. Manabe, R. J. Stouffer, *Nature* **378**, 165 (1995).
7. M. Vellinga, R. Wood, *Clim. Change* **54**, 251 (2002).
8. M. Schaeffer, F. M. Selten, J. D. Opsteegh, H. Goosse, *Geophys. Res. Lett.* **29**, 10.1029/2002GL015254 (2002).
9. G. L. Russell, D. Rind, *J. Clim.* **12**, 531 (1999).
10. Intergovernmental Panel on Climate Change, *Climate Change 2001: The Scientific Basis. Contributions of Working Group I to the Third Assessment Report of the Intergovernmental Panel on Climate Change*, J. T. Houghton *et al.*, Eds. (Cambridge Univ. Press, Cambridge, 2001).
11. A 20% reduction in overflow strength reported in (*29*) was not persistent. Continuing measurements show that the trend has stopped and perhaps changed sign in the past 2 or 3 years (B. Hansen, personal communication).
12. P. Wu, R. Wood, P. Stott, *Geophys. Res. Lett.* **31**, L02301 (2004).
13. See supporting data on *Science* Online.
14. In the last time frame, 1998 to 2002, only 62% of the Subpolar Basins' total volume can be estimated from measurements, versus 90% or better for all other time frames (*13*).
15. R. R. Dickson, J. Meincke, S.-A. Malmberg, A. J. Lee, *Prog. Oceanogr.* **20**, 103 (1988).
16. K. Aagaard, E. C. Carmack, *J. Geophys. Res.* **94**, 14485 (1989).
17. S. Häkkinen, *J. Geophys. Res.* **98**, 16397 (1993).
18. I. Belkin, *Geophys. Res. Lett.* **31**, L08306 (2004).
19. W. Schmitz, *Rev. Geophys.* **33**, 151 (1995).
20. J. Whitehead, *Rev. Geophys.* **36**, 423 (1998).
21. The time series of current meter measurements maintained since 1986 near Angmassalik, Greenland, has shown remarkably steady volume fluxes in the NSOW, although the properties (temperature, salinity) have fluctuated (R. R. Dickson, personal communication).
22. M. Bersch, *J. Geophys. Res.* **107**, 10.1029/2001JC000901 (2002).
23. T. Stocker, A. Schmittner, *Nature* **388**, 862 (1997).
24. R. Wood, A. Keen, J. Mitchell, J. Gregory, *Nature* **399**, 572 (1999).
25. S. Rahmstorf, A. Ganopolski, *Clim. Change* **43**, 353 (1999).
26. T. Fichefet *et al.*, *Geophys. Res. Lett.* **30**, 10.1029/2003GL017826 (2003).
27. P. Wu, R. Wood, P. Stott, *Geophys. Res. Lett.* **32**, L02703 (2005).
28. Q. Schiermeier, *Nature* **428**, 114 (2004).
29. B. Hansen, W. R. Turrell, S. Østerhus, *Nature* **411**, 927 (2001).

30. Supported by NSF grant OCE-0326778 (R.C.), a WHOI Independent Study Award (R.C., C.M.), and Norwegian Research Council grant 139 815/720 (NoClimII) (C.M.).

Supporting Online Material

www.sciencemag.org/cgi/content/full/308/5729/1772/DC1
Materials and Methods
Figs. S1 to S6
Table S1

6 January 2005; accepted 12 May 2005
10.1126/science.1109477

Secondary Evolutionary Escalation Between Brachiopods and Enemies of Other Prey

Michał Kowalewski,[1]* Alan P. Hoffmeister,[1] Tomasz K. Baumiller,[2] Richard K. Bambach[3]

The fossil record of predation indicates that attacks on Paleozoic brachiopods were very rare, especially compared to those on post-Paleozoic mollusks, yet stratigraphically and geographically widespread. Drilling frequencies were very low in the early Paleozoic (≪1%) and went up slightly in the mid-to-late Paleozoic. Present-day brachiopods revealed frequencies only slightly higher. The persistent rarity of drilling suggests that brachiopods were the secondary casualties of mistaken or opportunistic attacks by the enemies of other taxa. Such sporadic attacks became slightly more frequent as trophic systems escalated and predators diversified. Some evolutionarily persistent biotic interactions may be incidental rather than coevolutionary or escalatory in nature.

Our understanding of the long-term evolutionary dynamics of predator-prey interactions has advanced recently, primarily due to multiple synoptic studies of the post-Paleozoic marine mollusks (*1–5*). There is growing evidence that predatory (or parasitic) activities [in particular, those recorded by drill holes (*6*)] were widespread in the Paleozoic as well (*7–17*),

and compelling records of this are offered by brachiopod prey or hosts (*8*, *9*, *11–17*). Using brachiopods, we assembled multiple estimates of the Paleozoic history of trophic interactions and supplemented those estimates with data regarding present-day brachiopods (*6*).

We studied rhynchonelliform brachiopods (formerly referred to as Articulata) using (i) surveys of museum collections and (ii) field-based estimates compiled from the literature. We focused on drill holes left by predators or parasites (*6*). Our survey of 18 museum collections yielded 44,497 brachiopod specimens (molds and casts were excluded and >95% of specimens were articulated shells) representing 496 lower-taxon collections (LTCs). LTCs (minimal universal sampling units applicable across museums) are monospecific to congeneric collections from single sampling units that vary from individual bulk samples to pooled taxonomic sets from single lithostratigraphic units (formations or members). These data are thus sufficiently resolved for estimating long-term synoptic patterns at epoch-to-period resolution (*6*).

The museum data (*6*) point to a scarcity of drillings in Paleozoic brachiopods (Fig. 1 and tables S1 and S2): Drill-hole frequencies computed for all data pooled across collections and mean percentages for adequately sampled LTCs never exceeded 2% for any part of the Paleozoic and were below 1% for the pooled Paleozoic data (table S1). However, despite their overall rarity, drill holes were found in each geological period, and a notable fraction of adequately sampled LTCs ($n > 30$ specimens) yielded drilled individuals (Fig. 1, inset). Both estimates suggest that drilling frequencies remained low (<0.5%) throughout the lower-to-mid Paleozoic, increased slightly (but significantly) in the Carboniferous (0.5 to 1%), and then went up further (again subtly but significantly) in the Permian (1 to 2%) (Fig. 1 and table S1). The percentage of LTCs with drilled specimens (Fig. 1, inset) also increased from the Ordovician-Devonian to the Carboniferous-Permian: 8% versus 30% of LTCs with drilled specimens, respectively (log-likelihood $G = 21.1$, $P < 0.0001$, log-likelihood test).

The literature on drilled Paleozoic brachiopods provides a different way of assessing secular trends in drill-hole frequencies (*6*). In this case, a metric that is consistently accessible across all studies is the highest-drilled lower taxon (HDLT). This is because most studies are of localities already known for drilled specimens, and all studies reported drilling frequencies for the most frequently drilled species or genus found at those localities. The literature survey produced 34 HDLT estimates (tables S3 and S4), which represent diverse brachiopod genera from 14 lithostratigraphic units (predominately North American) encompassing 10 stratigraphic stages. Despite multiple studies on pre-Devonian drillers (*8*, *9*), the early Paleozoic literature yielded only one (late Silurian) HDTL estimate. That is, pre-Devonian rhynchonelliform brachiopods, drilled frequently enough to report HDLT estimates, have not been found so far in the fossil record. In contrast, numerous estimates are available from the Devonian through the Permian (Fig. 2). When pooled by stratigraphic stage, these estimates suggest a gradual increase in the average HDLT frequencies through the late Paleozoic (Fig. 2, inset), with mean HDLT estimates increasing notably from the Silurian-Devonian to the Carboniferous-Permian [$P < 0.05$ or $P < 0.1$, depending on the operational unit of analysis and the test used (table S3)].

Our survey of the present-day brachiopod collection housed at the Musée National d'Histoire Naturelle–Paris (Fig. 1 and table S1) revealed a similar pattern but also suggested that the trend of subtle increase in drilling frequencies continued after the Paleozoic. The overall drilling frequency is low, but many LTCs contained drilled specimens, including brachiopods from various lower taxa and nearly all major ocean basins of the world. The proportion of LTCs with drilled specimens is indistinguishable statistically from our late Paleozoic estimates (Fig. 1, inset, and table S1). However, the pooled frequency and mean LTC frequency both are higher than the Carboniferous-Permian estimates. This difference is significant for the pooled frequency and is nearly significant for mean LTC values (table S1). The brachiopod literature (*4*, *17–22*) suggests that after the end of the Paleozoic, drillings were also infrequent but sporadically high (*23*).

The multiple estimates consistently point to a significant but subtle secular increase in drilling frequencies from the early Paleozoic (Ordovician-Silurian) to the mid-to-late Paleozoic, and then up to even higher but still low frequencies in Recent ecosystems. These increases are consistent with macroevolutionary models postulating two major intervals of increased ecospace exploitation and evolutionary escalation (that is, an increase in predation pressures over evolutionary time scales): the mid-Paleozoic Marine Revolution (*7–10*, *24*), followed by the Mesozoic Marine Revolution (*1–5*, *24*). The trend is unlikely to be a spurious reflection of taphonomic trends, cryptic latitudinal gradients, or environmental shifts (*6*). However, because of the inclusion of a broad range of lower taxa, the data are poorly constrained phylogenetically and ecologically. To test whether the pattern is

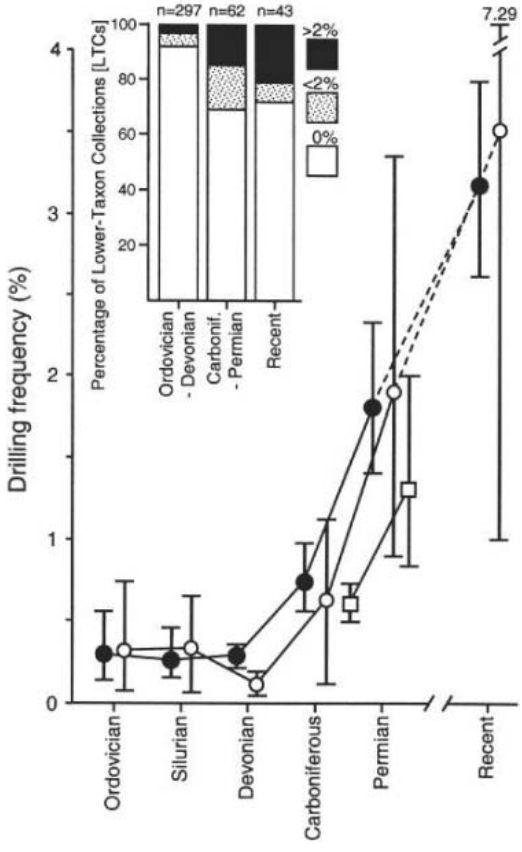

Fig. 1. Frequencies of predation traces (drill holes) in shells of brachiopod prey or hosts (*6*) averaged across multiple museum collections (tables S1 and S2). Solid symbols, with 95% binomial confidence intervals, represent overall percentages of drilled specimens per time period. Open symbols, with 95% bootstrap confidence intervals, represent mean drilling frequencies averaged across samples (LTC) with 30 specimens or more. Open squares, with 95% binomial confidence intervals, represent overall percentages of drilled specimens of the genus *Composita* (based on data assembled for the Carboniferous and Permian). Partly overlapping adjacent 95% confidence intervals remain significant as long as they do not overlap with adjacent estimates of means (see also statistical tests in table S1). Dashed segments of the lines connecting individual estimates mark a large temporal gap (from the Triassic through the Pleistocene). **(Inset)** Frequencies of LTCs (with $n \geq 30$ specimens) grouped on the basis of drilling frequencies and binned into three time intervals (Ordovician-Devonian, Carboniferous-Permian, and Recent). The proportion of samples with >0% drilling rates increased significantly from the Ordovician-Devonian to the Carboniferous-Permian ($G = 21.1$, $P < 0.0001$), but not from the Carboniferous-Permian to Recent ($G = 2.47$, $P = 0.29$). n = number of LTCs per time interval.

[1]Department of Geosciences, Virginia Polytechnic Institute and State University, Blacksburg, VA 24061, USA. [2]Museum of Paleontology, University of Michigan, Ann Arbor, MI 48109, USA. [3]Botanical Museum, Harvard University, 26 Oxford Street, Cambridge, MA 02138, USA.

*To whom correspondence should be addressed. E-mail: michalk@vt.edu.

reproducible at finer taxonomic scales, we generated a data set (n = 19,831 specimens) for a single genus (*Composita*) that is abundant in many late Paleozoic museum collections. These estimates tightly track the other two estimates from the Carboniferous to the Permian and are statistically indistinguishable from them (Fig. 1).

These patterns (Figs. 1 and 2 and tables S1 to S4) (*6*), when considered jointly, suggest that the drill holes do not record tight interactions between brachiopods and their own brachiopod-specialized enemies. First, in the case of coevolving and/or escalating trophic systems, the drilling frequencies tend to be much higher (*25*). For example, Cenozoic (and Recent) gastropods typically drilled (and drill) their mollusk or echinoid prey at frequencies (*3*, *4*, *26*, *27*) that are 10 to 20 times higher than those observed here for Paleozoic and Recent brachiopods. Second, the nearly static persistence of low drilling frequencies over evolutionary time scales would not be expected for tightly interacting brachiopod/driller systems: Extinctions and diversifications of victims and their enemies should lead to major temporal fluctuations in the frequency and strategy of drilling, as is observed for Cenozoic mollusk prey (*28*, *29*). There is also tentative evidence for an unusually high disparity in the size and shape of holes drilled in brachiopods (fig. S1 and table S5), which is more consistent with incidental attacks by diverse drillers than with targeted drillings by brachiopod-specialized enemies (*6*). Finally, if early drillers targeted brachiopods and then switched to more nutritious and increasingly abundant mollusks, as would be predicted by cost/benefit models, then drill holes in brachiopods should have become less frequent over time.

The patterns are more consistent with the hypothesis of secondary (or spurious) escalation between brachiopods and enemies of other prey or hosts. According to this hypothesis, the drillers preferentially attacked other organisms but sporadically drilled less nutritious, metabolically more sluggish, and perhaps less palatable (*30*) brachiopods. Such switches may have included opportunistic feedings (*31*); for example, present-day muricid gastropods may shift their diet (*32*) from barnacles, which often are killed without drilling (*33*), to mussels, which typically require drilling. Also, prey switches may have involved mistaken attacks (*34*, *35*) by stressed, inexperienced, or otherwise confused enemies of other prey or hosts.

Whereas many parasites tend to be highly host-specific, and thus are unlikely to display opportunistic behavior, externally drilling ectoparasites may be more flexible behaviorally. For example, Recent eulimid gastropods drill various echinoderms and often are associated with individual hosts only temporarily (*36*). Platyceratid gastropods, which are coprophagous or kleptoparasitic infesters of Paleozoic echinoderms, are a viable candidate for opportunistic or erroneous parasites of late Paleozoic brachiopods (*13*).

Apart from drilled echinoderms, the absence of notable Paleozoic drillings in putative primary prey or hosts can be attributable to multiple factors. The primary prey or host may have had an aragonitic skeleton; such Paleozoic taxa typically are preserved as molds or casts and thus rarely retain evidence of drilling attacks. A recent study comparing silicified shells of aragonitic bivalves with those of sympatric calcitic brachiopods showed that Permian mollusks were drilled at many times higher rates than were contemporaneous brachiopods from the same units (*16*). Also, drill holes may have been made in small fragile skeletons, or even in nonpreservable victims such as lightly biomineralized arthropods, that might have required drilling but would not have been preserved. Finally, drillers may have been facultative and drilled only or primarily when attacking brachiopods: Prey-specific or size-specific switches in attack behavior are documented in present-day ecosystems, and some predators drill only if other attack strategies fail (*37*).

The hypothesis of secondary escalation provides an explanation for a slow secular increase in drilling frequencies in brachiopods concordant with Paleozoic and Mesozoic Marine Revolutions. As ecosystems escalated, trophic interactions intensified, and ecospace exploitation widened, ecological pressures should have also increased. Elevated competition, greater food demands of metabolically more active faunas, higher failure rates of attacks on more active or better defended prey, and increased predation pressures on drillers themselves could all have contributed to more frequent incidences of opportunistic and mistaken attacks on brachiopods. Consistent with the escalation (*2*) and Red Queen (*38*) hypotheses, a subtle long-term increase in drilling frequency observed in brachiopods may thus be an expected testament of incidental damage inflicted on undesirable victims by increasingly abundant and diverse predators (*24*) of other prey. Such secondary escalation should not be equated with a true evolutionary escalation (*2*), being a mere side effect of escalating ecosystems manifested diffusively in brachiopods.

Organisms that are subject to incidental secondary interactions should not be used to directly test the evolutionary importance of biotic interactions. For example, it may be inappropriate to search for detectable evolutionary responses or test the hypothesis of escalation (*2*) by examining clades of occasionally drilled brachiopods. On the other hand, brachiopods may provide the best indirect means of measuring secular changes in the overall intensity of trophic interactions. That is, the frequency of opportunistic or erroneous attacks averaged across a wide spectrum of predatory and parasitic guilds may offer us a much more stable metric for assessing overall predatory pressures than could be provided by any specific predator/prey system that may show trends due to clade-specific diversification and extinction events. Finally, our study suggests that incidental interactions between organisms may be temporally persistent, globally widespread, and occasion-

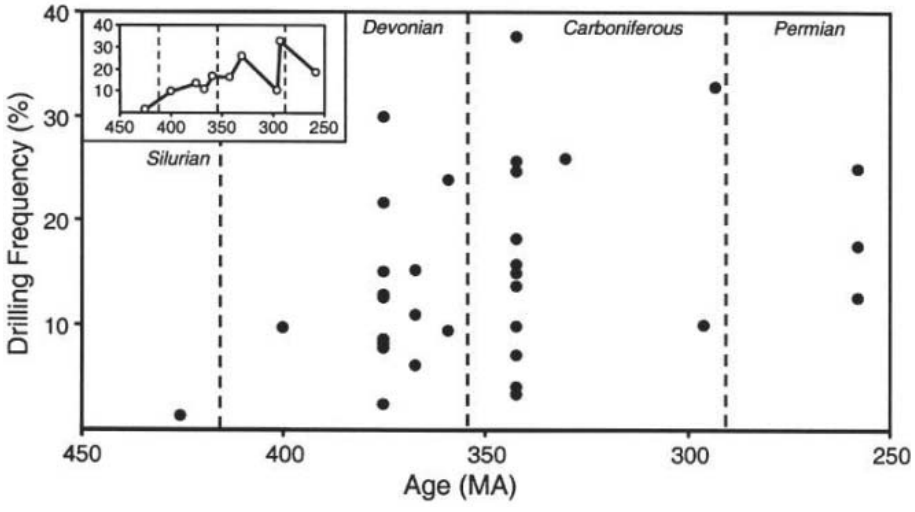

Fig. 2. Field-based estimates of drilling frequencies in the Paleozoic brachiopods compiled from the literature (tables S3 and S4). Each point represents a single HDLT frequency estimated in previous field studies (*6*). (**Inset**) An overall trend in mean HDLT averaged across all individual sites. The literature survey targeted the entire Paleozoic. Despite many studies of early Paleozoic drillers (*8*, *9*), HDLT estimates before the late Silurian are unavailable for rhynchonelliform brachiopods, suggesting that early Paleozoic calcitic brachiopods were drilled too infrequently to allow for quantitative analyses. MA, million years ago.

ally intense ecologically, even if their macroevolutionary consequences are unlikely to have been significant.

References and Notes

1. G. J. Vermeij, *Paleobiology* **3**, 245 (1977).
2. G. J. Vermeij, *Evolution and Escalation* (Princeton University, Princeton, NJ, 1987).
3. P. H. Kelley, T. A. Hansen, *Palaios* **8**, 358 (1993).
4. M. Kowalewski, F. T. Fürsich, A. Dulai, *Geology* **26**, 1091 (1998).
5. G. J. Vermeij, D. E. Schindel, E. Zipser, *Science* **214**, 1024 (1981).
6. Additional methodological details, data, and analyses are available as supporting material on *Science* Online.
7. P. W. Signor, C. E. Brett, *Paleobiology* **10**, 229 (1984).
8. C. E. Brett, S. E. Walker, in *The Fossil Record of Predation*, M. Kowalewski, P. H. Kelley, Eds. (Paleontological Society Papers 8, Yale University Reprographics and Imaging Services, New Haven, CT, 2002), pp. 93–118.
9. C. E. Brett, in *Predator-Prey Interaction in the Fossil Record*, P. H. Kelley, M. Kowalewski, T. A. Hansen, Eds. (Plenum, New York, 2003), pp. 401–432.
10. T. K. Baumiller, F. J. Gahn, *Science* **305**, 1453 (2004).
11. W. L. Ausich, R. A. Gurrola, *J. Paleontol.* **53**, 335 (1979).
12. S. A. Smith, C. W. Thayer, C. E. Brett, *Science* **230**, 1033 (1985).
13. T. K. Baumiller, L. Leighton, D. Thompson, *Palaeogeogr. Palaeoclimat. Palaeoecol.* **147**, 289 (1999).
14. L. R. Leighton, *Palaeogeogr. Palaeoclimat. Palaeoecol.* **201**, 221 (2003).
15. A. P. Hoffmeister, M. Kowalewski, T. K. Baumiller, R. K. Bambach, *Lethaia* **36**, 107 (2003).
16. A. P. Hoffmeister, M. Kowalewski, T. K. Baumiller, R. K. Bambach, *Acta Palaeontol. Pol.* **49**, 443 (2004).
17. E. M. Harper, *Palaeogeogr. Palaeoclimat. Palaeoecol.* **201**, 185 (2003).
18. E. M. Harper, D. S. Wharton, *Palaeogeogr. Palaeoclimat. Palaeoecol.* **158**, 15 (2000).
19. T. K. Baumiller, M. A. Bitner, *Palaeogeogr. Palaeoclimat. Palaeoecol.* **214**, 85 (2004).
20. J. H. Delance, C. C. Emig, *Palaeogeogr. Palaeoclimat. Palaeoecol.* **208**, 23 (2004).
21. E. M. Harper, L. S. Peck, *Polar Biol.* **26**, 208 (2003).
22. E. M. Harper, G. T. W. Forsythe, T. Palmer, *Palaios* **13**, 352 (1998).
23. Our data provide multiple estimates for the mid-to-late Paleozoic increase in drilling frequencies. The evidence for late Mesozoic increase is more circumstantial, however, being based on the late Cenozoic (Holocene) estimates only. However, the Paleozoic-to-Holocene increase is consistent with the Mesozoic Marine Revolution hypothesis. Moreover, recent literature compilations (*4*, *17*) do not indicate any significant increase in drilling between Paleozoic and Mesozoic brachiopods (i.e., the post-Paleozoic increase must have happened either in the latest Mesozoic or in the Cenozoic). Also, recent case studies indicate that exceptionally high drilling frequencies are occasionally observed in Cenozoic brachiopods, yielding HDLT estimates as high as 40% (*19*): a value higher than any of the 34 Paleozoic estimates reported here (Fig. 2).
24. R. K. Bambach, *Geobios* **32**, 131 (1999).
25. This argument is inconclusive when considered alone. If the drillers were highly facultative and attacked brachiopods by drilling only occasionally, the low frequencies would be a behavioral artifact and not evidence for a low level of trophic interactions. However, the low-frequency pattern is consistent with other more compelling lines of evidence discussed in the text.
26. J. H. Nebelsick, M. Kowalewski, *Palaios* **14**, 127 (1999).
27. P. H. Kelley, T. A. Hansen, in *Biotic Recovery from Mass Extinction Events*, M. B. Hart, Ed. (Geological Society Special Publication 102, Geological Society Publishing House, London, 1996), pp. 373–386.
28. G. P. Dietl, G. S. Herbert, G. J. Vermeij, *Science* **306**, 2229 (2004).
29. For example, naticid/mollusk interactions in the Cenozoic show major (possibly extinction-related) changes in drilling frequencies through time; often >10% shifts across adjacent time intervals are observed (*27*). In contrast, the overall shift observed here for the entire Phanerozoic history of drilling in brachiopods is ~3% and represents a slow increase over a period of ~500 million years.
30. C. W. Thayer, *Science* **228**, 1527 (1985).
31. G. C. Cadée, *Lethaia* **17**, 289 (1984).
32. G. Rilov, A. Gasitha, Y. Benayahub, *Mar. Environ. Res.* **54**, 85 (2002).
33. R. N. Hughes, S. DeB. Dunkin, *J. Exp. Mar. Biol. Ecol.* **77**, 45 (1984).
34. M. LaBarbera, *Paleobiology* **7**, 510 (1981).
35. S. E. Walker, S. B. Yamada, *Palaeontology* **36**, 735 (1993).
36. A. Warén, D. R. Norris, J. Templado, *Veliger* **37**, 141 (1994).
37. M. A. Steer, J. M. Semmens, *J. Exp. Mar. Biol. Ecol.* **290**, 165 (2003).
38. L. Van Valen, *Evol. Theory* **1**, 1 (1973).

39. We thank NSF (Geology and Paleontology Program, grants EAR-9909225 and 9909565), the Petroleum Research Fund (grants AC 37737 and AC 40735), and the Fulbright Commission for financial support; F. Gahn, B. Deline, E. Roberts, M. Tuura, and P. Shafer for help in processing museum samples; and S. Xiao, J. Huntley, G. Dietl, and two anonymous reviewers for useful comments on the manuscript.

Supporting Online Material

www.sciencemag.org/cgi/content/full/308/5729/1774/DC1
Materials and Methods
SOM Text
Fig. S1
Tables S1 to S5
References

8 April 2005; accepted 21 April 2005
10.1126/science.1113408

Patient-Specific Embryonic Stem Cells Derived from Human SCNT Blastocysts

Woo Suk Hwang,[1,2]* Sung Il Roh,[3] Byeong Chun Lee,[1] Sung Keun Kang,[1] Dae Kee Kwon,[1] Sue Kim,[1] Sun Jong Kim,[3] Sun Woo Park,[1] Hee Sun Kwon,[1] Chang Kyu Lee,[2] Jung Bok Lee,[3] Jin Mee Kim,[3] Curie Ahn,[4] Sun Ha Paek,[4] Sang Sik Chang,[5] Jung Jin Koo,[5] Hyun Soo Yoon,[6] Jung Hye Hwang,[6] Youn Young Hwang,[6] Ye Soo Park,[6] Sun Kyung Oh,[4] Hee Sun Kim,[4] Jong Hyuk Park,[7] Shin Yong Moon,[4] Gerald Schatten[7]*

Patient-specific, immune-matched human embryonic stem cells (hESCs) are anticipated to be of great biomedical importance for studies of disease and development and to advance clinical deliberations regarding stem cell transplantation. Eleven hESC lines were established by somatic cell nuclear transfer (SCNT) of skin cells from patients with disease or injury into donated oocytes. These lines, nuclear transfer (NT)–hESCs, grown on human feeders from the same NT donor or from genetically unrelated individuals, were established at high rates, regardless of NT donor sex or age. NT-hESCs were pluripotent, chromosomally normal, and matched the NT patient's DNA. The major histocompatibility complex identity of each NT-hESC when compared to the patient's own showed immunological compatibility, which is important for eventual transplantation. With the generation of these NT-hESCs, evaluations of genetic and epigenetic stability can be made. Additional work remains to be done regarding the development of reliable directed differentiation and the elimination of remaining animal components. Before clinical use of these cells can occur, preclinical evidence is required to prove that transplantation of differentiated NT-hESCs can be safe, effective, and tolerated.

Many human injuries and diseases result from defects in a single cell type. If defective cells could be replaced with appropriate stem cells, progenitor cells, or cells differentiated in vitro, and if immune rejection of transplanted cells could be avoided, it might be possible to treat disease and injury at the cellular level in the clinic (*1*). By generating hESCs from human NT blastocysts, in which the somatic cell nucleus comes from the individual patient—a situation where the nuclear [though not mitochondrial DNA (mtDNA)] genome is identical to that of the NT donor—the possibility of immune rejection might be eliminated if these cells were to be used for human treatment (*2*, *3*).

Recently, mouse models of severe combined immunodeficiency (SCID) (*4*) and Parkinson's disease (PD) (*5*) have been successfully treated through the transplantation of autologous differentiated mouse embryonic stem cells (mESCs) derived from NT blastocysts, a process also referred to as therapeutic cloning (*6*). In 2004, evidence was presented that a human NT-hESC line (NT-hESC-1) was derived by transferring the donor's cumulus cell nucleus into her own enucleated oocyte (*6*); however, questions remained as to whether the cell line had a parthenogenetic origin. In addition, it was not known whether NT-hESCs could be generated from NT procedures using nuclei from males, prepubescent girls, or postmenopausal

Table 1. Establishment of patient-specific NT-hESCs.

(A) Cell line	(B) Cell donors			(C) No. injected oocytes (no. of donors)	(D) No. fused oocytes (%)	(E) NT blastocysts		(F) NT-hESC lines established			
	Age (years)	Sex	Status			No.	% per fused oocyte	No.	% NT-hESCs per blastocyst	Mean no. oocytes injected per line	Mean no. fused oocytes per line
NT-hESC-2	10	M	SCI	8 (1)	5 (62.5)	1	20.0	1	100.0	8.0	5
NT-hESC-3	6	F	JD	18 (2; 1 > 30 years old)	6 (33.3)	2	33.3	1	50.0	18.0	6.0
NT-hESC-4 and -5	36	M	SCI	22 (1)	21 (95.5)	7	33.3	2	28.6	11.0	10.5
NT-hESC-6 and -7	24	F	SCI	23 (1)	18 (78.3)	6	33.3	2	33.3	11.5	9.0
NT-hESC-8*	33	F	SCI	5 (1)	4 (80.0)	2	50.0	1	50.0	5.0	4.0
NT-hESC-9	2	M	CGH	9 (1)	7 (77.8)	3	42.9	1	33.3	9.0	7.0
NT-hESC-10	56	M	SCI	12 (1)	7 (58.3)	1	14.3	1	100.0	12.0	7.0
NT-hESC-11	30	M	SCI	22 (2; 2 > 30 years old)	15 (68.2)	3	20.0	1	33.3	22.0	15.0
NT-hESC-12	35	M	SCI	48 (5; 4 > 30 years old)	34 (70.8)	6	17.6	1	16.6	48	34
Attempt I†	23	M	SCI	10 (2; 1 > 30 years old)	8 (80.0)	0	-	-	-	-	-
Attempt II†	20	M	SCI	8 (1)	4 (50.0)	0	-	-	-	-	-
Compilations				Σ Oocytes = 185, 125‡ Σ/Cycle = 10.2 oocytes; 12.5 oocytes‡	Σ = 129 (69.7)	Σ = 31	Mean = 24.0%	Σ = 11	Mean = 35.4% 40.9%‡	16.8 13.8‡	11.7 10.0‡

*Autologous SCNT was performed; that is, the donor's own fibroblast nuclei were transferred back into her own enucleated oocytes. †Successful NT development without blastocyst formation. ‡Rates with oocytes donated by women <30 years old (table S3).

women, or when using cell components from unrelated women. Finally, because NT-hESC-1 was grown on mouse feeders with likely xenograft contamination (*7*), the utility of those cells is largely preclinical. In our study, patient-specific NT-hESCs were established reliably and efficiently (~1 NT-hESC line per oocyte donation cycle) on human feeder cells and regardless of somatic cell donor sex or age. In addition, some lines were derived without the animal products used during immunosurgery. Immunosurgery exposes the ESC precursors, the inner cell mass cells (ICMs), through lysis of the blastocyst's outer trophectoderm cells by sequential exposure to antibodies followed by complement; however, residual animal byproducts, including calf serum and enzymes, still remain. Furthermore, 10 of the 11 new cell lines were generated from NT procedures using oocyte and somatic cell donors that were obtained from biologically unrelated individuals.

Oocyte donations by healthy women (with cell line -8 as the only exception) and somatic cell donations by patients conformed to the regulations and law in the Republic of Korea, in accordance with responsible institutional review board (IRB) review and oversight (*8*). Donors were fully aware of the scope of this study and each signed an informed consent form. Both of the parents of children under 18 years old donating somatic cells were similarly counseled, and each signed informed consent forms on behalf of their child. Patients voluntarily donated oocytes and somatic cells for therapeutic cloning research and relevant applications but not for reproductive cloning. Although expenses for public transportation and injections administered by medical personnel could have been provided, none of the donors requested this, and therefore no financial reimbursement in any form was paid (*9*).

Recruited patients had a genetic immunodeficiency disease [congenital hypogammaglobulinemia (CGH)], disorders caused by injury [spinal cord injury (SCI)], or another condition caused by complex autoimmune mechanisms [juvenile diabetes (JD)]. These three diseases are proposed to be treatable by single-cell-type transplantation with hematopoietic stem cells (of mesodermal origin), motor neurons or neuroprogenitors (ectodermal origin), or β-islet cells (endodermal origin), respectively. Patient-specific stem cells derived in this study are now expected to provide cells in a disease state that can be used to understand disease progression and assist in drug development. Because the stem cells generated with the use of patient cells are still likely to be defective, they probably cannot be directly used in cell transplantation to patients. In addition, before the cells can be used in the clinic, the biological properties of the patient-specific NT-hESCs must be defined, reliable differentiation procedures must be established, and the cells must be free of contaminating undifferentiated cells and potential pathogens.

Donor patients' fibroblasts were grown from skin biopsies (*9*). Individual cells were retrieved from the monolayer by trypsinization (*9*). Heterologous NTs were performed, in which donor somatic cell nuclei were transferred individually into enucleated oocytes from a biologically unrelated individual. However, for one cell line, NT-hESC-8, autologous NT was performed, in which the donor's own fibroblast nuclei were transferred into her own enucleated oocytes. Nine of the generated lines (and one of the unsuccessful attempts) used donated oocytes from unrelated individuals (biological or otherwise), whereas another successful line and one unsuccessful attempt used oocytes from a biologically unrelated family member. Details on oocyte and somatic cell donations and ovarian stimulation protocols are described, and the Korean version and translations by the Korean team into English of the informed consent forms are appended in (*9*). Enucleation, confirmation of the oocyte's DNA removal, NT, fusion, and activation were performed as described (*6*).

Eleven NT-hESC lines were derived using somatic cells from patients with SCI, JD, and CHG of both sexes and ranging from 2 to 56 years old (Table 1). Figure 1 shows results from male NT-hESC-2 (left columns) and female NT-hESC-3 (right columns), in which stem cell colonies display characteristic cobblestone-like appearances with circumscribed borders (Fig. 1, A and B) and express hESC pluripotency markers, including alkaline

[1]College of Veterinary Medicine, Seoul National University, Seoul 151-742, Korea. [2]School of Agricultural Biotechnology, Seoul National University, Seoul 151-742, Korea. [3]Medical Research Center, MizMedi Hospital, Seoul 135-280, Korea. [4]College of Medicine, Seoul National University, Seoul 110-744, Korea. [5]Hanna Women's Clinic, Seoul 137-872, Korea. [6]School of Medicine, Hanyang University, Seoul 471-701, Korea. [7]Pittsburgh Development Center, Magee-Womens Research Institute, Department of Obstetrics, Gynecology, and Reproductive Sciences and Department of Cell Biology and Physiology, University of Pittsburgh School of Medicine, Pittsburgh, PA 15213, USA.

*To whom correspondence should be addressed. E-mail: hwangws@snu.ac.kr (W.S.H.); gschatten@pdc.magee.edu (G.S.)

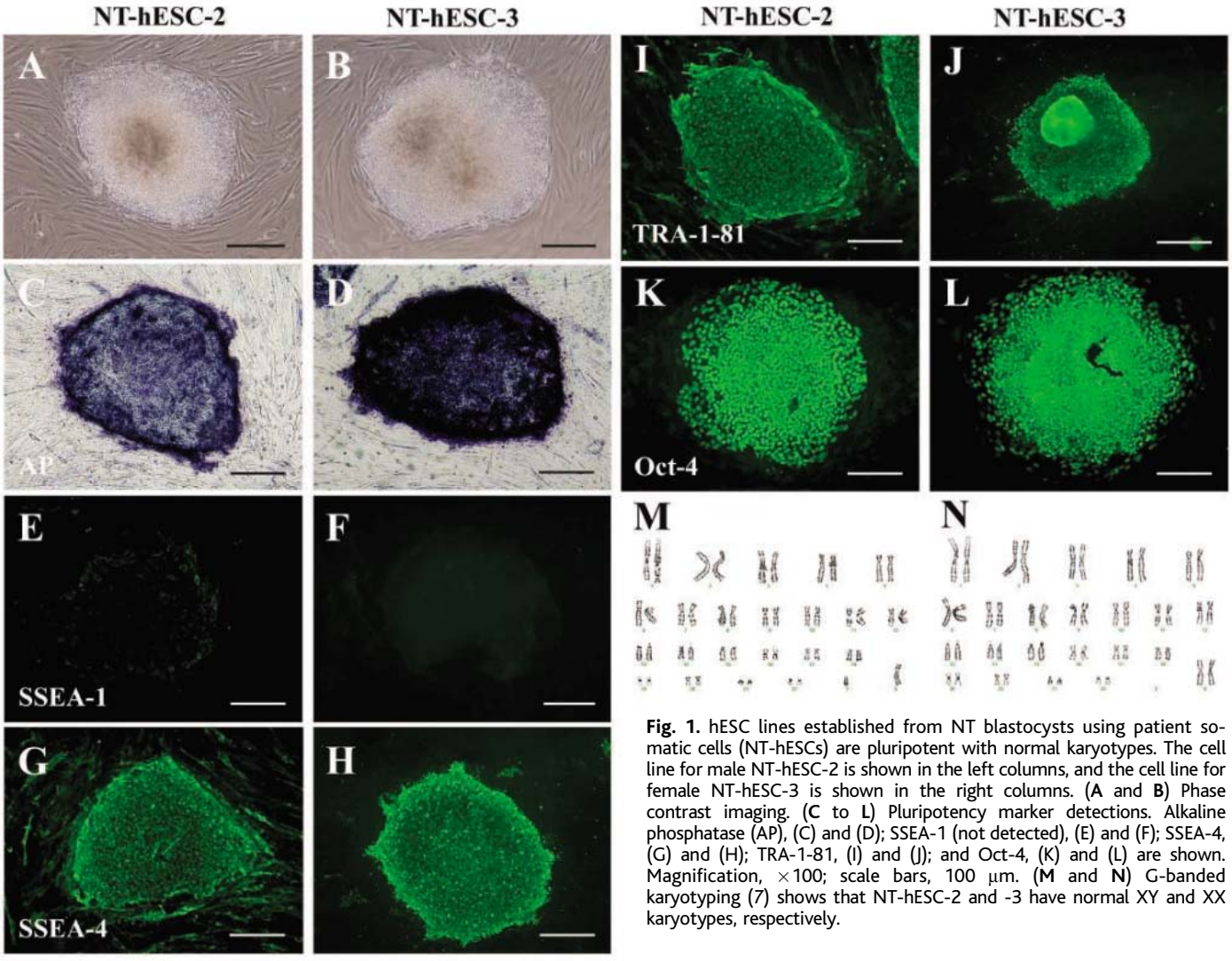

Fig. 1. hESC lines established from NT blastocysts using patient somatic cells (NT-hESCs) are pluripotent with normal karyotypes. The cell line for male NT-hESC-2 is shown in the left columns, and the cell line for female NT-hESC-3 is shown in the right columns. (**A** and **B**) Phase contrast imaging. (**C** to **L**) Pluripotency marker detections. Alkaline phosphatase (AP), (C) and (D); SSEA-1 (not detected), (E) and (F); SSEA-4, (G) and (H); TRA-1-81, (I) and (J); and Oct-4, (K) and (L) are shown. Magnification, ×100; scale bars, 100 μm. (**M** and **N**) G-banded karyotyping (7) shows that NT-hESC-2 and -3 have normal XY and XX karyotypes, respectively.

phosphatase (AP) (Fig. 1, C and D), stage-specific embryonic antigen 4 (SSEA-4) (Fig. 1, G and H), SSEA-3 (fig. S1A), tumor rejection antigen 1-81 (Tra-1-81) (Fig. 1, I and J), Tra-1-60 (fig. S1A), and octamer-4 (Oct-4) (Fig. 1, K and L), but not SSEA-1 (negative control; Fig. 1, E and F). Normal male (Fig. 1M) and female (Fig. 1N) karyotypes are shown for NT-hESC-2 and NT-hESC-3, respectively. For complete data on NT-hESC-4 through -11, see fig. S1, B and C, and Table 2.

DNA fingerprinting with human short tandem-repeat probes (Fig. 2 and fig. S2, A to D) shows with high certainty that every NT-hESC line derived here originated from the respective patient donor and that these lines were not the result of enucleation failures and subsequent parthenogenetic activation. In Fig. 2 (red), isogenic analysis in the loci amelogenin, D5S818, and the fibrinogen alpha chain gene (FGA) shows that the male lines -2 and -4 each precisely match the respective DNA fingerprints of the male NT donors, just as the female line -3 is an identical match with the female NT donor. The other male lines -5 and -9 to -12 also each match the respective male NT donors, just as the other female lines -6 to -8 each match the other female NT donors (fig. S2A; red are isogenic analyses in the amelogenin, D5S818, and FGA loci comparing NT-hESC-5 through NT-hESC-12, with their respective patient donor's DNA). DNA fingerprinting of donor oocytes was not performed because of their limited numbers and their central importance for the NT procedure. Data shown in fig. S2B [black; isogenic analysis in loci D19S433, von Willebrand factor gene (vWA), thyroid peroxidase gene (TPOX), and D18S51], fig. S2C [green; isogenic analysis in loci D3S1358, tyrosine hydroxylase gene 1 (THO1), D13S317, D16S539, and D2S1338], and fig. S2D [blue; isogenic analysis in loci D8S1179, D21S11, D7S820, and c-fms proto-oncogene for CSF-1 receptor gene (CSF1PO)] further confirmed the identical matches of NT-hESCs with each respective donor. The statistical probability that these lines may have been derived from another person is $<4.1 \times 10^{-16}$.

NT-hESCs have been efficiently established from a diverse group of patients. In Table 1, the somatic cell donor's sex, age, and disorder or disease (Table 1B) are shown in the left columns for each of the 11 new NT-hESC lines (NT-hESC-2 to -12; Table 1A). Eighteen women donated 185 oocytes for these studies (Table 1C), of which 125 oocytes were donated by 10 women under 30 years old (Table 1C, bottom row). On average, 10.2 oocytes were donated during each assisted reproductive technology (ART) stimulation cycle, and an average of 12.5 oocytes were donated per cycle by women under 30 (Table 1C, bottom row). Success varied, with nine lines derived from single cycles (Table 1C). NT-hESC-2 was established with five oocytes from a single cycle, but the derivation of NT-hESC-12 required 48 oocytes from five cycles (however, four of these donations were by women over 30; Table 1C). Lines NT-hESC-4 and -5 were established from a single cycle, as were NT-hESC-6 and -7 (Table 1C). The only line in which the oocytes and somatic cell were biologically related was NT-hESC-8, in which

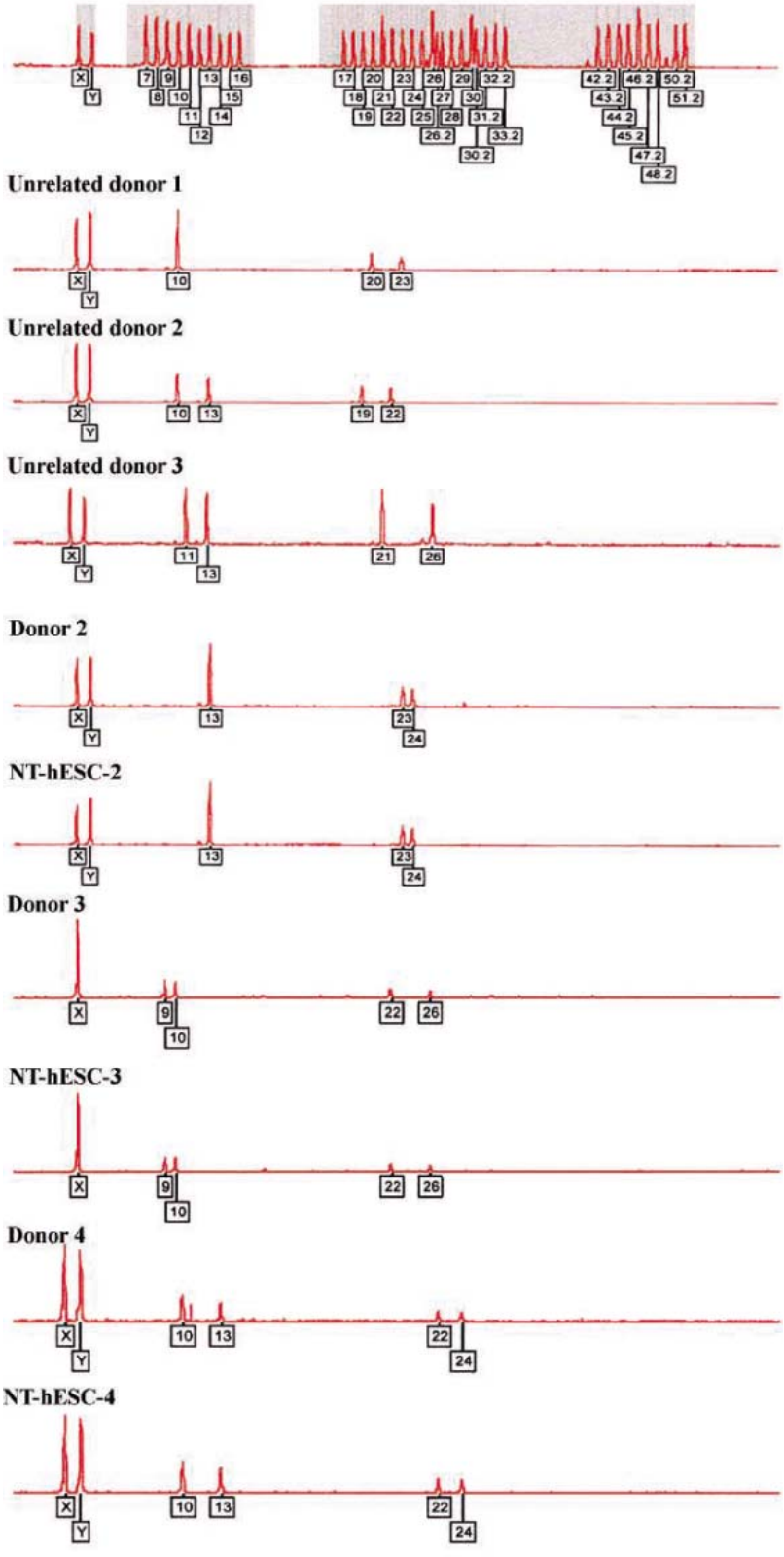

Fig. 2. DNA fingerprinting analysis of 3 of 11 NT-hESCs cell lines (-2 to -4) demonstrates genetic identities with donor patient nuclei (DNA fingerprinting of NT-hESC-5 through -12 are shown in fig. S2A). Isogenic analysis in loci amelogenin (chromosome location: X, p22.1 to 22.3; Y, p11.2); D5S818 (chromosome location 5p22 to 31); and FGA (chromosome location 4q28) is shown. The boxed numbers and corresponding peaks represent locations of polymorphisms for each short tandem-repeat marker at loci amelogenin (peak: X, Y); D5S818 (peak no. 9 to 13); and FGA (peak no. 18 to 26). Figure S2 provides additional DNA fingerprinting evidence.

the donor's own somatic cell was transferred into her own oocytes. Two cycles each were required for NT-hESC-3 and -11 (Table 1C). Only two NT-hESC attempts [NT-hESC attempt I, with oocytes from two donors (one donation from a woman older than 30), and attempt II, with a single donor's oocytes] were unsuccessful; i.e., NT constructs did not develop into blastocysts (Table 1A, bottom rows). Blastocyst development after NT occurred at high rates, with 129 fused NT constructs recovered from the original 185 injected oocytes (69.7%; range from 33.3 to 95.5%; Table 1D). Thirty-one NT blastocysts (24.0% of the fused NT oocytes; Table 1E) were generated. This rate was less than half the ~60% in vitro fertilization (IVF) blastocyst development rate with gametes from infertility patients reported by ART clinics (*10*).

Eleven NT-hESC lines were established from these 31 NT blastocysts (Table 1F; 35.4% average; range, 16.6 to 100%). 16.8 injected oocytes or 11.7 NT-fused oocytes were required for each established NT-hESC line (range, 5 to 48 injected or 4 to 34 fused NT oocytes, respectively). NT-hESC lines were established from 40.9% of NT blastocysts generated from oocytes donated by women under 30 (Table 1F, bottom). For each NT-hESC line when the oocytes were donated by women under 30, 13.8 injected oocytes or 10.0 NT-fused oocytes were needed (Table 1F, bottom). Derivation rates for NT-hESC lines from NT blastocysts were similar to those with fertilized blastocysts (*11*, *12*).

Neither nuclear donor sex (table S1, 33.3% NT-hESC lines per male blastocyst versus 40.0% NT-hESC lines per female blastocyst) nor age (table S2) influenced cell-line establishment with statistical significance. Oocyte donor age appears to be negatively correlated with success [oocytes donated by women older than 30 years were less successful (table S3), with 40.9% NT-hESC lines per NT blastocyst for oocytes donated by women younger than 30 years versus 22.2% for oocyte donors older than 30 years]. Whereas the limited sample size precludes findings of statistical significance, only two NT-hESC lines were established from the 60 oocytes donated by women older than 30 (3.3% NT-hESCs per oocyte), and the other nine lines were derived from the 125 oocytes donated by younger women (7.2%). It is premature to conclude whether technical confounders, the natural variability of oocytes and donor nuclei, or individual patient characteristics account for either very favorable outcomes (when some lines were established with a few oocytes) or unsuccessful outcomes [when NT-hESCs were not generated (Table 1, attempts I and II)].

Stem cells are defined (*13*) by their ability to self-renew as well as differentiate into somatic cells from all three embryonic germ layers: ectoderm, mesoderm, and endoderm. Differentiation of 7 of the 11 new NT-hESC lines (NT-hESC-2 through -11) (Table 2) was

analyzed both in teratomas (Fig. 3, A to X) and into embryoid bodies (EBs) (Fig. 3, Y to e, and fig. S3), and the remaining four cell lines investigated so far differentiated only in embryoid bodies (Table 2). Each NT-hESC line differentiated into all germ layers. The convoluted surfaces characteristic of ectodermal lineages, including skin epithelium, and retinal and primitive neuroepithelium, are shown in Fig. 3, A, B, I, J, Q, and R. Muscle cell bundles, distinctive cartilage nodules, renal tubules, and bone matrix, all derived from mesoderm, are shown in Fig. 3, C, D, G, K, L, O, Q, S, T, W, and X. Endoderm derivatives, including gastrointestinal and respiratory epithelia, are shown in Fig. 3, E to H, M, N, P, U, V, and X. Figure 3, Y to e, demonstrates in embryoid bodies that each line differentiates into cells labeled by monospecific lineage probes; for example, ectodermal cells [Fig. 3, Y to a; Y, NT-hESC-5; Z, NT-hESC-6; and a, NT-hESC-7; paired box gene (Pax 3/7), microtubule-associated protein 2 (MAP-2), and glial fibrillary acidic protein (GFAP)], mesodermal cells [Fig. 3, b to d; b, NT-hESC-8; c, NT-hESC-9; d, NT-hESC-10; atrial natriuretic peptide (ANP), CD34, and desmin, respectively], and endodermal cells [Fig. 3e, NT-hESC-11, myosin heavy chain (MHC)]. Figure S3 shows panels of immunohistochemical markers specific for each lineage in every line analyzed to date (Table 2).

The discoveries of Wilmut *et al*. (*14*) in sheep cloning, together with those of Thomson *et al*. (*1*) in deriving hESCs, have generated considerable enthusiasm for regenerative cell transplantation based on the establishment of patient-specific hESCs derived from NT blastocysts generated from a patient's own nuclei. This strategy, aimed at avoiding immune rejection through autologous transplantation, is perhaps the strongest clinical rationale for therapeutic cloning. By the same token, derivations of complex disease-specific NT-hESCs may accelerate discoveries of disease mechanisms. For cell transplantations, innovative treatments of murine SCID and PD models with the individual mouse's own NT-mESCs are encouraging (*4*, *5*). Human populations, unlike those of inbred mice, are genetically very diverse; consequently, conclusive proof of immune matching between the specific patient and her or his individualized NT-hESC line demands rigorous evidence. Toward this immune matching, MHC human leukocyte antigen (MHC HLA) isotypes of our stem cell lines are identical to those of the somatic cells from the corresponding patient donors (Table 3 for lines NT-hESC-2 through -4; table S4 for lines -5 through -12). MHC-HLA matching is crucial for immunological tolerance during organ donations, and in the absence of MHC-HLA matching, immunosuppressive medicines are required. This MHC-HLA matching provides additional evidence that parthenogenetic errors had not occurred. Each NT-hESC line matches the respective donor's for all HLA isotypes shown in Table 3 and table S4, suggesting that transplanted NT-hESCs will be tolerated. Yet caution is warranted in extrapolating from these in vitro data. Some histocompatibility antigens traffic through mitochondria (*15*), and mitochondria in these NT-hESCs are likely to be of either oocyte or heteroplasmic origin (except for autologous NT-hESC-8 and the original NT-hESC-1); thus, meticulous preclinical tolerance investigations in relevant preclinical animal models are a prerequisite for any consideration of clinical experimentation.

NT-hESCs were derived from 35.4% of the NT blastocysts (11 NT-hESC lines/31 NT blastocysts). This rate is more than 10 times the 3.3% reported earlier (*6*). In contrast, the rate of blastocyst development remains at ~24%. Direct derivations from either zona-free or zona-enclosed intact blastocysts were superior to derivations by immunosurgery (Table 2). Also, immunosurgery involves antibodies and complement, so the elimination of this method avoids animal contaminants, although alternatives for the animal enzymes and serum used in the fibroblast dissociation must now be perfected.

This 10-fold increase in NT-hESC derivation resulted from five protocol improvements discussed here, combined with 10 that were previously reported (*6*). The five improvements that we developed are as follows: (i) Human feeder cells, rather than murine ones, were established from the skin biopsy of donor 2, obtained under local anesthesia, and grown in 10% fetal bovine serum, 1% nonessential amino acids, and 10 μg of penicillin-streptomycin per milliliter of culture medium at 37°C in a humidified atmosphere of 5% CO_2 and 95% air. (ii) Donor nuclei were retrieved with 0.25% trypsin-EDTA for 30 s at 37°C and monitored carefully to avoid damage. (iii) Cumulus cell removal from the recipient oocytes demanded limited hyaluronidase exposure. (iv) Direct ES derivations from NT

Table 2. Summary of patient-specific NT-hESC lines. ZF-blast, zona-free blastocyst; ImmS, immunosurgery; Plurip, pluripotent. The check marks denote pluripotency demonstrated by both EBs and teratomas. Normal karyotypes have been shown for each line. Lines derived from male patients are shown in blue; lines derived from female patients are in pink.

NT-hESC	Isolation	Plurip	Differ	Pass no.	DNA	HLA
-2	ZF-blast	✓	✓	P40	Identical	Match
-3	Blast	✓	✓	P35	Identical	Match
-4, -5	ImmS	✓	✓	P26	Identical	Match
-6, -7	ImmS	✓	✓	P25	Identical	Match
-8	Blast	✓	✓	P21	Identical	Match
-9	ZF-blast	✓	EB	P20	Identical	Match
-10	ImmS	✓	EB	P19	Identical	Match
-11	ZF-blast	✓	EB	P19	Identical	Match
-12	ZF-blast	✓	EB	P7	Identical	Match

Table 3. Identical matches of MHC-HLA isotypes among NT-hESC lines -2, -3, and -4 with donors. A, B, C, DRB, and DQB represent gene loci. M, male; F, female. Asterisks indicate genotyping analysis. See table S4 for MHC-HLA matches with NT-hESC-5 through -12.

	MHC-I			MHC-II	
	HLA-A	HLA-B	HLA-C	HLA-DRB	HLA-DQB
Donor 2 (M)	A*01	B*37	Cw*06	DRB1*10	DQB1*0501
	A*31	B*51	Cw*14	DRB1*14	DQB1*0502
NT-hESC-2	A*01	B*37	Cw*06	DRB1*10	DQB1*0501
	A*31	B*51	Cw*14	DRB1*14	DQB1*0502
Donor 3 (F)	A*24	B*13	Cw*06	DRB1*04	DQB1*03
	A*24	B*44	Cw*14	DRB1*11	DQB1*03
NT-hESC-3	A*24	B*13	Cw*06	DRB1*04	DQB1*03
	A*24	B*44	Cw*14	DRB1*11	DQB1*03
Donor 4 (M)	A*02	B*60	Cw*03	DRB1*09	DQB1*0303
	A*11	B*62	Cw*08	DRB1*15	DQB1*0602
NT-hESC-4	A*02	B*60	Cw*03	DRB1*09	DQB1*0303
	A*11	B*62	Cw*08	DRB1*15	DQB1*0602

blastocysts were performed, rather than immunosurgery (Table 2). (v) Scientist-specific micromanipulation improvements were made during the most exacting steps of the oocyte's enucleation and during NT injection and fusion. The previous 10 important steps for NT blastocyst development are presented in (*6*, *9*). Neither autologous cytoplasmic matches nor fructose now appears essential. These combined 15 steps result in an NT-hESC line established with 16.8 injected or 11.7 NT-fused oocytes [fewer if donated by women younger than 30 (13.8 injected or 10.0 fused oocytes)] (Table 1F), which compares favorably with 10.5 oocytes donated each cycle (12.5 oocytes per cycle from women under 30 (Table 1C).

Our NT-hESC derivation rate is in line with some of the highest rates from IVF blastocysts (*12*). However, direct comparisons need to be tempered by the recognition that most IVF-hESC lines have been derived from clinically discarded, frozen embryos from infertility patients (*11*, *12*), whereas our studies relied on only prime fresh oocytes donated by fertile women expressly for this research.

Here we have described the establishment of patient-specific NT-hESCs with high success rates (Table 2): Average rates indicating that each oocyte donation cycle leads to the establishment of one patient-specific NT-hESC line. Furthermore, discoveries of the mechanisms of complex and multifactorial diseases, also called Research Cloning, are enabled because NT-hESC-9 is derived from a patient with CGH, and NT-hESC-3 is derived from a patient with JD. By extending NT-hESC procedures from previously autologous (*6*) to now heterologous NT, regardless of donor patient age (2 to 56 years old) or sex, these NT-hESCs can be evaluated in vitro and after transplantation into appropriate animal models for tolerance, efficacy, and safety.

NT-hESC derivation rates from NT-blastocysts increased more than 10-fold over our previous results (*6*). Although the cell lines in this study were derived on human feeder cells and were found to be free of known contaminants, the method for dissociating the patient's skin biopsy and primary fibroblast culture included fetal calf serum, trypsin, and collagenase (animal products). If preclinical results are encouraging, long before hESC lines could be used in the clinic, greater stringency is mandated, including methods to avoid xenoexposures. Furthermore, exacting documentation of the meticulous derivation, maintenance, and differentiation procedures would all need to be performed within current good manufacturer practice facilities, so that regulatory authorities such as the Korean and/or U.S. Food and Drug Administration could evaluate investigational new drug applications. However, these rates of NT-hESC establishment, combined with a time frame of less than 1 year from skin biopsy and oocyte donation to NT-hESC establishment, might be clinically relevant if therapeutic cloning were shown to be of medical value.

Molecular deviations between animals developing after fertilization versus those developing after reproductive cloning have been noted. In particular, epigenetic aberrations have been discovered in the genomic imprints of both cloned fetuses and offspring, as well as their placentas (*2*). Notwithstanding therapeutic interest, learning whether the erasure, reestablishment, and stability of genomic imprints in these NT-hESCs compare with those of IVF-derived hESCs (*16*) is essential. Other extranuclear or epigenetic influences include mitochondrial inheritance patterns in hESCs, let alone those in NT-hESCs, which are not understood. mtDNA heteroplasmy (*17*) could influence hESC stability or differentiation, as might homoplasmic oocyte mtDNA incompatibilities with the donor nucleus. Furthermore, the cells' mitotic spindle poles, or centrosomes, which are contributed by the sperm during human fertilization (*18*) and which, if imbalanced, have been shown to cause cancers (*19*, *20*), might replicate or divide inaccurately, leading to aneuploidies. Consequently, learning whether somatic centrosome transfer occurs during human NT, as it does during bovine NT (*21*), is important. Inactivation of the X

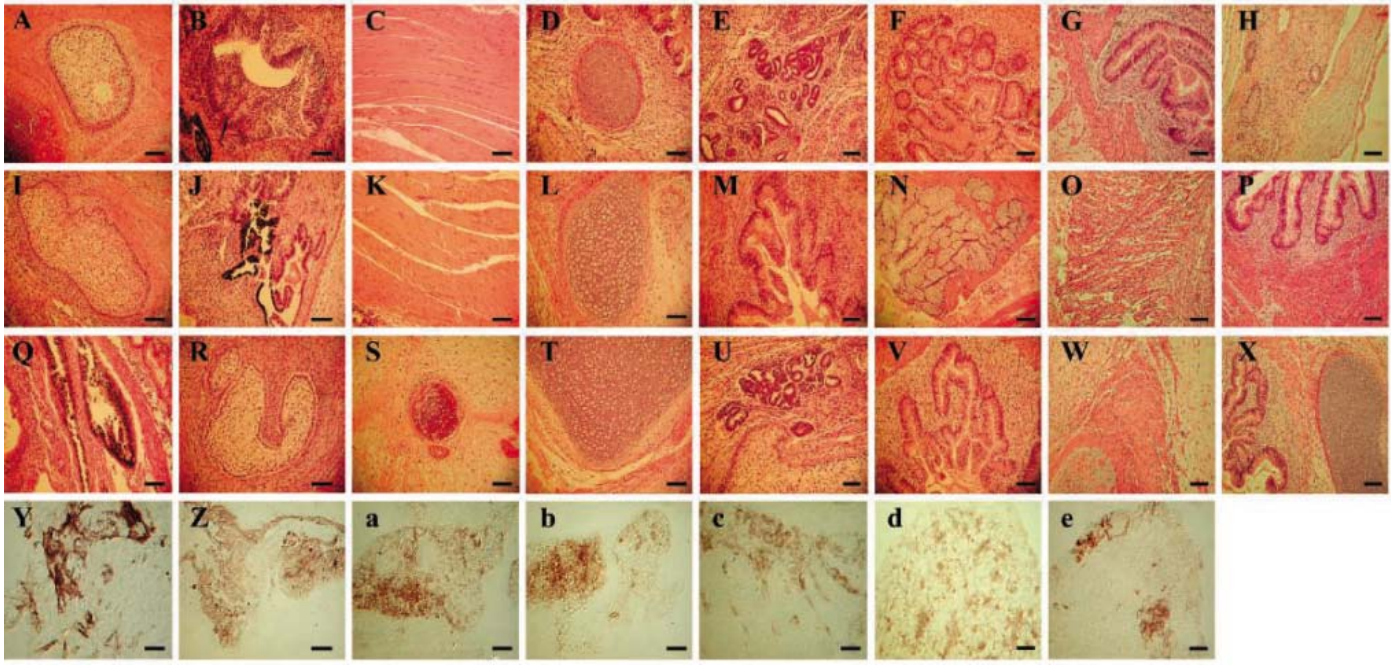

Fig. 3. Patient-specific human NT-hESCs differentiate into tissues from all three germ cell layers in vivo in teratomas (first three rows) and in vitro in EBs (bottom row). NT-hESC-2 (**A** to **H**), -3 (**I** to **P**), and -4 (**Q** to **X**) differentiated into all of the following somatic tissue types: skin [(A), (I), and (R)]; primitive neuroepithelium (B); striated muscle [(C) and (K)]; cartilage [(D), (L), and (T)]; renal tissues [(E) and (U)]; gastrointestinal epithelium [(F), (M), and (V)]; retina and primitive neuroepithelium [(J) and (Q)]; smooth muscle and respiratory epithelium [(G), (P), and (X)]; colon epithelium (H); mucosa gland (N); smooth muscle [(O) and (W)]; and bone (S). Immunohistochemical staining for EBs was performed for Pax3/7 (**Y**), MAP-2 (**Z**), GFAP (**a**), ANP (**b**), CD34 (**c**), desmin (**d**), and MHC (**e**). EBs also differentiated into all three germ layers expressing ectodermal [(Y), (Z), and (a)], mesodermal [(b) to (d)], and endodermal (e) marker genes. Figure S3 shows differentiation details for all NT-hESC lines. Magnification: ×100, (A) to (R); ×200, (S) to (Y). Scale bars, 100 μm.

chromosome, which is typically random in female mammals, is skewed in cloned female mice (*22*, *23*), causes recurrent spontaneous abortions in some pregnant women (*24*), and could result in misexpressions in NT-hESCs derived from women. Finally, the genomic stability of NT-hESCs, as well as their differentiation fidelity, including aging and telomerase/telomere behavior, also require rigorous investigations.

The somatic cell's adaptation to in vitro conditions may predispose human NT embryos to cell culture proliferation, with negligible potentials for implantation and none for normal development. Neither NT embryonic development nor NT-hESC establishment rates provide any encouragement for dangerous human reproductive cloning attempts. Cloned animals have adverse pregnancy outcomes, so regardless of cruel hoaxes (*25*), scientific evidence should further discourage reckless notions regarding human reproductive cloning. Human SCNT was optimized from porcine SCNT procedures in which ~150 NT embryos were transferred for pregnancy establishment (*26*–*28*). Furthermore, in rhesus monkeys, 135 cloned embryos transferred into 25 surrogates using some of these improved SCNT techniques (*29*) did not result in any pregnancies, although rhesus NT blastocysts developed and NT-ICMs were isolated.

Our work described here shows that stem cell lines can be generated using somatic cells from patients with disease and injury. It may also be possible to generate NT-hESC lines from patients with diseases and disorders of unknown causes. For example, NT-hESCs derived from early-onset Alzheimer's disease or autism patients might prove invaluable for mechanistic studies in vitro after differentiation into neuroprogenitors (*30*, *31*). In addition, biological insight gained through studying hESCs might find application to ART and assist in understanding genomic imprinting. The derivations of patient-specific NT-hESCs grown without animal cell co-culture may advance cell transplantation therapies as well as aid in the discovery of human developmental processes and the causes of many complex diseases.

References and Notes

1. J. A. Thomson *et al.*, *Science* **282**, 1145 (1998).
2. R. Jaenisch, *N. Engl. J. Med.* **351**, 2787 (2004).
3. M. Drukker, N. Benvenisty, *Trends Biotechnol.* **22**, 136 (2004).
4. W. M. Rideout 3rd, K. Hochedlinger, M. Kyba, G. Q. Daley, R. Jaenisch, *Cell* **109**, 17 (2002).
5. T. Barberi *et al.*, *Nat. Biotechnol.* **21**, 1200 (2003).
6. W. S. Hwang *et al.*, *Science* **303**, 1669 (2004).
7. M. J. Martin, A. Muotri, F. Gage, A. Varki, *Nat. Med.* **11**, 228 (2005).
8. Before beginning any experiments, we obtained approval for this study from the IRB for Human Subjects Research and Ethics Committee at Hanyang University Hospital, Seoul, Korea, which was required by existing regulations that were in place up to 31 December 2004. IRB approvals are included in (*9*). Oocyte and/or somatic cell donors were counseled by two IRB members to ensure that they were fully aware of the scope of the investigation, and each donor signed informed consent forms. Both of the parents of children under 18 years old donating somatic cells were similarly counseled, and each signed informed consent forms on behalf of their child. On 1 January 2005, the Republic of Korea's new regulation entitled Bioethics and Biosafety Act—Act No. 7150, requiring governmental licensing of SCNT using human oocytes and subsequent derivation of NT-hESCs (Therapeutic Cloning), became effective. On 12 January 2005, we received governmental approval in accordance with this new stem cell law. This law also required IRB approval from the College of Veterinary Medicine, Seoul National University, which was granted on 25 January 2005. When our previous report on NT-hESCs appeared online on 12 February 2004 (*6*), we imposed a voluntary moratorium on new NT-hESC derivations. In September 2004, we announced that we were again performing SCNT and deriving NT-hESCs, under the auspices and oversight of the Hanyang University IRB for Human Subjects Research and Ethics Committee. All IRB documents are included in (*9*).
9. Materials, methods, and IRB documents are available as supporting material on *Science* Online.
10. D. K. Gardner *et al.*, *Fertil. Steril.* **81**, 551 (2004).
11. C. A. Cowan *et al.*, *J. Med.* **350**, 1353 (2004).
12. S. J. Kim *et al.*, *Mol. Cells* **19**, 46 (2005).
13. A. H. Brivanlou *et al.*, *Science* **300**, 913 (2003).
14. I. Wilmut, A. E. Schnieke, J. McWhir, A. J. Kind, K. H. Campbell, *Nature* **385**, 810 (1997).
15. J. I. Semple *et al.*, *Gene* **314**, 41 (2003).
16. R. J. Rugg-Gunn, A. C. Ferguson-Smith, R. A. Pedersen, *Nat. Genet.* (published online 1 May 2005; in press, 2005).
17. J. C. St John, G. Schatten, *Genetics* **167**, 897 (2004).
18. C. Simerly *et al.*, *Nat. Med.* **1**, 47 (1995).
19. N. J. Quintyne, J. E. Reing, D. R. Hoffelder, S. M. Gollin, W. S. Saunders, *Science* **307**, 127 (2005).
20. B. R. Brinkley, *Trends Cell Biol.* **11**, 18 (2001).
21. C. S. Navara, N. L. First, G. Schatten, *Proc. Natl. Acad. Sci. U.S.A.* **93**, 5384 (1996).
22. S. Senda *et al.*, *Biochem. Biophys. Res. Commun.* **321**, 38 (2004).
23. L. D. Nolen *et al.*, *Dev. Biol.* **279**, 525 (2005).
24. M. C. Lanasa, W. A. Hogge, *Semin. Reprod. Med.* **18**, 97 (2000).
25. G. Schatten, R. Prather, I. Wilmut, *Science* **299**, 344 (2003).
26. C. J. Phelps *et al.*, *Science* **299**, 411 (2003).
27. L. Lai *et al.*, *Science* **295**, 1089 (2002).
28. G. S. Lee *et al.*, *Theriogenology* **63**, 973 (2005).
29. C. Simerly *et al.*, *Dev. Biol.* **276**, 237 (2004).
30. J. D. Rothstein, E. Y. Snyder, *Nat. Biotechnol.* **22**, 283 (2004).
31. O. Lindvall, R. McKay, *Proc. Natl. Acad. Sci. U.S.A.* **100**, 7430 (2003).

32. We thank foremost all donors. We also thank K. H. Han, J. H. Choi, J. T. Kang, S. G. Hong, and O. S. Kwon (Seoul National University); M. H. Kim, H. J. Jeong, E. K. Chun, and Y. J. Kim (MizMedi Hospital); and M. K. Koong and I. S. Kang (Samsung Cheil Hospital and Women's Healthcare Center) for assistance on NT-hESC culture; D. H. Chung (Seoul National University Hospital) for teratoma histopathology; J. Y. Kim and M. H. Park (Seoul National University Hospital) for HLA typing; and S. S. Yoo (Harvard Medical School) and the anonymous reviewers for their constructive critiques. All experiments were performed in Korea by Korean scientists, and all results were obtained in Korea using Korean equipment and Korean sponsorship. G.S and J.-H.P are grateful for the private philanthropy of the Magee-Womens Foundation, which supported their advisory roles in the analysis and for the interpretation and preparation for publication of these results obtained in Korea. No U.S. federal or Commonwealth of Pennsylvania funds were used in any aspect of this report. The authors are grateful for a graduate fellowship provided by the Ministry of Education, through BK21 program. This study was supported by grants from the Biodiscovery program of the Korean Ministry of Science and Technology to W.S.H. Until the formal establishment by the Republic of Korea of its National Center for Stem Cell Research, in which the previous NT-hESC line (-1) (*6*) and these new ones (-2 to -12) will be deposited and available for distribution, requests for cells and/or other materials should be addressed to W.S.H.

Supporting Online Material

www.sciencemag.org/cgi/content/full/1112286/DC1
Materials and Methods
SOM Text
Figs. S1 to S3
Tables S1 to S4
References

15 March 2005; accepted 12 May 2005
Published online 19 May 2005;
10.1126/science.1112286
Include this information when citing this paper.

Cladosporium Avr2 Inhibits Tomato Rcr3 Protease Required for *Cf-2*–Dependent Disease Resistance

Henrietta C. E. Rooney,[1]* John W. van 't Klooster,[2]* Renier A. L. van der Hoorn,[2] Matthieu H. A. J. Joosten,[2] Jonathan D. G. Jones,[1]† Pierre J. G. M. de Wit[2]†‡

How plants recognize pathogens and activate defense is still mysterious. Direct interaction between pathogen avirulence (Avr) proteins and plant disease resistance proteins is the exception rather than the rule. During infection, *Cladosporium fulvum* secretes Avr2 protein into the apoplast of tomato leaves and, in the presence of the extracellular leucine-rich repeat receptor-like Cf-2 protein, triggers a hypersensitive response (HR) that also requires the extracellular tomato cysteine protease Rcr3. We show here that Avr2 binds and inhibits Rcr3 and propose that the Rcr3-Avr2 complex enables the Cf-2 protein to activate an HR.

Plant disease resistance (*R*) genes mediate race-specific recognition of pathogens via perception of avirulence (*Avr*) gene products (*1*). Tomato (*Lycopersicon esculentum*) *Cf* genes confer resistance to leaf mold caused by *Cladosporium fulvum* and encode trans-

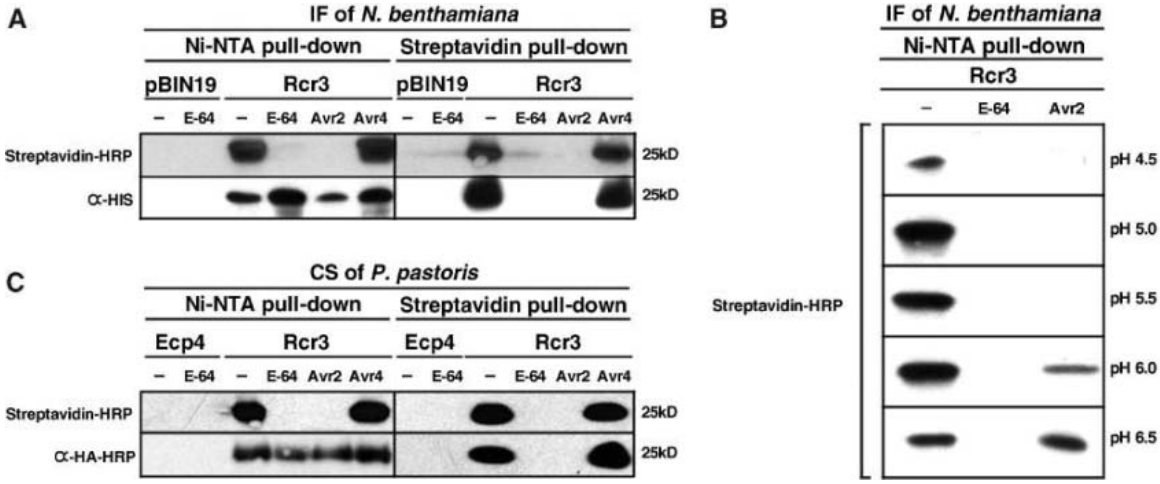

Fig. 1. The Rcr3 cysteine protease of tomato is inhibited by Avr2 of *C. fulvum*. (**A**) Inhibition of Rcr3 produced in *Nicotiana benthamiana* by Avr2. IF was isolated from *N. benthamiana* expressing either the empty vector (pBin19) or Rcr3-His-HA (Rcr3). Protease activity profiling with 220 nM DCG-04 was performed in the absence of inhibitor (–) or in the presence of E-64, His-FLAG-Avr2 (Avr2), or His-FLAG-Avr4 (Avr4). Rcr3-His-HA was captured (pulled down) by Ni-NTA beads (left) or by streptavidin beads (right), electrophoresed on an SDS gel, and detected with streptavidin-HRP or His-specific antibodies (α-His) (*28*). Detection with streptavidin-HRP reveals that Rcr3 is not biotinylated in the presence of E-64 or Avr2, whereas biotinylation of Rcr3 occurs without inhibitor or with Avr4, indicating that, like E-64, Avr2 inhibits Rcr3 cysteine protease activity. α-His always detects Ni-NTA–captured Rcr3-His-HA irrespective of whether Rcr3 is inhibited or not (left), whereas α-His only detects biotinylated Rcr3-His-HA when Rcr3 is not inhibited by E-64 or Avr2 (right). No biotinylated cysteine proteases were detected in the empty vector control (pBin19). (**B**) Inhibition of Rcr3 by Avr2 is pH-dependent. IF from *N. benthamiana* containing Rcr3-His-HA was profiled with 220 nM DCG-04 in the absence of inhibitor (–), and in the presence of E-64 (1120 nM) or Avr2 (140 nM), over a pH range from 4.5 to 6.5. Rcr3-His-HA was captured by Ni-NTA beads and detected with streptavidin-HRP to demonstrate biotinylation (*28*). Rcr3 is biotinylated in the absence of inhibitor (–), with highest amounts of biotinylation at pH values between 5.0 and 6.0. Inhibition of biotinylation of Rcr3 by E-64 is complete at all pH values, whereas inhibition by Avr2 decreases at pH values above 6.0. (**C**) Inhibition of Rcr3 produced in *Pichia pastoris* by Avr2. Culture supernatant (CS) was isolated from *P. pastoris* cultures expressing either His-FLAG-Ecp4 (Ecp4) or Rcr3-His-HA (Rcr3), and protease activity was profiled with 220 nM DCG-04 in the absence of inhibitor (–) or in the presence of E-64, His-FLAG-Avr2 (Avr2) or His-FLAG-Avr4 (Avr4). Subsequently, Rcr3 was captured by Ni-NTA beads (left) or by streptavidin beads (right), electrophoresed on an SDS gel, and detected with streptavidin-HRP or HA-specific antibodies (α-HA-HRP) (*28*). Detection with streptavidin-HRP reveals that in the presence of E-64 or Avr2, Rcr3 is not biotinylated, whereas biotinylation of Rcr3 occurs in the absence of inhibitor or in the presence of Avr4, indicating that, similar to E-64, Avr2 inhibits Rcr3 cysteine protease produced in *P. pastoris* in a similar way as Rcr3 produced in *N. benthamiana*.

membrane receptor-like proteins (RLPs) with extracellular leucine-rich repeats (LRRs) that mediate recognition of fungal Avrs secreted during infection (*2*). *Cf*-dependent perception of Avrs activates plant defense, including the HR, which results in host cell death at the site of penetration and limits pathogen ingress (*3*, *4*). How Cf proteins enable tomato to perceive Avrs is unknown. So far, no direct interaction between Cf proteins and Avr proteins has been detected (*5*). A direct interaction has only been demonstrated for two Avrs and LRR-containing proteins (*6*, *7*). The lack of a direct interaction led to the formulation of the guard hypothesis (*8*, *9*), proposing that Avrs are virulence factors that interact with host targets to facilitate pathogen growth in the host and that R proteins monitor the status of these host targets (*10*).

Cf-2, which originates from the wild tomato variety *L. pimpinellifolium*, confers resistance to *C. fulvum* in tomato (*11*) on the basis of perception of Avr2, a cysteine-rich protein secreted by the fungus (*12*). Cf-2 function also requires Rcr3 (*13*), a secreted tomato cysteine protease (*14*) that is not required by other *Cf* genes, including the highly homologous *Cf-5* gene (*13*, *14*). The *L. esculentum* allele encodes the Rcr3^{esc} protein that weakly activates *Cf-2*–dependent HR in tomato leaves in the absence of Avr2. The *L. pimpinellifolium* allele encodes Rcr3^{pim}, required for Cf-2 to confer an Avr2 response (*14*).

We hypothesized that Rcr3 is a target of Avr2. To test this hypothesis, we produced Rcr3 as a C-terminal 6xHistidine (His)- and hemagglutinin (HA)-tagged protein fusion (Rcr3-His-HA) both in *Nicotiana benthamiana* and in *Pichia pastoris*. Mature Rcr3 was recovered from intercellular fluid (IF) of *N. benthamiana* leaves by using the tags on the fusion protein (*14*). To monitor Rcr3 activity, we applied protease activity profiling at pH = 5 by using DCG-04, a biotinylated derivative of the irreversible cysteine protease inhibitor E-64 that has been used to profile cysteine protease activities from mammals (*15*), insects (*16*), and plants (*17*). DCG-04 treatment leads to irreversible labeling of cysteine proteases with biotin. Labeling of Rcr3 with 220 nM DCG-04 was assayed in the presence or absence of different concentrations of E-64 as a competitive inhibitor. After reaction with DCG-04, Rcr3-His-HA was precipitated with the use of Ni–nitrilotriacetic acid (NTA) (binding to His tag) or streptavidin (binding to biotin) beads. In the absence of E-64, DCG-04 biotinylates Rcr3, confirming that Rcr3 is a cysteine protease, whereas in the presence of 1120 nM E-64, Rcr3 is not biotinylated (Fig. 1A).

We tested whether Avr2 could inhibit biotinylation of Rcr3 by DCG-04. As a negative control, *C. fulvum* Avr4, which triggers *Cf-4*–dependent HR (*18*), was included. Both Avrs were expressed in *P. pastoris* as N-terminal His-FLAG-fusions and purified on a Ni-NTA column. In the presence of 140 nM Avr2, Rcr3 is not biotinylated (Fig. 1A), indicating that Avr2 inhibits Rcr3 activity (fig. S1). In the presence of Avr4, Rcr3 is biotinylated, showing that inhibition of Rcr3 by Avr2 is specific (Fig. 1A and fig. S1).

IF obtained from tomato has a pH of about 5 (*19*). To investigate the pH dependence of Rcr3 activity and its inhibition by Avr2, we incubated *N. benthamiana* IF containing Rcr3 with DCG-04 in the absence or presence of an excess of E-64 or Avr2 over a pH range from 4.5 to 6.5. Rcr3 activity is highest at pH of 5 to 6 and strongly decreases outside this range (Fig. 1B). Inhibition by E-64 is effective over the whole pH range, whereas inhibition by Avr2 is only effective below pH = 6 (Fig. 1B), indicating that the pH optimum for Rcr3 activity and its inhibition by Avr2 coincides with the pH of the apoplast of tomato (pH = 5). Rcr3 produced as a C-terminal His-HA fusion in *P. pastoris* is also inhibited by E-64 and Avr2 (Fig. 1C), indicating that Avr2 alone is sufficient to inhibit Rcr3 and that no additional plant factors are required. No biotinylation by

[1]Sainsbury Laboratory, John Innes Centre, Norwich NR4 7UH, UK. [2]Laboratory of Phytopathology, Wageningen University, Binnenhaven 5, 6709 PD Wageningen, Netherlands.

*These authors contributed equally to this work.
†These authors contributed equally to this work.
‡To whom correspondence should be addressed. E-mail: pierre.dewit@wur.nl

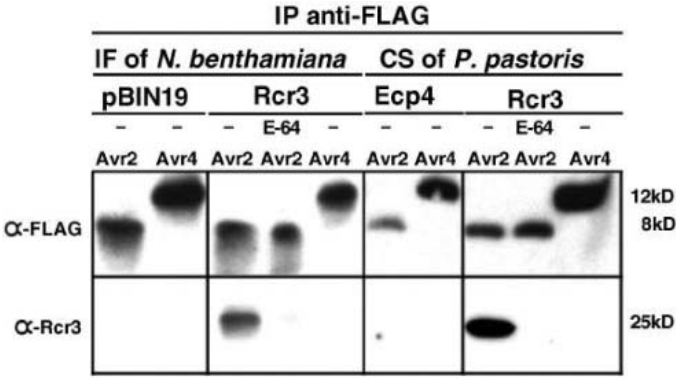

Fig. 2. Rcr3 and Avr2 physically interact. Rcr3-His-HA (Rcr3) was incubated with His-FLAG-Avr2 (Avr2), with or without pretreatment with E-64 or His-FLAG-Avr4 (Avr4), and then immunoprecipitated (IP) with FLAG-specific antibody (α-FLAG). IF from *N. benthamiana* expressing either the empty vector (pBin19) or Rcr3, or CS from *P. pastoris* expressing either His-FLAG-Ecp4 (Ecp4) or Rcr3, was incubated without inhibitor (–) or with an excess of E-64 before adding Avr2 or Avr4. After immunoprecipitation with α-FLAG beads, the Avr proteins were detected with α-FLAG, whereas co-immunoprecipitated Rcr3 was detected with α-Rcr3 (*28*). Rcr3 is only co-immunoprecipitated in the presence of Avr2 without preincubation with E-64.

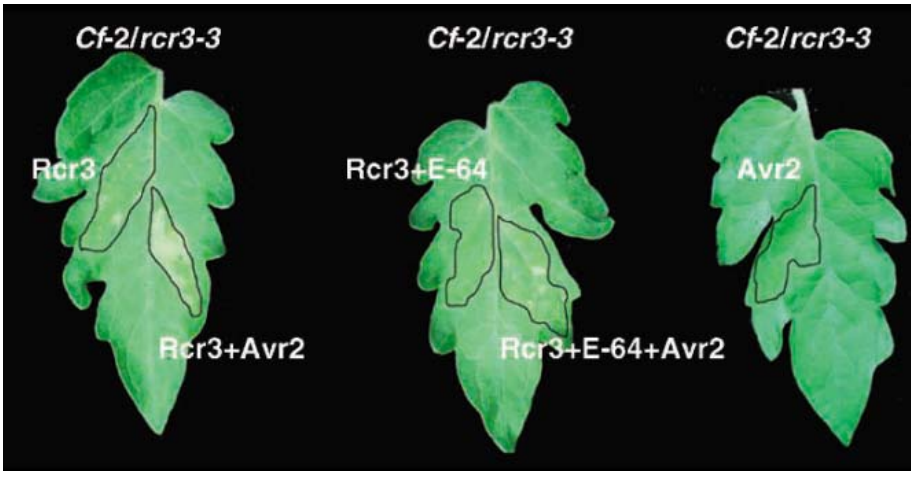

Fig. 3. Cf-2–mediated HR requires physical interaction between Rcr3 and Avr2. Fully expanded leaves of 5-week-old *Cf-2/rcr3-3* tomato were infiltrated with Rcr3-His-HA (Rcr3) produced in *N. benthamiana* (either alone or in combination with His-FLAG-Avr2 (Avr2), E-64, or E-64 and Avr2) or infiltrated with Avr2 alone (*28*). Leaves were photographed 3 days postinfiltration. The infiltrated sectors are outlined and the infiltrated compounds indicated. The HR is only triggered when Rcr3 and Avr2 can interact, whereas the HR is blocked when interaction of Rcr3 with Avr2 is prevented by preincubation of Rcr3 with E-64. Rcr3 produced in *P. pastoris* treated with the same compounds gave similar results (*21*).

DCG-04 of other cysteine proteases was observed in control IF from *N. benthamiana* nontransgenic for Rcr3 (Fig. 1A) or in control culture supernatant (CS) from *P. pastoris* nontransgenic for Rcr3 but expressing Ecp4, another protein secreted by *C. fulvum* (*20*) (Fig. 1C). This indicates that, at the DCG-04 concentration used (220 nM), no biotinylation of endogenous extracellular cysteine proteases could be detected.

Because Avr2 inhibits Rcr3, we expected a physical interaction between the two proteins. This was investigated by co-immunoprecipitation studies. His-FLAG-Avr2 or His-FLAG-Avr4 was added to *N. benthamiana* IF or culture supernatant (CS) of *P. pastoris* containing Rcr3-His-HA and immunoprecipitated with a FLAG-specific antibody (α-FLAG). As a control, Rcr3-His-HA was also preincubated with E-64 to block the active site before adding His-FLAG-Avr2. After immunoprecipitation, the samples were run on SDS gels and blotted, and Avr proteins and Rcr3 were detected with use of α-FLAG and an Rcr3-specific antibody (α-Rcr3), respectively (Fig. 2). Rcr3 co-immunoprecipitates with Avr2 but not with Avr4 (Fig. 2), indicating a specific interaction between Avr2 and Rcr3. Blocking the active site of Rcr3 by E-64 eliminates this interaction (Fig. 2). In the presence of Avr2, α-FLAG co-immunoprecipitates Rcr3 irrespective of the source of Rcr3, again indicating that the interaction between Avr2 and Rcr3 is independent of additional plant factors (Fig. 2). No signals were detected on blots probed with α-Rcr3 after immunoprecipitation of proteins from control *N. benthamiana* IF (marked pBin19 in Fig. 2) or control CS of *P. pastoris* nontransgenic for Rcr3 (marked Ecp4 in Fig. 2), indicating that α-Rcr3 is specific.

We tested whether native Rcr3 in tomato IF can be detected and inhibited by E-64 and Avr2. IF (6 ml) from different Cf tomato plants producing Rcr3 were labeled with 2.2 μM DCG-04 in the presence or absence of E-64 (28.6 μM) or Avr2 (6.9 μM). Biotinylated proteins were captured on streptavidin beads, run on an SDS gel, and probed with α-Rcr3 or streptavidin–horseradish peroxidase (HRP) (fig. S2). Native Rcr3 is detected by α-Rcr3 in Cf0 and Cf2 tomato lines, and its biotinylation by DCG-04 is inhibited by Avr2, whereas Rcr3 is absent in *Cf-2/rcr3-3* plants (*13*, *14*) (fig. S2; upper panel). In addition to Rcr3, several other apoplastic cysteine proteases are biotinylated that can be inhibited by Avr2 (fig. S2; lower panel).

To determine whether inhibition of Rcr3 by Avr2 is sufficient to trigger *Cf-2*–dependent HR, we infiltrated Rcr3 produced in *N. benthamiana*, either alone or in combination with Avr2, E-64, or E-64 and Avr2, or we infiltrated Avr2 alone, into *Cf-2/rcr3-3* tomato leaves (Fig. 3). Infiltration of Avr2 or Rcr3 alone or Rcr3 incubated with E-64 does not trigger an HR, whereas infiltration of Rcr3 incubated with Avr2 does. However, Rcr3 preincubated with an excess of E-64 to saturate the active site, and subsequently incubated with Avr2, does not trigger *Cf-2*–mediated HR, indicating that Cf-2 specifically recognizes the Rcr3-Avr complex. Similar results were obtained with *P. pastoris*–produced Rcr3 pretreated with the same compounds (*21*).

Inhibition of Rcr3 activity by Avr2 could be caused by either Avr2 acting solely as an inhibitor of Rcr3 or Avr2 being both a substrate and an inhibitor. However, we observed no degradation of Avr2 upon incubation with Rcr3 (Fig. 2), suggesting that Avr2 is not a substrate for Rcr3. Furthermore, if processing of Avr2 by Rcr3 were required for *Cf-2*–mediated HR, then Avr2 present in IF from Cf0 tomato plants (containing Rcr3) infected by Avr2-producing *C. fulvum* strains would induce an HR in *Cf-2/rcr3-3* tomato. This was not observed (*21*), indicating that Avr2 is an inhibitor, not a substrate, of Rcr3. However, inhibition of Rcr3 activity is not sufficient to initiate Cf-2–mediated HR (Fig. 3). Therefore, we propose that inhibition of Rcr3 by Avr2 induces a conformational change in Rcr3 that triggers the Cf-2 protein to activate HR. This model is consistent with the observation that the $Rcr3^{esc}$ protein alone provokes a weak *Cf-2*–dependent, Avr2-independent HR (*14*). We suggest that $Rcr3^{esc}$, which differs from $Rcr3^{pim}$ in one amino acid deletion and six amino acid changes, constitutively mimics the conformational change imposed on $Rcr3^{pim}$ (present in *Cf-2* plants) by Avr2 binding and weakly activates *Cf-2*–dependent HR in the absence of Avr2.

The role of Rcr3 cysteine protease activity for tomato and the importance of its inhibition by Avr2 for *C. fulvum* during infection are unknown, but secreted plant cysteine pro-

teases possibly have antimicrobial activity. *Rcr3* transcription is induced faster and transcripts accumulate to higher concentrations in incompatible compared with compatible interactions between tomato and *C. fulvum* (*14*), as do transcripts for pathogenesis-related proteins after infection by this fungus (*22*). Rcr3 is also induced in the absence of Cf-2, consistent with a role for Rcr3 in basal host defense (*14*). Furthermore, in addition to Rcr3, several other apoplastic cysteine proteases are inhibited by Avr2, suggesting that Avr2 is a general virulence factor facilitating growth of *C. fulvum* in the apoplast. Recently, it has been shown that a protease inhibitor from *Phytophthora infestans* interacts with and inhibits the plant serine protease P69B, which is induced during infection of tomato by this pathogen (*23*). Thus, inhibition of plant proteases may represent a general counterdefense used by invading pathogens.

The role of Rcr3 in the perception of Avr2 by Cf-2 is consistent with the guard hypothesis. The Rcr3-Avr2 complex, but not other Avr2-cysteine protease complexes, activates Cf-2. So far, all bacterial pathogens colonizing the apoplast of plants deliver their effector proteins into the plant cell by the type III secretion system where they interact with cytoplasmic virulence targets (*10*, *24*–*27*). In the case of RPM1- and RPS2-mediated resistance in *Arabidopsis*, the action of the Avr proteins AvrB, AvrRpm1, and AvrRpt2 on the guardee RIN4 is thought to trigger the activation of RPM1 (resistance to *Pseudomonas syringae* p. *maculicola* expressing *AvrRpm1*) or RPS2 (resistance to *P. syringae* pv. *tomato* expressing *AvrRpt2*) proteins (*24*–*27*). Similarly, in RPS5-mediated resistance in *Arabidopsis* the cysteine protease activity of the Avr protein, AvrPphB, on the guardee PBS1 is required to trigger the HR (*28*). Such indirect interactions between pathogen Avrs and plant R proteins may be more difficult for the pathogen to circumvent without a virulence penalty than direct interactions (*8*, *9*). In addition to Rcr3, other tomato cysteine proteases are inhibited by Avr2 that are not guarded by known Cf proteins. Characterization and functional analysis of these proteases will be the subject of future studies.

References and Notes

1. H. H. Flor, *Annu. Rev. Phytopathol.* **9**, 275 (1971).
2. M. H. A. J. Joosten, P. J. G. M. de Wit, *Annu. Rev. Phytopathol.* **37**, 335 (1999).
3. P. J. G. M. de Wit, *Neth. J. Plant Pathol.* **83**, 109 (1977).
4. G. Lazarovits, V. J. Higgins, *Can. J. Bot.* **54**, 224 (1976).
5. R. Luderer *et al.*, *Mol. Plant Microbe Interact.* **14**, 867 (2001).
6. L. Deslandes *et al.*, *Proc. Natl. Acad. Sci. U.S.A.* **100**, 8024 (2003).
7. M. Ron, A. Avni, *Plant Cell* **16**, 1604 (2004).
8. E. A. van der Biezen, J. D. G. Jones, *Trends Biochem. Sci.* **23**, 454 (1998).
9. R. A. L. van der Hoorn, P. J. G. M. de Wit, M. H. A. J. Joosten, *Trends Plant Sci.* **7**, 67 (2002).
10. J. H. Chang, A. K. Goel, S. R. Grant, J. L. Dangl, *Curr. Opin. Microbiol.* **7**, 11 (2004).
11. M. S. Dixon *et al.*, *Cell* **84**, 451 (1996).
12. R. Luderer, F. L. W. Takken, P. J. G. M. de Wit, M. H. A. J. Joosten, *Mol. Microbiol.* **45**, 875 (2002).
13. M. S. Dixon, C. Golstein, C. M. Thomas, E. A. van der Biezen, J. D. G. Jones, *Proc. Natl. Acad. Sci. U.S.A.* **97**, 8807 (2000).
14. J. Krüger *et al.*, *Science* **296**, 744 (2002).
15. D. Greenbaum, K. F. Medzihradszky, A. Burlingame, M. Bogyo, *Chem. Biol.* **7**, 569 (2000).
16. C. Kocks *et al.*, *Mol. Cell. Proteomics* **2**, 1188 (2003).
17. R. A. L. van der Hoorn, M. A. Leeuwenburgh, M. Bogyo, M. H. A. J. Joosten, S. C. Peck, *Plant Physiol.* **135**, 1170 (2004).
18. M. H. A. J. Joosten, T. J. Cozijnsen, P. J. G. M. de Wit, *Nature* **367**, 384 (1994).
19. C. Grignon, H. Sentenac, *Annu. Rev. Plant Physiol. Plant Mol. Biol.* **42**, 103 (1991).
20. R. Laugé, P. H. Goodwin, P. J. G. M. de Wit, M. H. A. J. Joosten, *Plant J.* **23**, 735 (2000).
21. P. J. G. M. de Wit *et al.*, unpublished data.
22. J. A. L. van Kan *et al.*, *Plant Mol. Biol.* **20**, 513 (1992).
23. M. Tian *et al.*, *J. Biol. Chem.* **279**, 26370 (2004).
24. M. J. Axtell, S. T. Chisholm, D. Dahlbeck, B. J. Staskawicz, *Mol. Microbiol.* **49**, 1537 (2003).
25. M. J. Axtell, B. J. Staskawicz, *Cell* **112**, 369 (2003).
26. D. Mackey, Y. Belkhadir, J. M. Alonso, J. R. Ecker, J. L. Dangl, *Cell* **112**, 379 (2003).
27. D. Mackey, B. F. Holt, A. Wiig, J. L. Dangl, *Cell* **108**, 743 (2002).
28. F. Shao *et al.*, *Science* **301**, 1230 (2003).
29. Materials and methods are available as supporting material on *Science* Online.

30. We thank M. A. Leeuwenburgh, Leiden University, Netherlands, and M. Bogyo, Stanford University, for providing DCG-04; J. Krüger and A. Heeze-Peck for useful suggestions; and B. P. H. J. Thomma for critically reading the manuscript. M.H.A.J.J. and R.A.L.v.d.H. were supported by a Vidi and Veni grant, respectively, from the Netherlands Organization for Earth and Life Sciences (ALW-NWO). P.J.G.M.d.W. was supported by the Center for Biosystems Genomics (CBSG). J.D.G.J. was supported at the Sainsbury Laboratory by the Gatsby Foundation, which also supported the Sainsbury studentship of H.C.E.R. Molecular interaction data have been deposited in the Biomolecular Interaction Network Database with accession codes 262290 and 262443.

Supporting Online Material

www.sciencemag.org/cgi/content/full/1111404/DC1
Materials and Methods
Tables S1 and S2
Figs. S1 and S2
References

23 February 2005; accepted 11 April 2005
Published online 21 April 2005;
10.1126/science.1111404
Include this information when citing this paper.

Nodulation Signaling in Legumes Requires NSP2, a Member of the GRAS Family of Transcriptional Regulators

Péter Kaló,[1,2] Cynthia Gleason,[1] Anne Edwards,[1] John Marsh,[1] Raka M. Mitra,[4*] Sibylle Hirsch,[1] Júlia Jakab,[2] Sarah Sims,[3] Sharon R. Long,[4] Jane Rogers,[3] György B. Kiss,[2] J. Allan Downie,[1] Giles E. D. Oldroyd[1†]

Rhizobial bacteria enter a symbiotic interaction with legumes, activating diverse responses in roots through the lipochito oligosaccharide signaling molecule Nod factor. Here, we show that *NSP2* from *Medicago truncatula* encodes a GRAS protein essential for Nod-factor signaling. NSP2 functions downstream of Nod-factor–induced calcium spiking and a calcium/calmodulin-dependent protein kinase. We show that NSP2-GFP expressed from a constitutive promoter is localized to the endoplasmic reticulum/nuclear envelope and relocalizes to the nucleus after Nod-factor elicitation. This work provides evidence that a GRAS protein transduces calcium signals in plants and provides a possible regulator of Nod-factor–inducible gene expression.

The legume/rhizobial symbiosis plays a crucial role in the introduction of fixed nitrogen into both agricultural and natural systems. Legumes form specialized organs, usually on the roots, and these "nodules" provide the low-oxygen environment required for the activity of bacterial nitrogenase. Within nodules, the bacteria reside in membrane-bound compartments within plant cells and differentiate into bacteroids, a specialized symbiotic form of the bacteria. Nod factor is central to the establishment of this symbiotic interaction. This lipochito oligosaccharide signal is produced by the bacteria in response to plant phenolics (*1*). Nod factor alone is sufficient to activate the majority of the early responses in the plant normally seen during the interaction with the bacteria, including the activation of cytosolic calcium spiking associated with the nucleus of epidermal root cells (*2*) and a wide range of plant genes (*3*). The recent identification of a gene (*DMI3*) encoding a calcium/calmodulin-dependent protein kinase (CCaMK) that functions in Nod-factor signaling (*4*, *5*) downstream of calcium

[1]Departments of Disease and Stress Biology and Molecular Microbiology, John Innes Centre, Norwich NR4 7UH, UK. [2]Institute of Genetics, Agricultural Biotechnology Center, Szent-Györgyi A. utca 4, 2100 Gödöllö, Hungary. [3]Wellcome Trust Sanger Institute, Hinxton, Cambridge CB10 1SA, UK. [4]Department of Biological Sciences, Stanford University, Stanford, CA 94305, USA.

*Present address: Department of Plant Biology, University of Minnesota, St. Paul, MN 55108, USA.
†To whom correspondence should be addressed. E-mail: giles.oldroyd@bbsrc.ac.uk

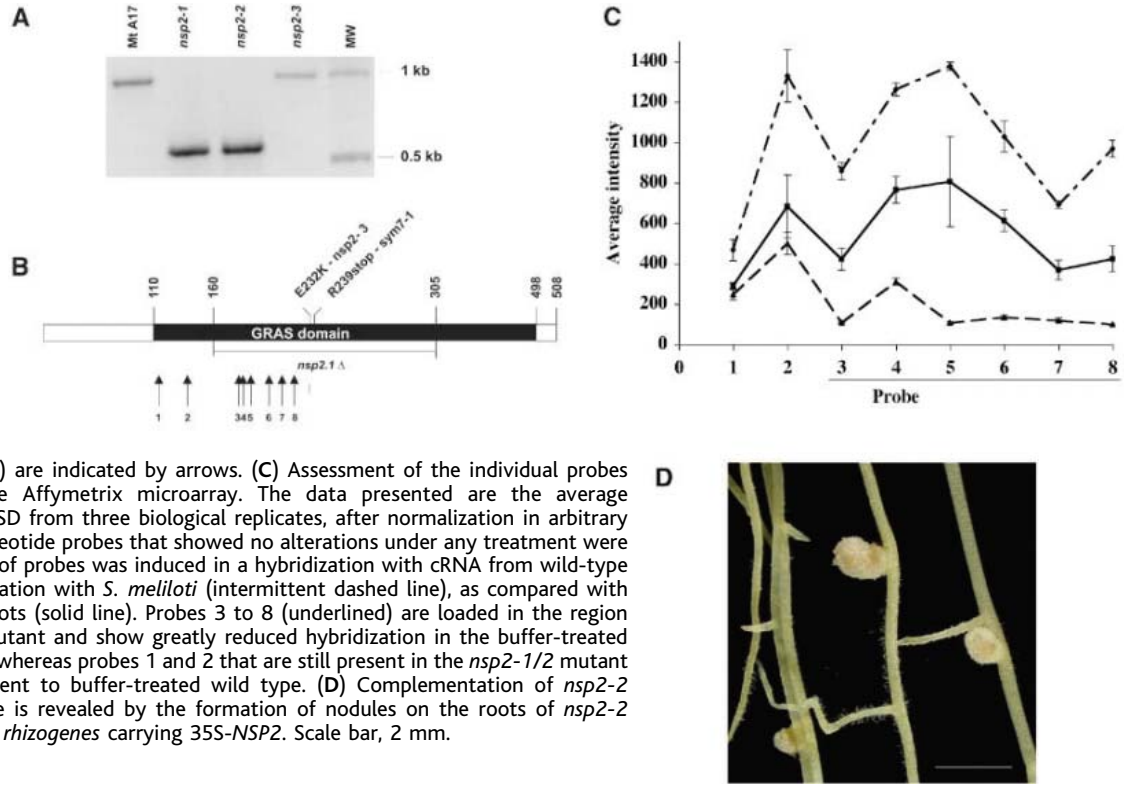

Fig. 1. (**A**) PCR amplification of a region of the *NSP2* gene reveals a deletion in *nsp2-1* and *nsp2-2* but not *nsp2-3*. Mt A17, wild-type plant; MW, molecular size marker. (**B**) *NSP2* encodes a GRAS protein with a conserved GRAS domain and variable N-terminal region. There are no introns contained in *NSP2*. The *nsp2-3* and pea *sym7-1* mutations are contained within the GRAS domain, as is the deletion in *nsp2-1* and *nsp2-2*. The positions of the Affymetrix oligonucleotide probes representing *NSP2* from (C) are indicated by arrows. (**C**) Assessment of the individual probes representing *NSP2* on the Affymetrix microarray. The data presented are the average hybridization intensities ± SD from three biological replicates, after normalization in arbitrary units. Three *NSP2* oligonucleotide probes that showed no alterations under any treatment were disregarded. The entire set of probes was induced in a hybridization with cRNA from wild-type roots 24 hours after inoculation with *S. meliloti* (intermittent dashed line), as compared with buffer-treated wild-type roots (solid line). Probes 3 to 8 (underlined) are loaded in the region deleted in the *nsp2-1/2* mutant and show greatly reduced hybridization in the buffer-treated *nsp2-1* roots (dashed line), whereas probes 1 and 2 that are still present in the *nsp2-1/2* mutant show hybridization equivalent to buffer-treated wild type. (**D**) Complementation of *nsp2-2* mutants by the *NSP2* gene is revealed by the formation of nodules on the roots of *nsp2-2* plants transformed with *A. rhizogenes* carrying 35S-*NSP2*. Scale bar, 2 mm.

spiking (*6*–*8*) highlights the importance of this calcium response.

Three genes of the model legume *Medicago truncatula* that are central to Nod-factor signaling, including the CCaMK, are also required for the symbiosis with arbuscular mycorrizal fungi (*9*). This suggests that aspects of early signaling are conserved between these two symbiotic interactions. The first committed steps for nodulation signaling downstream of the conserved pathway are represented by the *nodulation signaling pathway* genes *NSP1* and *NSP2* (*9*, *10*). Mutations in these genes reveal an essential role in Nod-factor signaling, because the majority of Nod-factor responses are absent or compromised in these mutants, whereas Nod-factor–induced calcium spiking is retained (*7*, *10*). This shows that the *NSP* gene products act downstream of both calcium spiking and the conserved pathway and therefore are likely to transduce the signal downstream of CCaMK. To date, little is known about the mechanisms of signal transduction downstream of plant calcium-activated kinases.

To better understand Nod-factor signaling and the integration of calcium signals in plants, we cloned the *NSP2* gene. *NSP2* was mapped to a region of chromosome 3, tightly linked to marker DK201 (*10*). Additional markers within this region from both *M. truncatula* and *M. sativa* revealed that the marker LAX3 is 0.08 cM from *NSP2*. LAX3 is contained on BAC 11A20, one of a small contig of BACs defined by DNA fingerprinting and extended by BAC

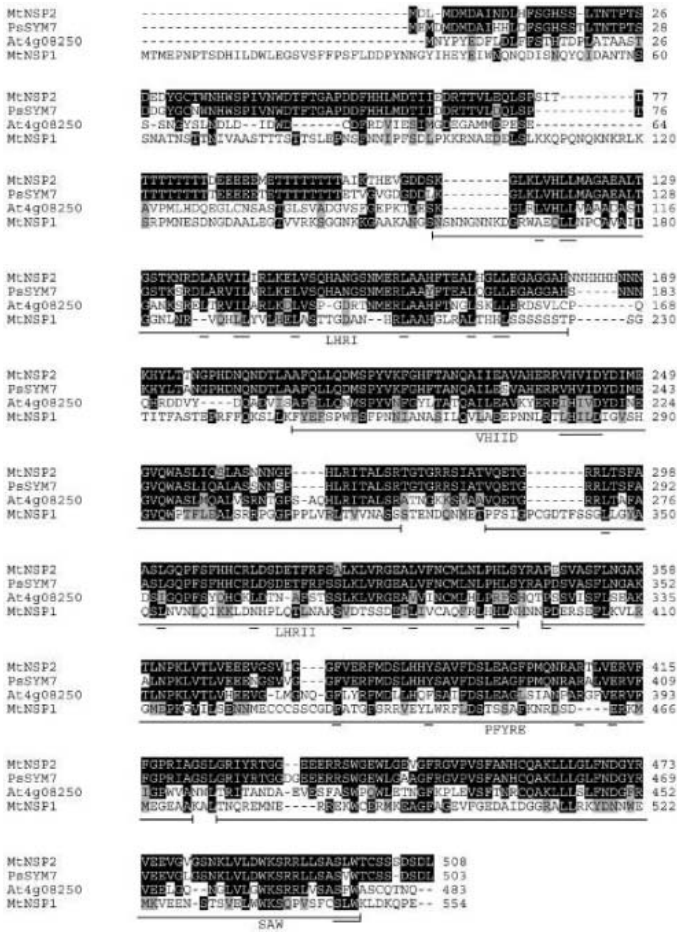

Fig. 2. Alignment of NSP2 with pea SYM7, At4g08250 (the closest *Arabidopsis* homolog), and NSP1. NSP2 and SYM7 show high similarity across the whole protein, including the variable N-terminal region, whereas the *Arabidopsis* protein shows homology only in the GRAS domain, indicating that although SYM7 is a true ortholog, the *Arabidopsis* protein is not. The GRAS domain contains two leucine-rich regions (LHRI and LHRII) and three separate conserved motifs: VHIID, PFYRE, and SAW. The conserved motifs (double underlined) are within regions (underlined) that contain additional conserved residues (not indicated).

walking (*11*) (fig. S1). Genetic markers associated with the ends of two BACs within the contig defined the region containing *NSP2* to 132 kb (*11*). Thirteen genes were predicted to be within this region, including multiple predicted transcription factors and an inositol phosphate kinase, all good candidates for playing a role in Nod-factor signaling.

We isolated the *DMI3* gene (CCaMK) on the basis of decreased transcript levels in the *dmi3-1* mutant, assayed with an Affymetrix microarray containing 9935 root-expressed *M. truncatula* genes (*5*). The *DMI3* transcript was destabilized in the *dmi3-1* mutant by a 14 base pair (bp) deletion that led to a frameshift, resulting in premature translational termination. A similar comparison of transcript levels between wild-type and *nsp2-1* roots identified 17 genes that show a greater than 2-fold reduction in the mutant. Among this list was one gene that is present within the *NSP2*-defined region. This gene, a member of the GRAS family of transcriptional regulators, showed a 3.84-fold decrease in the mutant, ranking it seventh relative to its fold reduction.

Analysis of the two fast neutron-generated *nsp2* mutants showed deletions within this GRAS gene (Fig. 1A), and sequencing revealed the same 435-bp deletion in both alleles (Fig. 1B). This deletion removes a major portion of the conserved GRAS domain but does not induce a frameshift. Therefore, we would not expect this deletion to destabilize the *NSP2* transcript as was the case in the *DMI3* transcript analysis. A comparison of the individual probes that represent this GRAS gene revealed that most of the Affymetrix oligonucleotide probes were contained within the region deleted in the *nsp2-1/2* mutant (Fig. 1B). The two probes that are not contained within the deletion show equivalent hybridization levels in both the wild type and the mutant (Fig. 1C). In contrast, the six probes contained within the deleted region showed substantially reduced expression in the mutant compared with the wild type. This indicates that the apparent reduction in transcript level was due to the lack of hybridization of the *nsp2-1* transcript to a subset of the probes rather than destabilization of this transcript.

An ethyl methane sulfonate mutant allele, *nsp2-3* (*12*), revealed a mutation that causes the nonconservative change E232K in the same GRAS gene (Fig. 1B). In contrast to *nsp2-1/2*, this allele shows a few small white nodules after rhizobial inoculation, which indicates that this mutation results in a weak mutant allele as compared with the presumed null of *nsp2-1/2*. We verified the identity of *NSP2* by complementation of *nsp2-2* with the *NSP2* cDNA under the regulation of the 35S promoter. This construct was introduced into the roots of *nsp2-2* mutant plants with *Agrobacterium rhizogenes.* This procedure results in the formation of a chimeric plant with transformed roots attached to an untransformed shoot. The transformed roots produced nodules (Fig. 1D), and no nodules were seen on roots of *nsp2* mutants transformed with *A. rhizogenes* alone or with CCaMK in the equivalent binary vector. This complementation validates the genetic identity of *NSP2*.

Pea *sym7-1* has a mutant phenotype similar to *nsp2-1/2*, and *SYM7* resides in an approximately syntenic position in the pea genome (*13*). Therefore, *SYM7* is a possible ortholog of *NSP2*. We isolated the homologous cDNA from pea using primers generated against the *M. truncatula* gene. The protein product shows 89.5% identity to the *M. truncatula* protein (Fig. 2). Analysis of the *sym7-1* sequence revealed a translation stop at the position equivalent to R239 in *M. truncatula* NSP2 (Fig. 1B). Thus, null mutations of *NSP2* show consistent phenotypes across two related species of legumes.

Analysis of *NSP2* expression levels on the Affymetrix microarrays revealed a 1.95 ± 0.05–fold induction of this gene 24 hours after treatment with the *M. truncatula* symbiont *Sinorhizobium meliloti* strain 1021 and a similar induction following Nod-factor treatment (Fig. 3A). This induction did not occur with SL44, a mutant strain of *S. meliloti* unable to generate Nod factor, or in mutants of plant genes known to be required for Nod-factor signal transduction (Fig. 3A). To verify these microarray data, we analyzed expression of *NSP2* by semiquantitative reverse transcription polymerase chain reaction (RT-PCR) and found a similar induction by both Nod factor and *S. meliloti* (Fig. 3B). Furthermore, quantitative real-time PCR analysis revealed a 1.6 ± 0.19–fold induction of *NSP2* 4 days after *S. meliloti* inoculation and a 3.2 ± 0.55–fold induction 7 days after inoculation. The RT-PCR data also revealed expression of *NSP2* in shoots and leaves (Fig. 3B). This shoot expression is surprising because the mutant phenotypes are restricted to the root, and complementation with *A. rhizogenes* indicates that root expression of *NSP2* is sufficient for nodulation. It is possible that *NSP2* has additional functions in shoots, but these must be either limited or redundant.

NSP2 encodes a gene with similarity to members of the GRAS family of putative transcriptional regulators. This gene family is found throughout the plant kingdom (*Arabidopsis* contains 33 members) and contains genes involved in gibberellin and phytochrome signaling, root development, axillary shoot development, and maintenance of the shoot apical meristem (*14*). *NSP2* contains a conserved GRAS domain and

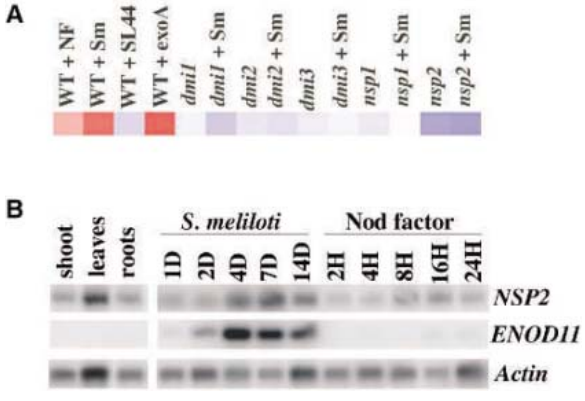

Fig. 3. (**A**) Expression of *NSP2* assayed on the Affymetrix microarray in roots from wild-type and Nod-factor signaling mutants. Red indicates higher levels than the median signal; blue indicates lower levels than the median, assessed as an average from three biological replicates. WT, wild type; NF, Nod factor; Sm, *S. meliloti;* SL44, *S. meliloti* mutant defective in Nod-factor production; exoA, *S. meliloti* mutant defective in exopolysaccharide production; *dmi* and *nsp*, plant mutants defective in Nod-factor signaling. (**B**) *NSP2* expression assayed by RT-PCR. *NSP2* is expressed in shoots, leaves, and roots and induced in roots treated with either *S. meliloti* or Nod factor. *ENOD11* is a gene induced during nodulation that acts as a positive control for *S. meliloti* inoculation. Overexposure of the blot reveals low levels of *ENOD11* after Nod-factor treatment. 1D to 14D, days after inoculation with *S. meliloti*; 2H to 24H, hours after treatment with Nod factor.

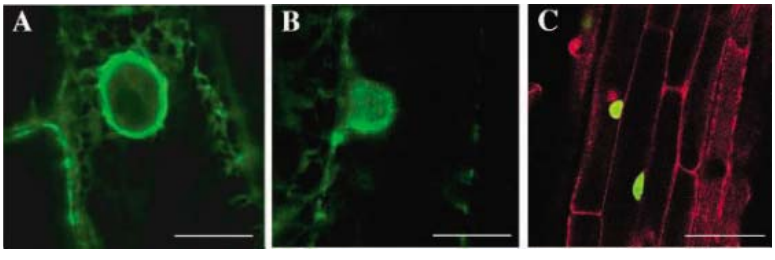

Fig. 4. NSP2 and CCaMK (DMI3) localization. Confocal sections through epidermal root cells expressing the NSP2-GFP and CCaMK-GFP fusions. (**A**) NSP2-GFP shows strong localization to the nuclear envelope and weaker localization in the endoplasmic reticulum, seen as a filamentous network emanating from the nuclear envelope. (**B**) Upon Nod-factor application, the nuclear envelope localization disappears and is replaced by diffuse fluorescence in the nucleus. (**C**) CCaMK shows strong nuclear localization that is unaffected by Nod-factor treatment. Scale bars in (A) and (B), 10 μM; scale bar in (C), 40 μM.

a variable N-terminal region, as observed in other family members. It shows closest similarity to At4 g08250 (Fig. 2), an *Arabidopsis* GRAS protein of unknown function. The GRAS domain consists of two leucine-rich regions that may indicate protein-protein interactions and some small invariantly conserved motifs whose functions are unknown (Fig. 2). Most GRAS domain proteins, including *NSP2*, show homopolymeric stretches of amino acids in the N-terminal region, and these are also found in the activation domain of transcription factors. This, coupled with the leucine-rich regions and the fact that many of these proteins show nuclear localization (*14*), suggests a possible role in transcriptional regulation. Smit *et al*. (*15*) reveal that *NSP1* also encodes a GRAS family member. However, the homology between *NSP1* and *NSP2* is mostly limited to the residues that are conserved throughout this family of proteins (Fig. 2). This is in contrast to the DELLA proteins, a group of closely related GRAS proteins that function in gibberellin signaling (*13*). It is likely that NSP1 and NSP2 fulfill similar, but nonredundant, functions.

We analyzed the localization of NSP2 with a C-terminal GFP fusion driven by the 35S promoter; this complements *nsp2-2*, indicating that this fusion protein is active. NSP2-GFP showed strong localization to the nuclear envelope and weaker localization to the ER (Fig. 4A), despite the fact that NSP2 does not contain a signal peptide or ER retention signal. After application of Nod factor, we saw a shift in NSP2-GFP with a specific loss in the nuclear envelope, but little change in the ER localization, and the gain of diffuse staining throughout the nucleus (Fig. 4B). Overexpression of proteins can cause spurious localization. However, we do not believe that the Nod-factor–induced relocalization is likely to be caused by overexpression. We used the nuclear envelope localization as a marker to assess the frequency of this relocalization event. We found that 85% of cells lacked the nuclear envelope localization 24 hours after 10^{-8} M Nod-factor treatment (n = 87, on three roots), as compared with only 3.7% of cells that lacked the nuclear envelope localization before Nod-factor treatment (n = 106, on three roots). However, this relocalization occurs much earlier, as 39% of cells lacked the nuclear envelope localization 4 hours after 10^{-9} M Nod-factor treatment (n = 111, on three roots). At this stage, we cannot differentiate between the retargeting of newly synthesized NSP2 after Nod-factor application and a shift of nuclear envelope–localized NSP2 to the nucleus. If NSP2 functions as a transcriptional regulator, which is proposed for GRAS family proteins, then its relocalization to the nucleus may be central to the regulation of its activity.

Because NSP2 appears to function downstream of CCaMK (DMI3), we analyzed the localization of CCaMK with both C- and N-terminal GFP fusions. These constructs complement the *dmi3* mutant, indicating appropriate localization. Both GFP CCaMK fusions show strong nuclear localization (Fig. 4C), and a similar localization was observed when this fusion was driven by the *DMI3* promoter (*15*). There was no change observed in the localization of CCaMK after Nod-factor treatment.

The phenotype of *nsp2* mutants indicates that NSP2 is essential for Nod-factor–induced gene expression and that NSP2 acts downstream of both calcium spiking (*10*) and CCaMK. A distinct possibility is the direct phosphorylation of NSP2 by CCaMK after the relocalization of NSP2 to the nucleus, but such an interaction between CCaMK and NSP2 still needs to be assessed. CCaMK is a common feature of both nodulation and mycorrhizal signaling, and specificity of these signaling pathways is most likely a function of differential regulation of this protein. NSP1 and NSP2 are the earliest known nodulation-specific proteins downstream of CCaMK, and their activation may be central to the maintenance of specificity in the Nod-factor signaling pathway. The mechanisms of transduction immediately downstream of CCaMK in both the nodulation and mycorrhizal pathways are likely to be similar, and there may be analogous mycorrhizal-specific GRAS proteins. The isolation of *NSP1* and *NSP2* provides the first insights into the nodulation-specific components of this signaling pathway downstream of CCaMK, and deciphering their mechanism of action will provide insights into calcium signaling in plants and the mechanisms of specificity in this multifunctional signaling pathway.

References and Notes

1. S. R. Long, *Plant Cell* **8**, 1885 (1996).
2. D. W. Ehrhardt, R. Wais, S. R. Long, *Cell* **85**, 673 (1996).
3. R. M. Mitra, S. L. Shaw, S. R. Long, *Proc. Natl. Acad. Sci. U.S.A.* **101**, 10217 (2004).
4. J. Levy *et al.*, *Science* **303**, 1361 (2004).
5. R. M. Mitra *et al.*, *Proc. Natl. Acad. Sci. U.S.A.* **101**, 4701 (2004).
6. G. E. Oldroyd, J. A. Downie, *Nat. Rev. Mol. Cell Biol.* **5**, 566 (2004).
7. R. J. Wais *et al.*, *Proc. Natl. Acad. Sci. U.S.A.* **97**, 13407 (2000).
8. S. A. Walker, V. Viprey, J. A. Downie, *Proc. Natl. Acad. Sci. U.S.A.* **97**, 13413 (2000).
9. R. Catoira *et al.*, *Plant Cell* **12**, 1647 (2000).
10. G. E. Oldroyd, S. R. Long, *Plant Physiol.* **131**, 1027 (2003).
11. Materials and methods are available as supporting material on *Science* Online.
12. B. B. Amor *et al.*, *Plant J.* **34**, 495 (2003).
13. P. Kaló *et al.*, *Mol. Genet. Genomics* **272**, 235 (2004).
14. C. Bolle, *Planta* **218**, 683 (2004).
15. P. Smit *et al.*, *Science* **308**, 1789 (2005).
16. We thank D. Barker for providing the *ENOD11*-GUS line, C. Gough for providing *nsp2-3*, T. LaRue and M. Ambrose for providing and maintaining the pea *sym7* mutant, and H. Miwa for help with the confocal microscope. This work was supported by the Biotechnology and Biological Sciences Research Council as a David Phillips Fellowship to G.O., a grant to G.O. and J.R., a Royal Society award to G.O., and a grant in aid to J.A.D. P.K. was partly supported by a Janos Bolyai postdoctoral fellowship, R.M. was a Howard Hughes Medical Institute (HHMI) predoctoral fellow, and S.R.L. was supported by HHMI and the U.S. Department of Energy. GenBank accessions: BAC 11A20 CR538722, BAC27D24 CR538723, *MtNSP2* AJ832138, *PsSYM7* AJ832139.

Supporting Online Material

www.sciencemag.org/cgi/content/full/308/5729/1786/DC1
Materials and Methods
Fig. S1
References

11 February 2005; accepted 22 April 2005
10.1126/science.1110951

NSP1 of the GRAS Protein Family Is Essential for Rhizobial Nod Factor–Induced Transcription

Patrick Smit,[1] John Raedts,[1] Vladimir Portyanko,[2] Frédéric Debellé,[3] Clare Gough,[3] Ton Bisseling,[1]* René Geurts[1]

Rhizobial Nod factors induce in their legume hosts the expression of many genes and set in motion developmental processes leading to root nodule formation. Here we report the identification of the *Medicago* GRAS-type protein Nodulation signaling pathway 1 (NSP1), which is essential for all known Nod factor–induced changes in gene expression. *NSP1* is constitutively expressed, and so it acts as a primary transcriptional regulator mediating all known Nod factor–induced transcriptional responses, and therefore, we named it a Nod factor response factor.

Nod factors are lipo-chitooligosaccharide–based signal molecules secreted by rhizobia that set in motion *Rhizobium*–legume root nodule symbiosis (*1*). Nod factors are essential for rhizobial infection and induction of cortical cell divisions, leading to nodule primordium formation. These processes are preceded by induction of at least 40 genes (*2*). Nod factors are most likely perceived by LysM domain–containing receptor kinases identified both in *Lotus japonicus* (lotus) (NFR1, NFR5) and *Medicago truncatula* (medicago) (LYK3, LYK4) (*3*–*5*). Subsequent Nod factor signal transduction requires another receptor kinase (DMI2 in medicago, SymRK in

lotus) and putative cation channel(s) (DMI1 in medicago, Pollux and Castor in lotus) (*6*–*9*). In medicago, these proteins are essential to induce Ca^{2+} spiking in the perinuclear region of root hairs within a few minutes after Nod factor application (*10*). These calcium spikes probably activate a calcium- and calmodulin-dependent protein kinase (DMI3 in medicago) that is also necessary for Nod factor signaling (*2*, *11*, *12*).

We fused the gene for green fluorescent protein (*GFP*) with *DMI3* to make *GFP-DMI3*, which is driven by the *DMI3* promoter (*DMI3::GFP-DMI3*) (*13*). This construct complements the *dmi3* mutant TRV25, which shows that the GFP-DMI3 fusion is biologically active (fig. S1). GFP-tagged DMI3 is located in the nucleus of epidermal root cells in both uninoculated roots and roots inoculated with *Sinorhizobium meliloti* Sm2011 [expressing monomeric red fluorescent protein (mRFP)] (*13*, *14*) (Fig. 1A). This suggests that activation of DMI3 and subsequent downstream Nod factor signal transduction occur in the nucleus. Putative targets of DMI3 are, therefore, primary transcription factors mediating Nod factor–induced gene expression. These transcription factors should be constitutively present in an inactive form, should be activated by Nod factor signaling, and, collectively, should be essential for all Nod factor–induced changes in gene expression. Such primary transcription factors have been identified, for example, in auxin signaling, and are called auxin response factors (ARFs) (*15*). Because Nod factor–activated primary transcription factors are analogous to ARFs, we named them Nod factor response factors (NRFs).

In addition to the aforementioned Nod factor–signaling genes, medicago *NODULATION SIGNALING PATHWAY 1* (*NSP1*) and *NSP2* are the only loci identified that are also essential for all known Nod factor–induced changes in gene expression (*2*, *16*, *17*). Genetic analyses showed that *NSP1* and *NSP2* gene products act directly downstream of DMI3 (*10*, *16*, *17*). Therefore, we postulate that at least one of these genes encodes an NRF. This report and the accompanying report of Kaló *et al*. describe the positional cloning of *NSP1* and *NSP2*, respectively, and show that both are excellent candidates for such NRFs (*14*).

We located *NSP1* on the short arm of chromosome 8 between markers 32C19F and 76L14R on the bacterial artificial chromosome (BAC) clone MtH2-37J10 (*13*). This region encompasses 50 kb and contains six putative genes (fig. S2). One of these encodes a putative transcription factor having all the motifs characteristic of proteins belonging to the GRAS transcription factor family (*18*). This putative transcription factor was mutated in all available *nsp1* mutants (B85, C54, C103, and C108) (*16*). The B85 mutant allele (*nsp1-1*) contains a premature stop codon and encodes a truncated protein of 239, instead of 554, amino acids. C54, C103, and C108 mutant alleles all have the same mutation, and therefore, we assume that they are siblings. This allele (*nsp1-2*) encodes a truncated protein of 487 amino acids, and it lacks the C-terminal SAW motif present in all GRAS proteins, which indicates that the SAW motif is essential for NSP1 functioning (Fig. 2). Introduction of the wild-type allele in B85 and C54, using *Agrobacterium rhizogenes*–mediated root transformation, resulted in infected root nodules on inoculation with *S. meliloti* Sm2011 (expressing GFP) (*13*) (fig. S3). This shows that *NSP1* encodes a GRAS-type protein essential for all known Nod factor–induced changes in gene expression.

GRAS-type transcription factors are in general involved in plant developmental processes (*19*). The involvement of NSP1 in Nod factor–induced nodule development is in line with such function. Also, *NSP2* encodes a putative GRAS-type transcription factor (*14*), although it is not similar to NSP1 (17% identity, 32% similarity) (Fig. 2). In contrast, NSP1 is highly homologous to two putative proteins of *Populus trichocarpa* (poplar) (here named HOMOLOG OF NSP1; PtHNO1 and PtHNO2), SCARECROW-LIKE 29 (SCL29) of *Arabidopsis*, and a putative protein of rice (OsHNO) (Fig. 2; fig. S4). The occurrence of putative orthologs in nonlegume plant species and the presence of only a single *NSP1*-type gene in medicago suggest that NSP1-type proteins have a nonsymbiotic function and that, during evolution, NSP1 has obtained an additional function in Nod factor signaling in legume species (fig. S5F).

NSP1 is preferentially expressed in roots, and its expression does not markedly change on *Rhizobium* inoculation (Fig. 3; figs. S5 and S6). Because *NSP1* and *NSP2* (*14*) are expressed before Nod factor signaling, and both are essential for all known Nod factor–induced changes in gene expression, they are NRFs and probably act in a cooperative manner.

Besides NSP1 and NSP2, another putative transcription factor essential for root nodule formation has been identified in lotus and pea, namely, NIN (*20*, *21*). Whether NIN is required

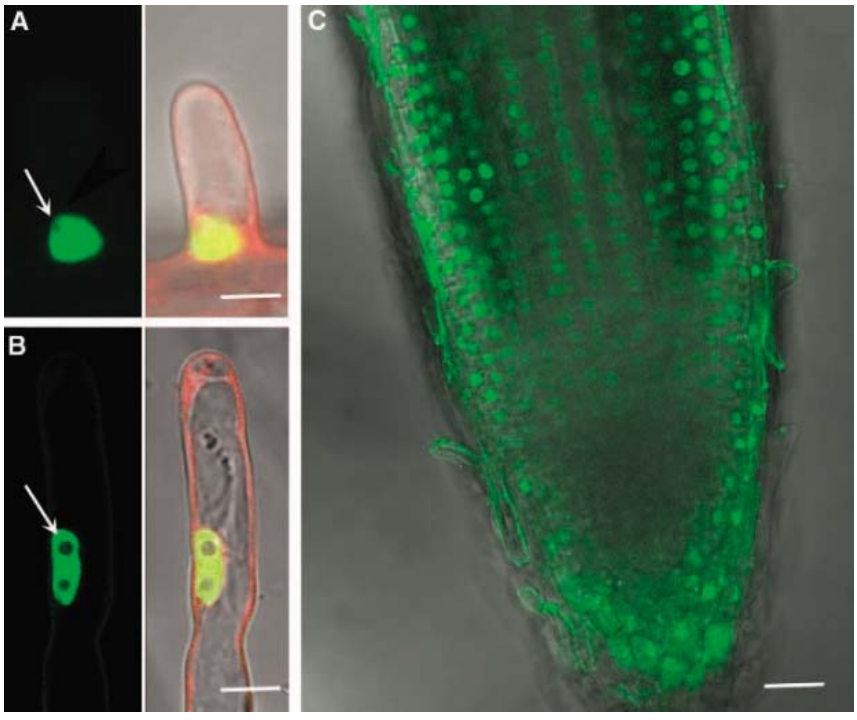

Fig. 1. Subcellular localization of DMI3 and NSP1 by using confocal microscopy. (**A**) TRV25 (*dmi3*) mutant transformed with *DMI3::GFP-DMI3*. Left, GFP-DMI3 localizes in the nucleus of a root hair cell. Right, Confocal sections of both GFP-DMI3 and DsRED (used as selection marker) signals are merged with a bright-field image. (**B**) C54 (*nsp1-2*) mutant transformed with *NSP1::GFP-NSP1*. Left, Localization of GFP-NSP1 in the nucleus of a root hair cell. Right, Confocal sections of both GFP-DMI3 and DsRED (selection marker) signals are merged with a bright-field image. (**C**) C54 (*nsp1-2*) mutant transformed with *NSP1::GFP-NSP1* 2 days after inoculation with *S. meliolti* Sm2011. Expression of GFP-NSP1 can be detected in all epidermal and cortical root cells. Green signal in cell walls of epidermal cells and cytoplasm of root cap cells is due to autofluorescence in the green channel. The nucleolus is devoid of GFP signal, which indicates that GFP-NSP1 and GFP-DMI3 are present in the nucleoplasm.

[1]Department of Plant Science, Laboratory of Molecular Biology, Wageningen University, Wageningen 6703 HA, Netherlands. [2]Department of Plant Biology, University of Minnesota, St. Paul, MN 55108, USA. [3]Laboratoire des Interactions Plantes-Microorganismes INRA-CNRS, BP27, 31326 Castanet-Tolosan Cedex, France.

*To whom correspondence should be addressed. E-mail: ton.bisseling@wur.nl

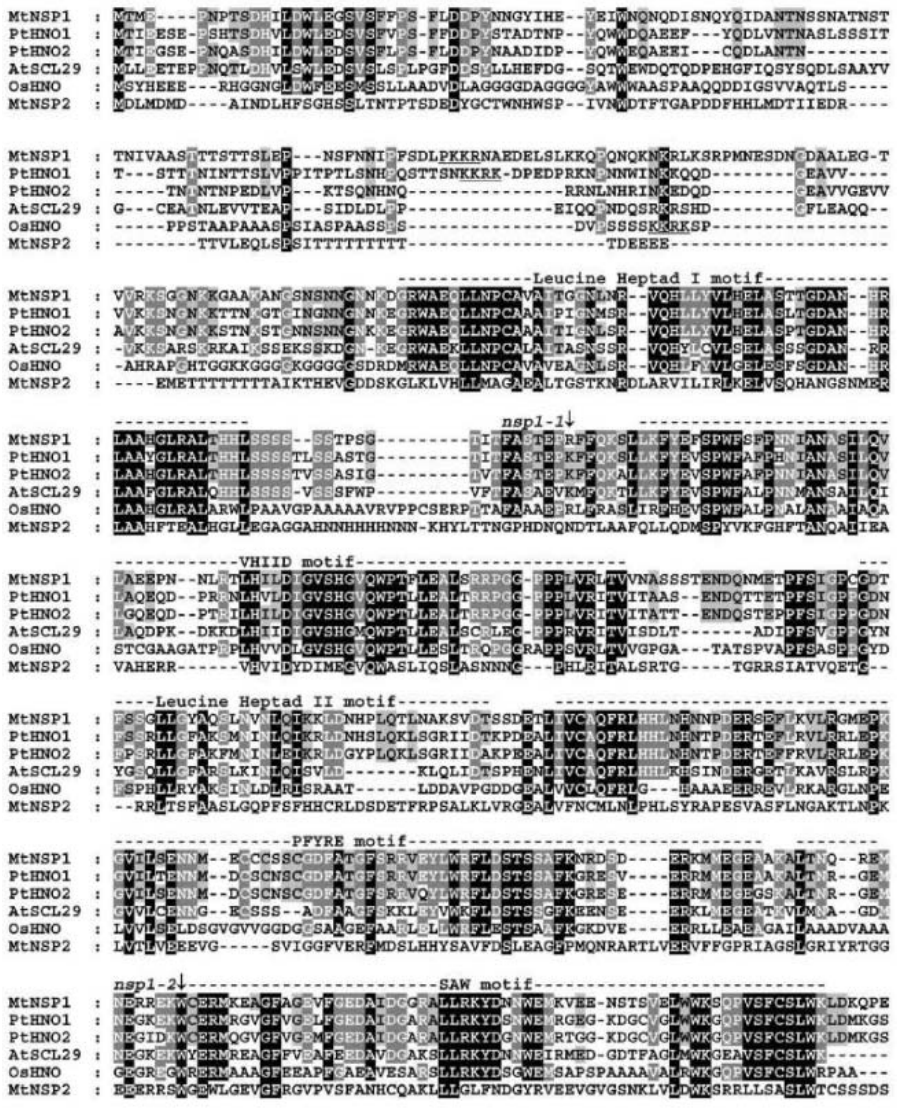

Fig. 2. Alignment of medicago NSP1 and NSP2, poplar PtHNO1 and PtHMO2, *Arabidopsis* SCL29, and rice OsHNO. Five conserved motifs specific for GRAS proteins are annotated (leucine heptad I, VHIID, leucine heptad II, PFYRE, and SAW motifs). Conserved amino acids in NSP1-type proteins are highlighted in shades of black and gray. Putative nuclear localization signals present in NSP1, PtHNO1, and OsHNO are underlined (*22*). Arrows indicate the premature translational stop in *nsp1-1* (B85) and *nsp1-2* (C54). Alignment was made using CLUSTALW (*23*). In order of homology to NSP1: PtHNO1 (66% identity, 77% similarity); PtHNO2 (63% identity, 74% similarity); AtSCL29 (48% identity, 63% similarity); OsHNO (36% identity, 50% similarity); and NSP2 (17% identity, 32% similarity).

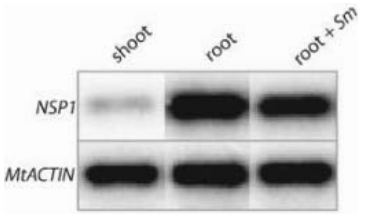

Fig. 3. Semiquantitative reverse transcription polymerase chain reaction (RT-PCR) analysis of *NSP1* expression. NSP1 is constitutively expressed in roots and not up-regulated on inoculation with *S. meliloti* (2 days). Expression of all five medicago *ACTIN* genes was used for normalization (see also figs. S5 and S6).

for Nod factor–induced gene expression is not known; however, *nin* mutants are blocked at a later stage of the interaction, as excessive root hair curling does occur (*16*, *17*, *20*, *21*). Therefore, it is unlikely that NIN is a primary transcription factor, which is also in line with its markedly increased expression when inoculated with rhizobia (*3*, *20*).

To determine whether NSP1 could be activated directly by DMI3, we determined its subcellular localization. We used a *GFP-NSP1* fusion driven by the 4-kb *NSP1* upstream region (*NSP1::GFP-NSP1*) (*13*). This construct complements both *nsp1* mutants (fig. S7). In roots transformed with this fusion construct, GFP-NSP1 is located in the nucleus of all epidermal and cortical root cells (Fig. 1, B and C). The nuclear localization of GFP-NSP1 is not altered after inoculation with *S. meliloti* Sm2011. Because DMI3 and NSP1 are both located in the nucleus, NSP1 could be directly activated by DMI3, but such interaction remains to be demonstrated. The subcellular localization of NSP1 differs from that of NSP2. In transgenic roots expressing *35S::NSP2-GFP*, the fusion protein is predominantly located in the nuclear envelope and the endoplasmic reticulum before Nod factor signaling (*14*). When Nod factor was added, NSP2-GFP accumulated in the nucleus (*14*). Because DMI3 is already localized in the nucleus in uninoculated plants, it is unlikely that the nuclear accumulation of NSP2 is controlled directly by DMI3. The colocalization of NSP1 and DMI3, together with the genetic analysis that shows that DMI3 acts directly upstream of NSP1, strongly supports that NSP1 is a target of DMI3.

References and Notes

1. G. E. Oldroyd, J. A. Downie, *Nat. Rev. Mol. Cell Biol.* **5**, 566 (2004).
2. R. M. Mitra, S. L. Shaw, S. R. Long, *Proc. Natl. Acad. Sci. U.S.A.* **101**, 10217 (2004).
3. S. Radutoiu *et al.*, *Nature* **425**, 585 (2003).
4. E. B. Madsen *et al.*, *Nature* **425**, 637 (2003).
5. E. Limpens *et al.*, *Science* **302**, 630 (2003).
6. G. Endre *et al.*, *Nature* **417**, 962 (2002).
7. S. Stracke *et al.*, *Nature* **417**, 959 (2002).
8. J. M. Ane *et al.*, *Science* **303**, 1364 (2004).
9. H. Imaizumi-Anraku *et al.*, *Nature* **433**, 527 (2005).
10. R. J. Wais *et al.*, *Proc. Natl. Acad. Sci. U.S.A.* **97**, 13407 (2000).
11. J. Levy *et al.*, *Science* **303**, 1361 (2004).
12. R. M. Mitra *et al.*, *Proc. Natl. Acad. Sci. U.S.A.* **101**, 4701 (2004).
13. Material and Methods are available as supporting material on *Science* Online.
14. P. Kaló *et al.*, *Science* **308**, 1786 (2005).
15. T. Ulmasov, G. Hagen, T. J. Guilfoyle, *Science* **276**, 1865 (1997).
16. R. Catoira *et al.*, *Plant Cell* **12**, 1647 (2000).
17. G. E. Oldroyd, S. R. Long, *Plant Physiol.* **131**, 1027 (2003).
18. L. D. Pysh, J. W. Wysocka-Diller, C. Camilleri, D. Bouchez, P. N. Benfey, *Plant J.* **18**, 111 (1999).
19. C. Bolle, *Planta* **218**, 683 (2004).
20. L. Schauser, A. Roussis, J. Stiller, J. Stougaard, *Nature* **402**, 191 (1999).
21. A. Y. Borisov *et al.*, *Plant Physiol.* **131**, 1009 (2003).
22. See www.psort.org/
23. See www.ebi.ac.uk/clustalw

24. We thank G. Kiss for providing marker U336, V. Penmetsa for B85 and C54 seeds, and M. Hartog and C. Franken for sequencing. The Dutch graduate school of Experimental Plant Sciences funded P.S. The U.S. Department of Energy, Energy Biosciences, funded V.P. by a grant to K. VandenBosch, award no. DE-GF02-01ER15201. EMBL accession numbers are as follows: Mth2-37J10, AJ972473; NSP1, AJ972478; nsp1-1, AJ972480; nsp1-2, AJ972481; 32C19F-A17, AJ972482; 32C19F-DZA, AJ972483; 74L14R-A17, AJ972484; 76L14R-DZA, AJ972485; MtRSH1, AJ972474; MtSRP, AJ972475, MtZFP, AJ972477; MtCHP, AJ972479; PtHNO1, AJ972486; PtHNO2, AJ972487.

Supporting Online Material

www.sciencemag.org/cgi/content/full/308/5729/1789/DC1
Materials and Methods
Figs. S1 to S7

14 February 2005; accepted 26 April 2005
10.1126/science.1111025

Major Dissociation Between Medial and Lateral Entorhinal Input to Dorsal Hippocampus

Eric L. Hargreaves,[1,2] Geeta Rao,[1] Inah Lee,[1]* James J. Knierim[1]†

Hippocampal place cells are a model system of how the brain constructs cognitive representations and of how these representations support complex behavior, learning, and memory. There is, however, a lack of detailed knowledge about the properties of hippocampal afferents. We recorded multiple single units from the hippocampus and the medial and lateral entorhinal areas of behaving rats. Although many medial entorhinal neurons had highly specific place fields, lateral entorhinal neurons displayed weak spatial specificity. This finding demonstrates a fundamental dissociation between the information conveyed to the hippocampus by its major input streams, with spatial information represented by the medial and nonspatial information represented by the lateral entorhinal cortex.

The hippocampus and related structures in the medial temporal lobe are crucial components of a brain system that mediates spatial learning, context-dependent learning, and episodic memory (*1*, *2*). These forms of learning have both spatial and nonspatial components, and hippocampal neurons correspondingly have both spatial and nonspatial firing correlates (*3*–*5*). Characterizing the pathways by which spatial and nonspatial information reach the hippocampus is critical for a full understanding of the neural circuitry underlying these forms of memory. The major cortical input to the hippocampus originates in the entorhinal cortex (Fig. 1A), which is divided into two parts on the basis of distinctive cytoarchitecture and connectivity patterns (*6*). The medial entorhinal cortex (MEC) receives its predominant input from the postrhinal cortex (parahippocampal cortex in primates) and forms the medial perforant path into the hippocampus. The lateral entorhinal cortex (LEC) receives its major input from the perirhinal cortex and forms the lateral perforant path (*7*).

The most salient behavioral correlate of hippocampal pyramidal cells in freely moving rats is the spatial location of the rat (*1*, *3*, *8*), and some entorhinal neurons have been shown to display spatial specificity as well (*9*–*12*). Different parts of the MEC and LEC project to different sites along the septal-temporal (dorsal-ventral) axis of the hippocampus (*13*), and accumulating evidence demonstrates functional heterogeneity along this axis (*6*, *14*, *15*). Therefore, it is imperative to precisely localize recording sites in the entorhinal cortex relative to their projections to the hippocampus. Neurons located within the dorsolateral band of the MEC (the band that projects to the dorsal hippocampus) fire in multiple discrete spots in an environment (*16*). These spots are reproducible across repeated sessions, and ensembles of these neurons represent the rat's location with precision. In contrast, cells in the ventromedial band of the MEC (the band that projects to the ventral hippocampus) do not display strong spatial tuning. Here we provide evidence for a major dissociation in spatial tuning along the orthogonal axis of the entorhinal cortex (i.e., between the LEC and the MEC).

Multiple single units were recorded while rats foraged for a food reward in a square chamber with a single white cue card on the west wall (*17*). Figure 1B shows the spatial firing-rate maps of the 10 cells with the highest spatial information scores (*18*) in the CA1 region of the hippocampus, the superficial layers of the MEC, and the superficial layers of the LEC. (The rate maps for all neurons in the sample are shown in fig. S1.) Entorhinal projections to the hippocampus originate in these superficial layers. Most CA1 and many MEC cells displayed very specific place fields, firing robustly and selectively in the square environment. In contrast, only a few cells in the LEC displayed spatial tuning, which was much less specific than that demonstrated by the MEC or CA1. Figure 1C shows the spatial information scores for all neurons from the superficial MEC (n = 52), superficial LEC (n = 68), and CA1 (n = 91). The differences among the three regions were highly significant [CA1: mean = 1.05 ± 0.06 SEM; MEC: mean = 0.61 ± 0.07; LEC: mean = 0.20 ± 0.02; $F(2,208) = 99.2$, $P < 0.0001$]. Post hoc Tukey tests showed that CA1 had higher spatial information scores than did the MEC [$q(208,3) = 6.7$, $P < 0.001$] and LEC [$q(208,3) = 19.8$, $P < 0.001$], and the MEC had higher spatial information scores than did the LEC [$q(208,3) = 11.0$, $P < 0.001$].

The LEC receives major cortical input from the perirhinal cortex (*6*, *7*). Perirhinal cortex neurons did not display strong spatial selectivity (mean = 0.19 ± 0.02, n = 70) (*19*). The MEC and LEC both receive strong input from the parasubiculum (*6*, *20*). In contrast to the perirhinal cortex, some parasubiculum cells displayed robust spatial tuning (mean = 0.59 ± 0.07, n = 30) (*21*, *22*). The information scores among the five regions (CA1, LEC superficial, MEC superficial, perirhinal, and parasubiculum) were significantly different [$F(4,306) = 75.4$, $P < 0.0001$]. Pairwise comparisons indicated that the parasubiculum was different from both the LEC [$q(306,5) = 8.9$, $P < 0.001$] and the perirhinal cortex [$q(306,5) = 11.2$, $P < 0.001$], but not from the MEC [$q(306,5) = 0.4$, $P > 0.5$, not significant (n.s.)]. Conversely, the perirhinal cortex was different from both the MEC [$q(306,5) = 12.8$, $P < 0.001$] and parasubiculum [$q(306,5) = 11.2$, $P < 0.001$], but not the LEC [$q(306,5) = 2.9$, $P > 0.2$, n.s.] (*23*).

Dorsal hippocampal neurons contain more specific place fields than do ventral hippocampal neurons (*15*). Because different anatomical bands of the MEC and LEC project to the dorsal and ventral hippocampus (Fig. 1A) (*13*), it is important to determine that both the MEC and LEC recording sites were in regions that project to the dorsal hippocampus, in order to make a valid comparison between the two areas. The locations of recording sites of the 12 rats of this study are shown on an unfolded flat-map representation of the dorsolateral projection bands of the MEC and LEC, which project to the dorsal half of the hippocampus (Fig. 2A) (see figs. S2 and S3 for individual maps for each rat and for precise localization of EC recording sites) (*13*) . Figure 2B shows representative histological sections of recordings from CA1 and the MEC, LEC, perirhinal cortex, and parasubiculum. All six MEC rats had tetrodes located in the dorsolateral band (hatched region); a few of the most rostral tetrode tracks encroached on the region that projects to the intermediate hippocampus. In four of the six LEC rats, the tetrodes were in the dorsolateral band, near the rhinal sulcus. In the remaining two rats, the LEC recording sites were in the intermediate band, which projects to the intermediate hippocampus (for one of these rats, no cells recorded in the LEC met inclusion criteria for this study). No strong place fields were recorded in the superficial layers of the LEC in either the intermediate or dorsolateral bands (fig. S4).

Although the quality of spatial information provided by superficial LEC neurons is lower than that provided by superficial MEC

[1]Department of Neurobiology and Anatomy, W. M. Keck Center for the Neurobiology of Learning and Memory, Post Office Box 20708, University of Texas Medical School at Houston, Houston, TX 77225, USA. [2]Center for Neural Science, New York University, New York, NY 10003, USA.

*Present address: Center for Memory and Brain, Boston University, 2 Cummington Street, Boston, MA 02215, USA.

†To whom correspondence should be addressed. E-mail: james.j.knierim@uth.tmc.edu

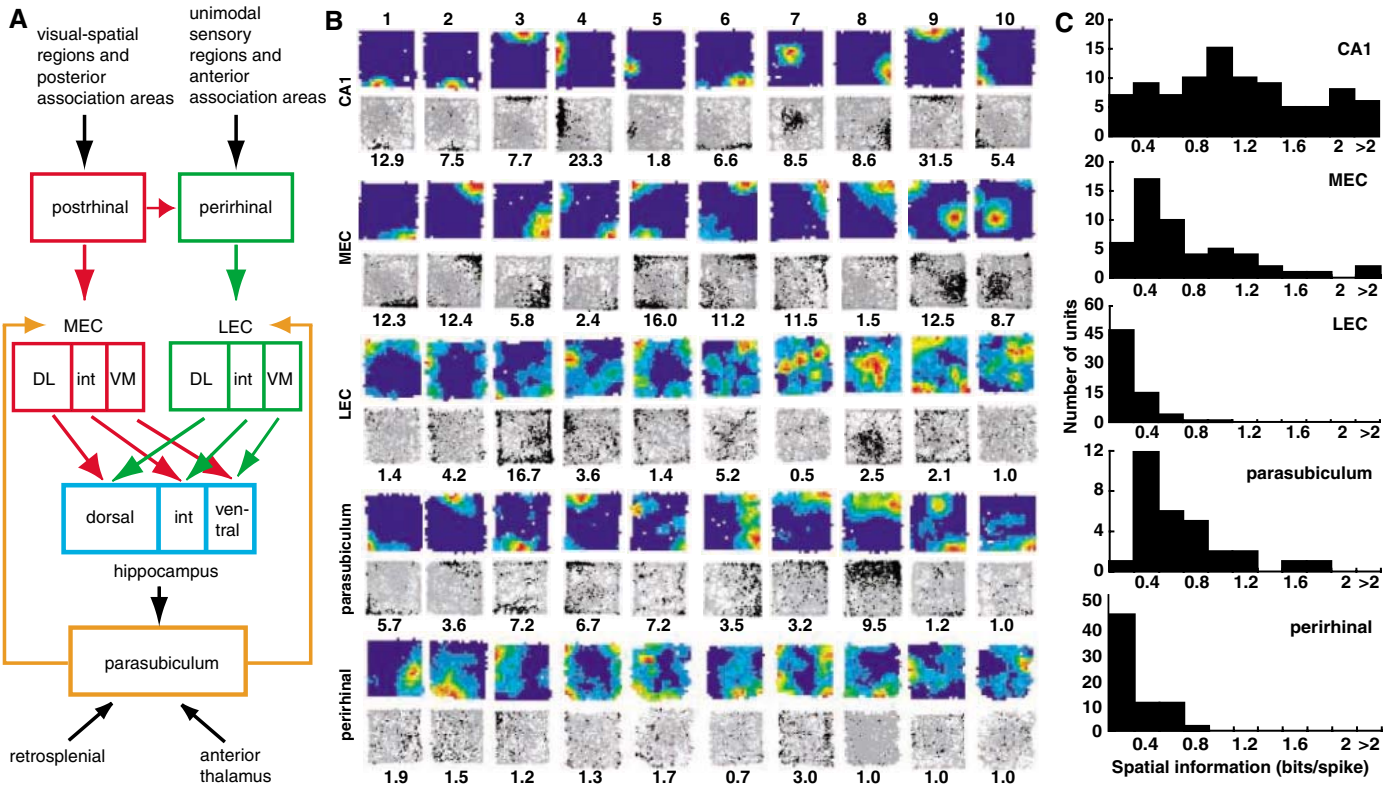

Fig. 1. Spatial firing properties in CA1 and parahippocampal areas. (**A**) Simplified connectivity between hippocampus and parahippocampal areas related to this study (*6*, *7*). Not all feedforward, feedback, or cross-stream pathways are represented. DL, dorsolateral band; int, intermediate band; VM, ventromedial band. (**B**) Firing-rate maps for the 10 cells showing the highest spatial information scores (ranked left to right) in each area. Red represents maximal firing, whereas blue represents no firing. The grayscale image below each rate map shows the trajectories of the rat in the 10-min session (gray lines) and the location of the rat when each spike was fired (black dots). Numbers represent the maximum firing rate for each cell. (**C**) Histograms of spatial information scores for each area. The spatial information score represents the amount of information (in bits per spike) about the rat's location that is conveyed by the firing of the cell (*18*). Note the differences in the *y*-axis scales.

neurons, some of the LEC rate maps displayed a modest amount of spatial selectivity (e.g., cells 4 and 8 of Fig. 1B). Putative spatial selectivity can arise as an artifact of inhomogeneous sampling of the environment, or of random bursts of activity, or from responsiveness to an aspect of the environment that is correlated with location (e.g., responsiveness to a localized odor). One test of true spatial selectivity is if the spatial firing patterns of a cell are replicated across repeated sessions. We systematically recorded successive sessions separated by 5 to 20 min in two rats (LEC rat 115 and MEC rat 123), and the firing-rate maps of superficial MEC cells were more correlated between the two sessions than the rate maps of superficial LEC cells [mean correlation for MEC = 0.63 ± 0.07, $n = 21$; for LEC = 0.30 ± 0.06, $n = 24$; $t(43) = 4.2$, $P < 0.0001$]. Because the paper covering the floor of the recording chamber was replaced between sessions, the reproducible firing patterns in MEC were not the result of floor-based odor cues. A similar analysis was performed for all cells in the sample by correlating the spatial firing patterns for the first half of a session with the spatial firing patterns for the second half. This analysis confirmed that CA1 and MEC spatial firing patterns were much more consistent within a session than were LEC patterns (fig. S5).

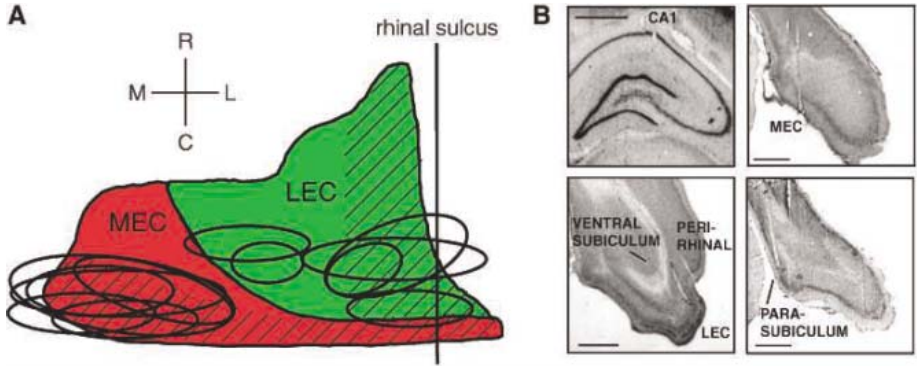

Fig. 2. Recording sites in the MEC and LEC. (**A**) Averaged flat-map reconstruction of the entorhinal cortex (*13*). The dorsolateral projection band, which sends projections to the dorsal half of the hippocampus, is shown hatched. Ovals denote the spread of tetrode penetrations for each rat. R, rostral; M, medial; C, caudal; L, lateral. (**B**) Representative histological sections showing tetrode tracks from CA1 and the LEC, perirhinal cortex, MEC, and parasubiculum. Scale bars, 1 mm.

The similarity of spatial information between the parasubiculum and the MEC raises questions about whether the spatial selectivity in the MEC is generated in the MEC from nonspatial postrhinal inputs (Fig. 1A) (*16*, *24*) or derived from the parasubiculum. In addition to its inputs from the subiculum, the parasubiculum receives input from the retrosplenial cortex and from the anterior thalamus (*6*, *25*), two regions that contain cells that represent head direction and movement through space (*26*, *27*). The parasubiculum may thus be part of a network that creates spatial representations on the basis of self-motion cues through interactions with the retrosplenial cortex and anterior thalamus, and then sends this

representation to the MEC. Regardless of the site of origin of the spatial signal, our results demonstrate a fundamental distinction between the functional correlates of the two major streams of input into the hippocampus from the neocortex. Superficial layers in the MEC contain exquisitely tuned "place cells," which may arise from a grid-like representation of space (fig. S6) (*16*). In contrast, there were few robust place cells in the superficial layers of the LEC under the present conditions of unstructured foraging in an environment with few spatial landmarks. Perhaps cells from the dorsolateral band of the LEC display spatial firing under other conditions (e.g., in a visually complex environment or in a more structured behavioral task). Alternatively, because CA1 neurons respond to individual items or discrete stimuli in conjunction with spatial location (*3*–*5*), it is possible that the LEC stream carries this nonspatial information from the perirhinal cortex into the hippocampus, where it is combined with spatial information from the MEC stream to create conjunctive object-place (or event-place) representations in the hippocampus proper (*28*, *29*). Consistent with this notion of parallel input streams, perirhinal cortex lesions disrupt exploratory behavior based on novel configurations of objects, whereas postrhinal cortex lesions disrupt exploratory behavior based on novel configurations of an object and a spatial context (*30*). This process may be a rodent analog of a dissociation in humans between item and source memory localized to the perirhinal and parahippocampal cortices, respectively (*31*).

References and Notes

1. J. O'Keefe, L. Nadel, *The Hippocampus as a Cognitive Map* (Clarendon Press, Oxford, UK, 1978).
2. H. Eichenbaum, *Neuron* **44**, 109 (2004).
3. J. O'Keefe, *Exp. Neurol.* **51**, 78 (1976).
4. E. R. Wood, P. A. Dudchenko, H. Eichenbaum, *Nature* **397**, 613 (1999).
5. M. A. Moita, S. Rosis, Y. Zhou, J. E. LeDoux, H. T. Blair, *Neuron* **37**, 485 (2003).
6. M. P. Witter, D. G. Amaral, in *The Rat Nervous System*, G. Paxinos, Ed. (Elsevier, New York, ed. 3, 2004), pp. 635–704.
7. R. D. Burwell, *Ann. N.Y. Acad. Sci.* **911**, 25 (2000).
8. R. Muller, *Neuron* **17**, 813 (1996).
9. C. A. Barnes, B. L. McNaughton, S. J. Mizumori, B. W. Leonard, L. H. Lin, *Prog. Brain Res.* **83**, 287 (1990).
10. S. J. Mizumori, K. E. Ward, A. M. Lavoie, *Brain Res.* **570**, 188 (1992).
11. G. J. Quirk, R. U. Muller, J. L. Kubie, J. B. Ranck Jr., *J. Neurosci.* **12**, 1945 (1992).
12. L. M. Frank, E. N. Brown, M. Wilson, *Neuron* **27**, 169 (2000).
13. C. L. Dolorfo, D. G. Amaral, *J. Comp. Neurol.* **398**, 25 (1998).
14. M.-B. Moser, E. I. Moser, *Hippocampus* **8**, 608 (1998).
15. M. W. Jung, S. I. Wiener, B. L. McNaughton, *J. Neurosci.* **14**, 7347 (1994).
16. M. Fyhn, S. Molden, M. P. Witter, E. I. Moser, M. B. Moser, *Science* **305**, 1258 (2004).
17. Materials and methods are available as supporting material on *Science* Online.
18. W. E. Skaggs, B. L. McNaughton, M. A. Wilson, C. A. Barnes, *Hippocampus* **6**, 149 (1996).
19. R. D. Burwell, M. L. Shapiro, M. T. O'Malley, H. Eichenbaum, *Neuroreport* **9**, 3013 (1998).
20. M. Caballero-Bleda, M. P. Witter, *J. Comp. Neurol.* **328**, 115 (1993).
21. J. S. Taube, *Hippocampus* **5**, 569 (1995).
22. Projections to the MEC and LEC originate in different regions of the parasubiculum (*20*). We did not sample the different regions adequately to determine whether there was a difference in spatial tuning between areas that project to the MEC or LEC, or to determine whether there were differences in spatial tuning between the dorsal and ventral parasubiculum.
23. Because there were no differences in the spatial information scores between the deep and superficial layers of either the parasubiculum or perirhinal cortex, recordings from these layers were combined for each area. Comparing the information scores of CA1, the superficial MEC, and the superficial LEC, with only the superficial cells of the parasubiculum or perirhinal cortex, yielded no change in the results.
24. R. D. Burwell, D. M. Hafeman, *Neuroscience* **119**, 577 (2003).
25. T. van Groen, J. M. Wyss, *Brain Res.* **518**, 227 (1990).
26. J. S. Taube, *J. Neurosci.* **15**, 70 (1995).
27. L. L. Chen, L. Lin, E. J. Green, C. A. Barnes, B. L. McNaughton, *Exp. Brain Res.* **101**, 8 (1994).
28. W. A. Suzuki, E. K. Miller, R. Desimone, *J. Neurophysiol.* **78**, 1062 (1997).
29. D. Gaffan, *Exp. Brain Res.* **123**, 201 (1998).
30. G. Norman, M. J. Eacott, *Behav. Neurosci.* **119**, 557 (2005).
31. L. Davachi, J. P. Mitchell, A. D. Wagner, *Proc. Natl. Acad. Sci. U.S.A.* **100**, 2157 (2003).

32. We thank M. Witter for reviewing recording site locations and M. Shapiro and J. Ferbinteanu for helpful comments on the manuscript. Supported by the Texas Higher Education Coordinating Board Advanced Research Program 011618-0180-1999 and by grants R01 NS039456 and K02 MH63297 from the Public Health Service.

Supporting Online Material

www.sciencemag.org/cgi/content/full/308/5729/1792/DC1
Materials and Methods
Figs. S1 to S6
References

31 January 2005; accepted 14 April 2005
10.1126/science.1110449

Early Asymmetry of Gene Transcription in Embryonic Human Left and Right Cerebral Cortex

Tao Sun,[1] Christina Patoine,[1] Amir Abu-Khalil,[2] Jane Visvader,[3] Eleanor Sum,[3] Timothy J. Cherry,[1] Stuart H. Orkin,[4] Daniel H. Geschwind,[2] Christopher A. Walsh[1]*

The human left and right cerebral hemispheres are anatomically and functionally asymmetric. To test whether human cortical asymmetry has a molecular basis, we studied gene expression levels between the left and right embryonic hemispheres using serial analysis of gene expression (SAGE). We identified and verified 27 differentially expressed genes, which suggests that human cortical asymmetry is accompanied by early, marked transcriptional asymmetries. *LMO4* is consistently more highly expressed in the right perisylvian human cerebral cortex than in the left and is essential for cortical development in mice, suggesting that human left-right specialization reflects asymmetric cortical development at early stages.

One of the most remarkable aspects of the human cerebral cortex is that the two hemispheres are specialized for distinct cognitive and behavioral functions. Whereas the right cerebral cortex regulates movement of the left side of the body and vice versa, ~90% of the human population is naturally more skilled with the right hand than with the left (*1*). This motor asymmetry is strongly correlated with language dominance: Language function is predominantly localized to a distributed network in the left perisylvian cortex in 97% of right-handers and ~60% of left-handers (*2*, *3*). Functional asymmetries exist in mathematical ability and in spatial and facial recognition as well. These functional asymmetries have been related to anatomical asymmetries of the cortex that are somewhat more subtle (*2*, *4*). For example, the posterior end of the sylvian fissure is higher in the right hemisphere than in the left (*5*). The planum temporale, a region in the posterior portion of the superior temporal sulcus in which Wernike's area resides, is larger in the left hemisphere than in the right in more than 65% of examined adult and 56 to 79% of examined fetus and infant brains, so the anatomical asymmetries are less marked than

[1]Howard Hughes Medical Institute, Beth Israel Deaconess Medical Center, and Department of Neurology, Harvard Medical School, New Research Building Room 0266, 77 Avenue Louis Pasteur, Boston, MA 02115, USA. [2]Department of Neurology, Program in Neurogenetics, University of California–Los Angeles School of Medicine, Los Angeles, CA 90095, USA. [3]Victorian Breast Cancer Research Consortium Laboratory, The Walter and Eliza Hall Institute of Medical Research, Melbourne, Victoria 3050, Australia. [4]Howard Hughes Medical Institute, Division of Hematology-Oncology, Boston Children's Hospital, and Department of Pediatrics, Dana-Farber Cancer Institute, Boston, MA 02115, USA.

*To whom correspondence should be addressed. E-mail: cwalsh@bidmc.harvard.edu

the functional ones (*6*, *7*). Although genetic factors connecting cerebral asymmetry and functional dominance have been supported (*8*), no molecular correlate of cerebral asymmetry has been identified.

We directly tested the hypothesis that left-right cortical asymmetry in humans results from differential gene expression at early embryonic stages, long before the onset of organized cerebral cortical function. By applying serial analysis of gene expression (SAGE), we measured gene expression levels between the left and right hemispheres in early (12- to 14-week-old) fetal human brains, during periods of neuronal proliferation and migration, and later (at 19 weeks), after these processes are largely completed (*9*). Brain tissues were first dissected from matching perisylvian regions in two hemispheres (Fig. 1, A to C). The cortex was then separated at the midline. On the medial side of the hemisphere, tissues were also dissected from the ventricular zone in the frontal and occipital regions (Fig. 1B). Total RNA was isolated, and 14 SAGE libraries were generated (Fig. 1D). To detect genes with differential expression levels, we compared the tag frequency for each gene between two SAGE libraries generated from the frontal, perisylvian, and occipital regions in the left-right hemispheres. To verify the statistical significance of differences in each comparison, we performed a Monte Carlo test and verified this using the χ test. Using the χ-squared distribution with one degree of freedom and confidence levels (P), we sorted genes within each comparison (e.g., left-right). A higher χ value indicates a greater statistically significant difference.

In all, 49 differentially expressed genes were identified by SAGE with $P > 99\%$ (χ value > 6.63) between the left-right perisylvian regions of a 12-week-old embryonic human cortex. Among them, 21 genes were highly expressed in the left region, whereas 28 genes were highly expressed in the right (Fig. 1E). Moreover, 68 genes were identified with $P > 99\%$ between the left-right perisylvian regions of a 14-week-old cortex (Fig. 1E). By combining analyses, we generated a list of statistically differentially expressed genes between the left-right hemispheres in the perisylvian regions (Fig. 1E and tables S1 to S5) and frontal and occipital regions (tables S9 to S12) of human embryonic brains at 12, 14, and 19 weeks. Differential gene expression levels detected by SAGE suggested an early transcriptional asymmetry between the left-right hemispheres in human embryonic brains.

One of the genes reproducibly asymmetrically expressed was the transcription factor *Lim Domain Only 4* (*LMO4*). Using SAGE analysis, we found that the human *LMO4* is more highly expressed in the perisylvian regions of the right hemisphere than in the left at both 12 and 14 weeks (Fig. 2A). In contrast, *LMO4* expression levels did not show significant differences between the left and right perisylvian regions at 19 weeks (Fig. 2A). We then quantified *LMO4* expression levels using real-time SYBR (Applied Biosystems)–green reverse transcription–polymerase chain reaction (RT-PCR) and confirmed higher *LMO4* expression in the right perisylvian regions than in the left of embryonic 12- and 14-week-old but not 19-week-old brains, using the same RNA samples for SAGE analysis (Fig. 2B). Moreover, we confirmed higher levels of *LMO4* expression in the right perisylvian region versus the left in second 12-week-old and 14-week-old brains and observed modest differences in two 16-week-old brains and one 17-week-old brain (Fig. 2B).

We next performed nonradioactive in situ hybridization on human embryonic brains and noted right-left differences in the extent of *LMO4* expression at 12 weeks. We serially sectioned the cortex in the frontal plane and performed in situ hybridization on at least 54 sections from this series, covering most of the frontal to occipital extent of the cerebral cortex (Fig. 2C). Consistent with the early expression of *Lmo4* in mice (see below), *LMO4* in this 12-week-old human brain was expressed in the ventral lateral cortical plate in a patchy fashion (Fig. 2, D to F). *LMO4* was also expressed highly and symmetrically in noncortical telencephalic structures, notably the putamen (Fig. 2F). We analyzed the medial-lateral extent of *LMO4* expression in the cortical plate in relation to the lateral border of the basal ganglia, defined by connecting the corticostriatal sulcus and the lateral border of the putamen (Fig. 2F). In this brain, *LMO4* expression was observed further dorsolateral in the cortical plate in the right hemisphere than the left, particularly in sections near the future perisylvian region (Fig. 2F).

We then confirmed asymmetric *LMO4* expression in several additional human fetal brains, focusing in the perisylvian region, using [^{35}S]-labeled radioactive in situ hybridization. At 14 weeks, *LMO4* was highly expressed in the cortical plate around the entire perimeter of the cortex. Although levels of *LMO4* expression in the right hemisphere

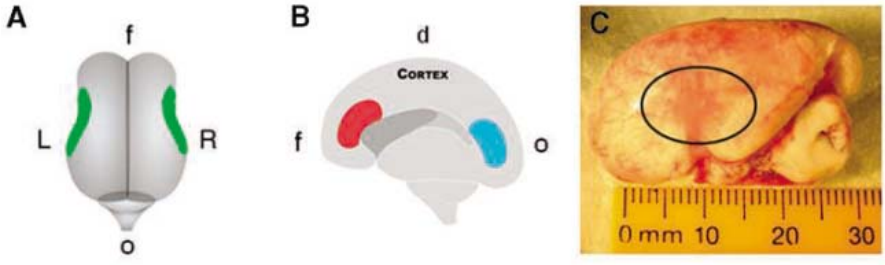

D

RNA Samples				SAGE Tags					
Code	Embryonic Stages	Sex	Application	Frontal Region		Perisylvian Region		Occipital Region	
				L	R	L	R	L	R
#1438	12.6 weeks	M	Making SAGE libraries	55,979	57,477	61,671	60,193	61,679	63,000
#1392	12.5 weeks	M	Verify SAGE data						
#1341	14 weeks	F	Making SAGE libraries	56,000	61,930	54,237	56,595	64,986	62,000
#1316	14 weeks	M	Verify SAGE data						
#1335	19.3 weeks	M	Making SAGE libraries			62,575	61,868		

E

Embryonic stages	12 weeks				14 weeks				19 weeks			
Confidence level	p>99%		95%<p<99%		p>99%		95%<p<99%		p>99%		95%<p<99%	
Comparison	L>R	L<R	L>R	L<R	L>R	L<R	L>R	L<R	L>R	L<R	L>R	L<R
Frontal Region	25	26	217	172	28	17	145	152	n/d	n/d	n/d	n/d
Perisylvian Region	21	28	189	180	38	30	194	117	14	14	166	196
Occipital Region	37	13	201	174	48	29	189	218	n/d	n/d	n/d	n/d

Fig. 1. Dissection of human embryonic brain tissues and generation of human SAGE libraries. (**A**) A top view of a 14-week-old human embryonic brain. Tissues were dissected from perisylvian regions in the left (L) and right (R) hemispheres. (**B**) A side view of a 14-week-old human embryonic right hemisphere. Tissues in the frontal (f, red) and occipital (o, blue) ventricular regions containing dividing cells were dissected. The dorsal cortex (d) is on the top. (**C**) The left side view of a 14-week-old human embryonic brain. The perisylvian region is circled. (**D**) Summary of human brain SAGE libraries. The male (M) and female (F) brains are listed. At least 55,000 tags were sequenced in each library. (**E**) Summary of differentially expressed genes detected by SAGE analysis between the left-right hemispheres. Numbers of genes that are highly expressed in the left (L > R) or right (L < R) hemisphere are listed with confidence levels $P > 99\%$ and $95\% < P < 99\%$. n/d, not detected.

were comparable to those in the left in broad areas of dorsomedial neocortex, paralleling the fact that there are no known anatomical asymmetries of these medial areas, it was consistently more highly expressed over broad areas of the right perisylvian cortex than the left (Fig. 2, G to J). At 16 weeks, asymmetric cortical expression was still observed, although it was diminished relative to earlier time points, consistent with the real-time RT-PCR analysis (Fig. 2, B, K, and L). Marked asymmetries in *LMO4* expression were seen in the perisylvian region of a human 17-week-old cortex studied by nonradioactive in situ hybridization (fig. S1) and were even more apparent than in the RT-PCR results (Fig. 2B). In a 19-week-old brain, consistent with RT-PCR results, left-right differences in *LMO4* expression were not obvious (fig. S1). Overall, the in situ hybridization analysis mirrored the SAGE and RT-PCR analysis, with clearer but variable asymmetries in expression among individuals at earlier stages and no clear asymmetry at the latest stage examined (19 weeks).

To better understand the dynamic change in *Lmo4* expression during cortical development, we analyzed *Lmo4* expression in mouse brains. Similar to its expression in the 12-week-old human embryonic brain, *Lmo4* was weakly expressed in the ventral cortex in the embryonic day 11.5 (E11.5) mouse brain, and its expression increased during development (Fig. 3A). *Lmo4* expression boundaries were fairly sharp at postnatal day 1 (P1) with expression being high in the anterior and posterior portions of the cortex, but with a large zone of nonexpression that overlapped the presumptive parietal cortex in between (Fig. 3D). However, this nonexpression zone disappeared at P17 (Fig. 3G). In coronal sections of E15.5 and P5 mouse cortices, *Lmo4* was expressed in the medial and lateral cortical areas as well (Fig. 3, B and E). *Lmo4* in the mouse showed apparent asymmetries in the cortical area in which it was highly expressed, and the expression pattern was quite dynamic (Fig. 3, A to G).

Because the levels of coronal sections may affect in situ hybridization signal, we mapped the *Lmo4* expression on serial sagittal sections to provide an accurate gene expression pattern (Fig. 3H). We divided the cortical expression of *Lmo4* in P1 brain into three regions: anterior (expression I), intermediate (nonexpression), and posterior (expression II) (Fig. 3I). The ratios of the length of each *Lmo4* expression region versus the full length of the cortex were calculated from the medial to lateral cortical regions and analyzed with histograms (Fig. 3, J and K). The *Lmo4* expression areas in the anterior were smaller in the left hemisphere than in the right in six tested brains (shown by one representative brain in Fig. 3J), but larger in the left than the right in four tested brains (shown by one representative brain in Fig. 3K). Correspondingly, the *Lmo4* nonexpression areas (intermediate) were larger in the left hemisphere than in the right in the same six tested brains (Fig. 3J) but smaller in the same four tested brains (Fig. 3K). However, we did not detect asymmetric *Lmo4* expression in the posterior cortex between the left-right hemispheres in any of the tested brains (Fig. 3, J and K). Thus, although *Lmo4* expression in mouse cortex was moderately asymmetrical in every individual brain tested so far, it was not consistently lateralized to the right or left

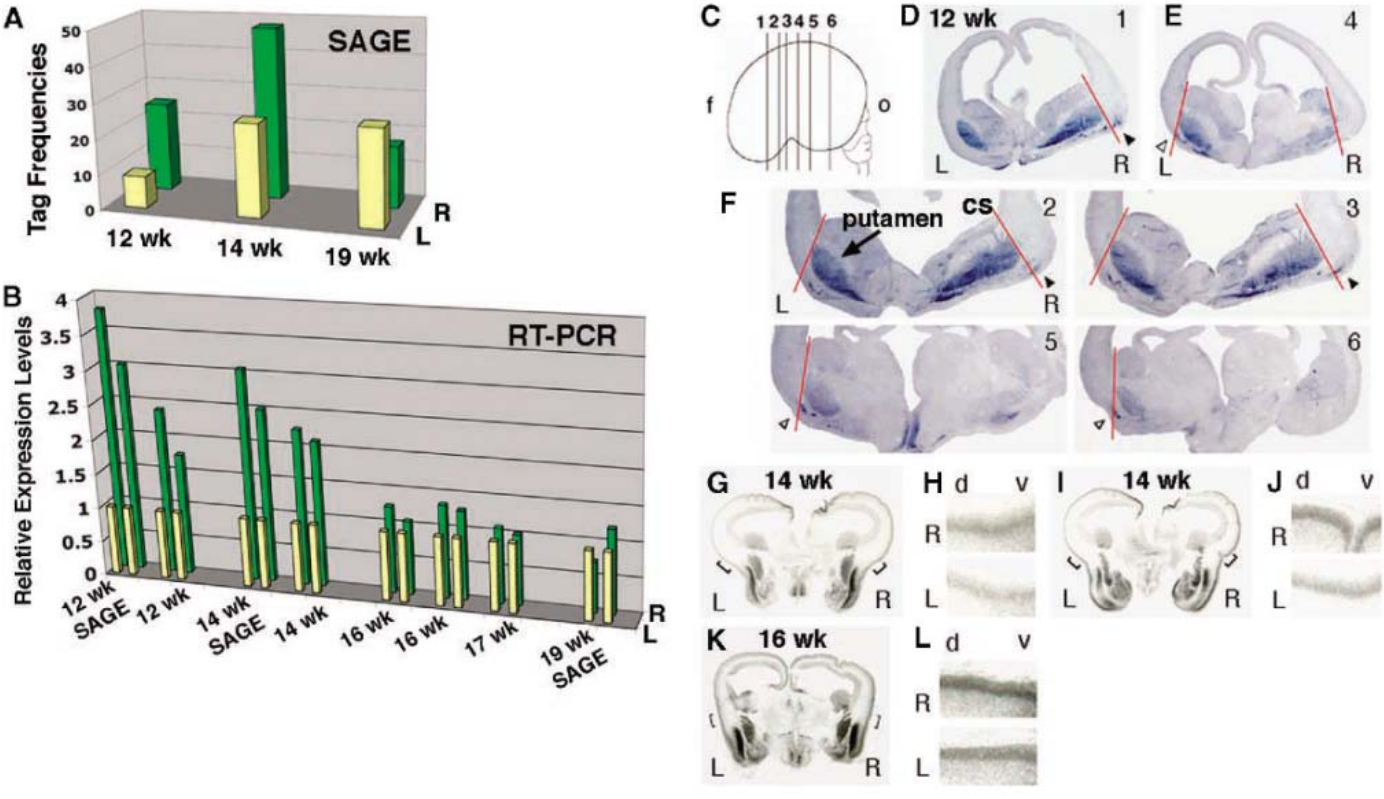

Fig. 2. Human *LMO4* was highly expressed in the right hemisphere as detected by SAGE, real-time RT-PCR, and in situ hybridization. (**A**) The human *LMO4* expression levels in the perisylvian regions measured by SAGE (tag frequencies) in 12-, 14-, and 19-week-old brains. wk, week. (**B**) The *LMO4* expression levels between the left and right hemispheres were verified by real-time RT-PCR in eight human embryonic brains (at 12 to 19 weeks). Two data points from duplicated experiments for each sample are illustrated. (**C** to **F**) *LMO4* expression in coronal sections cut from the frontal (f) to occipital (o) lobes of a human embryonic 12-week-old brain. The medial-lateral extent of *LMO4* expression in the cortical plate between the left (white arrowheads) and right (black arrowheads) hemispheres was defined by a red line connecting the corticostriatal sulcus (cs) and the lateral border of the putamen (arrow). Numbers in (D) through (F) indicate the sections shown in (C), (**G** to **L**). Human *LMO4* was more highly expressed in the cortical plates in the right hemispheres than in the left in coronal sections of [(G) to (J)] a 14-week-old brain and [(K) and (L)] a 16-week-old brain. (H), (J), and (L) show high-power views of selected areas in (G), (I), and (K), respectively. (G) and (I) illustrate two different rostral-caudal levels through the frontal lobe and presumptive perisylvian region. The dorsal (d) and ventral (v) areas of the cortex are labeled.

side. This may relate to behavioral and anatomical studies in mice, in which sensory-motor asymmetries, like paw preference, are observed in individual mice but are not biased on a population level to either the right or left hemisphere, as hand preference is in humans (*10*–*14*). The differences in mice and humans suggest the possibility that paw preference in rodents might reflect an early, perhaps stochastic, developmental asymmetry that is established perinatally, before paw usage, implying a transcriptional asymmetry that is not consistently lateralized to the left and right. Evolution of mechanisms that bias or entrain a modest and random asymmetry in lower organisms may have allowed the development of more consistent functional asymmetries in the human cortex (*15*).

To identify other differentially expressed genes between the left-right hemispheres, we focused on genes showing different expression levels measured by SAGE in the perisylvian regions of human embryonic 12-week-old brains. Using RNA samples for generating SAGE libraries, we verified 76 genes using real-time RT-PCR (tables S6 and S7) and found 39 genes (51%) showing consistent differential expression as measured by SAGE (table S6). To further test the reproducibility of verifying SAGE data, we verified expression levels of these 76 genes using a second 12-week-old brain. We found that 27 genes (36%) consistently showed differential expression (either left^{-high} or left^{-low}) in both brain samples (table S6). We also tested 17 genes that have lower χ values (<1.9) but have been implicated in cortical development and found 7 genes showing relatively significant differences of gene expression levels, although they were not detected by SAGE (table S8).

The left-right differences in *LMO4* expression in humans could potentially reflect either a differing topographic mapping in the two hemispheres or a difference in the tempo of cortical development, with the right hemisphere's development leading over the left. In mice, *Lmo4* expression marks anterior and posterior regions in the mouse cortex and is shifted in cortices of *Pax6* and *Fgf8* mutants, consistent with the suggestion that *Lmo4* expression at P0 to P5 reflects overall cortical topographic mapping (fig. S2). On the other hand, there is some evidence for the appearance of the several cortical sulci and gyri at earlier ages in human right hemisphere than in the left, for instance, the rolandic sulcus (which appears at 17 to 20 weeks) and the superior temporal fissure (at 23 weeks) (*2*, *7*, *16*). Thus, higher *LMO4* expression in the right than the left hemisphere could reflect the arrival of corresponding developmental stages sooner in the right than the left hemisphere. Either model, however, implies molecular events that greatly precede morphological asymmetries and provide potential insight into the mechanism of generation of asymmetry. Furthermore, the molecular events that regulate *LMO4* expression in humans may be secreted molecules, such as FGF8, and/or gradients in transcription factors in the ventricular zone, such as PAX6 and EMX2, as in mice. Indeed, some factors with potential roles in cortical development, such as *ID2* and *NEUROD6,* were asymmetric in SAGE and/or RT-PCR analyses in human embryonic 12-week-old brains (tables S6 and S8). Understanding the factors that regulate *LMO4* expression may ultimately identify earlier events in left-right brain asymmetry. On the other hand, our results generally confirm the earlier suggestion that genes previously implicated in visceral asymmetries are not detectably implicated in cerebral asymmetries (*3*, *17*). For instance, mutations that result in "situs inversus" in humans do not appear to disrupt the left-hemisphere localization of language, mathematical, and hearing abilities and handedness (*18*). Except possibly for the FGF signaling pathway, we did not detect significant differences of expression levels of genes regulating body asymmetry in the human

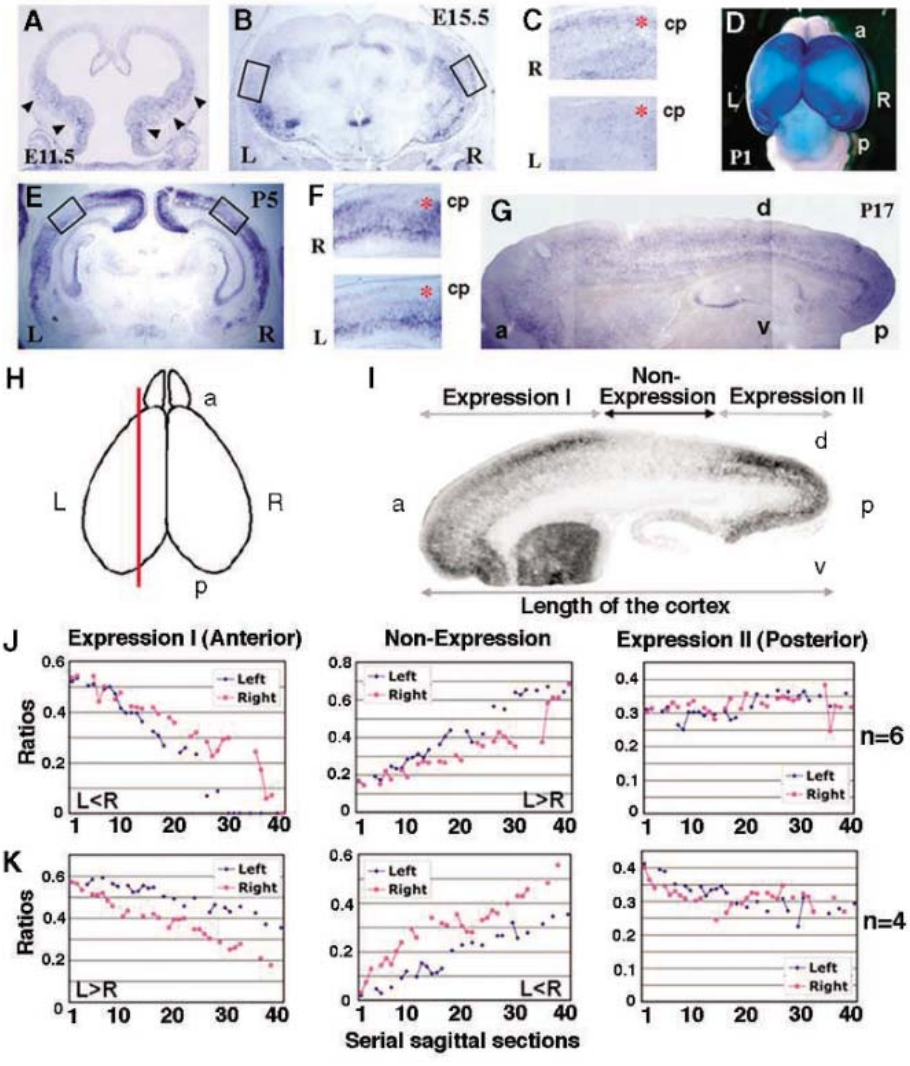

Fig. 3. The dynamic and asymmetric expression of *Lmo4* in mouse brains. (**A** to **F**) The patchy and asymmetric expression patterns of *Lmo4* are illustrated in [(A) to (C)] coronal sections of mouse brains from (A) E11.5 and (B) E15.5; (D) whole mount in situ hybridization from P1; and (E and F) coronal sections of P5 brain. (C) and (F) show high-power views of *Lmo4* expression in the cortical plates (cp) (red stars) in selected areas from (B) and (E), respectively. The dorsal cortex is on the left of (C) and (F). (**G**) *Lmo4* expression appears uniform in the cortical plate in a sagittal section of a P17 brain. (**H**) Schematic view of the forebrain from above, indicating the sagittal section shown in (I). (**I**) *Lmo4* expression was divided into the anterior (a) (Expression I), the posterior (p) (Expression II), and the nonexpression regions in sagittal sections of P1 mouse cortex. The dorsal (d) and ventral (v) areas of the cortex are labeled. (**J** and **K**) Asymmetric expression of *Lmo4* in the left-right hemispheres in representative P1 mouse cortices. The ratio of the size of each domain in the left versus the right hemisphere is plotted for serial sagittal sections. In total, six brains were similar to that in (J) and four brains to that in (K).

embryonic SAGE libraries, although asymmetries at earlier developmental stages cannot be ruled out (*3*, *19*).

Abnormalities of cerebral cortical asymmetry have been reported in a wide array of neuropsychiatric disorders, such as autism, schizophrenia, and dyslexia (*20*–*23*). The presence of early asymmetries in gene transcription in the two cerebral hemispheres thus provides potential pathways through which a number of developmental disorders may ultimately converge on the abnormal development of human cerebral asymmetry.

References and Notes

1. M. C. Corballis, *Behav. Brain Sci.* **26**, 199 (2003).
2. A. M. Galaburda, M. LeMay, T. L. Kemper, N. Geschwind, *Science* **199**, 852 (1978).
3. D. H. Geschwind, B. L. Miller, *Am. J. Med. Genet.* **101**, 370 (2001).
4. A. W. Toga, P. M. Thompson, *Nat. Rev. Neurosci.* **4**, 37 (2003).
5. M. LeMay, A. Culebras, *N. Engl. J. Med.* **287**, 168 (1972).
6. N. Geschwind, W. Levitsky, *Science* **161**, 186 (1968).
7. J. G. Chi, E. C. Dooling, F. H. Gilles, *Arch. Neurol.* **34**, 346 (1977).
8. D. H. Geschwind, B. L. Miller, C. DeCarli, D. Carmelli, *Proc. Natl. Acad. Sci. U.S.A.* **99**, 3176 (2002).
9. R. L. Sidman, P. Rakic, in *Histology and Histopathology of the Nervous System*, W. Haymaker, R. D. Adams, Eds. (C. C. Thomas, Springfield, IL, 1982).
10. F. G. Biddle, C. M. Coffaro, J. E. Ziehr, B. A. Eales, *Genome* **36**, 935 (1993).
11. P. Barneoud, H. Van der Loos, *Proc. Natl. Acad. Sci. U.S.A.* **90**, 3246 (1993).
12. D. R. Riddle, D. Purves, *J. Neurosci.* **15**, 4184 (1995).
13. P. Signore *et al.*, *Physiol. Behav.* **49**, 701 (1991).
14. R. L. Collins, *Brain Res.* **564**, 194 (1991).
15. A. R. Palmer, *Science* **306**, 828 (2004).
16. J. G. Chi, E. C. Dooling, F. H. Gilles, *Ann. Neurol.* **1**, 86 (1977).
17. J. Capdevila, K. J. Vogan, C. J. Tabin, J. C. Izpisua Belmonte, *Cell* **101**, 9 (2000).
18. D. N. Kennedy *et al.*, *Neurology* **53**, 1260 (1999).
19. A. Abu-Khalil, L. Fu, E. A. Grove, N. Zecevic, D. H. Geschwind, *J. Comp. Neurol.* **474**, 276 (2004).
20. M. R. Herbert *et al.*, *Brain* **128**, 213 (2005).
21. P. Falkai *et al.*, *Schizophr. Res.* **7**, 23 (1992).
22. K. Hugdahl *et al.*, *Scand. Audiol. Suppl.* **49**, 26 (1998).
23. A. M. Galaburda, M. T. Menard, G. D. Rosen, *Proc. Natl. Acad. Sci. U.S.A.* **91**, 8010 (1994).

24. We thank Y. F. Chen, J. Meschter, V. Petkova, and P. Grosu for technical support; S. Blackshaw, K. Polyak, and E. Fox for advice on SAGE; R. Vigorito, R. Johnson, and B. Poulos at the NIH-funded Brain and Tissue Banks; S. Dymecki for supplying *Pax6* mutant brains; and E. Meyers and G. Martin for *Fgf8* mutant brains. Supported by the McKnight Endowment Foundation, National Institute of Neurological Disorders and Stroke grant nos. RO1 R37 NS35129 (C.A.W.) and MH60233 (D.H.G.), and the James S. McDonnell Foundation (D.H.G.). T.S. is supported by an Advanced Postdoctoral Fellowship from the National Multiple Sclerosis Society and an NIH training grant from the Children's Hospital, Boston. S.H.O. and C.A.W. are Investigators of the Howard Hughes Medical Institute.

Supporting Online Material

www.sciencemag.org/cgi/content/full/1110324/DC1
Materials and Methods
Figs. S1 and S2
Tables S1 to S26
References and Notes

27 January 2005; accepted 12 April 2005
Published online 12 May 2005;
10.1126/science.1110324
Include this information when citing this paper.

Complementary Process to Response Bias in the Centromedian Nucleus of the Thalamus

Takafumi Minamimoto,* Yukiko Hori, Minoru Kimura†

Activity in several areas of the human brain and the monkey brain increases when a subject anticipates events associated with a reward, implicating a role for bias of decision and action. However, in real life, events do not always appear as expected, and we must choose an undesirable action. More than half of the neurons in the monkey centromedian (CM) thalamus were selectively activated when a small-reward action was required but a large-reward option was anticipated. Electrical stimulation of the CM after a large-reward action request substituted a brisk performance with a sluggish performance. These results suggest involvement of the CM in a mechanism complementary to decision and action bias.

When a large reward is expected as a result of a particular action, animals tend to choose this action more frequently than other alternatives (*1*, *2*). Animals that expect a reward carry out these activities quickly and with few errors (*3*–*5*). Studies have been undertaken to understand the neural correlates of decision-makers that assess the reward value of response options and set a "bias" to produce a particular response. Single-neuron activity reflects an expected reward and a schedule to obtain a reward in the cerebral cortex (*6*–*10*) and in the basal ganglia (*3*, *5*, *11*). Midbrain dopamine neurons transmit error of reward expectation (*12*–*14*) and motivation to action (*13*, *15*) to the striatum, limbic system, and cerebral cortex. On the other hand, the traditional models of how actions are produced may be fundamentally incomplete as the basis of goal-directed action mechanisms, because response bias is sometimes aborted when events do not occur as expected. Thus, an additional component, which plays complementary roles to response bias, seems to be required. Through both response bias and its complementary process, animals seem to be able to attain their final goals. However, the neural basis of this process has not been elucidated.

The centromedian/parafascicular (CM/PF) complex of the thalamus (*16*) has received little attention in studies of action and cognition, even though it has close connections to the basal ganglia and cerebral frontal cortex (*16*–*20*). Neurons in the monkey CM/PF complex respond to multimodal stimuli. Characteristically, the magnitude of a response is larger when the stimulus is unpredictable and contrary to expectation (*20*, *21*). This is in contrast to the basal ganglia, where signals of reward expectation are dominantly represented (*3*, *5*, *11*, *22*). Based on the complementary nature of neuronal activity between the CM/PF and the basal ganglia, it has been hypothesized that the CM/PF complements decision and action bias through the thalamostriatal projection and corticobasal ganglia loops (*21*, *23*). This study was designed to test this hypothesis, with special emphasis placed on the action-related CM neurons.

Two macaque monkeys (SJ and MA) were trained to perform GO-NOGO tasks in which visual stimuli asking for the GO or the NOGO actions appeared at an average probability of 0.5 (*24*). Performance of either the requested GO or NOGO action was rewarded by a large amount of water (+R), whereas the performance of the other action was rewarded with a small amount of water (−R) during a block of 60 to 120 trials. The action-reward association was then altered in the subsequent block (Fig. 1, A and B). Monkeys performed the large-reward GO trials more briskly than the small-reward trials. Average reaction times in the GO(+R) condition were shorter than those in the GO(−R) condition by 253 ms in monkey SJ (unpaired t test, $P < 0.0001$, 95% confidence interval (CI) 237 to 268 ms) and 89 ms in monkey MA ($P < 0.0001$, 95% CI 83 to 93 ms) (Fig. 1C). Movement times were shorter in the GO(+R) than in the GO(−R) condition by about 20 ms in both monkeys. Furthermore, the rate of error trials, such as reaction times that were too long (>3000 ms) or the initiation of incorrect actions, was higher in the small-reward trials (monkey SJ, GO trials, $P = 0.006$, 95% CI 0.34% to 1.91%; NOGO trials, $P = 0.023$, 95% CI 0.26% to 3.37%) (monkey MA, NOGO trials, $P = 0.002$, 95% CI 1.78% to 6.33%; GO trials, monkey made no error in +R or –R conditions).

The activity of 56 neurons (40 in monkey SJ and 16 in monkey MA) was recorded. The neurons showed burst discharges after un-

Department of Physiology, Kyoto Prefectural University of Medicine, Kawaramachi-Hirokoji, Kamigyo-ku, Kyoto 602-8566, Japan.

*Present address: Laboratory of Neuropsychology, National Institute of Mental Health, National Institutes of Health, Bethesda, MD 20892, USA.

†To whom correspondence should be addressed. E-mail: mkimura@koto.kpu-m.ac.jp

expected auditory and visual stimuli of long latencies that corresponded to previously described long-latency-facilitation (LLF)–type neurons (*20*, *21*); these neurons were primarily CM neurons (*24*). LLF neurons were activated by GO and NOGO requests, but the magnitude of their activation was much higher during the small-reward trials than during the large-reward trials, as shown in Fig. 2A. Although strong neuronal activation occurred in GO(−R) trials that were performed at longer reaction times than in GO(+R) trials, very long reaction-time trials were not always accompanied by markedly increased neuronal activation in the GO(−R) trial block (* in Fig. 2B). The activity in all recorded LLF neurons was markedly enhanced during small-reward conditions in both the GO and NOGO trials (Fig. 2C). Thirty-four of the 56 neurons (61%) showed a significant main effect of reward condition [two-way ANOVA; +R or −R, $P < 0.01$, variance explained by reward factor = 0.11 ± 0.04 (mean ± SD)] (*24*); of these, 33 were –R condition-selective. Thus, we concluded that LLF neurons were selectively activated when an action that was associated with a smaller reward between the two alternatives was requested and performed. Although neuronal activation occurred with a long latency (~300 to 450 ms) (table S1) after the GO(−R) request, it still preceded muscle activation (fig. S2) and sluggish release of the hold button by 162 ± 87 ms (mean ± SD) (Fig. 2D).

We next asked whether the expectation of a large reward modified LLF neuron activity. Another monkey (HD) was trained in a single block of trials in which GO(+R) and NOGO(−R) trials occurred at a ratio of 1:2. Thus, NOGO(−R) trials occurred more frequently and could repeat, although no more than three times. In this version of the task, the correct performance rate of NOGO(−R) trials increased significantly, with the number of trials since the last rewarded trial [post-reward trial number (PRN)] increasing from 1 to 3 [$F_{(2,\ 66)} = 25.0$, $P < 0.0001$, variance explained = 0.43] (Fig. 3A). There was also a significant shortening in the time to depression of the hold button to the start of each trial as the PRN increased [$F_{(2,\ 2525)} = 1026.7$, $P < 0.0001$, variance explained = 0.45], which suggests that the monkey's expectation of the reward trial had gradually increased. Correspondingly, neuronal activation during the NOGO(−R) trials increased in magnitude as the PRN increased (Fig. 3B). During the GO(+R) trials, small activations occurred with no clear dependency on the PRN (Fig. 3C). These results confirmed that neuronal activation was greater when the large-reward option was expected at higher probability. Furthermore, even in the NOGO(−R) trial, almost no activation occurred if the monkey released the hold button before the end of the hold period (Fig. 3B, Error). Thus, the critical nature of the activity was its specificity for the small-reward action and for pursuing the requested action.

Selective neuronal activation occurred after the GO(−R) request when the monkeys were expecting a GO(+R) request. This finding raised the question of whether artificial activation of the CM after a GO request could trigger the complementary process of the GO-action bias. If so, the activation effect would be expected to occur dominantly after a GO(+R) request. To answer this question, current pulses were delivered through microelectrodes at 300 to 400 ms after the GO request, when LLF neurons would have been activated after the GO(−R) request. One-eighth to one-half of the GO trials were randomly selected for stimulation. Following stimulation after the GO(+R) request, release of the hold button and depression of the target button was often much slower compared with the trials that took place without stimulation (Fig. 4A). At times, stimulation arrested the initiated GO action before the monkey reached the target button (* in Fig. 4A). In all of the 6 stimulated trials (5 blue filled circles in Fig. 4B and 1 arrest trial, not shown), the reaction and movement times were longer than the mean + 2 SD of the 27 trials that did not include stimulation (open circles). The effective stimulation rate (ESR) (*24*) was thus 100% (6 out of 6). The ESRs were significantly higher in the GO(+R) compared

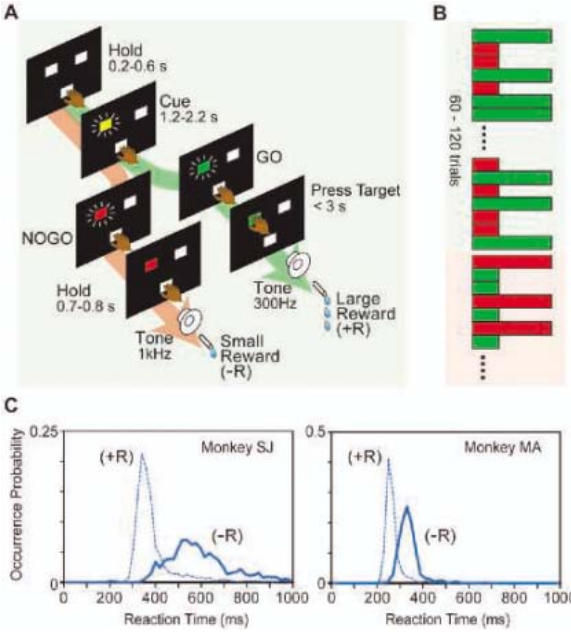

Fig. 1. Behavioral paradigm and monkey's performance. (**A**) Sequence of events in the GO-NOGO lever-release task in which the GO trials were followed by a greater reward (+R) than in the NOGO trials (–R). (**B**) Schemes for performance of the GO (green) and NOGO (red), large-reward (long bars) and small-reward (short bars) trials in a block of trials and their alternation in the next block. (**C**) Distribution of reaction times after a GO request under large-reward and small-reward conditions in two monkeys.

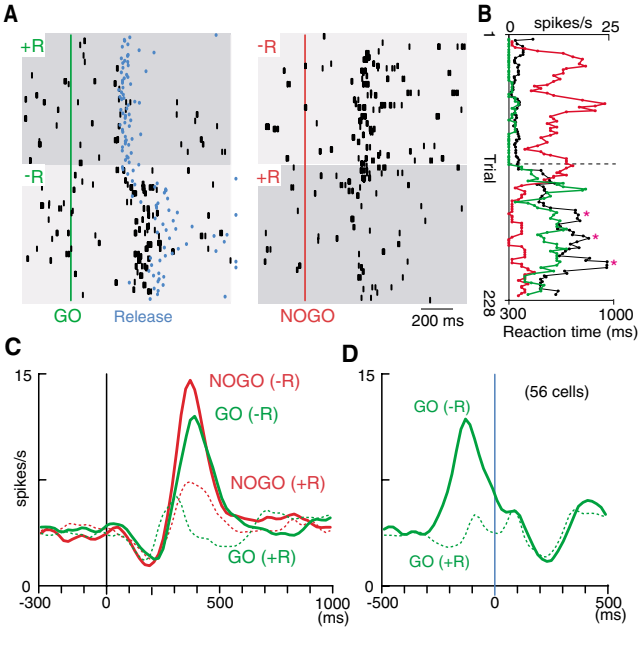

Fig. 2. Selective activation of LLF neurons during performance of a small-reward action. (**A**) The raster displays of spikes of a CM neuron (dark dots) are represented in order of occurrence of trials from top to bottom during two consecutive blocks of trials with different action-reward associations. Blue dots indicate the time of hold-button release. (**B**) Five-trial averages of neuronal activity during GO (green) and NOGO trials (red) and the reaction times in the GO trials (black). Asterisks indicate especially long reaction-time trials. (**C**) Ensemble average histograms of the activity of 56 LLF neurons before and after the GO or NOGO request (time 0). (**D**) Same as (C), except the activity was centered on hold-button release in the GO trials (time 0). The histograms were smoothed by Gaussian kernel (SD = 20 ms). Bin size is 20 ms.

with the GO(−R) trials (paired t test, $P = 0.012$, 95% CI 7.1% to 41.5%) (Fig. 4C). The average ESRs were significantly higher within the CM (mean ± SD, 62.4 ± 30.2%, $n = 16$) than outside the CM (37.9 ± 26.8%, $n = 28$) (unpaired t test, $P = 0.008$) (Fig. 4D). The effective sites were concentrated within the CM except for two, one of which was in the dorsal border of the dorsolateral parafascicular nucleus and the other of which was in the mediodorsal nucleus (MD). Thus, the effects of CM stimulation are consistent with characteristics of neuronal activity and support the hypothesis that the CM plays a complementary function to response bias.

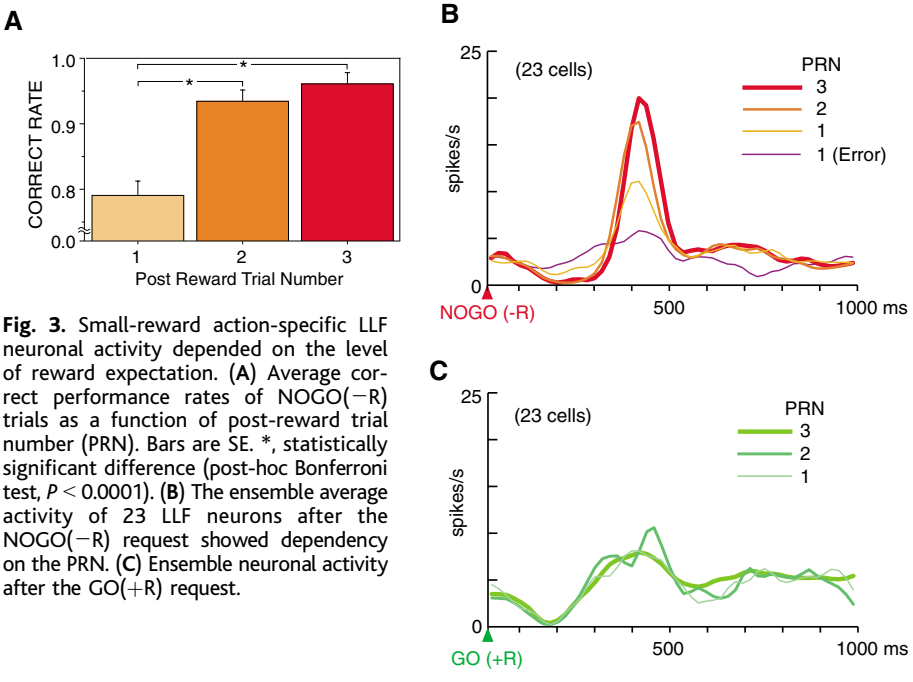

Fig. 3. Small-reward action-specific LLF neuronal activity depended on the level of reward expectation. (**A**) Average correct performance rates of NOGO(−R) trials as a function of post-reward trial number (PRN). Bars are SE. *, statistically significant difference (post-hoc Bonferroni test, $P < 0.0001$). (**B**) The ensemble average activity of 23 LLF neurons after the NOGO(−R) request showed dependency on the PRN. (**C**) Ensemble neuronal activity after the GO(+R) request.

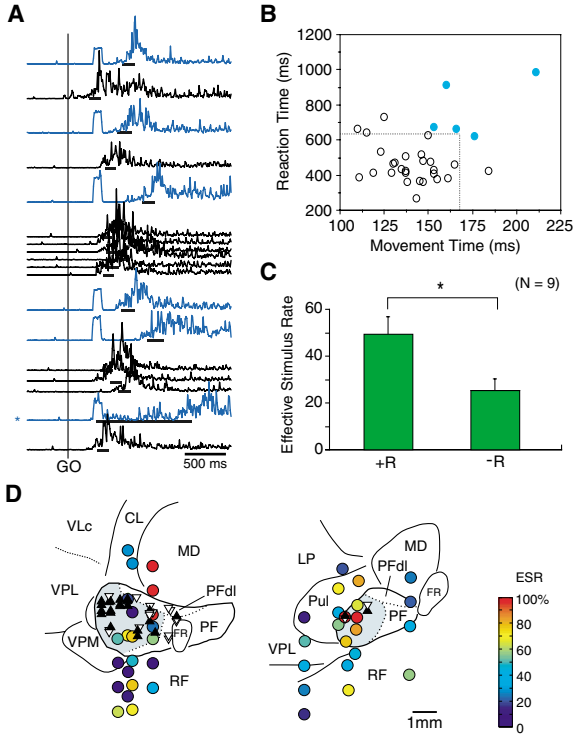

Fig. 4. Effects of electrical stimulation in and around the CM on task performance. (**A**) EMG traces of the flexor carpi ulnaris muscle during the large-reward GO trials with (blue) and without (dark) electrical stimulation (60 μA). The length of the lines beneath the traces indicates the time from release of the hold button to depression of the target button (movement time). *, trial with arrest. (**B**) Scatter plot of reaction and movement times of GO reaction with (filled blue circles) and without (dark open circles) stimulation. Dotted lines indicate the mean + 2 SD of the reaction and movement times. The arrest trial is not shown. (**C**) Average effective stimulation rates (ESRs) during large-reward (+R) and small-reward (−R) conditions. *, statistically significant difference (paired t test, $P < 0.05$). (**D**) Recording sites (triangles) and stimulation sites (circles) of neurons in monkey SJ. Filled triangles denote the location of neurons selectively activated during a small-reward condition. ESRs at the stimulation sites are color coded. CL, centrolateral nucleus; FR, fasciculus retroflexus; LP, lateral posterior nucleus; MD, mediodorsal nucleus; PF, parafascicular nucleus; PFdl, dorsolateral parafascicular nucleus; Pul, pulvinar; RF, reticular formation; VLc, ventrolateral nucleus caudal part; VPL, ventral posteriolateral nucleus; VPM, ventral posteriomedial nucleus.

Our data showed that LLF neurons were selectively activated when monkeys were forced to perform a small-reward action and that electrical activation of the CM region after a large-reward action request substituted brisk for sluggish task performance. Can these results be explained by assuming that the CM inhibits action and thus lengthens reaction time? The magnitude of neuronal activation was not monotonically related to reaction times (*24*), although it was proportional to the level of expectation of a large-reward option, which reflected response bias. Furthermore, the effectiveness of electrical activation of the CM on task performance was greater after a large-reward action request than after a small-reward action request. These additional observations do not support a general inhibitory role of the CM on action. However, they do suggest that the CM specifically participates in abolishing bias of the large-reward option of action and in pursuing the requested small-reward action, which is complementary to the response bias.

Our findings are consistent with previous reports (*20*, *21*) that showed that the magnitude of CM/PF neuron activation was larger when the stimuli were unpredictable or contrary to expectation. Although we have only limited knowledge about the network mechanisms that influence the characteristic activity of CM neurons, the basal ganglia (*16*, *19*, *20*) and cerebral cortex (*16*–*18*) likely play crucial roles. The cortico-basal ganglia-thalamocortical system may supply the CM with information about response bias (*3*, *11*), whereas information related to discrepancies in desirability between expected and actual options may be processed through their interaction with cortical areas that have been implicated in conflict monitoring, such as the anterior cingulate cortex (*10*, *25*). In other words, action- and cognition-related information in the cerebral cortex appears to be transformed in two contrasting ways through the cortico-basal ganglia loops: One way sets the bias with help from midbrain dopamine signals, whereas the other complementary process to the response bias might be mediated by signals transmitted by CM efferents.

References and Notes

1. E. L. Thorndike, *Animal Intelligence: An Experimental Study of the Associative Processes in Animals* (Macmillan, New York, 1898).
2. R. J. Herrnstein, *J. Exp. Anal. Behav.* **4**, 267 (1961).
3. J. Lauwereyns, K. Watanabe, B. Coe, O. Hikosaka, *Nature* **418**, 413 (2002).
4. M. Watanabe *et al.*, *Exp. Brain Res.* **140**, 511 (2001).
5. M. Shidara, T. G. Aigner, B. J. Richmond, *J. Neurosci.* **18**, 2613 (1998).
6. M. L. Platt, P. W. Glimcher, *Nature* **400**, 233 (1999).
7. L. P. Sugrue, G. S. Corrado, W. T. Newsome, *Science* **304**, 1782 (2004).
8. M. R. Roesch, C. R. Olson, *Science* **304**, 307 (2004).
9. M. I. Leon, M. N. Shadlen, *Neuron* **24**, 415 (1999).
10. M. Shidara, B. J. Richmond, *Science* **296**, 1709 (2002).
11. W. Schultz, *Nat. Rev. Neurosci.* **1**, 199 (2000).
12. W. Schultz, P. Dayan, P. R. Montague, *Science* **275**, 1593 (1997).

13. T. Satoh, S. Nakai, T. Sato, M. Kimura, *J. Neurosci.* **23**, 9913 (2003).
14. H. Nakahara, H. Itoh, R. Kawagoe, Y. Takikawa, O. Hikosaka, *Neuron* **41**, 269 (2004).
15. P. Redgrave, T. J. Prescott, K. Gurney, *Trends Neurosci.* **22**, 146 (1999).
16. M. Steriade, E. G. Jones, C. D. McCormick, in *Thalamus*, M. Steriade *et al.*, Eds. (Elsevier Science, Oxford, 1997), vol. 1, pp. 55–73.
17. H. J. Groenewegen, H. W. Berendse, *Trends Neurosci.* **17**, 52 (1994).
18. N. Hatanaka *et al.*, *J. Comp. Neurol.* **462**, 121 (2003).
19. Y. Smith, D. V. Raju, J. F. Pare, M. Sidibe, *Trends Neurosci.* **27**, 520 (2004).
20. N. Matsumoto, T. Minamimoto, A. M. Graybiel, M. Kimura, *J. Neurophysiol.* **85**, 960 (2001).
21. T. Minamimoto, M. Kimura, *J. Neurophysiol.* **87**, 3090 (2002).
22. A. M. Graybiel, T. Aosaki, A. W. Flaherty, M. Kimura, *Science* **265**, 1826 (1994).
23. M. Kimura, T. Minamimoto, N. Matsumoto, Y. Hori, *Neurosci. Res.* **48**, 355 (2004).
24. Materials and methods are available as supporting material on *Science* Online.
25. M. Botvinick, L. E. Nystrom, K. Fissell, C. S. Carter, J. D. Cohen, *Nature* **402**, 179 (1999).
26. We thank B. J. Richmond, H. Yamada, and K. Samejima for their helpful comments and R. Sakane for her technical assistance. This study was supported by a grant in aid from the Ministry of Education, Culture, Sports, Science, and Technology of Japan (MEXT).

Supporting Online Material
www.sciencemag.org/cgi/content/full/308/5729/1798/DC1
Materials and Methods
SOM Text
Figs. S1 to S3
Table S1
References

27 December 2004; accepted 6 April 2005
10.1126/science.1109154

A Mutation in the *TRPC6* Cation Channel Causes Familial Focal Segmental Glomerulosclerosis

Michelle P. Winn,[1,2]* Peter J. Conlon,[4] Kelvin L. Lynn,[5] Merry Kay Farrington,[1,2] Tony Creazzo,[3] April F. Hawkins,[1] Nikki Daskalakis,[1,2] Shu Ying Kwan,[2] Seth Ebersviller,[2] James L. Burchette,[5] Margaret A. Pericak-Vance,[1,2] David N. Howell,[5] Jeffery M. Vance,[1,2]* Paul B. Rosenberg[1]*

Focal and segmental glomerulosclerosis (FSGS) is a kidney disorder of unknown etiology, and up to 20% of patients on dialysis have been diagnosed with it. Here we show that a large family with hereditary FSGS carries a missense mutation in the *TRPC6* gene on chromosome 11q, encoding the ion-channel protein transient receptor potential cation channel 6 (TRPC6). The proline-to-glutamine substitution at position 112, which occurs in a highly conserved region of the protein, enhances TRPC6-mediated calcium signals in response to agonists such as angiotensin II and appears to alter the intracellular distribution of TRPC6 protein. Previous work has emphasized the importance of cytoskeletal and structural proteins in proteinuric kidney diseases. Our findings suggest an alternative mechanism for the pathogenesis of glomerular disease.

Focal and segmental glomerulosclerosis (FSGS) is an important cause of end-stage renal disease worldwide, and up to one-fifth of dialysis patients have been diagnosed with it (*1*, *2*). The prevalence of FSGS is increasing yearly, and the incidence is particularly high in the black population (*1*, *3*). FSGS is a pathological entity in which the glomerulus is primarily targeted. Typical manifestations of FSGS include proteinuria, hypertension, renal insufficiency, and eventual kidney failure. Our understanding of the pathogenesis of FSGS is incomplete, and there are no consistently effective treatments.

Analysis of disease-causing mutations in hereditary FSGS and congenital nephrotic syndromes has provided new insights into the pathogenesis of nephrotic syndrome. The previous identification of at least three genes causing familial FSGS and hereditary nephrotic syndromes underscores the substantial genetic heterogeneity in this disorder (*4*–*6*). These studies have highlighted the importance of abnormalities in the podocyte and the slit

[1]Department of Medicine, [2]Center for Human Genetics, [3]Department of Pediatrics, Duke University Medical Center, Durham, NC 27710, USA. [4]Department of Nephrology, Beaumont Hospital, Dublin, Ireland. [5]Department of Nephrology, Christchurch Hospital, Christchurch, New Zealand. [5]Department of Pathology, Duke University Medical Center and Durham VA Medical Center, Durham, NC 27710, USA.

*To whom correspondence should be addressed. E-mail: michelle.winn@duke.edu (M.P.W.); jeff@chg.duhs.duke.edu (J.M.V.); rosen029@mc.duke.edu (P.B.R.)

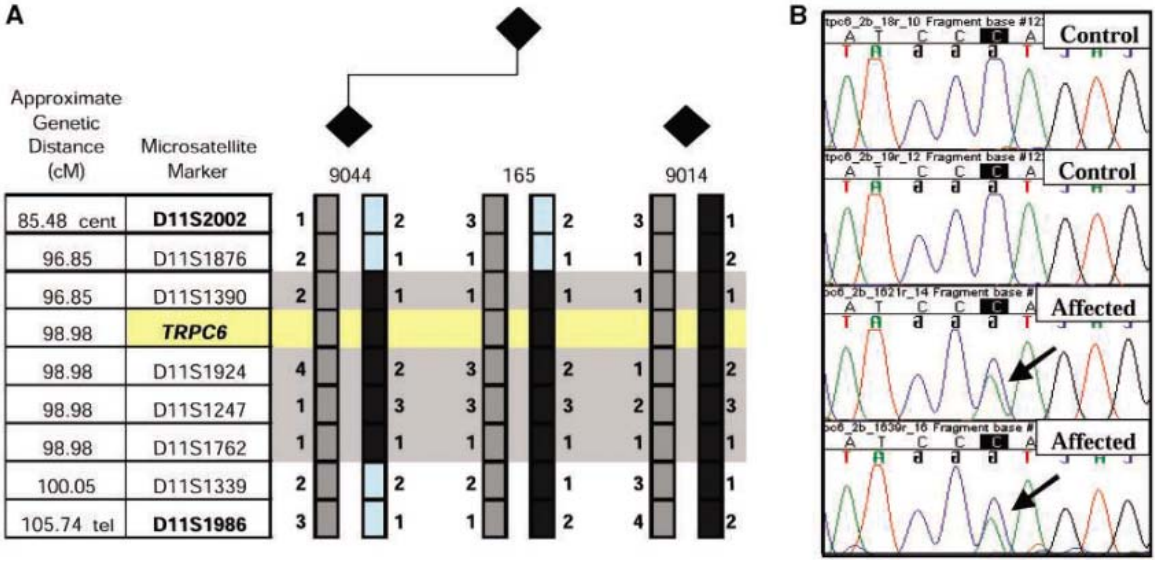

Fig. 1. (**A**) Minimal candidate region (MCR) of FSGS on human chromosome 11q. The area of interest is flanked by markers D11S1876 and D11S1339. The genetic distance from the centromere (cent) was obtained from http://genome.cse.ucsc.edu. Black squares indicate common alleles among affected individuals. Blue squares indicate recombination. Gray squares are alleles inherited from the nonaffected parent. Individual 165 is the parent of individual 9044. Individual 9014 provides an example of the ancestral affected haplotype. All individuals represented are affected. The MCR is defined by individual 9044. Microsatellite markers in bold indicate original flanking markers. The horizontal gray box (including *TRPC6* in yellow) indicates the candidate gene region. tel, telomere. (**B**) Sequence chromatogram of exon 2 of *TRPC6*. The arrows highlight the C/A mutation.

diaphragm of the glomerulus in the development of the severe proteinuria that characterizes the nephrotic syndrome.

Previously, we identified and characterized a large New Zealand family of British origin who have autosomal dominant hereditary FSGS (fig. S1) (*7*). The character of the disease in this family is particularly aggressive. Affected individuals typically present with high-grade proteinuria in their third or fourth decade, and approximately 60% progress to end-stage renal disease (ESRD). The average time between initial presentation and the development of ESRD is 10 years. A genomic screen performed on this kindred localized the disease-causing mutation to chromosome 11q (*8*).

Haplotype analyses reduced the minimal candidate region to an approximate 2.1-centimorgan (cM) area defined by critical recombination events at D11S1390 and D11S1762 (Fig. 1A). This region contains several known genes as well as multiple novel and predicted genes, which were systematically screened for mutations by direct sequencing. After examination of 42 other candidate genes, *transient receptor potential cation channel 6* (*TRPC6*) (GenBank accession number NP_004612) emerged as a candidate on the basis of reports of detection of *TRPC6* mRNA in the kidney (*9*, *10*). We therefore sequenced each of the 13 exons of the *TRPC6* gene, along with their intron/exon boundaries. Primer sequences are provided (table S1). As shown in Fig. 1B, we discovered a missense mutation (C335A) in exon 2 from affected individuals, causing a proline-to-glutamine substitution at position 112 (P112Q) within the first ankyrin repeat of the *TRPC6* protein. This variant was present in all of the affected individuals (20 affected; 1 probably affected) in our kindred, and there were no nonpenetrant carriers. The change was not found in any of the public databases of single-nucleotide polymorphisms. Furthermore, we found no evidence of the substitution in 614 chromosomes screened from a group of Caucasian controls without known renal disease, 33 of whom were from New Zealand. The allele frequencies from all markers used for linkage in this kindred and from the New Zealand controls are similar to those from the other Caucasian controls. Pro^{112} is highly conserved in evolution and is present in TRPC protein homologs from multiple species (fig. S2).

Our previous finding that familial FSGS does not recur in affected patients after renal transplantation indicates a critical role for the kidney in disease pathogenesis (*11*). Although expression of *TRPC6* mRNA has been reported in multiple tissues, including the kidney, its distribution in the kidney is not clear (*9*, *10*). Therefore, to define the spatial distribution of *TRPC6* protein expression in the human kidney, we performed immunohistochemistry of normal human renal cortex tissue with a rabbit antibody raised against a specific human *TRPC6* peptide (Fig. 2, A and B). Immunofluorescence staining revealed *TRPC6* expression throughout the kidney in glomeruli and tubules. This is consistent with a recent study detecting *TRPC6* mRNA in isolated glomeruli (*12*). The expression of *TRPC6* in glomeruli is particularly noteworthy because abnormal podocyte function appears to be a final common pathway in a variety of proteinuric kidney diseases (*13*). To verify these immunofluorescence findings, we carried out fluorescence in situ hybridization (FISH) in human kidney sections (Fig. 2, C to F). These studies confirmed diffuse expression of *TRPC6* mRNA in glomeruli and tubules in a pattern that is virtually identical to that seen with staining for antibody to *TRPC6*.

To determine the effect of the P112Q mutation on *TRPC6* function, we studied human embryonic kidney (HEK) 293 cells transfected with mutant ($TRPC6^{P112Q}$) or wild-type (WT) *TRPC6* (*14*). The WT *TRPC6* was cloned from a human kidney cDNA library. On Western blots, the abundance and mobility of the P112Q mutant were comparable to those of WT *TRPC6* (fig. S3). Diacylglycerol (DAG) is a potent activator of *TRPC6* (*15*). We therefore measured the intracellular calcium concentration ($[Ca^{+2}]_i$) using Fura fluorescence in HEK 293 cells expressing either the WT *TRPC6* or $TRPC6^{P112Q}$ after exposure to the DAG analog OAG (1-oleoyl-2-acetyl-sn-glycerol). OAG perfusion increased late Ca^{+2} transients in cells transfected with WT *TRPC6* as expected (Fig. 3A and fig. S4). Peak intracellular concentrations were significantly higher in cells expressing $TRPC6^{P112Q}$ as compared with WT controls ($[Ca^{2+}]_i$ of $TRPC6^{P112Q}$ = 181 ± 25 nM versus $[Ca^{2+}]_i$ of WT *TRPC6* = 106 ± 15 nM; $P < 0.05$).

Angiotensin II, acting through its AT1 receptor, plays a critical role in the generation of proteinuria and in the progression of kidney injury in a number of kidney diseases, including FSGS (*16*). AT1 receptors, coupled to heterotrimeric guanine nucleotide–binding proteins (G proteins), activate phospholipase C–β (PLC-β) isoforms that hydrolyze phosphatidylinositol 4,5-bisphosphate (PIP_2). This triggers the production of inositol 1,4,5-

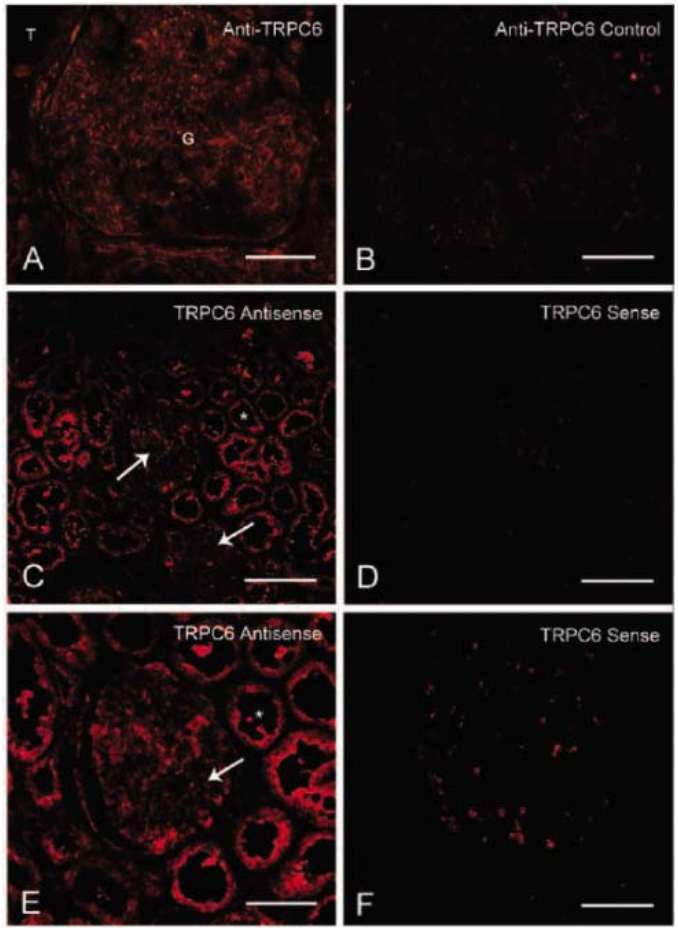

Fig. 2. Immunofluorescence staining and FISH of normal human renal cortical tissue for *TRPC6*. (**A**) Immunofluorescent staining of normal human renal cortical tissue with rabbit antibody against human *TRPC6*. In this representative photomicrograph, specific staining within a glomerulus (G) and the epithelium of surrounding tubules (T) is easily seen. (**B**) Negative control of an adjacent section also stained with the primary antibody to TRPC6 in the presence of the immunizing peptide. There is minimal nonspecific staining. Scale bars in (A) and (B), 25 μm. [(C) and (E)] FISH of *TRPC6* mRNA in normal human renal cortex. (**C**) *TRPC6* antisense probe generated from nucleotides 2301 to 3621 from *TRPC6* mRNA (GenBank accession number AJ006276). (**D**) Hybridization with the corresponding *TRPC6* sense probe. Scale bar, 90 μm. (**E** and **F**) High-power photomicrographs of the same sense and antisense probes. Scale bar, 40 μm. Widespread expression of *TRPC6* mRNA was detected throughout the kidney in both glomeruli and tubular epithelia. Background staining in (D) and (F) reflects autofluorescence from red blood cells trapped at the time of kidney harvest. Arrows highlight glomeruli. Asterisks are centered in renal tubules.

trisphosphate ($InsP_3$), and DAG releases internal calcium stores and activates Ca^{+2} entry (*17*). We examined whether the P112Q mutation would affect angiotensin II–dependent (that is, receptor-operated) calcium signaling. HEK 293 cells were cotransfected with the AT1 receptor (AT–yellow fluorescent protein) and with either WT *TRPC6* or *TRPC6*^{P112Q}. $[Ca^{+2}]_i$ changes were measured after exposure to angiotensin II (Fig. 3B and fig. S5). As in the OAG experiments, the peak angiotensin II–stimulated $[Ca^{+2}]_i$ was higher in cells expressing the mutant protein as compared with WT controls ($[Ca^{2+}]_i$ *TRPC6*^{P112Q} = 640 ± 66 nM versus $[Ca^{2+}]_i$ WT *TRPC6* = 357 ± 46 nM; $P < 0.05$).

To examine the effects of the P112Q mutation on ion flux, we measured current using the whole-cell patch-clamp technique (Fig. 3C). After patch break, HEK 293 cells expressing WT *TRPC6* or *TRPC6*^{P112Q} channels were held at –60 mV for the duration of the experiment. In normal Na^+ extracellular solution, we detected large inward currents in cells transfected with WT *TRPC6*. These currents were significantly increased in cells transfected with the mutant *TRPC6*^{P112Q} protein (WT *TRPC6* = 1.03 ± 0.23 nA versus *TRPC6*^{P112Q} = 4.21 ± 0.10 nA; $P = 0.02$). The addition of uridine triphosphate (UTP), carbachol, or angiotensin II augmented the inward currents in cells expressing WT *TRPC6* or *TRPC6*^{P112Q}. However, the magnitude of the agonist-stimulated current was two to three times greater in cells transfected with mutant than with WT *TRPC6* protein. Control green fluorescent protein–transfected cells showed no appreciable UTP current in comparison to the *TRPC6* transfected cells. The enhanced UTP currents established at baseline and after stimulation with $G_q/11$ agonist support the Ca^{+2} measurements found in our Fura-2 experiments. Thus, the results of the $[Ca^{+2}]_i$ measurements, along with whole-cell current recordings using both endogenous (P2Y2; UTP) and ectopically expressed (AT1R; Ang-2) G_q receptors for *TRPC6* WT and mutant channels, indicate that the P112Q mutation in *TRPC6* causes a gain of function. Ca^{+2} entry is enhanced and is particularly exaggerated in response to G-protein agonists such as angiotensin II.

We also evaluated the subcellular localization of the mutant *TRPC6* protein by surface biotinylation experiments (Fig. 3D). A greater fraction of the mutant protein was associated with the plasma membrane as compared with the WT protein (densitometry measurements were as follows: WT *TRPC6* = 1210.33 versus *TRPC6*^{P112Q} = 23126.67 units; $P = 0.05$). In control experiments, no difference was found in the surface expression of the transferrin receptor (TfR) in cells transfected with either WT *TRPC6* or *TRPC6*^{P112Q}. Our findings are in accordance with reports by others (*18*, *19*). This enhanced cell surface expression of *TRPC6*^{P112Q} protein suggests a mechanism of exaggerated calcium signaling and flux.

Mutations in several other proteins have been identified in familial nephrotic syndrome and hereditary FSGS. Nephrin (*NPHS1*), the

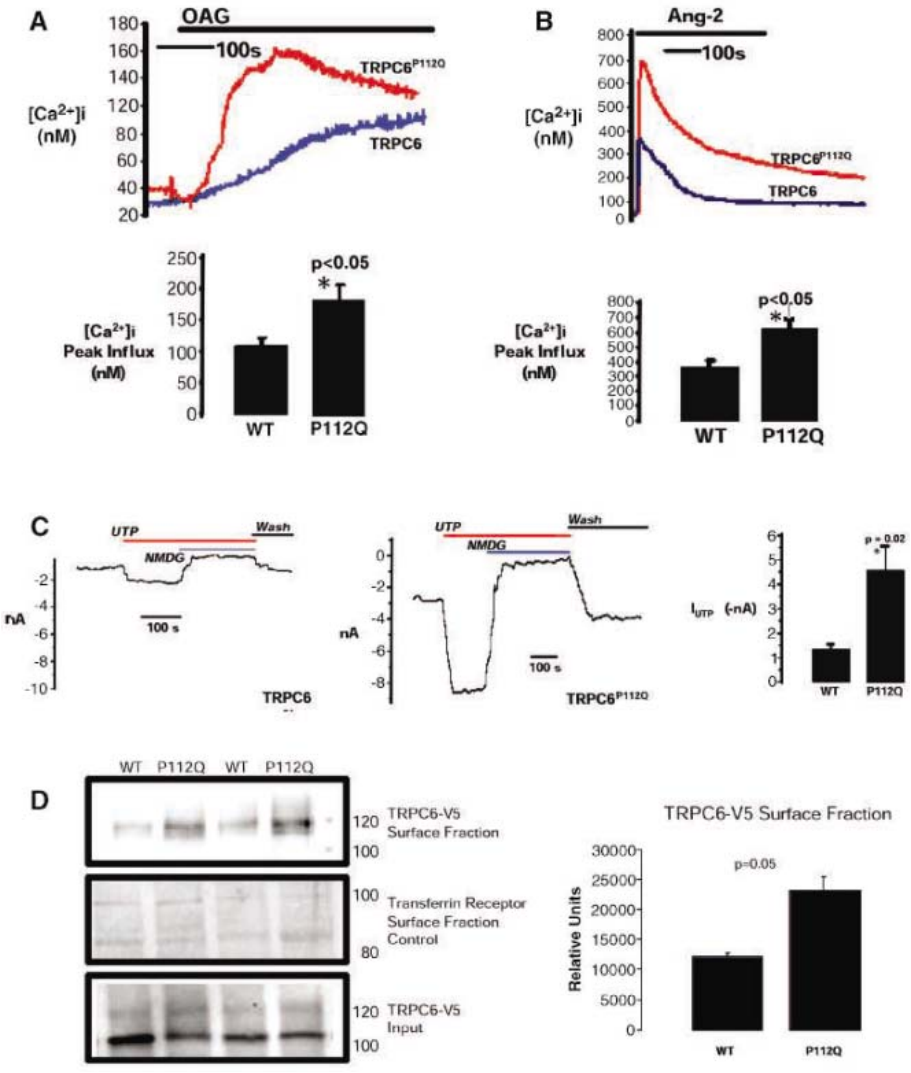

Fig. 3. The *TRPC6*^{P112Q} mutant enhances the influx of calcium into cells via DAG-mediated and receptor-operated pathways. (**A**) $[Ca^{2+}]_i$ was measured after OAG perfusion. *TRPC6*^{P112Q}-transfected cells had significantly higher calcium concentrations than cells transfected with WT *TRPC6*. The peak influx $[Ca^{2+}]_i$ is depicted in the bar graph below the tracing. (**B**) Angiotensin II (Ang-2)–induced $[Ca^{2+}]_i$ was measured. The peak influx $[Ca^{2+}]_i$ is depicted in the bar graph below the tracing. Again, *TRPC6*^{P112Q}-transfected cells had significantly higher calcium concentrations than cells transfected with WT *TRPC6*. Each trace represents the mean value derived from 15 to 20 cells in a single experiment, and each experiment was replicated three times, with similar results. The error bars represent the standard deviation. (**C**) Whole-cell current recordings of HEK 293 cells expressing either WT *TRPC6* or *TRPC6*^{P112Q} protein. Considerable inward currents in normal Na^+ extracellular solution were observed in WT *TRPC6* cells. However, inward currents were significantly larger in *TRPC6*^{P112Q} cells. When cells were perfused with 100 μM UTP, even larger inward currents were obtained. Cells expressing the *TRPC6*^{P112Q} mutation conducted two to three times more current than did the WT *TRPC6*–expressing cells, as depicted in the bar graph next to the current recordings. NMDG, *N*-methyl-D-glucamine; wash, washout of NMDG with physiological solution. (**D**) Surface expression experiments in HEK 293 cells transfected with *TRPC6* protein. Biotinylation was used to quantitate cell surface expression of *TRPC6* proteins. Cells expressing *TRPC6*-V5 or *TRPC6*^{P112Q}-V5 were incubated with biotin-SS reagent, followed by pull-down with streptaviden agarose beads. Immunoblotting with an antibody to V5 made of surface and whole-cell lysates demonstrates increased surface expression of the *TRPC6*^{P112Q} as compared to WT *TRPC6* protein. Immunoblotting with an antibody to TfR is located in the middle row and shows no difference in the surface expression of the constitutively active plasma membrane receptor (the 95-kD band). Each experiment was replicated four times, with similar results. Densitometry measurement in relative units are depicted in the bar graph next to the immunoblot (the results from all four replicants are quantitated). The error bars represent the standard error.

cause of Finnish nephropathy, is a protein of unknown function that localizes to the glomerular slit diaphragm and appears to form a zipperlike structure (*20*). Podocin (*NPHS2*) appears to anchor elements of the slit diaphragm to the cytoskeleton (*21*). Mutations in alpha-actinin 4 (*ACTN4*) may alter functions of the actin cytoskeleton in the podocyte (*6*, *22*). CD2-associated protein (*CD2AP*) has been implicated in glomerular function on the basis of mouse studies (*23*). *CD2AP* also appears to have important interactions with nephrin and podocin at the slit diaphragm.

TRP channels have been implicated in diverse biological functions such as cell growth, ion homeostasis, mechanosensation, and PLC-dependent calcium entry into cells. Calcium as a second messenger affects many of these same cellular functions. We speculate that the exaggerated calcium signaling conferred by the $TRPC6^{P112Q}$ mutation disrupts glomerular cell function or causes apoptosis (*24*). We further speculate that the mutant protein may amplify injurious signals triggered by ligands such as angiotensin II that promote kidney injury and proteinuria. Clinical manifestations of renal disease do not appear until the third decade in individuals with the $TRPC6^{P112Q}$ mutation. This is in contrast to individuals with Finnish nephropathy and steroid-resistant nephrotic syndrome, who typically develop proteinuria in utero or at birth (*5*). This delay may reflect the difference between these recessive disorders and the autosomal-dominant mechanism of inheritance in the family described here; in that family, the presence of one normal *TRPC6* allele may postpone the onset of kidney injury. Patients with autosomal-dominant FSGS due to mutations in the *ACTN4* gene also have a delayed onset of kidney disease.

Our studies identify *TRPC6* as a disease gene causing hereditary FSGS. Because ion channels tend to be amenable to pharmacological manipulation, our study raises the possibility that *TRPC6* may be a useful therapeutic target in treating chronic kidney disease.

References and Notes

1. T. Srivastava, S. D. Simon, U. S. Alon, *Pediatr. Nephrol.* **13**, 13 (1999).
2. A. Hurtado *et al.*, *Clin. Nephrol.* **53**, 325 (2000).
3. S. M. Korbet, R. M. Genchi, R. Z. Borok, M. M. Schwartz, *Am. J. Kidney Dis.* **27**, 647 (1996).
4. M. Kestilä *et al.*, *Mol. Cell* **1**, 575 (1998).
5. N. Boute *et al.*, *Nat. Genet.* **24**, 349 (2000).
6. J. M. Kaplan *et al.*, *Nat. Genet.* **24**, 251 (2000).
7. M. P. Winn *et al.*, *Kidney Int.* **55**, 1241 (1999).
8. M. P. Winn *et al.*, *Genomics* **58**, 113 (1999).
9. A. Riccio *et al.*, *Brain Res. Mol. Brain Res.* **109**, 95 (2002).
10. R. L. Garcia, W. P. Schilling, *Biochem. Biophys. Res. Commun.* **239**, 279 (1997).
11. P. J. Conlon *et al.*, *Kidney Int.* **56**, 1863 (1999).
12. C. S. Facemire, P. J. Mohler, W. J. Arendshorst, *Am. J. Physiol. Renal Physiol.* **286**, F546 (2004).
13. P. Mundel, S. J. Shankland, *J. Am. Soc. Nephrol.* **13**, 3005 (2002).
14. The HEK 293 cell line was originally derived from human embryonic kidney tissue, and its morphological features bear little or no resemblance to those of mature renal cell lineages. Thus, the absence of *TRPC6* expression in HEK cells probably has little bearing on whether the protein is actually expressed in mature kidney tissue. Examples of this phenomenon are the angiotensin receptors, which are not expressed in HEK cells but are expressed throughout the kidney.
15. T. Hofmann *et al.*, *Nature* **397**, 259 (1999).
16. M. W. Taal, B. M. Brenner, *Kidney Int.* **57**, 1803 (2000).
17. T. Balla, P. Varnai, Y. Tian, R. D. Smith, *Endocr. Res.* **24**, 335 (1998).
18. B. B. Singh *et al.*, *Mol. Cell* **15**, 635 (2004).
19. V. J. Bezzerides, I. S. Ramsey, S. Kotecha, A. Greka, D. E. Clapham, *Nat. Cell Biol.* **6**, 709 (2004).
20. V. Ruotsalainen *et al.*, *Proc. Natl. Acad. Sci. U.S.A.* **96**, 7962 (1999).
21. S. Roselli *et al.*, *Am. J. Pathol.* **160**, 131 (2002).
22. C. H. Kos *et al.*, *J. Clin. Invest.* **111**, 1683 (2003).
23. K. Schwarz *et al.*, *J. Clin. Invest.* **108**, 1621 (2001).
24. Y. Hara *et al.*, *Mol. Cell* **9**, 163 (2002).

25. We thank the members of the family described here, the Center for Human Genetics core facilities for assistance, J. Burch for technical assistance, and R. S. Williams for helpful discussions. Supported in part by grants from NIH.

Supporting Online Material

www.sciencemag.org/cgi/content/full/1106215/DC1
Materials and Methods
Figs. S1 to S5
Table S1
References

8 October 2004; accepted 13 April 2005
Published online 5 May 2005;
10.1126/science.1106215
Include this information when citing this paper.

Protein Crystallization System

The Crystal Farm CF-150 is a benchtop system for high-throughput protein crystallization. It features the same technology as the CF-400 model in a smaller footprint. The Crystal Farm is a fully integrated, web-based incubation and imaging system for protein crystallization screening and optimization. By providing high-throughput protein crystallization automation, Crystal Farm addresses the critical quest for high-speed structure-based drug discovery and design. The system combines capacity for up to 15,000 simultaneous experimental conditions with patent-pending "Cool Flash" imaging technology, and includes a web-browser-based interface that controls all system functions either locally or remotely, including priority-based image scheduling, viewing, and scoring. Experimental results stored in an SQL database can be easily mined for monitoring and optimizing crystallization experiments.

Bruker AXS For information 800-234-XRAY www.bruker-biosciences.com

DNA Methods Development Kit

The GenomeLab Methods Development Kit contains multiple chemistries for DNA sequencing on the CEQ Series Genetic Analysis Systems. A complement to Beckman Coulter's CEQ Quick Start and DTCS kits, this new kit contains a set of core reagents plus a choice of nucleotide mixtures—dITP for routine sequencing and dGTP for sequencing through difficult G-C rich and polymerase hard stop regions. The dGTP chemistry is effective for those problematic templates in which standard terminator kits produce data with early signal loss.

Beckman Coulter For information 800-742-2345 www.beckmancoulter.com

Electroporation-Competent Cells

The ElectroTen-Blue cells were created to transform large DNA molecules with high efficiency. The cells exhibit the high electroporation efficiency (Hee) phenotype. The Hee phenotype improves survival of these cells during electroporation treatment, dramatically improving transformation efficiency. The high cloning efficiency makes this strain a suitable host for generating large, more representative libraries. ElectroTen-Blue cells make it possible to clone methylated DNA, such as eukaryotic genomic DNA. ElectroTen-Blue cells are deficient in all known *E. coli* K12 restriction systems to decrease the likelihood of generating unrepresentative libraries. Absence of these endogenous bacterial restriction systems increases the efficiency of introducing eukaryotic DNA into *E. coli*, and increases the size and representation of libraries constructed with methylated or hemi-methylated DNA.

Stratagene For information 800-424-5444 www.stratagene.com

Fast Gram Stain

The Endosafe PDS Gram ID is a three-minute Gram stain assay. This new assay makes use of a handheld reader and disposable cartridge pre-loaded with all the materials needed to run a single-step Gram determination. The test measures the presence of the cell walls in a microbial isolate. The measurement is interpreted by the software to indicate whether a sample contains Gram negative or positive bacteria, yeasts, or mold. More than 70 organisms have been tested with the PTS Gram ID for accuracy and specificity. The test is easy to perform; simply load a sample into each of the four sample reservoirs of the disposable cartridge and in about three minutes, the PTS will indicate the result. There is no subjectivity or interpretation of results and up to 100 results can be saved in memory and downloaded to lab management software.

Charles River Laboratory For information 877-CRIVER1 www.criver.com

Cell-Based Assay Monitoring

The RT-CES system makes use of new biosensor technology for label-free, real-time monitoring of cell-based assays. The core of the system is the microelectronic cell-sensor arrays integrated into the bottom of the microtiter plates, which provide continuous, quantitative information about the biological status of attached cells. Any changes to cell number, size, morphology, or attachment quality is detected in real-time without the use of reporter reagents. The integrated software allows data to be collected and saved automatically as often as every minute over virtually any time period. The instrument is suitable for drug discovery and research applications involving cancer research, receptor/ligand interaction, cytotoxicity, apoptosis, and toxicology. It is available in both 16- and 96-well formats.

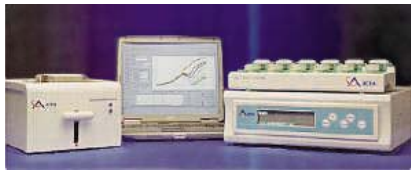

ACEA Biosciences For information 866-308-2232 www.aceabio.com

New Fluorescent Proteins

Invitrogen has released the first in a series of fluorescent protein vectors based on the jellyfish *Aequorea victoria*. The recently released Vivid Colors Emerald Green (EmGFP) and Yellow (YFP) fluorescent proteins have been enhanced for greater fluorescence intensity. The vectors are enabled by Gateway cloning technology for rapid, directional cloning. Convenient TOPO-cloning forms and Lenti-versions will be available in the near future.

Invitrogen For information 800-955-6288 www.invitrogen.com

Reverse Transcription Kit

The Quantitect Reverse Transcription Kit makes real-time, two-step reverse-transcription polymerase chain reaction (RT-PCR) faster and more convenient. Only 20 min are required to synthesize first-strand cDNA and eliminate genomic DNA contamination. The cDNA yields are high, allowing sensitive detection of even low-abundance genes.

Qiagen For information 800-426-8157 www.qiagen.com

For more information visit GetInfo, *Science*'s new online product index at *http://science.labvelocity.com*

From the pages of GetInfo, you can:
- Quickly find and request free information on products and services found in the pages of *Science*.
- Ask vendors to contact you with more information.
- Link directly to vendors' Web sites.

Newly offered instrumentation, apparatus, and laboratory materials of interest to researchers in all disciplines in academic, industrial, and government organizations are featured in this space. Emphasis is given to purpose, chief characteristics, and availability of products and materials. Endorsement by *Science* or AAAS of any products or materials mentioned is not implied. Additional information may be obtained from the manufacturer or supplier by visiting www.science.labvelocity.com on the Web, where you can request that the information be sent to you by e-mail, fax, mail, or telephone.

ScienceCareers.org

Classified Advertising

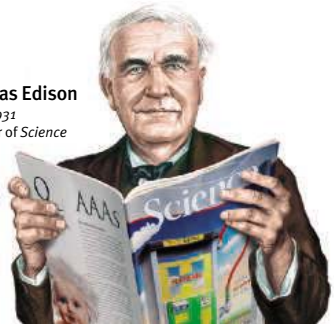

Thomas Edison
1847–1931
Founder of *Science*

For full advertising details, go to **www.sciencecareers.org** and click on **How to Advertise,** or call one of our representatives.

United States & Canada

E-mail: advertise@sciencecareers.org
Fax: 202-289-6742

JILL DOWNING
(CT, DE, DC, FL, GA, MD, ME, MA, NH, NJ, NY, NC, PA, RI, SC, VT, VA)
Phone: 631-580-2445

KRISTINE VON ZEDLITZ
(AK, AZ, CA, CO, HI, ID, IA, KS, MT, NE, NV, NM, ND, OR, SD, TX, UT, WA, WY)
Phone: 415-956-2531

KATHLEEN CLARK
Employment: AR, IL, LA, MN, MO, OK, WI, Canada; Graduate Programs; Meetings & Announcements (U.S., Canada, Caribbean, Central and South America)
Phone: 510-271-8349

EMNET TESFAYE
(Display Ads: AL, IN, KY, MI, MS, OH, TN, WV; Line Ads)
Phone: 202-326-6740

BETH DWYER
(Internet Sales Manager)
Phone: 202-326-6534

Europe & International

E-mail: ads@science-int.co.uk
Fax: +44 (0) 1223-326-532

TRACY HOLMES
Phone: +44 (0) 1223-326-525

HELEN MORONEY
Phone: +44 (0) 1223-326-528

CHRISTINA HARRISON
Phone: +44 (0) 1223-326-510

JASON HANNAFORD
Phone: +81 (0) 52-789-1860

To subscribe to *Science*:
In U.S./Canada call 202-326-6417 or 1-800-731-4939
In the rest of the world call +44 (0) 1223-326-515

Science makes every effort to screen its ads for offensive and/or discriminatory language in accordance with U.S. and non-U.S. law. Since we are an international journal, you may see ads from non-U.S. countries that request applications from specific demographic groups. Since U.S. law does not apply to other countries we try to accommodate recruiting practices of other countries. However, we encourage our readers to alert us to any ads that they feel are discriminatory or offensive.

POSITIONS OPEN

The Department of Microbiology and Molecular Biology at Brigham Young University (BYU) announces the availability of a permanent (continuing faculty status track) **FACULTY POSITION.** Review of applications will begin July 1, 2005, and continue until the position is filled. Applicants should have a Ph.D. degree and postdoctoral experience. Candidates are expected to develop a strong teaching capability in medical microbiology or parasitology and have a research emphasis focusing on molecular mechanisms of pathogenesis. Candidates must demonstrate a high potential for establishment of an externally funded research program. Apply online at website: **http://yjobs.byu.edu** through faculty application; attach curriculum vitae and one-page statements of teaching philosophy and of research interests and goals. Contact: **Dr. Byron Murray, Chair, Search Committee, Department of Microbiology and Molecular Biology, Brigham Young University, Provo, UT 84602. Telephone: 801-422-7403; e-mail: byron_murray@byu.edu.** Additional departmental information is available at **website: http://mmbio.byu.edu.** Preference is given to qualified members in good standing of the sponsoring church, The Church of Jesus Christ of Latter-day Saints. *BYU is an Equal Employment Opportunity Employer.*

CHAIR
Department of Pharmaceutical Sciences
Midwestern University
College of Pharmacy–Glendale

Midwestern University College of Pharmacy–Glendale invites applications and nominations for the position of Chair of the Department of Pharmaceutical Sciences at the **ASSOCIATE** or **PROFESSOR** level. The Department of Pharmaceutical Sciences encompasses the disciplines of medicinal chemistry, pharmaceutics, pharmacokinetics, and pharmacology/physiology. The position is full-time, twelve-month, and tenure-track.

The successful applicant will have a Ph.D. in pharmaceutical sciences or a related discipline and a strong commitment to pharmacy education and scholarship. A professional degree in pharmacy is desirable but not required. Responsibilities of the Chair position include teaching and providing leadership and mentoring to the departmental faculty in the areas of teaching, scholarship, and service.

While the College places a high priority on teaching excellence, faculty are supported and expected to engage in scholarly activities. For further information about the College of Pharmacy–Glendale, please visit our **website: http://www.midwestern.edu/CPG.**

Applicants should submit curriculum vitae, statement of management philosophy, and contact information for a minimum of three references to: **Chair, Pharmaceutical Sciences Search Committee, Midwestern University College of Pharmacy–Glendale, 19555 North 59th Avenue, Glendale, AZ 85308.** *Midwestern University is an Equal Opportunity Employer.*

Tulane University School of Medicine, Department of Medicine, Section of Nephrology, is searching for a **POSTDOCTORAL FELLOW** (Ph.D. or M.D.) with background in cell and molecular biology for a laboratory involved in the study of the pathogenesis and treatment of hypertension. Experience with small animal experimentation, Western and Northern blots, enzyme assays preferred. Work in a modern laboratory with updated equipment. Excellent working environment and collaborative arrangements. Competitive salary and benefits. Send curriculum vitae and names/contact of three references to: **Jules B. Puschett, M.D., Department of Medicine SL12, 1430 Tulane Avenue, New Orleans, LA 70112-2699.** *Affirmative Action/Equal Opportunity Employer.*

POSITIONS OPEN

BRITISH COLUMBIA LEADERSHIP CHAIR IN ENVIRONMENTAL AND FOREST GENOMICS

The University of Victoria seeks applications for a prestigious British Columbia Leadership Chair in Environmental and Forest Genomics, appointed to the Centre for Forest Biology (**website: http://web.uvic.ca/forbiol/home/**) in the Department of Biology (**website: http://web.uvic.ca/biology/**). This position is subject to funding. The Chair is an endowed position that will be filled at the **PROFESSOR** level. The successful candidate will be an internationally recognized leader in the application of genomics to ecophysiology, ecosystem function, and forest health. The Chairholder must have strong leadership skills, demonstrated excellence in research, a very strong publication record, a proven ability to maintain a high profile, externally funded research program, and a keen commitment to undergraduate and graduate teaching. The Chairholder will conduct innovative research on the response of forests to environmental change and reinforce and broaden collaborations between Uvic researchers and local industry, regional government laboratories, and the international community. The Chairholder will establish an interdisciplinary program to advance understanding of forest processes on scales spanning genes to forests and bring to British Columbia genomic knowledge applied to forest biology. This will add significant depth to existing forest biological research being conducted by molecular biologists, phytopathologists, and physiologists at the University of Victoria, Genome BC, the Canadian Forest Service, and the British Columbia Ministry of Forests Research Branch.

Applications should be sent to: **Dr. William Hintz, Chair, Department of Biology, University of Victoria, P.O. Box 3020, STN CSC, Victoria, B.C. V8W 3N5, Canada. Fax: 250-721-7120; e-mail: biochair@uvic.ca.** The closing date for the position is September 30, 2005, but applications will be accepted until the position is filled. Curriculum vitae and research and teaching statements should be included as well as contact information (names, addresses, fax, e-mail) for four referees.

The University of Victoria is an Equity Employer and encourages applications from women, persons with disabilities, visible minorities, Aboriginal peoples, people of all sexual orientations and genders, and others who may contribute to the further diversification of the University.

All qualified applicants are encouraged to apply; however, in accordance with Canadian Immigration requirements, Canadians and permanent residents will be given priority.

VISITING FACULTY POSITION
CELL BIOLOGY/NEUROBIOLOGY
Bowdoin College

The Biology Department and the Biochemistry and Neurobiology Interdisciplinary Programs of Bowdoin College invite applications for a one-year Visiting Assistant Professor beginning in January 2006. Candidates should have received their Ph.D. by December 2005. Teaching responsibilities for the year include a course in cell biology/biochemistry, a course in neurobiology, mentoring the research of honors and independent study students, and possibly teaching one nonmajors course. Review of applications will begin August 17, 2005. Possible extension of the position through spring 2007. Please send curriculum vitae, a statement describing your teaching philosophy and research interests, and three letters of reference to: **Amy Johnson, Chair, Biology Department, 6500 College Station, Bowdoin College, Brunswick, ME 04011.** For further information about the College, the Department, and the program, please see our **website: http://www.bowdoin.edu.**

Bowdoin College is committed to equality through Affirmative Action and is an Equal Opportunity Employer. We encourage inquiries from candidates who will enrich and contribute to the cultural and ethnic diversity of our College. Bowdoin College does not discriminate on the basis of age, race, creed, color, religion, marital status, gender, sexual orientation, veteran status, national origin, or disability status in employment, or in our education programs.

Events in Drug Discovery

Focus on Global Pharma

THE ENTIRETY OF THE PHARMACEUTICAL BUSINESS, FROM DISCOVERY TO MANUFACTURING, FORMS THE SUBJECT FOR FORTHCOMING MEETINGS ON TWO CONTINENTS. BY PETER GWYNNE

IBC Life Sciences:
http://www.ibcusa.com
http://www.drugdisc.com

Two events later this year will celebrate the increasingly global nature of the pharmaceutical business. Between August 8 and August 11 at the Boston Convention and Exhibition Center in Massachusetts, U.S.A., the 10th annual Drug Discovery Technology & Development World Congress will paint the big picture of the industry's requirements to improve the productivity of drug discovery and development across the entire pipeline. Two months later and half a world away in Mumbai, India, the second annual presentation of Drug Discovery to Clinical Trials: Global Partnering and New Science will provide a forum for individuals and companies involved in drug discovery, clinical trials, and manufacturing and will cast a bright light on recent progress in the Asia-Pacific region. That event will take place from October 5 to October 7 at the Renaissance Mumbai Hotel and Convention Center. Both meetings are organized by IBC Life Sciences; sponsoring publications include this journal.

The expected attendance of more than 5,000 individuals from roughly 40 countries makes Boston's World Congress the world's largest gathering of drug discovery scientists and biotechnologists. The event will feature case studies of successful drug and biological research projects and unbiased technology critiques and evaluations coupled with examples of ways in which companies are optimizing their interfaces between discovery and development – a critical factor in the industry given the current pressure to move products along the pipeline.

In keynote speeches, U.S. Food and Drug Administration acting commissioner Lester Crawford will outline "New Regulatory Directions for the 21st Century" and John LaMattina, president of Pfizer Global Research and Development, will discuss "Pharmaceutical R&D – The World's Hope for Tomorrow's Cures." And in a keynote panel moderated by Robert Ruffolo, president of R&D for Wyeth Pharmaceuticals and senior vice president of Wyeth, Crawford will join George Poste, a pharmaceutical industry veteran who now heads Arizona State University's Arizona Biodesign Institute, to explore "The Industry and Regulatory Interface in Drug Development."

As its scientific themes, the Congress will present symposia in five specific areas. They are: promising approaches to drug discovery and development; success factors in the transition from discovery to clinic; protein and antibody therapeutics; business ventures and deal-making; and gaining value from discovery informatics. The event will also feature peer-reviewed poster sessions, technology-specific workshops, and case studies from the pharmaceutical business. More than 400 companies have signed up to offer booths in the exhibit hall on the 9th, 10th, and 11th of August. Networking events will include cocktail receptions and *Science*'s career fair. And a gala dinner on the Congress's first evening will highlight the fourth annual Pharmaceutical Achievement Awards, which will recognize significant accomplishments by individuals and organizations in the global pharmaceutical and biotechnology industries.

Michael Keenan of IBC Life Sciences emphasizes that information presented during the Congress will provide individuals with examples and ideas that they can apply in their own work environments. IBC has designed the program to appeal to both bench scientists and middle and upper level managers.

The event in Mumbai will provide a forum at which biopharmaceutical companies from North America, Europe, and the Asia-Pacific region can discuss scientific advances, business strategies, and partnerships. IBC has split the event into seven specific topic areas. A review of the Asia-Pacific landscape in drug development and clinical trials will examine the opportunities and sectors of strength for the pharmaceutical and biotechnology industries in Australia, China, India, Japan, Malaysia, Singapore, South Korea, Taiwan, and Thailand. A series of panel discussions will deal with drug regulation and the protection of intellectual property. In a third panel, scientists and executives will present case studies of partnerships in drug discovery and development.

Symposia on science and technology will target drug and biologic discovery, global clinical trials and the lessons learned from them, and opportunities in manufacturing, biogenerics, and delivery/formulations. Finally, a showcase on emerging Asian companies that will run throughout the conference will highlight a selection of companies from that continent involved in drug discovery, clinical trials, and manufacturing. As at the Boston Congress, the Mumbai event will feature poster sessions and an exhibit hall that will showcase the latest technologies, products, and services in the biopharma field.

Organizers encourage scientists and managers from beyond Asia to attend. Why? The event will provide insights into Asia's explosive growth in biopharmaceuticals and the opportunities that this phenomenon offers in terms of new markets for non-Asian organizations' products and services.

To find more information on the two conferences, you can visit the website http://www.drugdisc.com. Alternatively, you can write to Ellen Massa at IBC USA Conferences, Inc., One Research Drive, Suite 400A, P.O. Box 5195, Westborough, MA 01581-5195 U.S.A., e-mail her at emassa@ibcusa.com, or phone her at +1 508-614-1213.

A former science editor of Newsweek, *Peter Gwynne (pgwynne767@aol.com) covers science and technology from his base on Cape Cod, Massachusetts, U.S.A.*

NATIONAL INSTITUTE OF ALLERGY AND INFECTIOUS DISEASES

POSTDOCTORAL POSITIONS AVAILABLE

The Chemokine System in Lymphocyte Biology

Postdoctoral training positions are available in the Inflammation Biology Section (IBS), Laboratory of Molecular Immunology, National Institute of Allergy and Infectious Diseases (NIAID), National Institutes of Health (NIH), Bethesda, Maryland. The NIAID is a major research component of the NIH and the Department of Health and Human Services.

The IBS is seeking candidates with a Ph.D. and/or M.D. degree to study the chemokine system in lymphocyte biology as related to immunity and inflammation. Projects in the laboratory focus on the regulation of expression, signaling, and function of lymphocyte chemokine receptors and include using chemokine receptors to understand T cell differentiation in humans. Ordinarily, an interview will be required. Salary will be determined based on education and research experience. Health benefits are available through the NIH.

Please apply electronically by sending letter of interest, curriculum vitae, and names and contact information of three references to: **Joshua M. Farber, M.D., email: jfarber@niaid.nih.gov**

For students, recent graduates, and postdoctoral, research, and clinical fellows.

Your on-line guide to training with the best at the world's largest biomedical research institution.

In Bethesda, Maryland, and at other NIH laboratories.

Office of Intramural Training and Education
Bethesda, Maryland
20892
800.445.8283

opportunity *clicks*

www.training.nih.gov

National Institutes of Health
Virtual Career Center
at the tip of your mouse

www.training.nih.gov/careers

-EXPLORE CAREER OPTIONS
-CONTINUE YOUR EDUCATION
-SEARCH FOR A JOB

Careers in science, medicine, and beyond at the college, postbaccalaureate, graduate, and postdoctoral levels

Office of Intramural Training and Education
(800) 445-8283

WWW.NIH.GOV

Interview/Hire the World's Best Scientists

Reach innovative young scientists at the forefront of their fields

Attend the Job Fair for NIH Postdoctoral, Research, and Clinical Fellows

Date: October 20, 2005
Time: 10:30 am - 3:00 pm
Place: Natcher Conference Center
National Institutes of Health
Bethesda, Maryland

Access 3800 doctoral scientists and clinicians in training at the NIH

Register by September 15th at: **www.training.nih.gov/jobfair**

Office of Intramural Training and Education

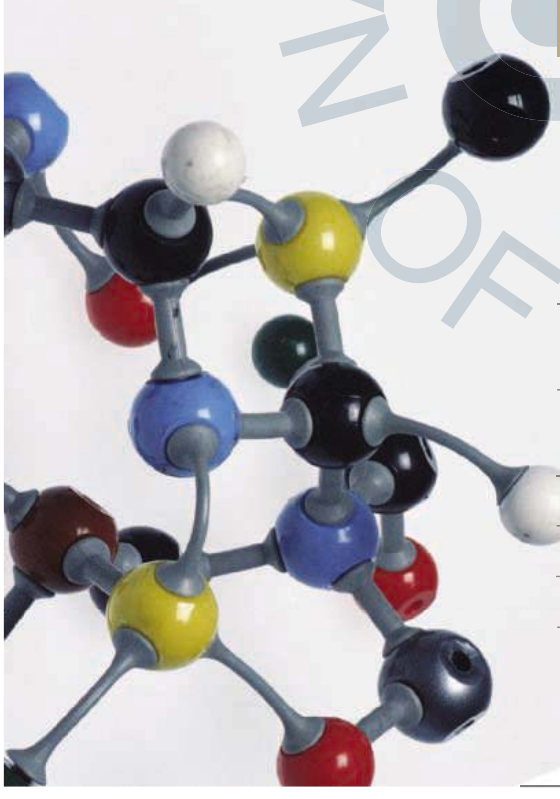

Postdoctoral Research Training at NIH

Launch a career to improve human health

Work in one of 1250 of the most innovative and well-equipped biomedical research laboratories in the world

Explore new options in interdisciplinary and bench-to-bedside research

Develop the professional skills essential for success

Earn an excellent stipend and benefits

Click on www.training.nih.gov

Office of Intramural Training and Education

香港城市大學
City University of Hong Kong

City University of Hong Kong is one of eight higher education institutions directly funded by the Government of the Hong Kong Special Administrative Region through the University Grants Committee (Hong Kong). It aims to become one of the leading universities in the Asia-Pacific region through excellence in teaching and research. In two recent studies, City University of Hong Kong is ranked among the top 200 universities in the world, and among the top ten universities in the Greater China region. The student population is approximately 23,000 enrolled in over 100 programmes at the associate degree, undergraduate and postgraduate levels. The medium of instruction is English.

The University invites applications and nominations for :

Head *[Ref. A/447/49]*
Department of Biology and Chemistry

The Department of Biology and Chemistry provides quality education in biology and chemistry as well as environmental science and technology. The study programmes offered are applied in nature and specially designed to meet the local and regional employment needs.

The Department strongly fosters interdisciplinary applied research. Staff expertise lies in environmental biology and chemistry, ecology, ecotoxicology, bioactive compounds, organic chemistry, computational chemistry, inorganic chemistry, microbiology, biochemistry and biotechnology. Members of the Department play a central role in the establishment of the Centre for Marine Environmental Research and Innovative Technology (MERIT) supported by a HK$45 million Area of Excellence Grant from the Government. Other areas such as bioactive products and catalysis are also increasing in strength.

Qualifications for Appointment
The Head of Department will be expected to provide strong academic leadership in the development of teaching and applied research within the Department, as well as providing effective managerial leadership. Candidates should possess strong academic and professional qualifications, substantial relevant experience in tertiary education, and an internationally recognized record of research and scholarship.

Salary and Conditions of Service
The successful candidate will be offered appointment to an academic rank commensurate with the appointeeís qualifications and experience. The appointment will either be on superannuable terms with provision for superannuation benefits, or on a fixed-term contract with contract-end gratuity. The appointee will be offered the headship appointment concurrently for an initial period of three years. The University offers competitive salaries and employee benefits, including annual leave, medical and dental schemes, and, where applicable, passage allowance. Provision of housing benefit is under review.

Application and Information
Further information on the post and the University is available at http://www.cityu.edu.hk, or from the Human Resources Office, City University of Hong Kong, Tat Chee Avenue, Kowloon, Hong Kong (Fax : (852) 2788 1154 or (852) 2788 9334/E-mail: hrklau@cityu.edu.hk). Please send the nomination or application in the form of an application letter, enclosing a current curriculum vitae, to the Human Resources Office by **22 July 2005**. Please quote the reference of the post in the application and on the envelope.

The University reserves the right to consider late applications and nominations, and to fill or not to fill the position.

OPEN TO

INSPIRE

Follow a path to insight and illumination.

The Novartis Institutes for BioMedical Research is seeking highly motivated postdoctoral fellows to work at its cutting-edge research facilities in Cambridge, MA. Would you like to join us on the new frontier of lifesaving drug discovery?

Our openings include positions in the following areas:

- Automation Technologies, Biology (5291BR)
- Cardiovascular, Heart Failure (3656BR)
- Cardiovascular, Stem Cell (5818BR)
- Developmental Molecular Pathways, Biology (5004BR)
- Diabetes and Metabolism, Mechanistic Enzymology (1517BR)
- Lead Discovery Center, Preclinical Profiling/ Toxicology (1415BR)
- Lead Discovery Technologies, Computational Lab (3248BR)
- Models of Disease Center, Epigenetics (5742BR)
- Molecular Pathways, Biology (5015BR)
- Molecular Resonance Imaging, Atherosclerosis (5377BR)
- Neurobiology (4619BR)

To view descriptions of these positions and to apply, visit www.nibr.novartis.com and follow the links to Careers and Job Opportunities. Be sure to apply directly to the corresponding Job ID number listed above.

Novartis is committed to embracing and leveraging diverse backgrounds, cultures, and talents to achieve competitive advantage.
Novartis is an equal opportunity employer. M/F/D/V

NOVARTIS
NOVARTIS INSTITUTES FOR BIOMEDICAL RESEARCH

The New Pathway to Drug Discovery

www.nibr.novartis.com

THE UNIVERSITY of York

DEPARTMENT OF BIOLOGY

Research Fellows Recruitment Day - 9 September 2005

Do you hold a bioscience research fellowship or are you considering applying for one?

Would you like to hold it at a department with an outstanding reputation and world-class research facilities?

We would like to invite you to apply to attend our Research Fellows Recruitment Day at York, with the opportunity to introduce yourself and your work to a department that is keen to host ambitious researchers who are building a career in science.

The Department of Biology is holding a Research Fellows Recruitment Day on 9 September 2005. We will be inviting outstanding researchers from across the bioscience spectrum who hold or are applying for Fellowships to look round our facilities and meet our academic and research staff. Researchers will have the opportunity to give a presentation about their work and attend an interview to discuss their science and career plans. We are keen to offer places to a number of researchers for the duration of their fellowship, along with the opportunity to obtain a guarantee of a permanent position on the expiry of the fellowship.

We can offer:

- The chance to be part of a dynamic, multidisciplinary department (5-ranked in the last two RAE exercises)
- Superb research facilities including the innovative Technology Facility, housing more than £6m of state-of-the-art equipment in key technologies
- Opportunities to collaborate with colleagues across the biological spectrum, and with other departments with which we have strong links, such as Chemistry and the Hull York Medical School
- Mentorship and the opportunity to develop skills and experience of value in academia, industry and beyond.
- An attractive campus environment 2 km from the centre of one of the most beautiful cities in Britain.

Eligibility Requirements:

- A relevant PhD, and experience at post-doctoral level
- An excellent publication record (or other proof of research success)
- A coherent and well-developed research plan

For further information and details of how to apply please go to our website at http://www.york.ac.uk/depts/biol/research/rfrecruit.htm or contact Glenda Foster on gfm500@york.ac.uk

Informal enquiries may be made to Professor Dale Sanders, Head of Department (bio-personnel@york.ac.uk), or Professor Ottoline Leyser, Chair of Research Committee (hmol1@york.ac.uk).

Closing date: 15 July 2005.

The University of York is committed to diversity and has policies and developmental programmes in place to promote equality of opportunity. It particularly welcomes applications from ethnic minority candidates.

www.york.ac.uk

Director

The DHHS/FDA/Center for Drug Evaluation and Research (CDER), Office of Pharmaceutical Science (OPS), Office of Testing and Research (OTR) is recruiting a Director at FDA's Research Laboratory located in Rockville, and White Oak, Maryland.

Qualifications: Basic qualifications require a doctoral degree (M.D., Ph.D., D.V.M., D. Sc., etc.), a doctoral level knowledge of pharmacology or closely related fields, and extensive knowledge in the development of pharmaceutical products with a strong record of peer-reviewed original research.

Duties: The Director is the Office/Center's principal adviser in all matters related to the planning and conducting of pharmaceutical and biomedical research and in developing regulatory scientific standards involving clinical pharmacology, applied pharmacology, pharmaceutical analysis, and product quality research. As a recognized expert, the incumbent participates fully in policy formulation, planning and evaluating programs, including oversight of the pharmacological/toxicological/pharmacokinetic/pharmacyodynamics and product quality aspects of pharmaceutical and biomedical research as they pertain to the Center's regulatory mission. Provides the executive leadership and scientific direction to a staff of 85+ multidisciplinary scientists engaged in pharmaceutical and biomedical laboratory research in order to provide scientific advice and assistance to the drug review programs and other organizational components of the Center. Recommends policies and standards based on research findings, which affect regulatory decision making. Plans and conducts research to study the manufacturing aspects of ensuring product quality including researching new technologies which can improve manufacturing techniques and processes and determining the effects of formulation components and composition on manufacturing processes and product design.

Salary Range: $103,947 - $180,100 per annum. This position may be filled as either Senior Biomedical Research Service (SBRS), Title 42 or Commissioned Corps.

How to Apply: Submit curriculum vitae or brief resume with cover letter indicating that you are applying for the SBRS position of Director, Office of Testing and Research (OTR), Office of Pharmaceutical Science (OPS), Center for Drug Evaluation (CDER), Food and Drug Administration (FDA) to: **FOOD AND DRUG ADMINISTRATION, Center for Drug Evaluation and Research, Office of Pharmaceutical Science, Rockwall Building 2, Room 1065, 5515 Security Lane, Rockville, Maryland 20852, Attn: Jim Keady, Project Manager.**

More information on this position can be obtained by contacting **Jim Keady** at **keadyj@cder.fda.gov**, on **301-443-5205** (phone), **301-443-5225** (fax) or **Sharon Miller** at **millersh@cder.fda.gov** on **301-443-5236**.

FDA IS AN EQUAL OPPORTUNITY EMPLOYER WITH A SMOKE FREE ENVIRONMENT

ambit
BIOSCIENCES

Quantitative Biochemist

Ambit Biosciences is recruiting a highly motivated biochemist with outstanding quantitative skills. Candidates should have significant expertise in protein structure/function relationships and ligand binding thermodynamics and kinetics. The successful candidate will contribute to a major technology development effort [*Nature Biotechnology* **23:** 329, 2005].

Qualifications: Ph.D. in biochemistry, biophysics, or equivalent with postdoctoral experience. Expertise in quantitative biochemistry is essential, and structural biology experience is desirable. Candidates must be rigorous, creative, conscientious and must work effectively in a fast-paced, team-oriented environment.

Ambit is located in sunny San Diego and is primarily focused on kinase inhibitor drug discovery and development.

Email curriculum vitae with **Job code: P-400** to **hr@ambitbio.com**.

ÉCOLE POLYTECHNIQUE FÉDÉRALE DE LAUSANNE

Faculty Position in Aerothermodynamics of Turbomachines

at Ecole Polytechnique Fédérale de Lausanne (EPFL)

The EPFL plans a substantial expansion in energy sciences and technologies, in particular through an intensive search for internationally renowned experts.

As part of this, the Institute of Energy Sciences has an opening at the **Assistant Professor (tenure-track)** level. Senior candidates shall nevertheless also be considered. We seek outstanding individuals in the area of aerothermodynamics of turbomachines.

The new professor will be in charge of the Laboratory of Thermal Turbomachines (LTT) and must hence have the capacity to maintain and develop both a fundamental and applied research activity with international visibility. Possible directions of these activities are advanced experimental and/or numerical methods (including reactive flow modeling), linked to high power density machines for advanced energy conversion. The successful candidate will lead important projects and build cooperation with other laboratories as well as with industrial partners, and will contribute to the teaching of thermal sciences within the Mechanical Engineering undergraduate and graduate programs.

Significant start-up resources and research infrastructure will be available. We offer internationally competitive salaries and benefits, as well as a world-class, dynamic research environment. Applications, including curriculum vitae, publications list, concise statement of research and teaching interests as well as the

names and addresses (including e-mail) of at least five referees, should be sent by **August 31st, 2005** to:

Professor Michel Declercq, Dean
EPFL School of Engineering
Station 11
CH-1015 Lausanne
Switzerland

More information about EPFL and its Institute of Energy Sciences are available at :
http://www.epfl.ch or http://ise.epfl.ch

EPFL is an equal opportunity employer.

APPLICATION SCIENTIST

This position primarily helps customers with their technical questions and problems, but involves everything from trouble-shooting optics to experimental design and helping with internal and external research and development and education.

Our ideal candidate is a great communicator with significant related lab experience in fluorescence microscopy, sample preparation and imaging. Minimum of a Masters in related field (Biology, Chemistry, Physics or Microscopy), Ph.D. preferred. Good customer service skills, with customer service experience preferred. Ability to travel, on average, eight to twelve days per quarter. Second language helpful: German, Japanese or languages from India or China.

As an employee-owned company, Chroma is able to offer an extremely generous package of benefits and compensation. In return, we ask all employee-owners to be self-motivated, independent workers willing to strategize and work towards the long-term prosperity of the company.

Please forward your resume to:
Human Resources Director
Chroma Technology Corp
PO Box 489
Rockingham, VT 05101
or by email:
dsensor@chroma.com

NO PHONE CALLS PLEASE

CHROMA *An Employee-Owned Company and Equal Opportunity Employer*

Chroma Technology Corp is a leader in the manufacture of thin film coatings for high performance optical filters.

GenomeCanada

VICE-PRESIDENT, RESEARCH

Genome Canada is seeking a Vice-President, Research who will be the *Voice of Genomics and Proteomics Research in Canada*.

Responsibilities include:

- Shape Canadian genomics and proteomics research into world leadership in key areas
- Ensure Canada's capabilities, competitiveness and exciting potential in this field of research
- Support Canada's most promising investigators
- Nurture relationships with Canadian and international stakeholder groups and Genome Centres across Canada

The candidate will be joining an innovative team in Ottawa, Canada, working in a rapidly evolving environment. You have the following qualities, experience and education:

- An advanced University degree and a respected history of discoveries, publications, awards, ideally focused on genomics/proteomics
- Clear academic recognition, with a history of peer reviewed support from national research funding agencies
- A broad personal and professional network of Canadian and international relationships among leaders and executives in diverse academic, industry and government settings
- Knowledge and experience in the area of Intellectual Property and commercialization
- Bilingualism (English and French) would be an asset.

The successful candidate will enjoy a competitive salary based on experience.

Full details about this unique opportunity and about Genome Canada are available at www.genomecanada.ca/Careers

Please forward your resumé by
July 8, 2005
By email or fax to:

Hélène Meilleur
hmeilleur@genomecanada.ca
Fax: (613) 751-4474

National Health Research Institutes

Position of the President

The National Health Research Institutes (NHRI) – a non-profit research organization registered with the Department of Health, Government of Taiwan, the Republic of China – invites applicants for the position of President.

I. The NHRI was founded in January 1996. The incumbent President, Dr. Cheng-Wen Wu will step down from the post on December 31, 2005, following the completion of his 10-year term. Accordingly, the Institutes invites applicants for the Position of President.

II. The missions of the NHRI are to advance medical development and to promote health welfare of people in Taiwan. The responsibilities of the Institutes include:

1. To coordinate and integrate researches of local medical research organizations.
2. To conduct investigations on diseases of importance, especially to Taiwan.
3. To study the policies and regulations related to medical development, health care and disease prevention.
4. To promote new technologies and products derived from medical research and development.

III. The President of the NHRI is employed and reports to the Board of Directors and is authorized by the Board to be the representative of NHRI. Candidates should possess the qualifications listed below:

1. Recognition of the objectives and spirits of NHRI and familiarity with the development of scientific research in Taiwan. In addition, the candidates shall possess strong leadership qualities in administration.
2. Outstanding academic achievements and reputation.
3. Excellent character and integrity.
4. Behavior in accordance with justice and beyond political (partisan) and personal interests.

IV. The application shall include:

1. A letter of intent
2. Curriculum vitae
3. A list of publication
4. A copy each of five major recent publications
5. Three referees, including their names, addresses, telephone numbers, fax numbers and e-mail.

Please send the application materials to:
National Health Research Institutes (Taipei Office)
10F, 3, Yuanqu Street, Taipei 115, Taiwan, R.O.C.
Fax: 886-2-2655-8768
E-mail: cjy@nhri.org.tw

** Please mark on the envelope "Application for the Position of President of NHRI".*
*** Nominators should have the nominees' consent for nomination.*

V. The evaluation and processing of the applications will begin on August 1, 2005.

University of Heidelberg

The **Center for Molecular Biology** of the University of Heidelberg (ZMBH) invites applications for a

Full Professorship in Molecular Biology (W3)

The successful candidate will contribute to the research and teaching activities at the ZMBH in molecular and cellular biology.

Research and teaching programmes and scientific job openings are summarized at the ZMBH's website (http://www.zmbh.uni-heidelberg.de or http://www.zmbh.uni-heidelberg.de/jobs/default.html).

The ZMBH presently houses 14 independent research groups and offers an excellent research environment including central facilities for biomolecular chemistry, biocomputing, light microscopy, animal house as well as centralized administration and technical services.

This is essentially a permanent position. The first contract will be based on regulation § 50 Abs. 1 LHG and will be temporary. Exceptions to the temporal initial contract can be made under special circumstances and especially for applicants from outside Germany or outside academia if she/he would not consider the position otherwise. Should the position be made permanent after the initial period then this will not require a new application process.

The University of Heidelberg has a policy of raising the proportion of women in academic positions and therefore specifically invites the application of women scholars with the necessary qualifications. Under German law disabled applicants with full qualifications are to be preferred.

Applications should be sent by **01.07.2005** to the **Director of the ZMBH, Prof. Dr. Bernd Bukau, Im Neuenheimer Feld 282, D-69120 Heidelberg, Germany.**

CHAIRPERSON
DEPARTMENT OF CHEMICAL AND BIOMOLECULAR ENGINEERING
UNIVERSITY OF MARYLAND, COLLEGE PARK

Applications and nominations are invited for the position of Professor and Chairperson of the Department of Chemical and Biomolecular Engineering. The Department has reached an especially exciting point in its long history. In addition to the recent change in the department's name from the Department of Chemical Engineering to the Department of Chemical and Biomolecular Engineering, a number of junior faculty have recently joined the department and, in concert with the senior faculty, new areas of biologically related research are currently being explored. A renovation of the building in which the department resides is expected to be completed this summer. As an integral part of the highly rated A. James Clark School of Engineering at the University of Maryland, we seek a dynamic individual to lead the department into an energetic new era.

Selection criteria include: Earned doctorate in Chemical Engineering or closely related field, Integrity, Creativity, Excellent interpersonal skills, Strong leadership abilities, Record of achievement in research and scholarship, Commitment to education, Potential for excellence as manager and administrator, and Compatibility with College and Department growth plans.

With a budget of $10.7 million, the Department has 16 full-time faculty, 5 emeritus and 4 adjunct faculty working on research in the areas of biochemical and metabolic engineering, nanoparticle technology, complex fluids, polymer engineering, and process systems engineering. The department has 100 undergraduate students, 60 graduate students 80% of whom are pursuing a PhD degree.

Applications should include a cover letter, complete curriculum vitae and names of at lease five references and should be received by **August 1, 2005** for best consideration. Submit applications to: **Professor David Barbe, Professor and Associate Director, Maryland Technology Enterprise Institute, 2115 Potomac Building, University of Maryland, College Park, Maryland 20742-3415.**

The University of Maryland is an Equal Opportunity Affirmative Action Employer. Women and under represented minority candidates are particularly encouraged to apply.

POSITIONS OPEN

DEVELOPMENTAL PRIMATOLOGY

The Program in Biological Anthropology, Harvard University, seeks a faculty member at **ASSISTANT (TENURE TRACK), ASSOCIATE (TENURE TRACK),** or **FULL PROFESSOR** level interested in the developmental biology of humans and related primates from an evolutionary perspective.

All aspects of the relationship between genotype and developing phenotype relevant to primates/humans are appropriate, including gene expression, embryogenesis through postnatal development of major organ systems, physiology, and behavior.

This search is part of a broader initiative to develop a large and comprehensive research program in evolutionary developmental biology at Harvard University, which will involve several departments in both the Faculty of Arts and Sciences and Harvard Medical School. Successful applicants will interact with colleagues in biological anthropology with interests in human/primate genetics and genomics, behavioral ecology, reproductive ecology, functional/developmental anatomy, and paleobiology, as well as with the wider community in the life sciences.

Applicants should submit curriculum vitae, statements of research and teaching interests, representative publications, and the names and addresses of three references to: **Daniel E. Lieberman, Peabody Museum, 11 Divinity Avenue, Cambridge, MA 02138, U.S.A.** If possible, please have letters of reference submitted at the time of initial application. Letters of nomination from third parties are also welcome. Review of applications and nominations will begin October 1, 2005.

Further information about biological anthropology is available at **website: http://www.bioanth.harvard.edu/.** Send inquiries to **e-mail: mlynch@fas.harvard.edu.** *Harvard University is an Affirmative Action/Equal Opportunity Employer. Applications from or nominations for women and minority candidates are encouraged.*

POSITIONS OPEN

POSTDOCTORAL FELLOW

A Postdoctoral/Research Associate position is available immediately in the areas of prostate cancer, tumor suppressor, and drug discovery. Candidates must have a Ph.D. or equivalent with a significant background in biochemistry, molecular biology, and/or cell biology. Please submit your curriculum vitae and names of three references to: **Dr. Zhou Wang, Northwestern University Feinberg School of Medicine, Department of Urology, Tarry 16-763, 303 E. Chicago Avenue, Chicago, IL 60611. Fax: 312-908-7275; e-mail: wangz@northwestern.edu.** *Northwestern University is an Affirmative Action/Equal Opportunity Employer. Women and minorities are encouraged to apply.*

Multiple **POSTDOCTORAL POSITIONS** are available in the Division of Nephrology at University of Utah. The research concerns mechanisms of renal control blood pressure and chronic renal failure. The research program is currently supported by four NIH grants. Strong background in molecular biology and renal physiology is desirable. Please send curriculum vitae along with contact information of three references and a brief statement of research interest to: **Dr. Tianxin Yang, Associate Professor, Salt Lake City, UT 84132. E-mail: tianxin.yang@hsc.utah.edu; telephone: 801-582-1565, extension 4334.**

Position open for **RESEARCH ASSISTANT PROFESSOR,** Department Cancer Biology, Vanderbilt University, Nashville, Tennessee. Requires Ph.D. plus a minimum of three years postdoctoral work in cancer research, chemokines, and inflammation. Must have excellent publication record and written and verbal communication skills. Position entails management of current research, grant and manuscript preparation, and an individual research project. Send resume to **e-mail: linda.w.horton@vanderbilt.edu.**

POSITIONS OPEN

ASSOCIATE OR FULL PROFESSOR BIOLOGICAL SCIENCES

The Department of Biological Sciences and the College of the Environment and Life Sciences at the University of Rhode Island (URI) are focused on enhancing our rapidly growing Marine Biology Program and seek candidates to fill a leadership position for this effort at the level of Associate or Full Professor (tenure track). The successful candidate will be expected to provide vision and leadership for the Department and College to promote the goal of excellence in research and undergraduate/graduate education in marine biology. This initiative complements the University's existing focus on advancing the life sciences and follows closely our recent reorganization of biological sciences within the College of the Environment and Life Sciences, and approval of a new $50 million life sciences research and education building. Required: Ph.D. in biological sciences or a related discipline; an international reputation as an outstanding scientist in an area of marine biology, including externally funded research and outstanding publications in marine biology. For additional qualifications and information, visit the University's **website: http://www.uri.edu/human_resources** and the Department's **webpage: http://www.uri.edu/artsci/bio.** Review of applications will begin August 1, 2005, and continue until the position is filled. Submit (no e-mails or faxes, please) curriculum vitae, copies of three published papers, statements of research interests and teaching philosophy, and the names and contact information of five potential references to: **Cheryl A. Wilga, Search Chair, (Requisition #SM011079), University of Rhode Island, P.O. Box G, Kingston, RI 02881.** *URI is an Affirmative Action/Equal Employment Opportunity Employer and values diversity.*

POSITIONS OPEN

CORNELL UNIVERSITY

Joan and Sanford I. Weill Medical College

TENURE-TRACK POSITIONS GENETIC MEDICINE Weill Medical College Cornell University

As part of a significant enhancement of its basic biomedical science research programs and laboratory facilities, Weill Medical College of Cornell University is seeking to recruit tenure-track faculty at all levels to its newly formed Department of Genetic Medicine. We are especially interested in candidates with a focus on embryonic stem cells including the characterization of genes controlling pathways critical to ectoderm, endoderm, and mesenchymal differentiation, and the role of stem cells in organ repair after injury. Candidates with an interest in nuclear cell transfer are of specific interest. Exceptional candidates in other related/appropriate fields of interest regarding embryonic stem cells will also be considered. Candidates for junior positions should demonstrate the potential of establishing a vigorous independent research program. Candidates for senior positions should have an outstanding publication record, as well as substantial recent success in obtaining peer-reviewed grant support. Appointment of these independent, tenure-track faculty will be in the Department of Genetic Medicine chaired by Ronald G. Crystal, M.D.

Recruited faculty will receive generous startup support, will occupy newly constructed laboratories, will participate in The Ansary Stem Cell Center and will have access to the Arthur and Rochelle Belfer Gene Therapy Core Facility. Candidates may participate in the Graduate School of Medical Sciences Program which includes faculty from the Weill Medical College and the Sloan-Kettering Institute, and in the Tri-Institutional M.D.-Ph.D. Program which also includes faculty from The Rockefeller University.

Applications should include curriculum vitae, statement of research interests, and three letters of recommendation. Applications should be sent to:

Jennifer J. Cameron
Genetic Medicine Recruitment Committee (RC)
Box #27
Weill Medical College of Cornell University
1300 York Avenue
New York, NY 10021

Equal Employment Opportunity/Affirmative Action/Minorities/Females/Persons with Disabilities/Veterans.

ASSISTANT/ASSOCIATE PROFESSOR Department of Neurosciences College of Medicine Medical University of South Carolina, Charleston

The Department of Neurosciences at the Medical University of South Carolina (MUSC) seeks applications for a faculty position in primate cognitive neurophysiology. Candidates will be partaking in the development of a new primate research facility established in collaboration between MUSC and Alpha Genesis, and located in Yemassee (90 minutes from Charleston, South Carolina). Applicants must have a strong academic record of independent research with a Ph.D. or M.D. degree and expertise in single unit recordings in rhesus monkeys. Newly renovated laboratory space and attractive startup package and benefits available.

Applicants must apply online at **website: http://www.musc.edu/hrm/careers/faculty.htm.** Position requisition number is 041704. Applicants should also submit online a cover letter expressing their interest and qualifications, curriculum vitae, and three references addressed to: **Neurophysiology Search Committee, Department of Neurosciences, Medical University of South Carolina, 173 Ashley Avenue, BSB 403, Charleston, SC 29425.** *MUSC is an Equal Employment Opportunity/Affirmative Action Employer.*

POSITIONS OPEN

The Department of Basic Pharmaceutical Sciences in the School of Pharmacy at The University of Louisiana at Monroe (ULM) invites applications for a twelve-month, tenure-track faculty position. This position includes an attractive recruitment package of salary, startup, and laboratory space. Candidates should have an earned Doctorate in pharmaceutics, or a related field, with research interests in drug delivery, metabolism, or materials science. The successful candidate is expected to develop an independent, externally funded research program, and contribute to teaching professional and graduate courses in the area of pharmaceutics. Located in Monroe, Louisiana, a city whose metropolitan area population exceeds 100,000, the ULM campus offers a tranquil and cordial setting encompassing 238 acres, over 50 buildings, and an off-campus farm. Qualified individuals should submit their curriculum vitae, list of three references, and a statement of how their current interests and future goals might complement the strengths of the Department to: **William Kolling, Ph.D., Chair, Search Committee, School of Pharmacy, University of Louisiana at Monroe, 700 University Avenue, Monroe, LA 71209-0470. E-mail: kolling@ulm.edu.** *The University of Louisiana at Monroe is an Equal Opportunity/Affirmative Action Employer.*

POSTDOCTORAL POSITION

Postdoctoral position available immediately at Harvard Institutes of Medicine, Beth Israel Deaconess Medical Center to study mechanisms of autoimmune disease mechanism and dendritic cell biology. Research position will complement ongoing projects in the laboratory studying animals generated with autoimmune disease phenotype, dendritic cell dysfunction, and hematopoietic cell defects. Applicants should be highly motivated with a Ph.D. and/or M.D. degree and a strong background in immunology and molecular biology. Experience in signal transduction, stem cells, animal transplantation is a plus. The fellow will be part of a multidisciplinary research division in cancer and stem cell biology. Interested applicant should send curriculum vitae, a statement of scientific interest and career goals, names of three references or letters of recommendation to: **Dr. Bing Lim, HIM 955, Harvard Institutes of Medicine, 77 Louis Pasteur Avenue, Boston, MA 02115** at **e-mail: blim_science2005@yahoo.com.**

POSTDOCTORAL POSITIONS

Postdoctoral positions are available to work on genetic pathogenesis of lung cancer. Our laboratory is generating various compound mutant mouse models that develop lung cancers. We are seeking **POSTDOCTORAL FELLOWS** to further characterize these mutant mice and to perform chemoprevention and treatment studies with novel agents. Potential candidate must have documented experience of one or more years in molecular biology techniques or mouse modeling. Please send curriculum vitae with three references to: **Kwok-Kin Wong, M.D., Ph.D., Dana Farber Cancer Institute, 44 Binney Street, Dana Building 810B, Boston, MA 02115. E-mail: kwong1@partners.org**. *Dana Farber Cancer Institute is committed to hiring a diverse work force.*

Two **POSTDOCTORAL POSITIONS** available immediately to study chemoprevention of lung cancer using lung-specific p53 mutant mice as model and adult stem cell therapy in acute lung injury and fibrosis. *One position requires U.S. residency.* Applicant should have Ph.D. degree and molecular biology experience; animal experience is a plus. Please submit curriculum vitae and three references to: **Kam-Meng Tchou-Wong, Ph.D., Department of Environmental Medicine, New York University School of Medicine, 57 Old Forge Road, Tuxedo, NY 10987** or via **e-mail: tchouk02@med.nyu.edu.**

POSITIONS OPEN

CHAIR OF PHARMACOLOGY The University of Texas Southwestern Medical Center

The University of Texas (UT) Southwestern Medical Center is seeking candidates for the Chairman of the Department of Pharmacology. Candidates should have an established international record of superb achievement in areas relevant to academic pharmacology, a strong vision for basic science, and be prepared to lead the department in UT Southwestern's multi-departmental quest for excellence. The Department occupies new space and has existing strengths in several areas. Applicants should send curriculum vitae to:

Eric N. Olson
Chairman
Department of Molecular Biology
University of Texas
Southwestern Medical Center at Dallas
5323 Harry Hines Boulevard
Dallas, TX 75390-9148

UT Southwestern is an Equal Opportunity Employer.

VETERINARY PATHOLOGIST

The Department of Pathobiology at the University of Florida College of Veterinary Medicine is seeking a veterinary pathologist for a tenure-track position at the rank of **ASSISTANT/ASSOCIATE** or **FULL PROFESSOR.** Applicants should have a D.V.M. or equivalent degree and a record of research accomplishment in infectious disease/emerging pathogens and/or immunologic mechanisms. Applicants having a Ph.D. degree and American College of Veterinary Pathologists certification are preferred. Primary responsibilities will be to conduct a competitive program in research and to teach pathology. Teaching may be at the professional, graduate, resident, and/or postdoctoral levels. The Department has excellent research facilities and programs in infectious disease and comparative immunology (**website: http://www.vetmed.ufl.edu/path.htm**). The University of Florida is developing a campus-wide program of excellence to study emerging pathogens. Applicants should submit a letter outlining professional goals, curriculum vitae, and a list of three references to:

Dr. William Castleman
Department of Pathobiology
College of Veterinary Medicine
P.O. Box 110880
University of Florida
Gainesville, FL 32611—0880

Informal inquiries are welcome (**e-mail: castlema@ufl.edu; telephone: 352-392-4700, extension 3920**). Review of applicants is ongoing and will continue until the position is filled. The start date is flexible and negotiable. *The University of Florida is an Equal Opportunity/Equal Acess/Affirmative Action Employer.*

BIOINFORMATICS CORE POSITION

The Wadsworth Center (**website: http://www.wadsworth.org**) is seeking a Ph.D. scientist to provide bioinformatic and biostatistical support for a wide range of biomedical research projects, including studies employing micro-arrays and other genome-scale approaches. The successful applicant will have a firm grounding in statistics, documented scholarship in one or more relevant areas of bioinformatics with a track record of collaborative research, and an interest in interacting with a multidisciplinary community of scientists in a state-of-the-art computational facility. Applicants should submit (preferably via e-mail) curriculum vitae and summary of expertise and collaborations, and arrange to have three reference letters sent to: **Dr. Carmen Mannella, Wadsworth Center, New York State Department of Health, P.O. Box 509, Albany, NY 12201-0509. E-mail: carmen@wadsworth.org.** *The Wadsworth Center is an Affirmative Action/Equal Opportunity Employer.*

Immunology and Infectious Disease Careers

A *Science* Advertising Supplement

Science's qualified circulation of 129,590[1] plus our pass-along readers brings total global weekly readership to over 710,000.[2]

When you run your ad in this issue it will be distributed at three Gordon Research Conferences. These exclusive conferences are by invite only so your ad will reach the best and the brightest.

- Applied & Environmental Microbiology 24–29 July, New London, CT
- Cancer Models & Mechanisims 24–29 July, Smithfield, RI
- Human Genetics & Genomics 24–29 July, Newport, RI

Don't forget — When you post your job on ScienceCareers.org it is also searchable on six additional websites.

Just added:
This issue of *Science* will include an exclusive editorial focus on important genome papers. This means additional media coverage and readership of an important issue. Be a part of it by including your recruitment or image ad.

1 *Science* June 2004 BPA Publisher's Statement.
2 *Science* June 2004 circulation as applied to 14 January 2000 Harvey Readership Survey and 2002 Harvey Cumulative Report, publisher's own data.

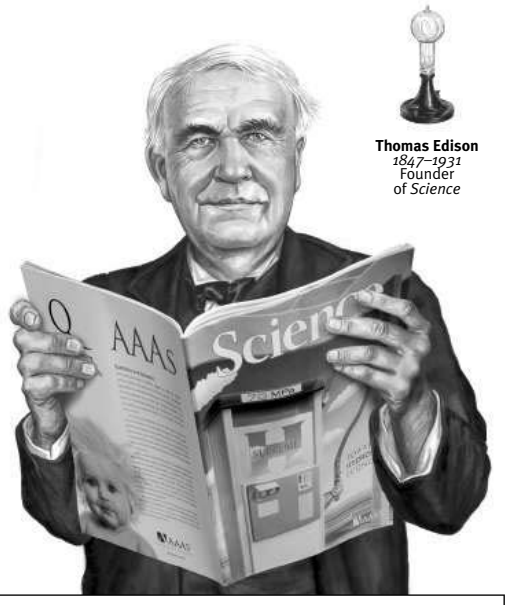

Thomas Edison
1847–1931
Founder
of *Science*

Issue date 15 July 2005
Reserve ad space by 28 June 2005

More ways to reach immunologists

- **Send an Exclusive Job Alert**
  Over 2,500 scientists have signd up to receive job alerts for immunology and infectious disease opportunities.
- **Search our Resume/CV Database**
  Our Resume/CV Database contains over 4,000 resumes of scientists working in immunology or infectious diseases.

To advertise contact:

U.S. Daryl Anderson
Phone: (202) 326-6543
E-mail: advertise@sciencecareers.org

Europe and International
Tracy Holmes
Phone: +44 (0) 1223 326 500
E-mail: ads@science-int.co.uk

Japan Jason Hannaford
Phone: +81 (0) 52 789-1860
E-mail: jhannaford@sciencemag.jp

ScienceCareers.org
We know science AAAS

Believe it!

DNA Sequencing for $2.50 per reaction.

- Read length up to 900 bases.
- High quality electropherograms.
- Fast turnaround.
- Plasmid and PCR purification available.

$2.50 per reaction!

POLYMORPHIC
Polymorphic DNA Technologies, Inc.℠

Polymorphic exclusively uses ABI 3730XL sequencers.
Data delivered via secure FTP, email or CD.
No charge for standard sequencing primers.
96 sample minimum order.
96 well plates only- no tubes.

www.polymorphicdna.com
info@polymorphicdna.com

1125 Atlantic Ave., Ste. 102
Alameda, CA 94501

888.362.0888

For more information please visit
www.polymorphicdna.com

New from R&D Systems:

Faster, Smarter, Easier, Better

Quality | Selection | Performance | Results

We are pleased to announce our renovated, redesigned website with more powerful search functions and user-friendly navigation. The new design will complement our new look and organization of reagents into seven key areas of research:

Cancer, Development, Endocrinology, Immunology, Neuroscience, Proteases, & Stem Cells.

On **www.RnDSystems.com**, you'll be able to search or browse our expansive product database by research topic, product type, or molecule letter. And as you've come to expect, you'll continue to have access to our product inserts, minireviews and online literature. Visit us online or call us for a free guide to using the new, improved website.

www.RnDSystems.com | (800) 343-7475

U.S. & Canada
R&D Systems, Inc.
Tel: (800) 343-7475
info@RnDSystems.com

Europe
R&D Systems Europe Ltd.
Tel: 0800 37 34 15
info@RnDSystems.co.uk

Germany
R&D Systems GmbH
Tel: 0800 909 4455
infogmbh@RnDSystems.co.uk

France
R&D Systems Europe
Tel: 0800 90 72 49
info@RnDSystems.co.uk

R&D SYSTEMS